Theoretical Analysis of Blood Flow through Arteries

By

Shagufta Ijaz

Department of Mathematics
Quaid-i-Azam University
Islamabad, Pakistan
2016

Theoretical Analysis of Blood Flow through Arteries

By

Shagufta Ijaz

Supervised By

Prof. Dr. Sohail Nadeem

Department of Mathematics
Quaid-i-Azam University
Islamabad, Pakistan
2016

Theoretical Analysis of Blood Flow through Arteries

By

Shagufta Ijaz

A Dissertation Submitted in the Partial Fulfillment of

the requirements for the degree of

DOCTOR OF PHILOSOPHY

IN

MATHEMATICS

Supervised By

Prof. Dr. Sohail Nadeem

Department of Mathematics
Quaid-i-Azam University
Islamabad, Pakistan
2016

Contents

Nomenclature **4**

1 Introduction **6**

2 Theoretical analysis of metallic nanoparticles on blood flow through tapered elastic artery with overlapping stenosis **12**

2.1 Mathematical formulation 13

2.2 Solution of the problem 17

2.3 Thermophysical properties of blood and copper 19

2.4 Results and discussion 19

3 Study of radially varying magnetic field on blood flow through catheterized tapered elastic artery with overlapping stenosis **32**

3.1 Mathematical formulation 33

3.2 Solution of the problem 36

3.3 Appendix 38

3.4 Thermophysical properties of blood and copper 38

3.5 Results and discussion 39

4 Examination of nanoparticles as a drug carrier on blood flow through catheterized composite stenosed artery with permeable walls **54**

4.1 Mathematical formulation 55

4.2 Solution of the problem 58

4.3 Appendix 60

4.4 Results and discussion 60

5 Impulsion of nanoparticles as a drug carrier for the theoretical investigation of stenosed arteries with magnetic effects 75

5.1 Fundamental equation of induced magnetic field 76

5.2 Formulation of the problem 77

5.3 Solution of the problem 80

5.4 Appendix 83

5.5 Results and discussion 84

6 Nanoparticles analysis on blood flow through tapered catheterized elastic artery with overlapping stenosis 102

6.1 Fundamental equation of Buongiorno's model 102

6.2 Mathematical formulation 103

6.3 Solution of the problem 105

6.4 Appendix 108

6.5 Results and discussion 109

7 Single wall carbon nanotube (SWCNT) examination on blood flow through a multiple stenosed artery with variable nanofluid viscosity 120

7.1 Mathematical formulation 121

7.2 Solution of the problem 124

7.3 Appendix 126

7.4 Thermophysical properties of blood and SWCNT 126

7.5 Results and discussion 126

8 Influence of metallic nanoparticles on blood flow through arteries having both stenosis and aneurysm 139

8.1 Mathematical formulation 140

8.2 Solution of the problem 143

8.3 Appendix 145

8.4 Results and discussion 145

9 Theoretical examination of nanoparticles as a drug carrier with slip effects on the wall of stenosed arteries **160**

9.1 Mathematical formulation . . . 161

9.2 Solution of the problem . . . 163

9.3 Appendix . . . 165

9.4 Results and discussion . . . 165

10 Conclusions **187**

10.1 Heat and mass transfer results . . . 187

10.2 Hemodynamic theoretical results . . . 188

10.2.1 Nanoparticles effects . . . 188

10.2.2 Permeable wall and slip effects . . . 188

10.2.3 Magnetic effects . . . 188

10.2.4 Thermal and velocity slip effects . . . 189

10.2.5 Variable nanofluid viscosity effects . . . 189

10.2.6 Combination of aneurysm and stenosis effects . . . 189

10.2.7 Other important findings . . . 190

10.3 Axial velocity results . . . 190

10.4 Trapping results . . . 190

References **191**

Nomenclature

English words	
$h(z)$	height of stenosis
e_0	radius of normal artery
L	length of artery
$L_o, \overline{L}$	length of stenosis
R_{en}	Reynolds number
n	shape of stenosis
t	time
u_0	averaged velocity
p	pressure
S_{rz}	shear stress
L	length of stenosed artery
Q	embedding parameter
P_{rn}	Prandtl number
H_a	Hartmann number
N_t	thermophoresis parameter
N_b	Brownian motion parameter
S^2	Strommers number
G_r	Grashof number
B_r	local nanoparticle Grashof number
J_θ	current density distribution
R_m	magnetic Reynolds number
F	flow rate
T_o, T_1	constant temperature on walls
u, v, w	components of velocity
r, z	radial and axial directions
C_o, C_1	nanoparticles concentration on walls
H_z, H_r	axial, radial induced magnetic field

D_a	Darcy number
s	dimensionless slip parameter
$Q_1(t)$	time-variant parameter
Greek words	
γ	thermal slip
$\boldsymbol{\kappa}$	velocity slip
α	viscosity parameter
ε	catheter radius
η	inclination angle
ϕ	tapering parameter
δ	maximum height of stenosis
λ	resistance impedance
ω	angular frequency
ζ	tapering parameter
β	heat source parameter
α_o	amplitude constant
Φ	nanoparticle volume fraction
θ	temperature
d_i, α_i, β_i	indicates position of stenosis
a_i, b_i, c_i	constants
x_i, m_i, g_i	constants

Chapter 1

Introduction

Blood is considered as a vital fluid having major importance in physiopathology that remains a factor of heart failure and other diseases. Blood is a very much concentrated suspension with a variety of cells such as red blood, white blood cells and platelets that are suspended in a continuous phase called plasma. Plasma is an aqueous solution of organic substances and electrolytes mainly proteins. Plasma behaves as a viscous fluid whose viscosity depends mainly on temperature as water does and exhibits non-viscous properties at low shear rate while flowing in the small diameter arteries. The main objective of the blood flow model in arteries is to evaluate hemodynamic effects for which artery wall experiences due to different factors like the fluid flow geometry, the pulsatile blood flow and the blood rheology behavior (i.e., viscous or non-viscous properties of fluid). Further, it is important to discuss the correlation between abnormal biological events and flow pattern characteristics and arterial diseases like thrombosis, atherosclerosis and stenosis. The hemodynamic effects play important roles in the access of arterial diseases and regulation of vascular biology (see Mann et al. [1]) and some other researchers have also discussed this study [2, 3].

Arterial Stenosis is a disease that developed in the form of the obstruction in the lumen of the blood vessel and it disturbs the normal blood circulation causing major concerns to health in the form of strokes brain ischemia, cardiac ischemia etc. Atherosclerosis is attributed to the addition of fat, cholesterol and lipid, so forth on the inner wall of the blood vessel and this blockade may harm the internal cells of the walls and may promote to the growth of the stenosis [4, 5]. One of the most serious significance of these arterial diseases is an increase in resistance

to blood flow, which leads to reduction of blood flow in the affected vascular bed.

The mechanics of circulation of the blood through stenosed arteries have been discussed theoretically and experimentally by many researchers [6, 7]. Liu et al. [8] discussed the blood flow through models of stenotic and tapered arteries. Here they deliberated that the stenosis disturbs the flow field at the throat of the stenosis. Siegel et al. [9] discussed the physiologic stress levels that are experienced by platelets and endothelial cells in the region of vascular stenosis. Morgan et al. [10] discussed an incompressible blood flow through an axisymmetric stenosis. Here they found that the theoretical calculations of flow separation characteristics and pressure drop are in reasonably good agreement with the experimental measurements. The blood vessel walls may be movable, flexible and permeable. Cholesterol is considered as one of the major reasons to increase in permeability of the arteries and the further theoretical studies related to this topic are [11, 12].

Stenosis or atherosclerosis may develop in series (multiple), non-symmetric, symmetric, irregular, composite and overlapping or bell shaped manner. Perhaps one could consider effects of stenosis that may develop with different shapes in the realm of formation of arterial narrowing which may provide more help to design and to construct upgraded artificial organs. Chakravarty et al. [13] discussed the problem of the blood flow through confined vessel segments with an overlapping stenosis. They discussed two dimensional and non-linear mathematical model of blood flow in tapered arteries with the presence of overlapping stenosis. Ellahi et al. [14] discussed the arterial blood flow through composite stenosis under the mild stenosis case by treating blood as micropolar fluid. Mekheimer et al. [15] discussed a micropolar fluid model for axis-symmetric blood flow through radially symmetric but axially non-symmetric mild stenosis tapered arteries. Some other geometrical configurations of the stenosis proposed by different researchers are $[16 - 18]$.

Blood flow through arteries becomes more complicated due to development of aneurysm. Aneurysm is a like a balloon dilation found on the walls of a blood artery and are usually seen in arteries such as carotid, cerebral, thoracic, abdominal, femoral, renal etc. It develops gradually as time passes and grows faster as it becomes larger. The role of hemodynamics in the growth of aneurysms has been the subject of several studies [19, 20]. Mukhopadhyay et al. [21] analyzed the systematic analysis of flow features in a tube and modelled as an artery,

having a local aneurysm in the presence of hematocrit. Kumar et al. [22] discussed the pulsatile suspension flow in a dilated vessel. They discussed the pulsatile suspension flow characteristics by analyzing the flow, pressure and stress fields.

The interaction and combination of aneurysm and stenosis further complicate the hemodynamics in diseased arterial vessels. Pincombe et al. [23] discussed the effects of stenosis and dilatations of the coronary arteries with various combinations on the resistance impedance to flow by considering blood as Bingham fluid model. Prasad et al. [24] discussed the steady flow of Jeffrey fluid through a tube with both constriction and dilatations. Numerous theoretical and experimental studies of fluid dynamics through different geometries of constriction or expansion have been discussed to evaluate the flow pattern (see [25, 26]).

The tapering effects are a substantial characteristic of mammalian arterial systems and considered mathematically by many researchers in order to create resemblance with the living organism. Biswas et al. [27] discussed the steady blood flow analysis through arterial stenosis along tapering wall phenomena. Zaman et al. [28] discussed the two-dimensional model to analyze the unsteady pulsatile flow of blood through tapered stenosed arteries. Sankar et al. [29] considered a computational model to analyze the unsteady flow of blood through tapered narrow arteries. Mekheimer et al. [30] discussed the diverging, converging and non-tapered effects by considering the time-variant anisotropically elastic arteries.

The procedure of catheterization is important and has turn into a standard tool for the treatment and diagnosis in latest medical applications. The inclusion of a catheter into an artery produces the annular region between the arterial wall and the catheter wall. A catheter is composed of polyester based thermoplastic polyurethane, chlorides and medical grade polyvinyl etc. The insertion of the catheter into arteries will change the flow field and modify the hemodynamics conditions that occur in the artery before catheterization [31, 32]. Mekheimer et al. [33] discussed the study that is related to the surgical technique for the injection of a catheter through stenotic arteries. They explored the movement of physiological fluid on behalf of blood in the gap between two eccentric tubes. Srivastav et al. [34] discussed the blood flow in a narrow catheterized artery. They investigated by using a two-phase macroscopic model of blood. Verma et al. [35] discussed the problem of the blood flow through a symmetric stenosis during artery catheterization by assuming blood to behave like a viscous fluid.

The use of external magnetic field in biotechnology has many applications for the advance development of instruments for cell separation, magnetic tracers, cancer treatment and for the reduction of bleeding during surgeries. To decrease the heart rate in biological systems the influence of external magnetic is helpful as described in [36]. The study of electromagnetic fields in medical science was firstly introduced by Kolin [37]. Recently, several mathematical models have been considered by a number of investigators to discuss the behavior of the blood flow under the effect of magnetic field. Stud et al. [38] discussed the influence of moving magnetic field on blood flow. They observed that the influence of suitable moving magnetic field speed up the blood. Korchevskii et al. [39] explored the possibility of regulating the blood movement in human system by applying magnetic field. The significant contributions of current years to this topic are cited as [40, 41].

The circulation of the blood through arteries with no slip condition has been discussed by many researchers in which they assumed that the fluid layer moves with next to the boundary surface [42, 43]. Misra et al. [44] considered a theoretical model of the blood flow through a stenosed arterial segment with no-slip condition at the vessel wall. However, there is another mechanism available in literature which considered the hypothesis of slippage, which states that the velocity of the fluid is linearly proportional to the shear stress. The flow problems that exhibit boundary slip conditions have important applications, such as in internal cavities and polishing valves of artificial hearts. Sinha et al. [45] considered the influence of externally imposed periodic body acceleration on the blood flow through a stenosed arterial segment by taking velocity slip conditions into account. Recently, Ponalagusamy et al. [46] considered the mathematical models for the blood flow through stenosed arterial segment with velocity slip condition at the constricted wall.

Mostly, the studies that are mentioned above arteries carrying blood were considered to being horizontal however various arteries in biological systems are not horizontal such as bifurcated arteries. Chakraborty et al. [47] explored the blood flow through radially symmetric but axially non-symmetric stenosis in an inclined artery. Mekheimer et al. [48] explored the analysis of the blood flow through inclined catheterized arteries with a balloon (angioplasty). Biswas et al. [49] discussed tapered inclined arteries with the catheter insertion. Here they considered suitable flow geometry to investigate the effect of shape parameters on the stenotic

wall. For some further studies in this direction are given in [50, 51].

The circulation of blood plays an important role for heat transferred analysis in tissues. A variation of temperature and heat transfer rates in living organism depends on the blood perfusion, arterial blood flow, metabolic heat generation, thermal properties of blood and tissue. The heat transfer in tissue is a complex process and discussed by many researchers [52, 53]. Ogulu et al. [54] examined the heat transfer analysis on the circulation of blood in a diseased artery. They discussed here that the heat distributions also effect the circulation of blood in cardiovascular system. Chakravarty et al. [55] presented a model to discuss the dynamic response of heat and mass transfer in bifurcated arteries by considering stenotic conditions. Tashtoush et al. [56] discussed the influence of temperature distributions on a blood flow through multi-stenosis arteries. They investigated here the effects of stenosis with Nusselt number and shear stress.

The viscosity of blood in physiological system is not constant and may depend not only on the diameter of vessel but also depend on radial coordinate, hematocrit ratio, temperature and pressure. In fact, blood viscosity decreases when temperature of blood increases, which will help to increase the blood flow rate and reduces coagulation factors [57]. Shit et al. [58] discussed the blood flow model through a stenosed artery with hematocrit depended variable viscosity. Nadeem et al. [59] discussed the blood flow through a tapered stenosed artery with a temperature dependent viscosity by treating blood as Jeffrey fluid. Misra et al. [60] discussed dependence of blood viscosity on hematocrit. Gupta et al. [61] discussed the mathematical model of the blood flow with radial dependent viscosity in a stenosed artery.

In biomedical applications, the use of nanotechnology giving a unique chemical and physical property has the potential to provide intensely advance diagnostic methods and capable devices for more effective molecular exposure [62 – 64]. Nanotechnology based drug delivery has various advantages and provides a mechanism for solving the problems associated with conventional drug delivery systems. A small amount of nanoparticles, when dispersed and suspended into the base fluid can provide dramatic enhancements in the thermal properties of the considered base fluid. The nanoparticles are nanometer-sized particles of carbides, oxides, metals, or nanotubes and these nanoparticles have applications in biomedicine i.e. radiation therapy for cancer treatment, deliver drugs by targeting rotted arteries which have developed

as a noninvasive method to contest heart disease especially copper nanoparticles that corrects abnormal heart enlargement called hypertrophic cardiomyopathy [65] etc. Gentile et al. [66] discussed longitudinal transport of nanoparticles in blood vessels by considering blood as Casson fluid. Fluids with nanoparticles firstly proposed by Choi [67] and after him highlighted by others [68 − 73]. Buongiorno [74] discussed the different method to analyze the effects of nanoparticle dispersion with in the base fluid.

The blood mediated nanoparticle distribution is a growing and new field in the development of diagnostics and therapeutics. A nanoparticle with magnetic properties adds a new dimension where they can be manipulated with application of an external magnetic field. The magnetic nanoparticles as a drug agent has gained much attention based on their ease of preparation and ability to transport a drug directly to the centre of the disease. The concept of nanoparticles with magnetic field effects for drug delivery application is discussed by many researchers [75, 76].

The suspended nanoparticles within the base fluid alone are not enough to enhance thermal conductivity due to dependence on the shape and size of the particles. Recently, Murshed et al. [77] demonstrated that a carbon nanotube (CNT) provides six times better thermal conductivity as compared to other materials. Carbon nanotubes are long, thin cylinders of carbon which were discovered by Iijima et al. [78] and now captivate a wide range of industries as well as scientists interest due to their fascinating chemical and physical properties. They hold potential for applications in medicine, gene, and drug delivery areas. There are three key features of CNT i.e. single, double and multiple wall carbon nanotubes. One of the most important potential applications of single wall carbon nanotubes is in the domain of nano electronics and as a result of SWCNT's is highly conductive. Further discussed by many researchers as [79, 80].

In understanding with all above literature, present thesis is devoted for theoretical analysis of blood flow through stenosis with help of mathematical models. The nanoparticles are utilized here as a drug carrier to discuss the hemodynamic effects of stenosis. The considered nano mathematical models are simplified for mild stenosis (or aneurysm) case and then solved by using exact and HPM techniques. The detail description on the HPM technique can be found in [81]. The main outcomes are obtained after the graphical and flow pattern illustration. The thesis consists of ten chapters that are authors own work which is published in reputed international journal.

Chapter 2

Theoretical analysis of metallic nanoparticles on blood flow through tapered elastic artery with overlapping stenosis

In this chapter, the mathematical model of blood flow through an elastic artery with overlapping stenosis under the influence of metallic nanoparticles is discussed. To do this an appropriate mathematical geometry of the overlapping stenosis is considered with tapering effect. The governing equations for a mild stenosis case have been modeled to obtain exact solutions of velocity, temperature and pressure gradient. The expressions of impedance resistance to flow and wall shear stress are computed to discuss hemodynamic effects of stenosis. The effects of different emerging flow parameters are discussed through graphs for different values of interest. The obtained results from nano contributions are also discussed with comparison to the pure blood case $\Phi = 0.00$. At the end, it is concluded that the contribution of metallic nanoparticles is important as drug carrier to decrease the significances of the wall shear stress and resistance impedance to flow when compared to the pure blood case.

2.1 Mathematical formulation

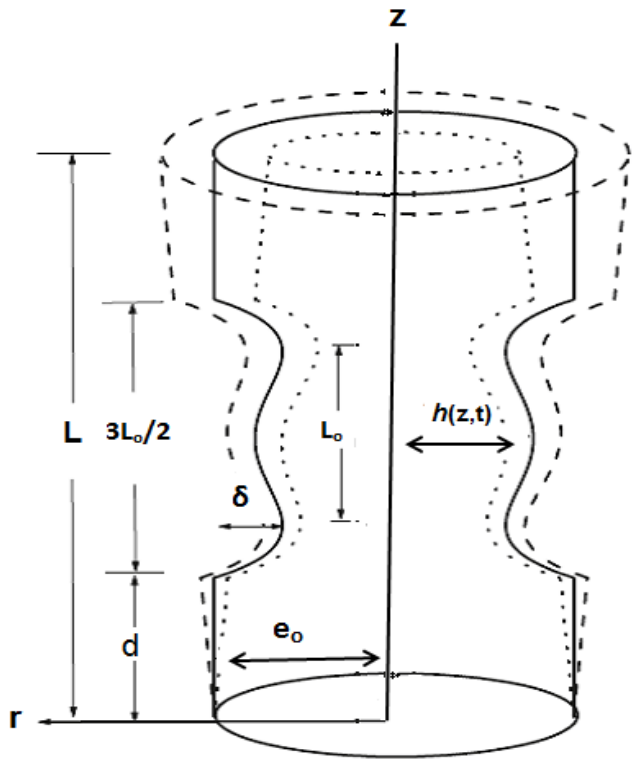

Fig. (2.1): Geometry of overlapping stenosed artery.

Let us consider the laminar and the incompressible viscous nanofluid flowing through a vertical tube of length L with overlapping stenosis. Let $(r,\ \theta,\ z)$ be defined as coordinates in the cylindrical polar coordinate system where z axis is taken along the axis of the artery, while θ and r are taken along the circumferential and radial directions respectively. Also, we have considered that $r = 0$ as the axis of the symmetry of the tube and heat transfer phenomenon is taken into account by giving temperature T_o to the wall of the artery. The geometry of the elastic arterial wall of the time-variant overlapping stenosis for different taper angles is defined as

$$\begin{aligned}\overline{h}(z,\,t) &= [(\zeta^*\overline{z}+e_0)-\frac{\delta\cos\phi}{L_0}(\bar{z}-d)\{11-\frac{94}{3L_0}(\bar{z}-d)+\frac{32}{L_0^2}(\bar{z}-d)^2 \\ &\quad -\frac{32}{3L_0^3}(\bar{z}-d)^3\}]Q_1(t), \qquad d\le\bar{z}\le d+\frac{3}{2}L_0, \\ &= (\zeta^*\bar{z}+e_0)Q_1(t), \qquad \text{otherwise,} \end{aligned} \tag{2.1}$$

where $h(z,\,t)$ defined as the radius of the tapered arterial segment in the trapped region, e_0 as the constant radius in the non-stenotic region, ϕ as the tapered angle, $\frac{3}{2}L_0$ as the length of overlapping stenosis, d as the location of the stenosis, $\delta\cos\phi$ is taken to be the critical height of the overlapping stenosis and ζ =tanϕ represents the slope of the tapered vessel. We can explore the possibility of different shapes of the artery, the converging tapering ($\phi<0$), non-tapered artery ($\phi=0$) and the diverging tapering ($\phi>0$). The time-variant parameter is taken to be

$$Q_1(t)=1-\alpha_o(\cos\omega t-1)\exp[-\alpha_o\omega t], \tag{2.2}$$

where α_o is a constant, ω represents the angular frequency of the forced oscillation and t is the time. The governing equations for conservation of mass, momentum and temperature for viscous fluid can be written as

$$\frac{\partial\overline{u}}{\partial\overline{r}}+\frac{\overline{u}}{\overline{r}}+\frac{\partial\overline{w}}{\partial\overline{z}}=0, \tag{2.3}$$

$$\rho_{nf}\left(\frac{\partial\overline{u}}{\partial\overline{t}}+\overline{u}\frac{\partial\overline{u}}{\partial\overline{r}}+\overline{w}\frac{\partial\overline{u}}{\partial\overline{z}}\right)=-\frac{\partial\overline{p}}{\partial\overline{r}}+\mu_{nf}\left(\frac{\partial^2\overline{u}}{\partial\overline{r}^2}+\frac{1}{\overline{r}}\frac{\partial\overline{u}}{\partial\overline{r}}+\frac{\partial^2\overline{u}}{\partial\overline{z}^2}-\frac{\overline{u}}{\overline{r}^2}\right), \tag{2.4}$$

$$\rho_{nf}\left(\frac{\partial\overline{w}}{\partial\overline{t}}+\overline{u}\frac{\partial\overline{w}}{\partial\overline{r}}+\overline{w}\frac{\partial\overline{w}}{\partial\overline{z}}\right)=-\frac{\partial\overline{p}}{\partial\overline{z}}+\mu_{nf}\left(\frac{\partial^2\overline{w}}{\partial\overline{r}^2}+\frac{1}{\overline{r}}\frac{\partial\overline{w}}{\partial\overline{r}}+\frac{\partial^2\overline{w}}{\partial\overline{z}^2}\right)+g(\rho\gamma)_{nf}(\overline{T}-T_0), \tag{2.5}$$

$$\left(\frac{\partial\overline{T}}{\partial\overline{t}}+\overline{u}\frac{\partial\overline{T}}{\partial\overline{r}}+\overline{w}\frac{\partial\overline{T}}{\partial\overline{z}}\right)=\frac{K_{nf}}{(\rho c_p)_{nf}}\left(\frac{\partial^2\overline{T}}{\partial\overline{r}^2}+\frac{1}{\overline{r}}\frac{\partial\overline{T}}{\partial\overline{r}}+\frac{\partial^2\overline{T}}{\partial\overline{z}^2}\right)+\frac{Q_0}{(\rho c_p)_{nf}}. \tag{2.6}$$

In above equations $\overline{u}$ and $\overline{w}$ are defined as components of velocity in radial and axial directions, $\overline{T}$ as the temperature of fluid, Q_0 as constant heat absorption or heat generation. For the proposed nanofluid model μ_{nf} is defined as viscosity, K_{nf} as thermal conductivity, ρ_{nf} as density, γ_{nf} as thermal expansion coefficient and $(\rho c_p)_{nf}$ as heat capacitance and the thermo physical properties are given as

$$\begin{aligned}
&\mu_{nf} = \frac{\mu_f}{(1-\Phi)^{2.5}},\ \alpha_{nf} = \frac{K_{nf}}{(\rho c_p)_{nf}},\ \rho_{nf} = (1-\Phi)\rho_f + \Phi\rho_s,\\
&(\rho c_p)_{nf} = (1-\Phi)(\rho c_p)_f + \Phi(\rho c_p)_s, (\rho\gamma)_{nf} = (1-\Phi)(\rho\gamma)_f + \Phi(\rho\gamma)_s,\\
&\frac{K_{nf}}{K_f} = \frac{(K_s+2K_f) - 2\Phi(K_f - K_s)}{(K_s+2K_f) + \Phi(K_f - K_s)},
\end{aligned} \tag{2.7}$$

here for base fluid ρ_f is defined as density, μ_f as viscosity, γ_f as thermal expansion coefficient, $(\rho c_p)_f$ as heat capacitance and K_f as thermal conductivity, while for solid nanoparticle ρ_s is defined as density, γ_s as thermal expansion coefficient, $(\rho c_p)_s$ as heat capacitance, K_s as thermal conductivity and Φ as the volume fraction. Non-dimensional variables are defined as

$$\begin{aligned}
&r = \frac{\overline{r}}{e_0},\ z = \frac{\overline{z}}{L_0},\ w = \frac{\overline{w}}{u_o},\ u = \frac{L_0\overline{u}}{u_o\delta},\ p = \frac{e_0^2\overline{p}}{u_o L_0 \mu_f},\\
&t = \frac{\overline{t}u_o}{L_0},\ R_{en} = \frac{e_0 u_o \rho_f}{\mu_f},\ G_r = \frac{g\gamma_f\rho_f e_0^2 T_0}{u_0\mu_f},\ L = \frac{\overline{L}}{L_0}\\
&\beta = \frac{Q_0 e_0^2}{T_0 K_f},\ \theta = \frac{\overline{T} - T_0}{T_0},\ P_{rn} = \frac{c_p\mu_f}{K_f}.
\end{aligned} \tag{2.8}$$

After using Eq. (2.8), Eqs. (2.3) to (2.6) take the following form

$$\delta^*\left(\frac{\partial u}{\partial r} + \frac{u}{r}\right) + \frac{\partial w}{\partial z} = 0, \tag{2.9}$$

$$\frac{\rho_{nf}}{\rho_f} R_{en}\epsilon^3\delta^*\left(\frac{\partial u}{\partial t} + \delta^* u\frac{\partial u}{\partial r} + w\frac{\partial u}{\partial z}\right) = -\frac{\partial p}{\partial r} + \frac{\mu_{nf}}{\mu_f}\epsilon^2\delta^*\left(\frac{\partial^2 u}{\partial r^2} + \frac{1}{r}\frac{\partial u}{\partial r} + \epsilon^2\frac{\partial^2 u}{\partial z^2} - \frac{u}{r^2}\right), \tag{2.10}$$

$$\frac{\rho_{nf}}{\rho_f}R_{en}\epsilon\left(\frac{\partial w}{\partial t}+\delta^* u\frac{\partial w}{\partial r}+w\frac{\partial w}{\partial z}\right)=-\frac{\partial p}{\partial z}+\frac{\mu_{nf}}{\mu_f}\left(\frac{\partial^2 w}{\partial r^2}+\frac{1}{r}\frac{\partial w}{\partial r}+\epsilon^2\frac{\partial^2 w}{\partial z^2}\right)+\frac{(\rho\gamma)_{nf}}{(\rho\gamma)_f}G_r\theta, \quad (2.11)$$

$$R_{en}P_{rn}\epsilon^2\left(\frac{\partial \theta}{\partial t}+\delta^* u\frac{\partial \theta}{\partial r}+w\frac{\partial \theta}{\partial z}\right)=\frac{K_{nf}}{K_f}\frac{(\rho c_p)_f}{(\rho c_p)_{nf}}\left(\frac{\partial^2 \theta}{\partial r^2}+\frac{1}{r}\frac{\partial \theta}{\partial r}+\epsilon^2\frac{\partial^2 \theta}{\partial z^2}\right)+\beta\frac{(\rho c_p)_f}{(\rho c_p)_{nf}}. \quad (2.12)$$

In the above expressions G_r represents as the Grashof number, R_{en} is the Reynolds number, P_{rn} is the Prandtl number, β is non-dimensional heat source parameter with respect to fluid and u_0 is the averaged velocity. Using mild stenosis case $\delta^* = \frac{\delta}{e_0} \ll 1$ and taking extra condition $\epsilon = \frac{e_0}{L_0} \approx O(1)$, the constitutive Eqs. (2.10) to (2.12) can be written as

$$\frac{\partial p}{\partial r}=0, \quad (2.13)$$

$$\frac{\partial p}{\partial z}\frac{\mu_f}{\mu_{nf}}=\frac{\partial^2 w}{\partial r^2}+\frac{1}{r}\frac{\partial w}{\partial r}+\frac{\mu_f}{\mu_{nf}}\frac{(\rho\gamma)_{nf}}{(\rho\gamma)_f}G_r\theta, \quad (2.14)$$

$$\frac{\partial^2 \theta}{\partial r^2}+\frac{1}{r}\frac{\partial \theta}{\partial r}+\beta\frac{K_f}{K_{nf}}=0. \quad (2.15)$$

Boundary conditions and geometry of stenosis in dimensionless form are defined as

$$\begin{aligned} h(z,\ t) &= [(\zeta z+1)-\delta^*\cos\phi(z-d^*)\{11-\frac{94}{3}(z-d^*)+32(z-d^*)^2- \\ &\quad \frac{32}{3}(z-d^*)^3\}]Q_1(t), \qquad d^* \le z \le d^*+\frac{3}{2}, \\ &= (\zeta z+1)Q_1(t), \qquad \text{otherwise}, \end{aligned} \quad (2.16)$$

$$\frac{\partial w}{\partial r}=0 \ \ at \ \ r=0, \quad w=0 \ \ at \ \ r=h(z), \quad (2.17)$$

$$\frac{\partial \theta}{\partial r}=0 \ \ at \ \ r=0, \quad \theta=0 \ \ at \ \ r=h(z), \quad (2.18)$$

where

$$\delta^* = \frac{\delta}{e_0},\ d^* = \frac{d}{L_0},\ \zeta = \frac{\zeta^* L_0}{e_0}. \tag{2.19}$$

2.2 Solution of the problem

The exact solutions of Eqs. (2.14) and (2.15) are written as

$$\theta = -\frac{1}{4}\beta(r^2 - h^2)\left(\frac{K_s(1-\Phi) + K_f(2+\Phi)}{K_s(1+2\Phi) + 2K_f(1-\Phi)}\right), \tag{2.20}$$

$$w = \frac{(1-\Phi)^{2.5}}{4}\left(\frac{dp}{dz} - h^2 q_1\right)(r^2 - h^2) + \frac{q_1(1-\Phi)^{2.5}}{16}(r^4 - h^4), \tag{2.21}$$

where

$$q_1 = \frac{G_r\beta}{4}\left((1-\Phi) + \Phi\frac{\rho_s\gamma_s}{\rho_f\gamma_f}\right)\left(\frac{K_s(1-\Phi) + K_f(2+\Phi)}{K_s(1+2\Phi) + 2K_f(1-\Phi)}\right). \tag{2.22}$$

The flow rate F that is given as

$$F = \int_0^h rw dr. \tag{2.23}$$

Using Eqs. (2.21) and (2.22) into Eq. (2.23), we get the expression for pressure gradient in terms of the flow rate as follows

$$\frac{dp}{dz} = -\frac{16}{h^4(1-\Phi)^{2.5}}\left(F - \frac{h^6 q_1(1-\Phi)^{2.5}}{24}\right). \tag{2.24}$$

In above F is constant flow rate and the pressure drop across the length of the overlapping stenosis is given as

$$\Delta p = \int_0^L \left(-\frac{dp}{dz}\right) dz. \tag{2.25}$$

Using above Eq. (2.25), the impedance resistance experienced by the flowing blood in the arterial segment can be evaluated as

$$\lambda = \frac{\Delta p}{F} = \left\{ \int_0^{d^*} \Sigma(z) \mid_{h=(\zeta z+1)Q_1(t)} dz + \int_{d^*}^{d^*+\frac{3}{2}} \Omega(z) dz + \int_{d^*+\frac{3}{2}}^{L} \Sigma(z) \mid_{h=(\zeta z+1)Q_1(t)} dz \right\}, \tag{2.26}$$

where

$$\Omega(z) = \frac{16}{h^4(1-\Phi)^{2.5}F}\left(F - \frac{h^6 q_1(1-\Phi)^{2.5}}{24}\right), \tag{2.27}$$

$$\Sigma(z) = \Omega(z) \mid_{h=(mz+1)Q_1(t)} . \tag{2.28}$$

Expression for the wall shear stress is given as

$$S_{rz} = -\frac{\mu_{nf}}{\mu_f}\left(\frac{\partial w}{\partial r}\right)_{r=h}. \tag{2.29}$$

Using Eqs. (2.21) and (2.22) in Eq. (2.29), we get the expression for wall shear stress in the stenotic region

$$S_{rz} = -\frac{1}{(1-\Phi)^{2.5}}\left(\frac{1}{2}\left(-h^2 q_1 + \frac{dp}{dz}\right) h(1-\Phi)^{2.5} + \frac{h^3 q_1}{4}(1-\Phi)^{2.5}\right). \tag{2.30}$$

The expression of flow pattern is obtain by using Eqs. (2.21) to (2.22) and utilizing $\psi = 0$ at $r = h$ in the following

$$w = \frac{1}{r}\frac{\partial \psi}{\partial r}. \tag{2.31}$$

2.3 Thermophysical properties of blood and copper

The experimental values of the various physical parameters are presented in the following table

Physical properties	blood	Cu
$c_p(J/kgK)$	3594	385
$\rho(kg/m^3)$	1063	8933
$K(W/mK)$	0.492	400
$\gamma \times 10^{-5}(1/K)$	0.18	1.67

Table (2.1): Thermo physical properties.

2.4 Results and discussion

In order to understand the quantitative effects of the different flow parameter the graphs of wall shear stress, impedance resistance to flow and temperature distribution are plotted by considering three distinct types of tapering effects (diverging tapering $\varphi = 0.01$, converging tapering $\varphi = -0.01$ and non-tapered arteries $\varphi = 0.00$). In particular the graphs are plotted by keeping the parameter constant such as $\alpha_o = 0.1$, $\omega = 7.854$, $t = 0.5$, $L = 3$, $d^* = 0.75$ [29], further parameters are defined as $\Phi = 0.00 - 0.09$, $\beta = 0.1$, $\delta = 0.2$, $F = 0.01$, $G_r = 0.9$, $z = 1.5$. Figs. (2.2) to (2.5) are strategized to show that wall shear stress is essential in understanding the development of arterial disease between the stenotic segment $0.75 \leq z \leq 2.25$. The stresses on the wall of overlapping stenotic arteries gain its higher magnitude at the critical locations where the stenosis is considered maximum, while its magnitude decreases where the stenosis is considered minimum. One may observe from these graphs that the convergent tapering effects gives higher results for wall shear stress as comparing with other non-tapered and divergent tapering effects. The wall shear stress for different values of heat source parameter β is given in Fig. (2.2). It is analyzed that stresses on wall of arteries decreases with an increase in heat source parameter β. This increase is due to increase in internal heat source i.e. metabolic process, which accelerates flow of blood and shift stenotic pressure to the wall of arteries. The wall shear stress for different values of Grashof number G_r is plotted in Fig.(2.3). It is analyzed that wall shear stress decreases due to increase in the viscous forces as compare to the buoyancy

forces. Fig. (2.4) relates to the variation of wall shear stress S_{rz} for different values of stenosis height δ against the axial distance z. It is illustrated from this graph that stress on the wall of arteries is increases, as if we increase the stenosis height δ. This justifies the results of tapering phenomena that stresses on the wall are higher for contracted arteries as compare to the expanded arteries. Fig. (2.5) is plotted for different values of nanoparticles volume fraction Φ and analyzed that the stresses on the wall of arteries decreases with an increase in nanoparticles volume fraction. It is also observed from this figure that the stresses on the wall is higher for the pure blood case when compared to the other cases ($\Phi = 0.01$, $\Phi = 0.02$). Figs. (2.6) to (2.8) show the variation of the resistance impedance to flow along the maximum height of stenosis δ for different values of tapering angle φ. From these graphs it is depicted that resistance impedance to flow gives higher results for converging tapering as comparing to other tapering effects. It is also concluded that resistance to blood flow is directly proportional to stenosis height δ i.e., if we increase stenosis height δ, the resistance to blood flow in the presence of time variant overlapping stenosis will get the higher amplitude. The effects of Grashof number G_r is given in Figs. (2.6). It is analyzed that resistance impedance to flow decreases with an increase in the viscous forces. The wall shear stress for heat source parameter β is plotted in Fig. (2.7) and it observed from this figure that with an increase in internal heat source parameter flow is accelerated and resistance to blood flow decreases. Fig. (2.8) is plotted to show the resistance impedance to flow for nanoparticles volume fraction Φ. It is observed from this figure that nanoparticles with high thermal conductivity reduces resistance to blood flow and concluded that they are useful as drug carrier to heal the consequences of stenosed arteries. The variations of temperature profile for different values of stenosis height δ, nanoparticle volume fraction Φ and heat source parameter β are shown in Figs. (2.9) to (2.11). It is analyzed from these graphs that temperature profile gives higher results for divergent tapering as comparing to other tapering and maximum temperature occurs at $r = 0$. The temperature profile for different values stenosis height δ is given in Fig. (2.9). It is observed from these graphs that temperature profile decreases with an increase in the values of stenosis height δ. The variation of temperature profile for heat source parameter β is given in Fig. (2.10) and observed that the temperature profile increases with an increase in the values of heat source parameter β because of increase in the thermal state of the fluid i.e. through metabolic process. From Fig. (2.11),

it is analyzed that temperature profile decreases with an increase in the nanoparticles volume fraction, which means nanoparticles with high thermal conductivity are useful to dissipate heat. It is also observed that the temperature distribution remain higher for pure blood case. Figs. (2.12) and (2.13) are plotted against time t for almost four and three cardiac phases. In these graphs the magnitude of first cycle starts decreasing to obtain its minimum then starts increasing to obtain its maximum then replicate its form again to obtain the starting point of the second cycle and so on. It is observed that these graphs decay as the time t increases. This graphical illustration shows that the resistance impedance to blood flow and wall shear stress contributes better results for convergent tapering. Trapping characterized an interesting phenomenon for the blood flow in an overlapping stenosed artery that is discussed through Figs. (2.14) to (2.16) for non-tapered arteries, other associated arteries are discussed in Fig. (2.14). Fig. (2.14) is plotted for convergent and divergent tapering arteries. It is depicted that trapping bolus shift towards lower side for expanded arteries ($\phi > 0$), while shift towards upper side for contracted arteries ($\phi < 0$). The effects of stenosis height δ and time t are discussed in Figs. (2.15) and (2.16). It is observed from these graphs of streamlines that the number of trapping bolus increases with an increase in the values time t and stenosis height δ. Tables (2.2, 2.3) are plotted for velocity and temperature profile. It is observed from table (2.2) the temperature profile decreases throughout the considered stenosed artery with an increase in the nanoparticle volume fraction Φ. The velocity table (2.3) is plotted for different values of the nanoparticle volume fraction Φ. It is observed from this table that velocity starts increasing at the center of the arteries between the regions $-0.4 \leq r \leq 0.4$, while starts decreasing near the walls of considered stenosed elastic arteries. This table also indicate that velocity gives higher altitude for pure blood case ($\Phi = 0.00$) near the wall of the arteries and gives higher altitude for nano blood cases ($\Phi = 0.02, 0.04$) at the center of the stenosed arteries ($-0.4 \leq r \leq 0.4$).

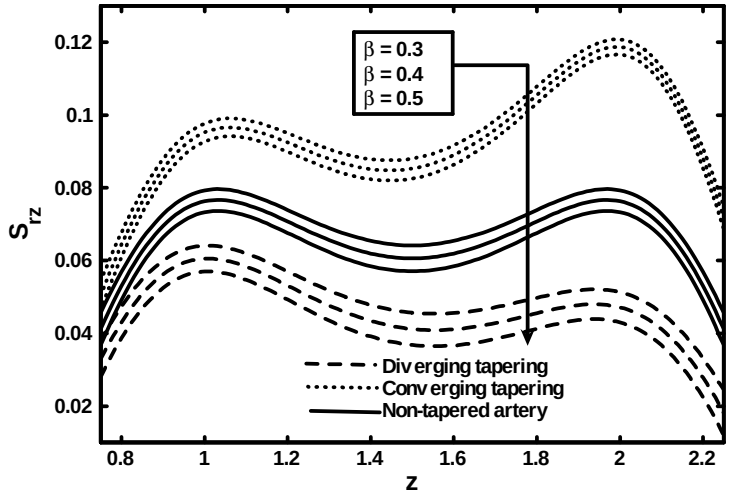

Fig. (2.2): Variation of wall shear stress for different values of heat source parameter β.

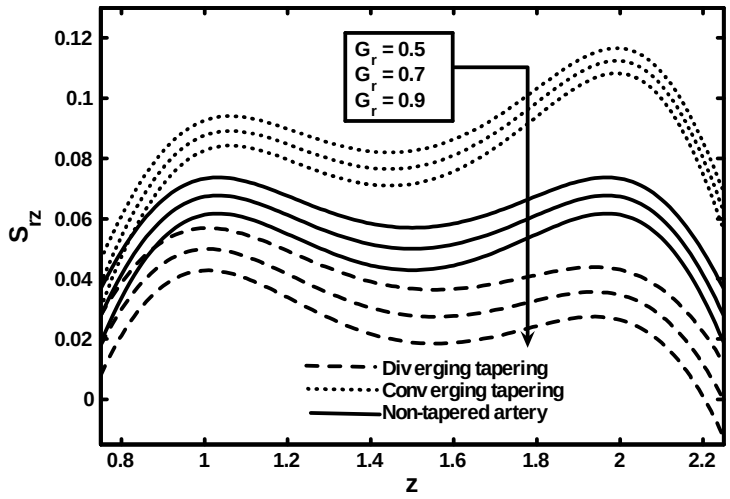

Fig. (2.3): Variation of wall shear stress for different values of Grashof number G_r.

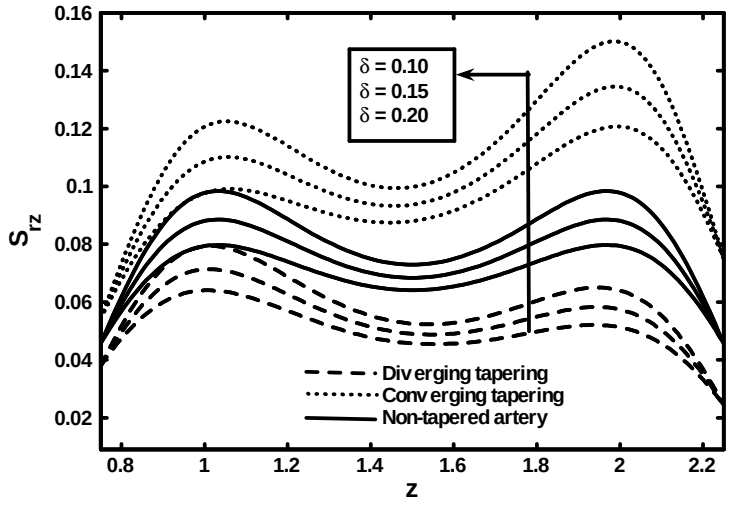

Fig. (2.4): Variation of wall shear stress for different values of stenosis height δ.

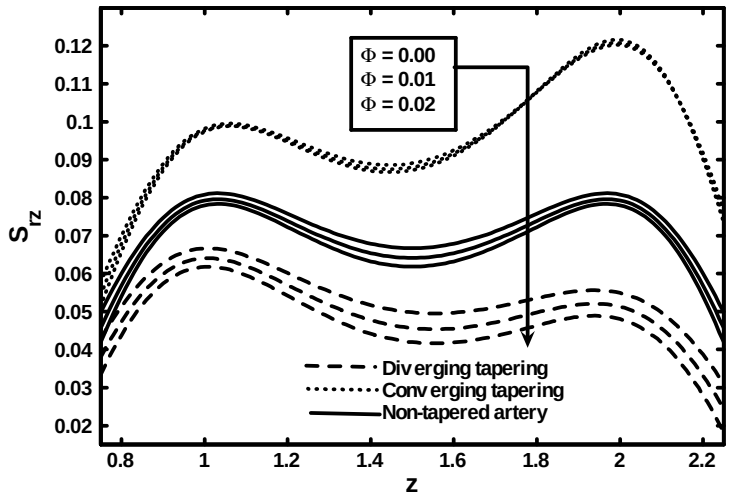

Fig. (2.5): Variation of wall shear stress for different values of nanoparticles volume fraction Φ.

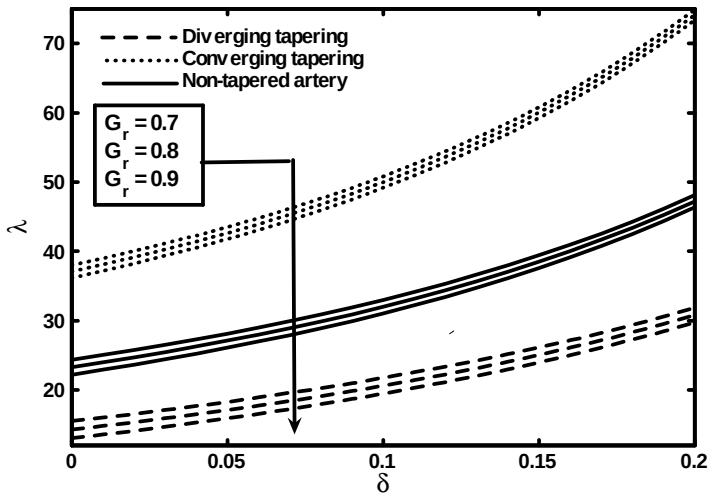

Fig. (2.6): Variation of resistance impedance for different values of Grashof number G_r.

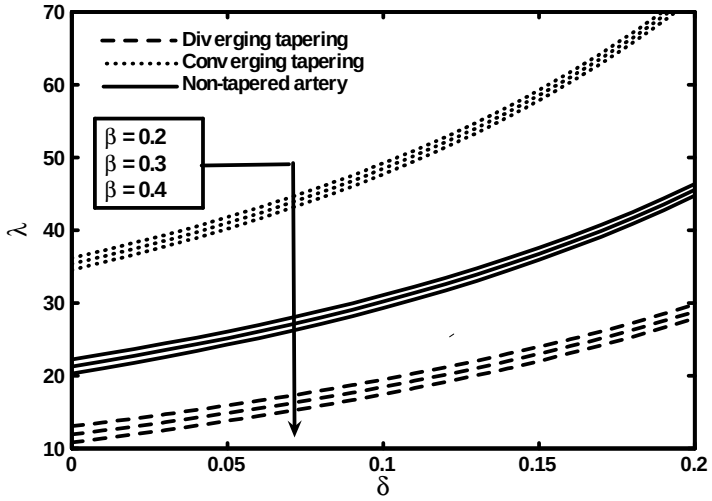

Fig. (2.7): Variation of resistance impedance for different values of heat source parameter β.

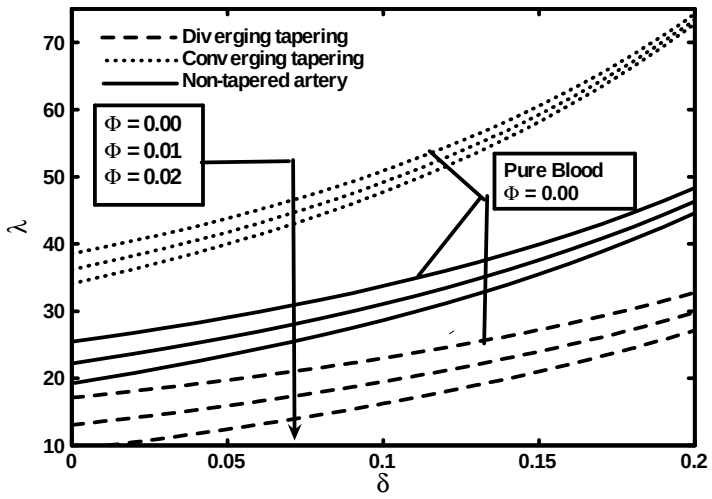

Fig. (2.8): Variation of resistance impedance for different values of nanoparticles volume fraction Φ.

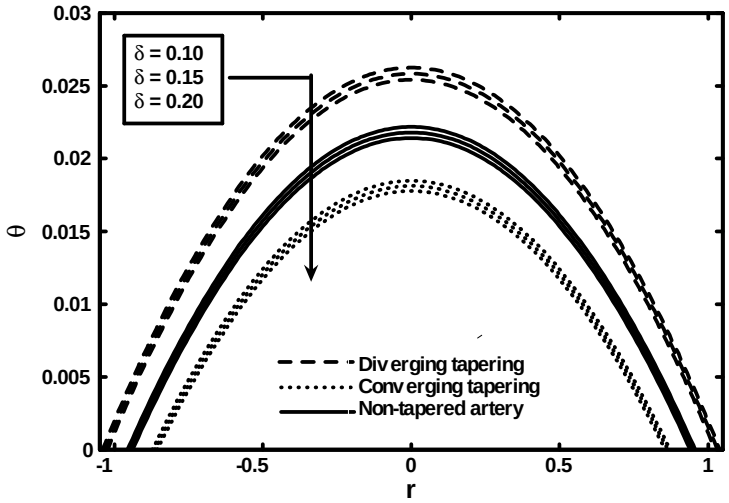

Fig. (2.9): Variation of temperature profile different values of stenosis height δ.

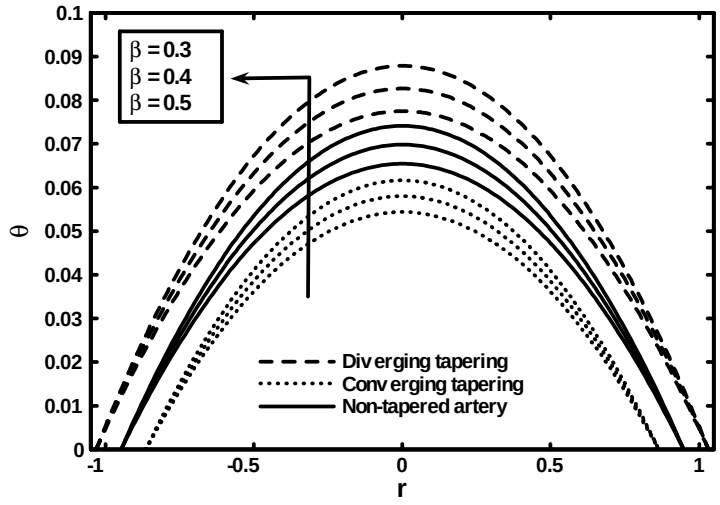

Fig. (2.10): Variation of temperature profile for different values of heat source parameter β.

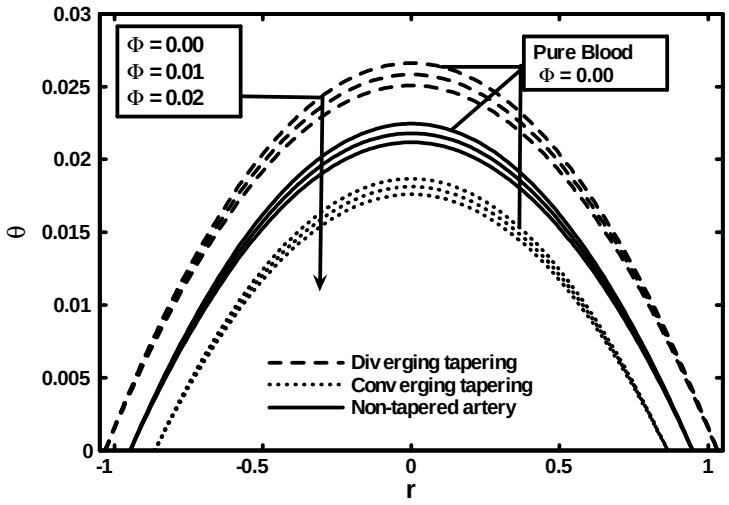

Fig. (2.11): Variation of temperature profile for different values of nanoparticles volume fraction Φ.

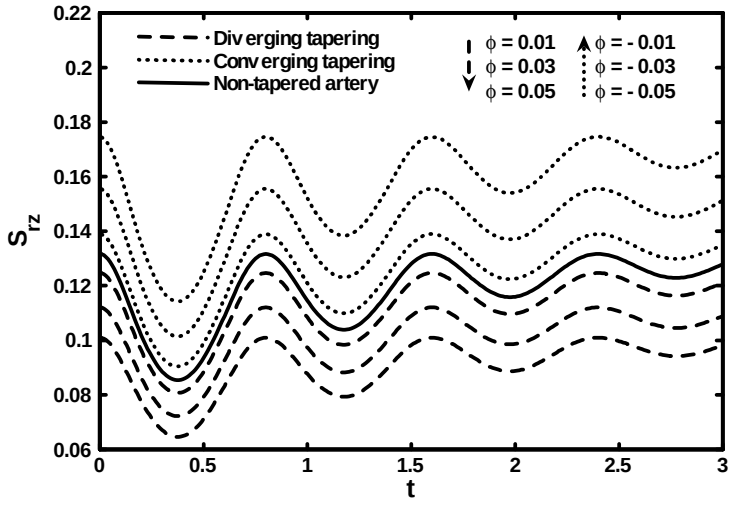

Fig. (2.12): Variation of wall shear stress for different values tapering angles against t.

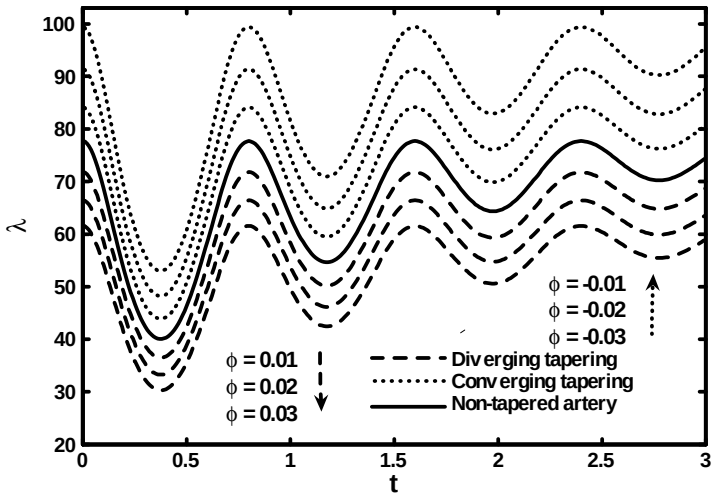

Fig. (2.13): Variation of resistance impedance for different for different values of tapering angles against t.

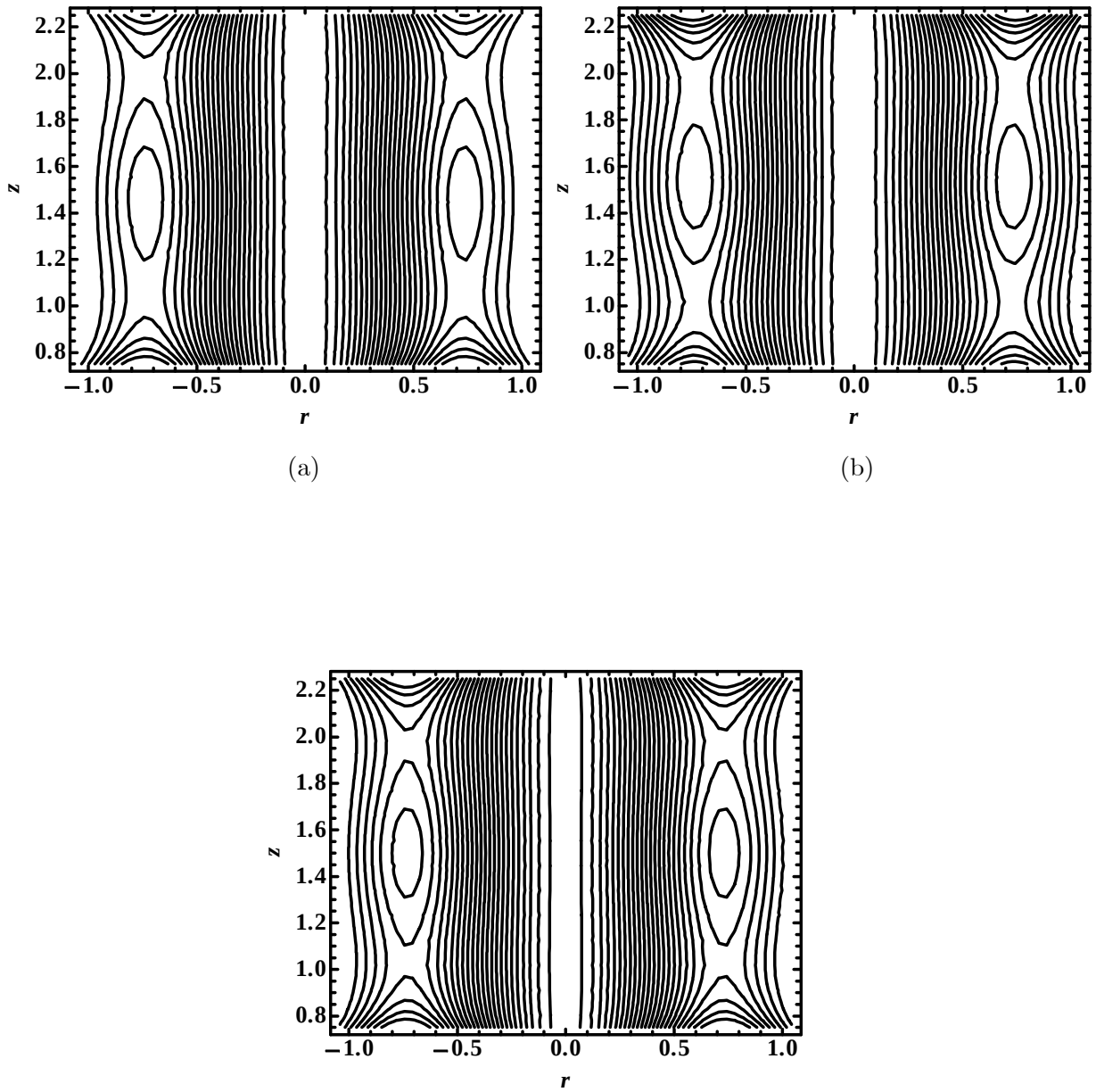

(a) (b)

(c)

Fig. (2.14): Blood flow pattern for different values of (a) $\varphi < 0$, (b) $\varphi > 0$, (c) $\varphi = 0$.

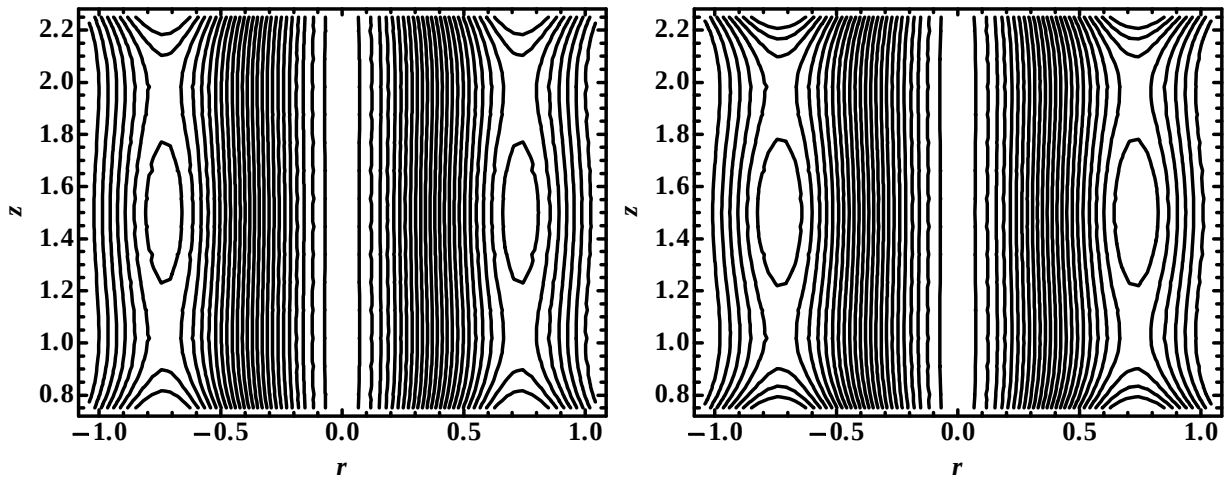

(a)

(b)

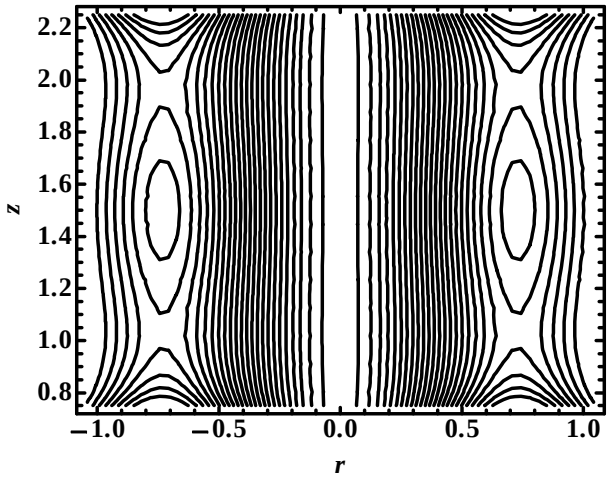

(c)

Fig. (2.15): Blood flow pattern for different values of (a) $\delta = 0.03$, (b) $\delta = 0.04$, (c) $\delta = 0.05$.

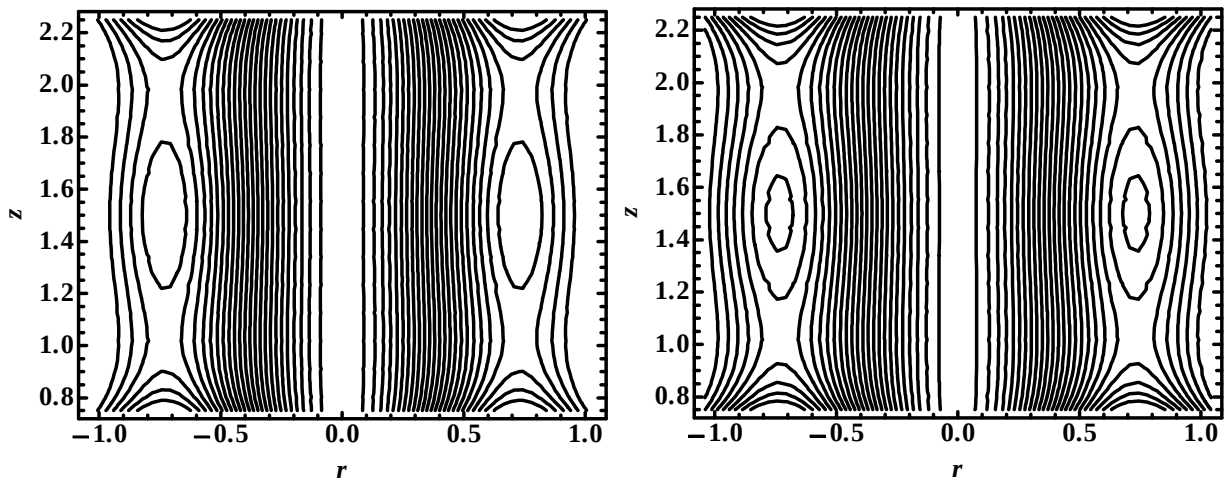

(a) (b)

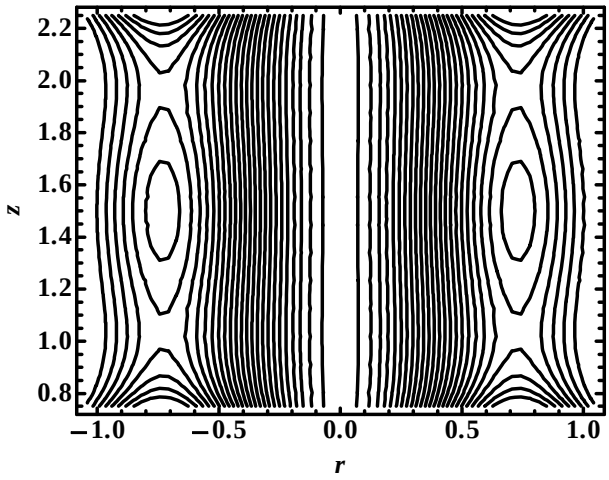

(c)

Fig. (2.16): Blood flow pattern for different values of (a) $t = 0.3$, (b) $t = 0.4$, (c) $t = 0.5$.

θ	Non-tapered artery			Diverging tapering			Converging tapering		
r	Φ=0.00	Φ=0.02	Φ=0.04	Φ=0.00	Φ=0.02	Φ=0.04	Φ=0.00	Φ=0.02	Φ=0.04
$-h$	0.0000	0.0000	0.0000	0.0000	0.0000	0.0000	0.0000	0.0000	0.0000
-0.8	0.0065	0.0061	0.0057	0.0106	0.0100	0.0094	0.0027	0.0025	0.0023
-0.6	0.0135	0.0127	0.0119	0.0176	0.0166	0.0157	0.0097	0.0091	0.0086
-0.4	0.0185	0.0174	0.0164	0.0226	0.0213	0.0201	0.0147	0.0138	0.0130
-0.2	0.0215	0.0202	0.0191	0.0256	0.0241	0.0228	0.0177	0.0167	0.0157
0.0	0.0225	0.0212	0.0199	0.0266	0.0251	0.0237	0.0187	0.0176	0.0166
0.2	0.0215	0.0202	0.0191	0.0256	0.0241	0.0228	0.0177	0.0167	0.0157
0.4	0.0185	0.0174	0.0164	0.0226	0.0213	0.0201	0.0147	0.0138	0.0130
0.6	0.0135	0.0127	0.0119	0.0176	0.0166	0.0157	0.0097	0.0091	0.0086
0.8	0.0065	0.0061	0.0057	0.0106	0.0100	0.0094	0.0027	0.0025	0.0023
h	0.0000	0.0000	0.0000	0.0000	0.0000	0.0000	0.0000	0.0000	0.0000

Table (2.2): Variations of temperature profile for the nanoparticles volume fraction Φ.

w	Non-tapered artery			Diverging tapering			Converging tapering		
r	Φ=0.00	Φ=0.02	Φ=0.04	Φ=0.00	Φ=0.02	Φ=0.04	Φ=0.00	Φ=0.02	Φ=0.04
$-h$	0.0000	0.0000	0.0000	0.0000	0.0000	0.0000	0.0000	0.0000	0.0000
-0.8	0.0127	0.0125	0.0124	0.0148	0.0146	0.0144	0.0076	0.0075	0.0074
-0.6	0.0266	0.0264	0.0265	0.0248	0.0248	0.0248	0.0277	0.0276	0.0275
-0.4	0.0367	0.0369	0.0371	0.0322	0.0325	0.0327	0.0421	0.0422	0.0423
-0.2	0.0428	0.0432	0.0435	0.0366	0.0372	0.0376	0.0509	0.0511	0.0513
0.0	0.0449	0.0453	0.0457	0.0381	0.0388	0.0393	0.0538	0.0541	0.0544
0.2	0.0428	0.0432	0.0435	0.0366	0.0372	0.0376	0.0509	0.0511	0.0513
0.4	0.0367	0.0369	0.0371	0.0322	0.0325	0.0327	0.0421	0.0422	0.0423
0.6	0.0266	0.0264	0.0265	0.0248	0.0248	0.0248	0.0277	0.0276	0.0275
0.8	0.0127	0.0125	0.0124	0.0148	0.0146	0.0144	0.0076	0.0075	0.0074
h	0.0000	0.0000	0.0000	0.0000	0.0000	0.0000	0.0000	0.0000	0.0000

Table. (2.3): Variations of velocity profile for the nanoparticles volume fraction Φ.

Chapter 3

Study of radially varying magnetic field on blood flow through catheterized tapered elastic artery with overlapping stenosis

In this chapter a precise model has been developed for studying the influence of metallic nanoparticles on blood flow through catheterized tapered elastic arteries with radially varying magnetic field. The model is solved under the mild stenosis approximation by considering blood as viscous fluid. The influence of different flow parameters associated with this problem such as Hartmann number, nanoparticle volume fraction, Grashof number and heat source parameter is analyzed by plotting the graphs of velocity profile, temperature distribution, wall shear stress, resistance impedance to flow and stream lines. The influence of the radially varying magnetic field on resistance impedance to flow is analyzed and it is observed that the significantly strong magnetic force tends to increase in resistance.

3.1 Mathematical formulation

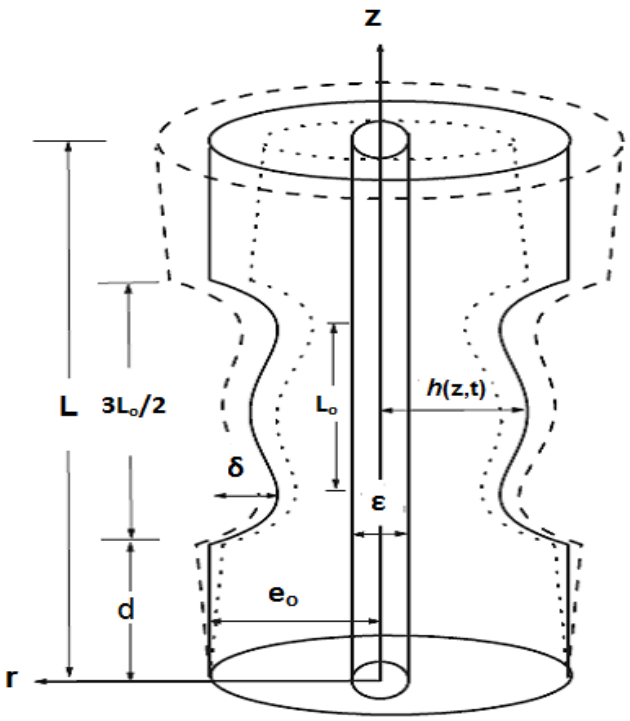

Fig. (3.1): Geometry of overlapping stenosed artery.

Heat transfer phenomenon is taken into account by giving temperature T_1 to the wall of the artery, T_o to the wall of the catheter and radially varying magnetic field is applied in the normal direction of the blood flow. The governing equations for conservation of mass, momentum and temperature for viscous nanofluid can be written as

$$\frac{\partial \overline{u}}{\partial \overline{r}} + \frac{\overline{u}}{\overline{r}} + \frac{\partial \overline{w}}{\partial \overline{z}} = 0, \tag{3.1}$$

$$\rho_{nf}\left(\frac{\partial \overline{u}}{\partial \overline{t}} + \overline{u}\frac{\partial \overline{u}}{\partial \overline{r}} + \overline{w}\frac{\partial \overline{u}}{\partial \overline{z}}\right) = -\frac{\partial \overline{p}}{\partial \overline{r}} + \mu_{nf}\left(\frac{\partial^2 \overline{u}}{\partial \overline{r}^2} + \frac{1}{\overline{r}}\frac{\partial \overline{u}}{\partial \overline{r}} + \frac{\partial^2 \overline{u}}{\partial \overline{z}^2} - \frac{\overline{u}}{\overline{r}^2}\right), \tag{3.2}$$

$$\rho_{nf}\left(\frac{\partial \overline{w}}{\partial \overline{t}}+\overline{u}\frac{\partial \overline{w}}{\partial \overline{r}}+\overline{w}\frac{\partial \overline{w}}{\partial \overline{z}}\right) = -\frac{\partial \overline{p}}{\partial \overline{z}}+\mu_{nf}\left(\frac{\partial^2 \overline{w}}{\partial \overline{r}^2}+\frac{1}{\overline{r}}\frac{\partial \overline{w}}{\partial \overline{r}}+\frac{\partial^2 \overline{w}}{\partial \overline{z}^2}\right)+ g(\rho\gamma)_{nf}(\overline{T}-T_1)-\sigma_{nf}B_o^2(r)\overline{w}, \tag{3.3}$$

$$\left(\frac{\partial \overline{T}}{\partial \overline{t}}+\overline{u}\frac{\partial \overline{T}}{\partial \overline{r}}+\overline{w}\frac{\partial \overline{T}}{\partial \overline{z}}\right)=\frac{K_{nf}}{(\rho c_p)_{nf}}\left(\frac{\partial^2 \overline{T}}{\partial \overline{r}^2}+\frac{1}{\overline{r}}\frac{\partial \overline{T}}{\partial \overline{r}}+\frac{\partial^2 \overline{T}}{\partial \overline{z}^2}\right)+\frac{Q_0}{(\rho c_p)_{nf}}, \tag{3.4}$$

in above equations for the given nanofluid model σ_{nf} denotes the electrical conductivity and the thermo physical properties with respect to blood and copper nanoparticles are given as

$$\begin{aligned}
&\mu_{nf}=\frac{\mu_f}{(1-\Phi)^{2.5}},\quad \alpha_{nf}=\frac{K_{nf}}{(\rho c_p)_{nf}},\quad \rho_{nf}=(1-\Phi)\rho_f+\Phi\rho_s,\\
&(\rho c_p)_{nf}=(1-\Phi)(\rho c_p)_f+\Phi(\rho c_p)_s,\quad (\rho\gamma)_{nf}=(1-\Phi)(\rho\gamma)_f+\Phi(\rho\gamma)_s,\\
&\frac{K_{nf}}{K_f}=\frac{(K_s+2K_f)-2\Phi(K_f-K_s)}{(K_s+2K_f)+\Phi(K_f-K_s)},\ \frac{\sigma_{nf}}{\sigma_f}=1+\frac{3\left(\frac{\sigma_s}{\sigma_f}-1\right)\Phi}{\left(\frac{\sigma_s}{\sigma_f}+2\right)-\left(\frac{\sigma_s}{\sigma_f}-1\right)\Phi}.
\end{aligned} \tag{3.5}$$

In above equation, σ_f denotes the electrical conductivity for fluid, while σ_s denotes the electrical conductivity for solid nanoparticle. Non-dimensional variables are defined as,

$$\begin{aligned}
r &= \frac{\overline{r}}{e_0},\ w=\frac{\overline{w}}{u_o},\ u=\frac{L_0\overline{u}}{u_o\delta},\ p=\frac{e_0^2\overline{p}}{u_oL_0\mu_f},\ t=\frac{\overline{t}u_o}{L_0},\\
\beta &= \frac{Q_0e_0^2}{(T_0-T_1)K_f},\ R_{en}=\frac{e_0u_o\rho_f}{\mu_f},\ G_r=\frac{g\gamma_f\rho_fe_0^2(T_0-T_1)}{u_0\mu_f},\\
\theta &= \frac{\overline{T}-T_1}{T_0-T_1},\ z=\frac{\overline{z}}{L_0},\ H_a(r)=B_o(r)e_o\sqrt{\frac{\sigma_f}{\mu_f}},\ L=\frac{\overline{L}}{L_0}.
\end{aligned} \tag{3.6}$$

Here H_a represents the Hartmann number. Utilizing above Eq. (3.6), mild stenosis case $\delta^*=\frac{\delta}{e_0}\ll 1$, extra condition $\epsilon=\frac{e_0}{b}\approx O(1)$ and taking $H_a(r)=\frac{H_a}{r}$, the governing Eqs. (3.2) to (3.4) can be written as

$$\frac{\partial p}{\partial r}=0, \tag{3.7}$$

$$\frac{\partial p}{\partial z}\frac{\mu_f}{\mu_{nf}} = \frac{\partial^2 w}{\partial r^2} + \frac{1}{r}\frac{\partial w}{\partial r} + K_2\theta - \frac{M^2}{r^2}w, \tag{3.8}$$

$$\frac{\partial^2 \theta}{\partial r^2} + \frac{1}{r}\frac{\partial \theta}{\partial r} + \beta K_1 = 0, \tag{3.9}$$

where

$$\begin{aligned} K_1 &= \left(\frac{k_s(1-\Phi)+k_f(2+\Phi)}{k_s(1+2\Phi)+2k_f(1-\Phi)}\right), \\ K_2 &= \left((1-\Phi)+\Phi\frac{\rho_s\gamma_s}{\rho_f\gamma_f}\right)(1-\Phi)^{2.5}G_r,\ M^2 = (H_a)^2K_3, \\ K_3 &= \left(1+\frac{3\left(\frac{\sigma_s}{\sigma_f}-1\right)\Phi}{\left(\frac{\sigma_s}{\sigma_f}+2\right)-\left(\frac{\sigma_s}{\sigma_f}-1\right)\Phi}\right)(1-\Phi)^{2.5}. \end{aligned} \tag{3.10}$$

The geometry of stenosis in dimensionless form is defined as

$$\begin{aligned} h(z,\ t) &= [(\zeta z+1) - \delta\cos\phi(z-d^*)\{11 - \frac{94}{3}(z-d^*) + 32(z-d^*)^2 - \frac{32}{3} \\ &\quad (z-d^*)^3\}]Q_1(t), \qquad d^* \le z \le d^* + \frac{3}{2}, \\ &= (\zeta z+1)Q_1(t), \qquad \text{otherwise}, \end{aligned} \tag{3.11}$$

with

$$\delta = \frac{\delta^*}{e_0},\ d^* = \frac{d}{L_0}. \tag{3.12}$$

Corresponding boundary conditions are defined as

$$w = 0 \ \ at \ \ r = h(z,t), \ \ w = 0 \ \ at \ \ r = \varepsilon, \tag{3.13}$$

$$\theta = 0 \ \ at \ \ r = h(z,t), \ \ \theta = 1 \ \ at \ \ r = \varepsilon. \tag{3.14}$$

3.2 Solution of the problem

The exact solutions of temperature distribution and velocity profile using Eqs. (3.13) and (3.14) are written as

$$\begin{aligned}\theta &= \frac{1}{4(\ln h-\ln \varepsilon)}(4(\ln h-\ln r)+\beta K_1(h^2(\ln r-\ln \varepsilon)+r^2(-\ln h+\\ &\ln \varepsilon)+(\ln h-\ln r)\varepsilon^2)),\end{aligned} \tag{3.15}$$

$$\begin{aligned}w &= \frac{dp}{dz}\frac{(1-\Phi)^{2.5}}{(h^{2M}-\varepsilon^{2M})(-4+M^2)}r^{-M}(\varepsilon^M r^M(\varepsilon^M r^2-\varepsilon^2 r^M)+h^{2+M}(-\varepsilon^{2M}+\\ &r^{2M})+h^{2M}(\varepsilon^{2+M}-r^{2+M}))+\frac{1}{(h^{2M}-\varepsilon^{2M})(-4+M^2)^2(-16+M^2)}(K_2 r^{-M}\\ &(-4b_2(-16+M^2)(\varepsilon^M r^M(\varepsilon^M r^2-\varepsilon^2 r^M)+h^{2+M}(-\varepsilon^{2M}+r^{2M})+h^{2M}(\varepsilon^{2+M}\\ &-r^{2+M}))+(-4+M^2)(-b_3(-16+M^2)(\varepsilon^M r^M(\varepsilon^M r^2-\varepsilon^2 r^M)+h^{2+M}(-\varepsilon^{2M}\\ &+r^{2M})+h^{2M}(\varepsilon^{2+M}-r^{2+M}))-b_1(-4+M^2)(\varepsilon^M r^M(r^4\varepsilon^M-r^M\varepsilon^4)+h^{4+M}(\\ &-\varepsilon^{2M}+r^{2M})+h^{2M}(\varepsilon^{4+M}-r^{4+M})))+(b_2(64-20M^2+M^4)(h^{2+M}(\varepsilon^{2M}\\ &-r^{2M})\ln h-\varepsilon^{2+M}(h^{2M}-r^{2M})\ln\varepsilon+(h^{2M}-\varepsilon^{2M})r^{2+M}\ln r))).\end{aligned} \tag{3.16}$$

Flow rate is given as

$$F=\int_{\varepsilon}^{h} rw dr. \tag{3.17}$$

Using Eq. (3.16) into Eq. (3.17), we get the expression for pressure gradient as follows

$$\frac{dp}{dz}=\frac{4(F-b_5(z))(h^{2M}-\varepsilon^{2M})(-4+M^2)^2}{(1-\Phi)^{2.5}b_4(z)}. \tag{3.18}$$

Since F is constant for all sections between the two coaxial tubes, the pressure drop across the length of the overlapping stenosis is given as

$$\Delta p = \int_0^L \left(-\frac{dp}{dz}\right) dz. \tag{3.19}$$

Using above Eq. (3.19), the impedance resistance can be evaluated as

$$\lambda = \frac{\Delta p}{F} = \left\{ \int_0^{d^*} \Sigma_o(z) \mid_{h=(\zeta z+1)Q_1(t)} dz + \int_{d^*}^{d^*+\frac{3}{2}} \Omega_o(z) dz + \int_{d^*+\frac{3}{2}}^{L} \Sigma(z)_o \mid_{h=(\zeta z+1)Q_1(t)} dz \right\}, \tag{3.20}$$

where

$$\Omega_o(z) = -\frac{4(F - b_5(z))(h^{2M} - \varepsilon^{2M})(-4 + M^2)^2}{(1-\Phi)^{2.5} F b_4(z)}. \tag{3.21}$$

Expression for the wall shear stress is given as

$$\begin{aligned} S_{rz} \;=\; & \frac{dp}{dz}\frac{-1}{h(h^{2M} - \varepsilon^{2M})(-4 + M^2)}(h^{2+2M}(-2 + M) - 2h^M \varepsilon^{2+M} M + h^2 \varepsilon^{2M} \\ & (2 + M))) + \frac{(1-\Phi)^{2.5}}{h(h^{2M} - \varepsilon^{2M})(-4 + M^2)^2(-16 + M^2)}(K_2(-b_3(64 - 20 \\ & M^2 + M^4)(h^{2+2M}(-2 + M) - 2h^M \varepsilon^{2+M} M + h^2 \varepsilon^{2M}(2 + M)) + b_2(-16 + \\ & M^2)(h^{2+2M}(-2 + M)^2 + 8h^M \varepsilon^{2+M} M - h^2 \varepsilon^{2M}(2 + M)^2) - b_1(-4 + M^2)^2 \\ & (h^{4+2M}(-4 + M) - 2h^M \varepsilon^{4+M} M + h^4 \varepsilon^{2M}(4 + M)) - b_2(64 - 20M^2 + M^4) \\ & (h^2(h^{2M}(-2 + M) + \varepsilon^{2M}(2 + M)) \ln h - 2h^M \varepsilon^{2+M} M \ln \varepsilon))). \end{aligned} \tag{3.22}$$

3.3 Appendix

$$b_1 = -\frac{\beta K_1}{4},\ b_2 = \frac{-4+\beta K_1(h^2-\varepsilon^2)}{4(\ln h - \ln \varepsilon)},\ b_3 = \frac{(4\ln h + \beta K_1(-h^2 \ln \varepsilon + \varepsilon^2 \ln h)}{(4(\ln h - \ln \varepsilon))},$$
$$b_4 = (-16h^{2+M}\varepsilon^{2+M}M + \varepsilon^{2M}(-\varepsilon^4(-2+M)^2 + h^4(2+M)^2) + h^{2M}(-h^4(-2+M)^2$$
$$+\varepsilon^4(2+M)^2)),\ b_5 = \frac{1}{48(h^{2M}-\varepsilon^{2M})(-16+M)^2(-4+M^2)^3)}(K_2(12b_3(-16+M^2)$$
$$(-4+M^2)(16h^{2+M}\varepsilon^{2+M}M + \varepsilon^{2M}(\varepsilon^4(-2+M)^2 - h^4(2+M)^2) + h^{2M}(h^4(-2+M)^2$$
$$-\varepsilon^4(2+M)^2)) + 8b_1(-4+M^2)^2(12h^{4+M}\varepsilon^{2+M}(h^2+\varepsilon^2)M + \varepsilon^{2M}(\varepsilon^6(-4+M)(-2+$$
$$M) - h^6(2+M)(4+M)) + h^{2M}(h^6(-4+M)(-2+M) - \varepsilon^6(4+M)(2+M)) + 3b_2$$
$$(-16+M^2)(256h^{2+M}\varepsilon^{2+M}M + h^{2M}(\varepsilon^4(-6+M)(2+M)^3 - h^4(-2+M)^3(6+M))$$
$$+\varepsilon^{2M}(h^4(-6+M)(2+M)^3 - \varepsilon^4(-2+M)^3(6+M))) + 12b_2(64-20M^2+M^4)$$
$$(8h^{2+M}\varepsilon^{2+M}M(\ln h + \ln \varepsilon) + \varepsilon^{2M}(-h^4(2+M)^2 \ln h + \varepsilon^4(-2+M)^2 \ln \varepsilon) +$$
$$h^{2M}(h^4(-2+M)^2 \ln h - \varepsilon^4(2+M)^2 \ln \varepsilon)))).$$

3.4 Thermophysical properties of blood and copper

The experimental values of various parameters are tabulated below,

Physical properties	blood	copper
$c_p(J/kgK)$	3594	385
$\rho(kg/m^3)$	1063	8933
$k(W/mK)$	0.492	400
$\gamma \times 10^{-5}\ (1/K)$	0.18	1.67
$\sigma\ (s/m)$	6.67×10^{-1}	5.96×10^{7}

Table (3.1): Thermo physical properties.

3.5 Results and discussion

The main purpose of this chapter is to discuss the combined effect of the stenosis with radially varying magnetic field on the wall shear stress and resistance impedance to flow. The effect of the important parameters such as the Hartmann number H_a, Grashof number G_r, nanoparticles volume fraction Φ and heat source parameter β for three different types of tapering effects are discussed in this section through graphical illustrations. These graphs are plotted by keeping the parameter constant such as $\Phi = 0.00 - 0.09$, $\beta = 0.1$, $L = 3$, $\delta = 0.2$, $F = 0.01$, $d^* = 0.75$, $G_r = 0.9$, $\alpha_o = 0.1$, $\omega = 7.854$, $t = 0.5$, $H_a = 0.9$, $z = 1.5$, $\varepsilon = 0.1$. The magnitude of wall shear stress is plotted between the stenotic segment $0.75 \leq z \leq 2.25$, which is essential to understand the arterial disease because of its strong correlation with the constriction of the arteries. The graphs of wall shear stress along axial displacement z are plotted in Figs. $(3.2) - (3.6)$ with different tapering effects and observed from these figures that the wall shear stress having overlapping stenosis gives higher altitude for converging tapering as compare to the diverging tapering and non-tapered arteries. Fig. (3.2) describe the influence of heat source parameter β on the graph of wall shear stress and it is concluded here that the stresses on wall of arteries decreases with an increase in internal heat source through metabolic process. The wall shear stress for different values of Grashof number G_r is given in Fig. (3.3). From this graph of wall shear stress it is analyzed that stresses on the wall of arteries decreases with an increase in the values of the Grashof number. From Fig. (3.4) it is analyzed that stresses on wall of the artery increases with an increase in the values of stenosis height δ. The wall shear stress for different values of nanoparticles volume fraction Φ is given in the Fig. (3.5). It is depicted that increase in the nanoparticles volume fraction minimizes the stresses on the considered arterial wall segment. In Fig. (3.6), it is observed that the stresses on the wall of arteries start increasing with an increase in the Hartmann number H_a. It is observed that this result is attained due to decrease in axial velocity near the throat of stenosis. The variation of resistance impedance to flow λ with stenosis height δ is given in Figs. $(3.7) - (3.10)$ for different values of tapering angle φ. It is illustrated from these graphs that converging tapering arteries gives higher results for resistance impedance to flow as comparing to other tapering arteries. It is important to note that resistance to blood flow is directly proportional to stenosis height δ. From Fig. (3.7), we have observed that with an increase in the Grashof number

G_r the resistance to blood flow decreases with an increase in viscous forces. The effects of heat source parameter β are given in Fig. (3.8). It is illustrated from this graph that with an increase in heat source parameter β the viscosity of the fluid decreases, that reduces the resistance impedance to blood flow. Fig. (3.9) is plotted to show that the influence of volume fraction Φ on resistance impedance to blood flow and concluded that the metallic nanoparticles help to minimize the effects of resistance impedance to blood flow. The variations of Hartmann number H_a are given in Fig. (3.10). It is observed that with an increase in the intensity of magnetic field the resistance impedance to blood flow increases. It is due to the fact that when magnetic field is applied normal to the fluid, random motion of the particles within the considered base fluid gets slower down and hence flow of blood is retarded. The variations of temperature profile for different values of nanoparticle volume fraction Φ and heat source parameter β is shown in Figs. (3.11) and (3.12). The variation of temperature profile for heat source parameter β is given in Fig. (3.11) and observed that the temperature profile increases with an increase in the values of heat source parameter β. This graph indicates that with an increase in the internal heat source of the fluid, temperature profile gets higher altitude ($\beta > 0$). From Fig. (3.12), it is analyzed from this profile that temperature decreases with an increase in the nanoparticles volume fraction but shows temperature distribution remains higher for pure blood case $\Phi = 0.00$. Figs. (3.13) and (3.14) are strategized versus time t for almost four and three cardiac phases. In these graphs we observed that the scale of first cycle starts decreasing to obtain its minimum then starts increasing to obtain its maximum then repeat its form again to obtain the starting point of the second cycle and so on. It is illustrated from these figures that fluctuation starts decaying as the time t increases. Trapping illustrates as an interesting phenomenon for the blood flow pattern in an overlapping stenosed artery with radially varying magnetic field that is discussed through Figs. $(3.15) - (3.19)$ for non-tapered arteries and trapping for other associated arteries are discussed in Fig. (3.15). In Fig. (3.15), it is observed that trapping bolus shift towards lower side for divergent tapering when compared to convergent and non-tapered arteries. The influence of stenosis height δ is given in Fig. (3.16). It is observed from these trapping phenomena that stream lines become closer with an increase in the stenosis height δ. From Figs. (3.17) and (3.18), it is observed that the number of trapping bolus increases with an increase in the values of Grashof number G_r

and heat source parameter β. The trapping phenomena for Hartmann number H_a are discussed in Fig. (3.19). It is depicted in these figures that the number of trapping bolus increases with an increase in the intensity of magnetic field. The tables (3.2) and (3.3) are plotted to show the variations of velocity profile for different values of nanoparticles volume fraction Φ and Hartmann number H_a against radial direction r. Table (3.2) illustrates that the variations of velocity profile for different values of nanoparticles volume fraction Φ increases near the wall of the catheter between the region $\varepsilon \leq r \leq 0.5$ $(\phi < 0, \phi = 0)$, $\varepsilon \leq r \leq 0.6$ $(\phi > 0)$, while starts decreasing near the wall of the arteries between the region $0.5 < r \leq h$ $(\phi < 0, \phi = 0)$, $0.6 < r \leq h$ $(\phi > 0)$. Table (3.3) is prepared for velocity profile for different values of Hartmann number H_a and it is observed from this table that the velocity profile increases near the wall of the artery between the region $0.5 < r \leq h$, while starts decreasing near the wall of the catheter between the region $\varepsilon \leq r \leq 0.5$.

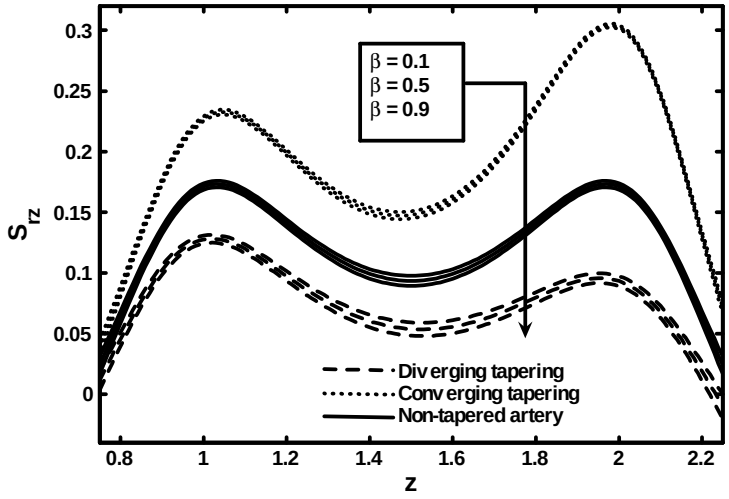

Fig. (3.2): Variation of wall shear stress for different values of heat source parameter β.

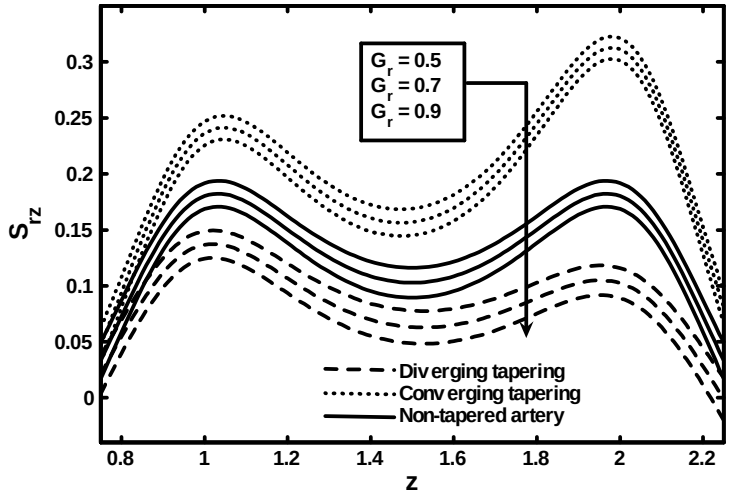

Fig. (3.3): Variation of wall shear stress for different values of Grashof number G_r.

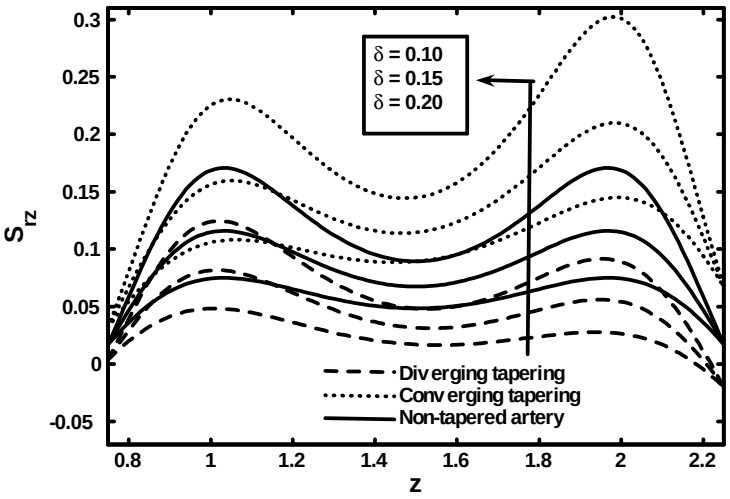

Fig. (3.4): Variation of wall shear stress for different values of stenosis height δ.

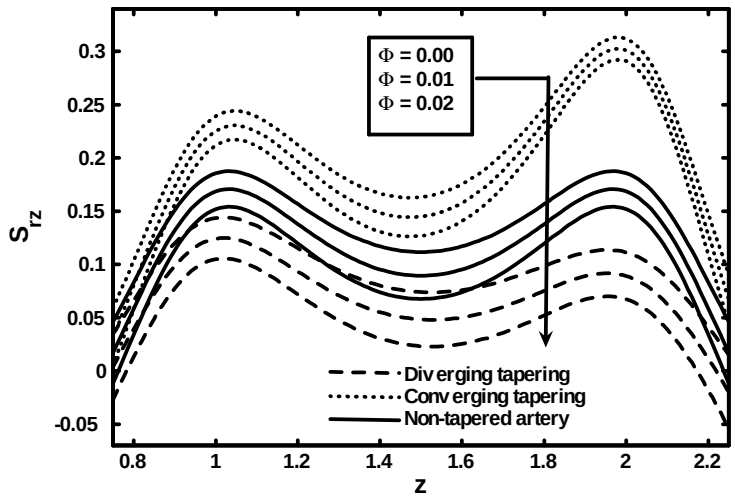

Fig. (3.5): Variation of wall shear stress for different values of nanoparticles volume fraction Φ.

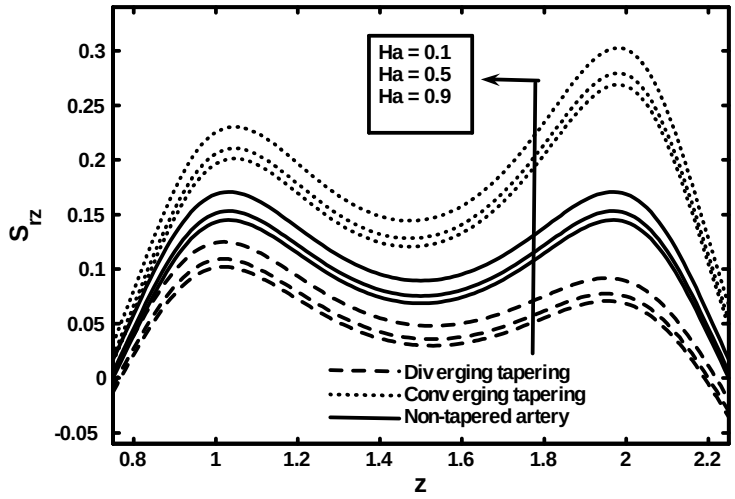

Fig. (3.6): Variation of wall shear stress for different values of Hartmann number H_a.

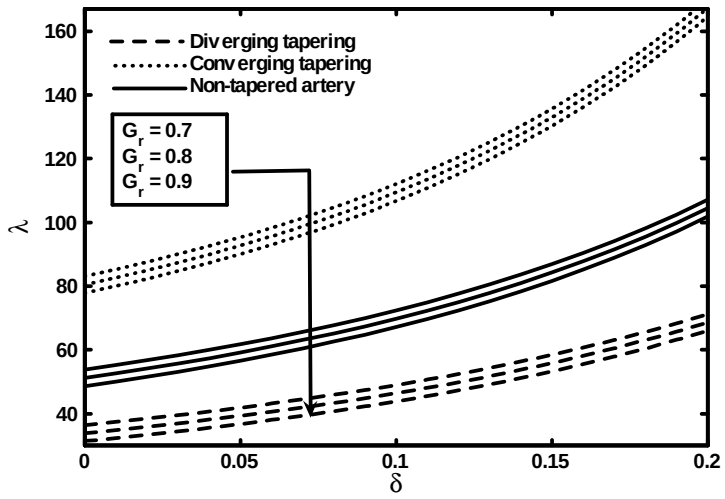

Fig. (3.7): Variation of resistance impedance for different values of Grashof number G_r.

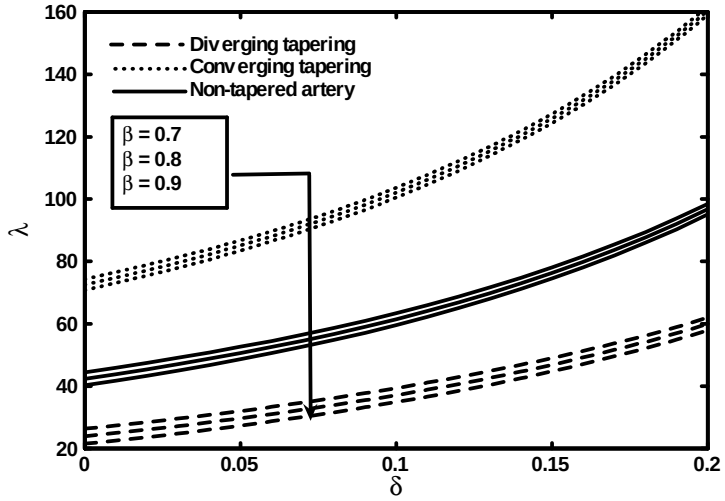

Fig. (3.8): Variation of resistance impedance for different values of heat source parameter β.

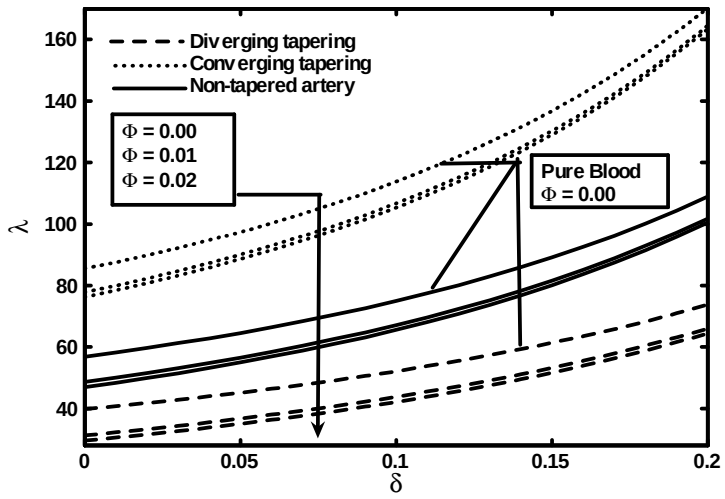

Fig. (3.9): Variation of resistance impedance for different values of nanoparticles volume fraction Φ.

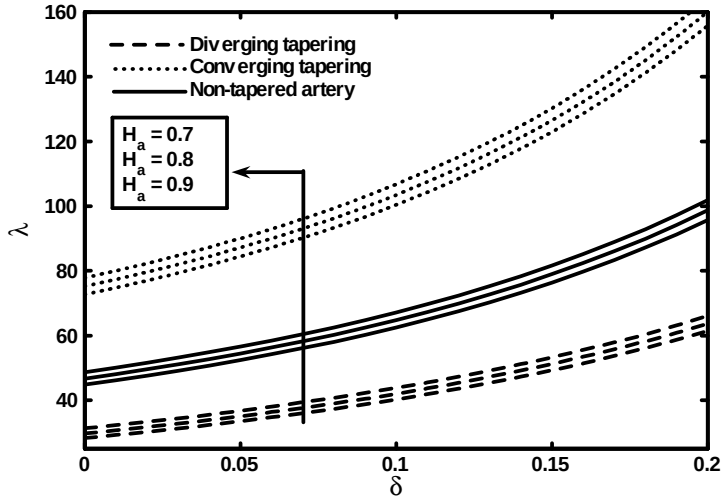

Fig. (3.10): Variation of resistance impedance for different values of Hartmann number H_a.

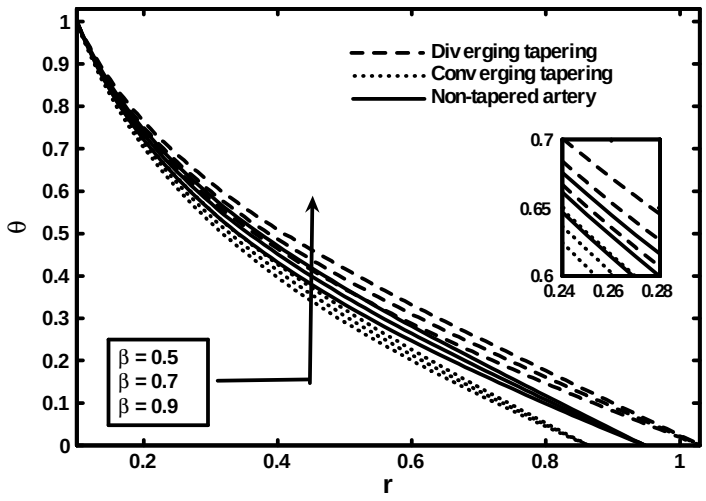

Fig. (3.11): Variation of temperature profile different values of heat source parameter β.

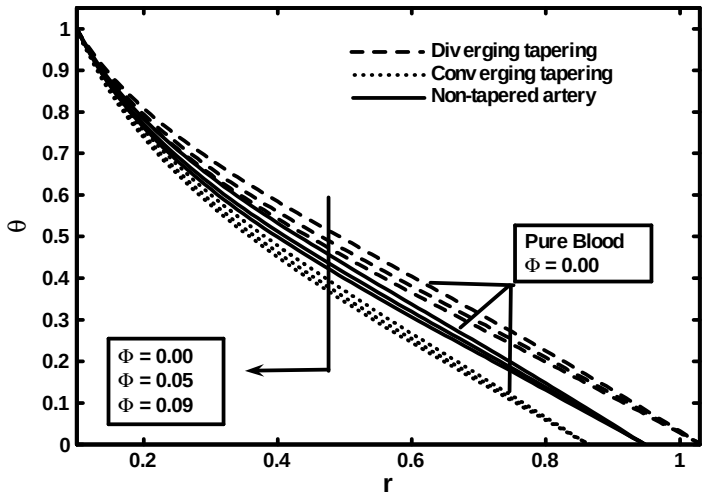

Fig. (3.12): Variation of temperature profile for different values of nanoparticles volume fraction Φ.

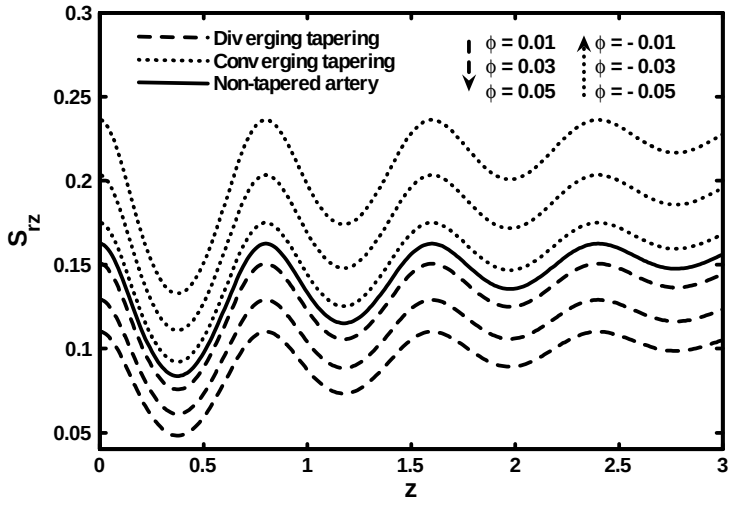

Fig. (3.13): Variation of wall shear stress for different values of the tapering angles against t.

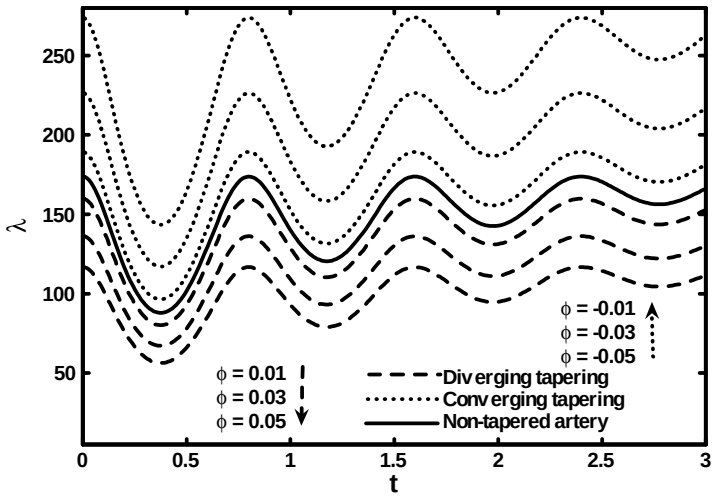

Fig. (3.14): Variation of resistance impedance for different values of the tapering angles against t.

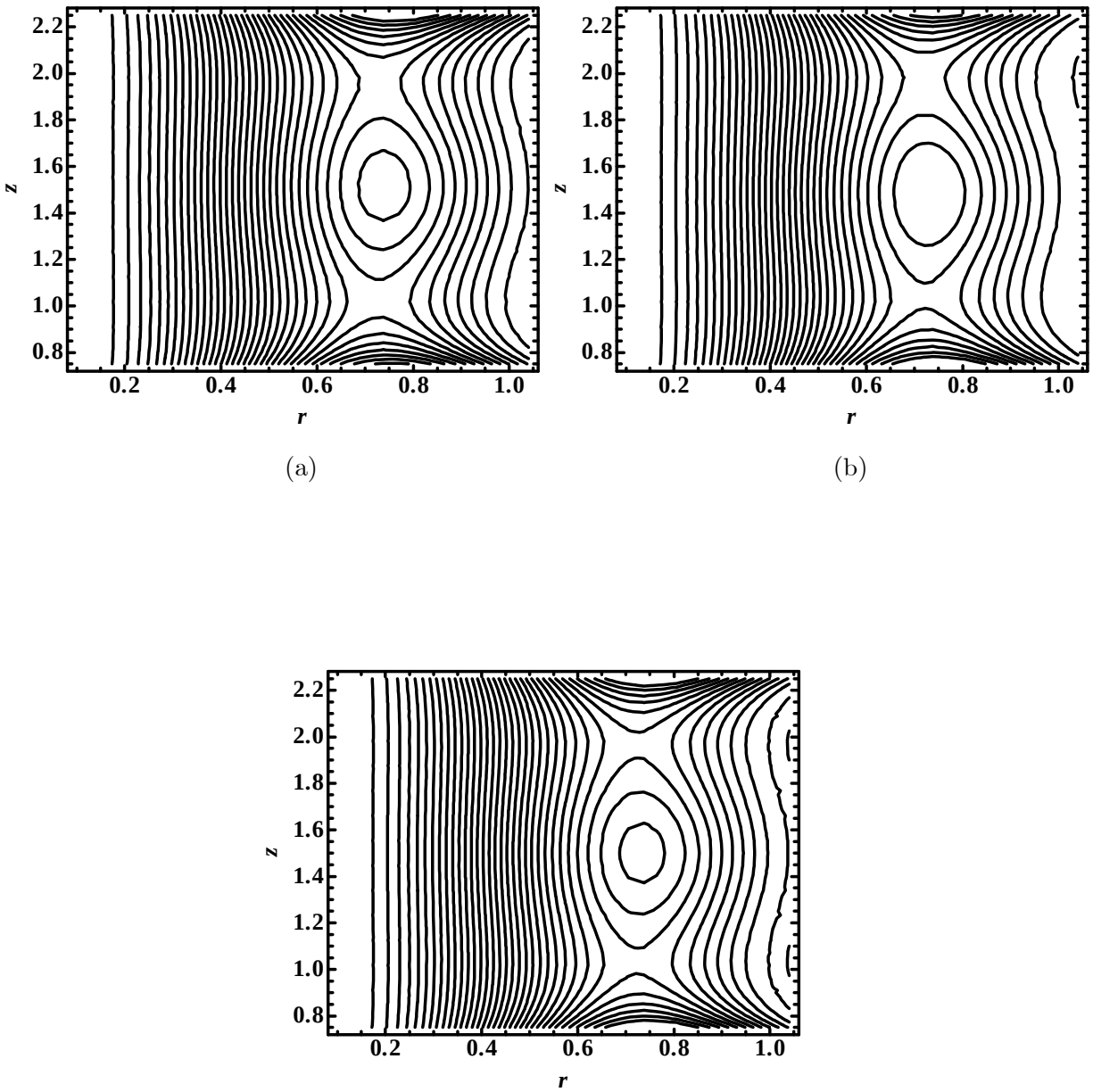

(a) (b)

(c)

Fig. (3.15): Blood flow pattern for different values of (a) $\varphi > 0$, (b) $\varphi < 0$, (c) $\varphi = 0$.

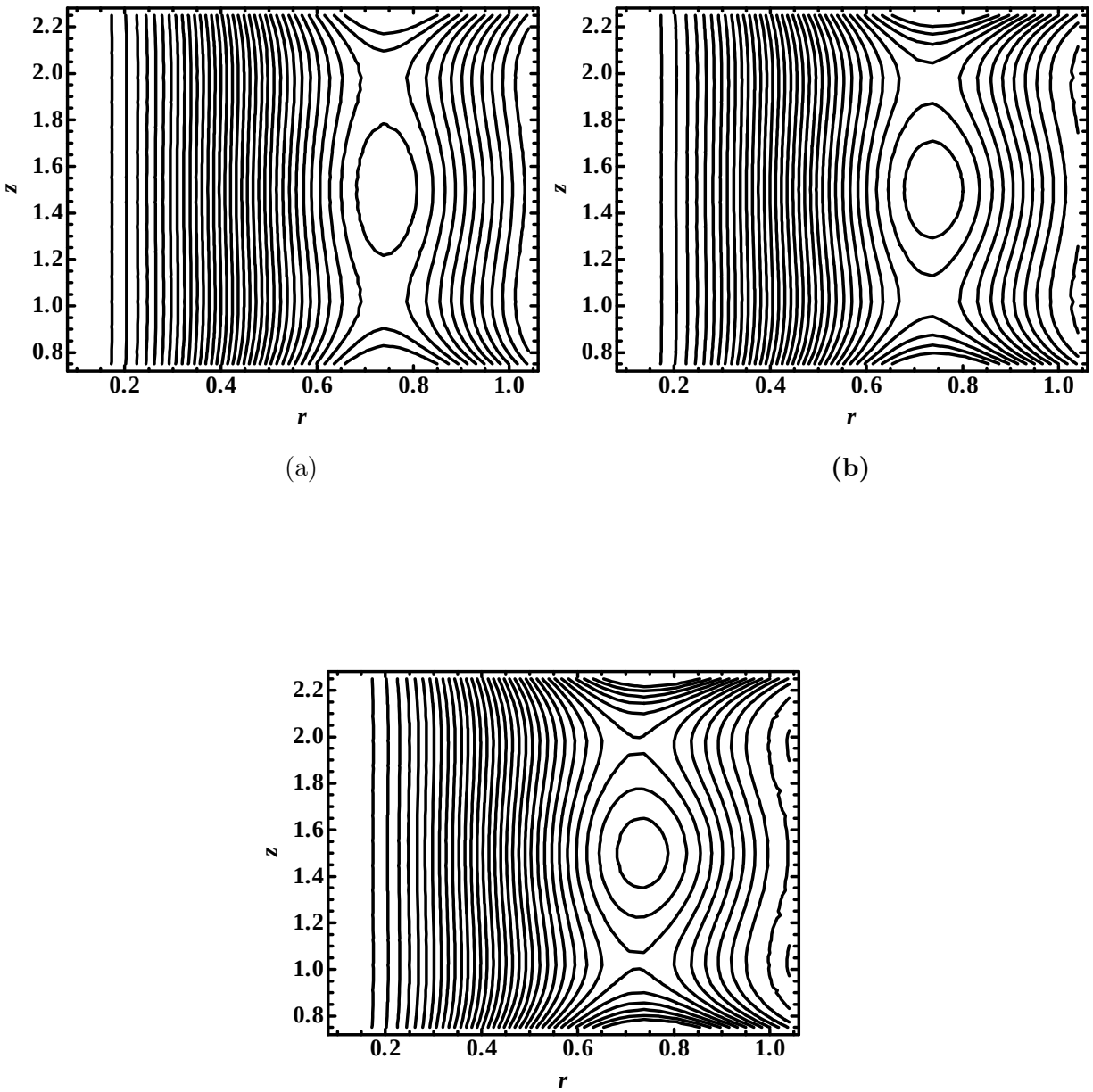

(a) (b)

(c)

Fig. (3.16): Blood flow pattern for different values of (a) $\delta = 0.03$, (b) $\delta = 0.05$, (c) $\delta = 0.07$.

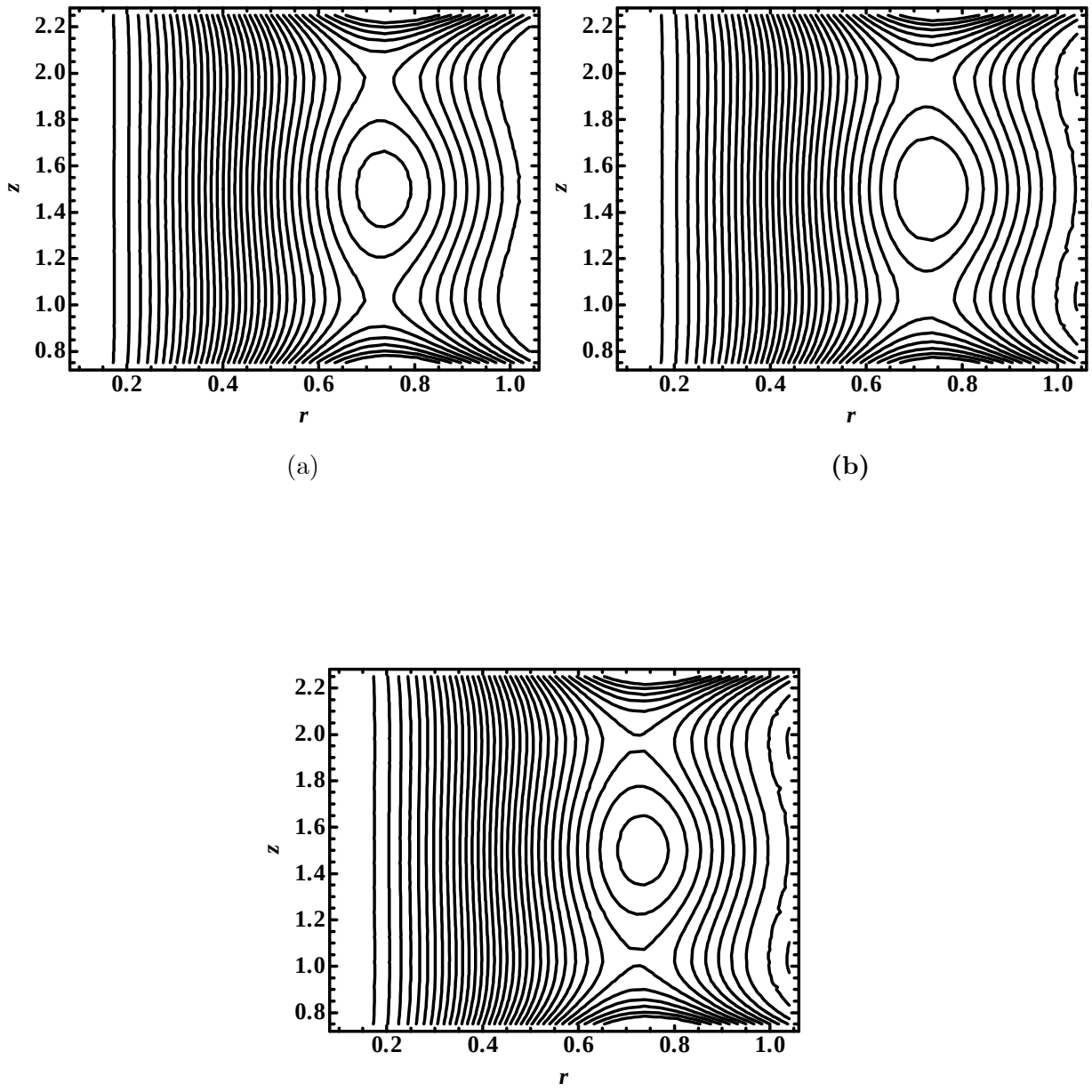

(a) (b)

(c)

Fig. (3.17): Blood flow pattern for different values of (a) $\beta = 1.3$, (b) $\beta = 1.33$, (c) $\beta = 1.36$.

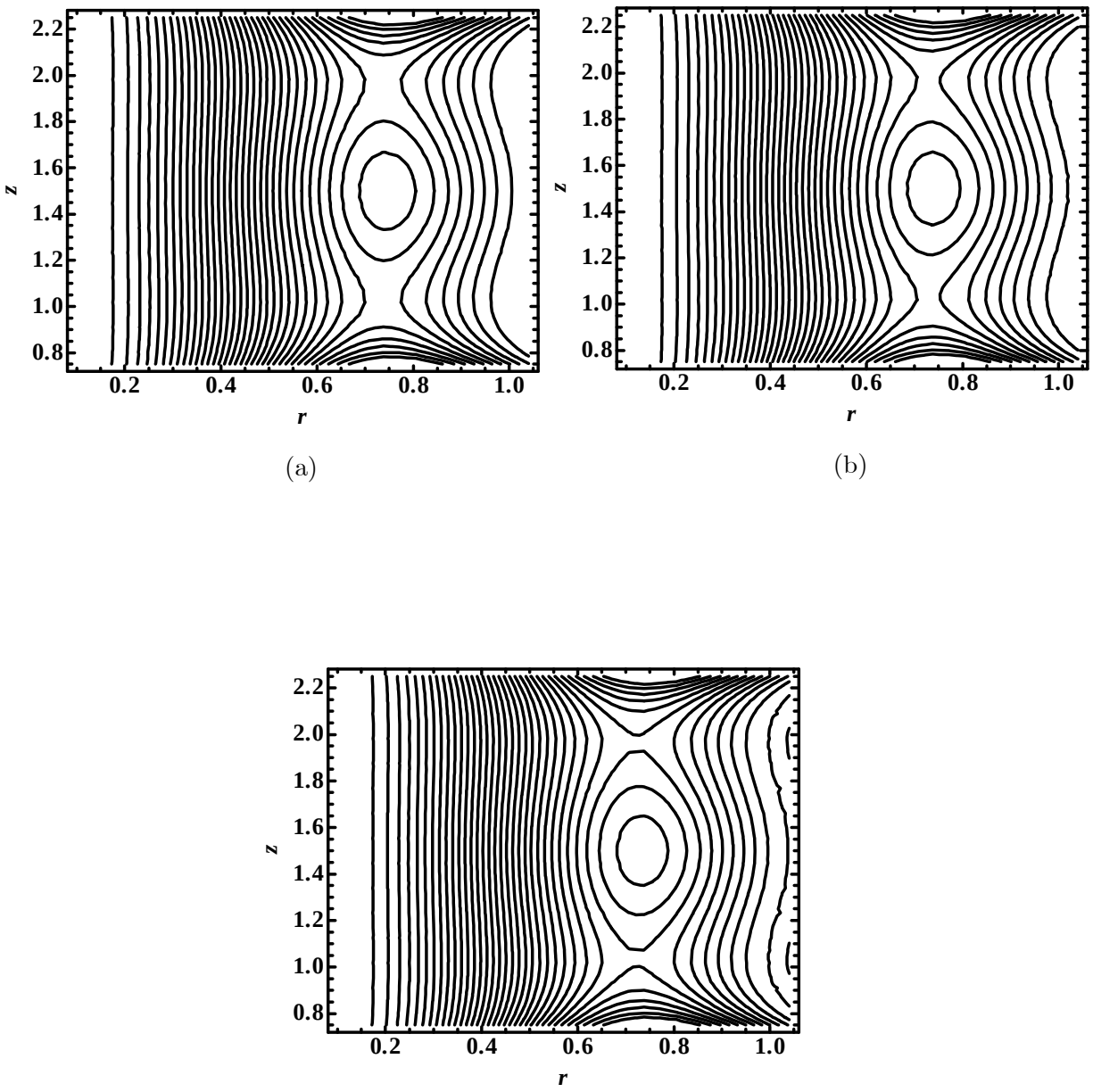

(a) (b)

(c)

Fig. (3.18): Blood flow pattern for different values of (a) $G_r = 1.9$, (b) $G_r = 2.0$, (c) $G_r = 2.1$.

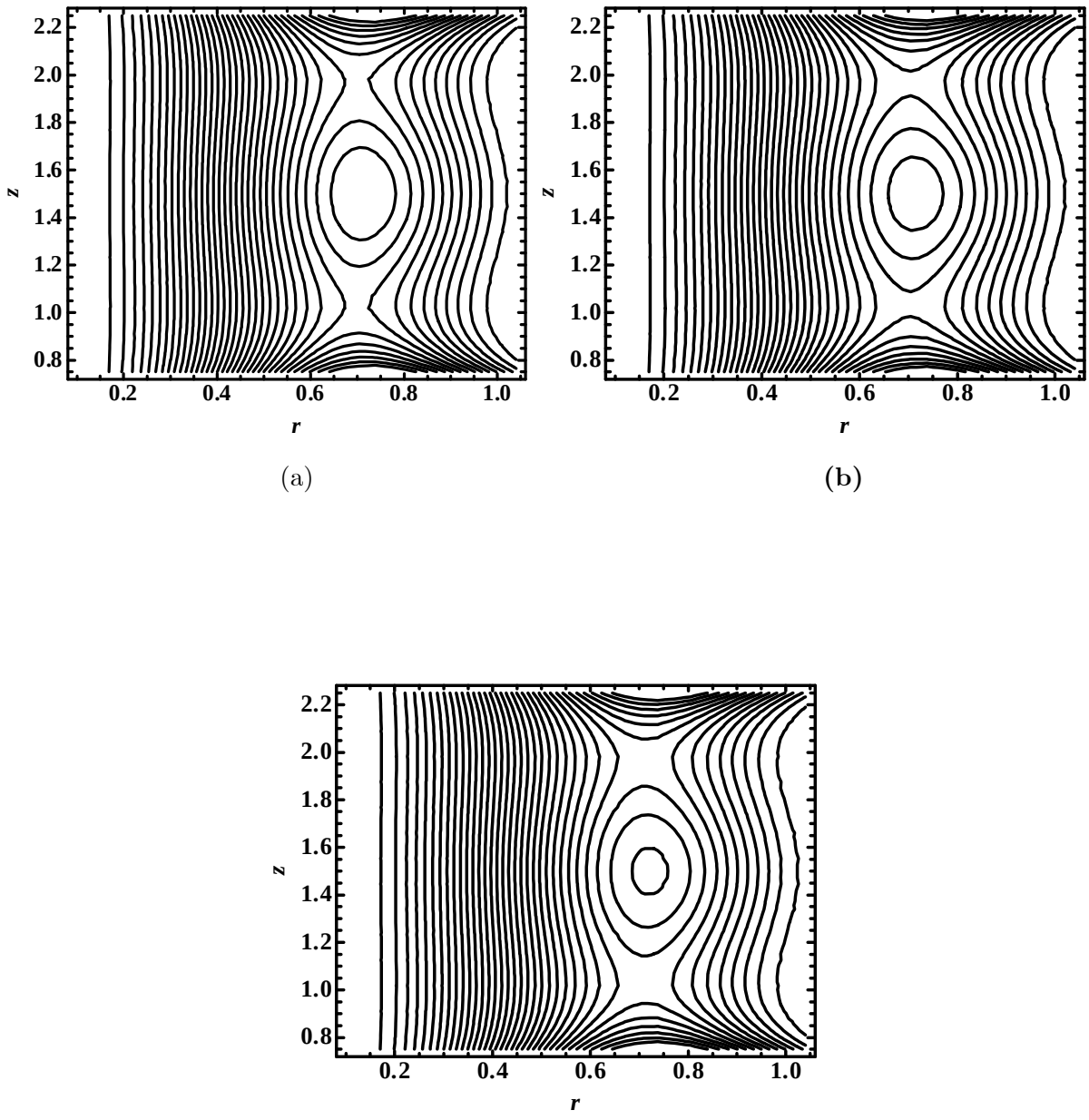

(a) (b)

(c)

Fig. (3.19): Blood flow pattern for different values of (a) $H_a = 0.1$, (b) $H_a = 0.3$, (a) $H_a = 0.6$.

w	Non-tapered artery			Diverging tapering			Converging tapering		
r	Φ=0.00	Φ=0.02	Φ=0.04	Φ=0.00	Φ=0.02	Φ=0.04	Φ=0.00	Φ=0.02	Φ=0.04
ε	0.0000	0.0000	0.0000	0.0000	0.0000	0.0000	0.0000	0.0000	0.0000
0.2	0.0228	0.0294	0.0354	0.0197	0.0273	0.0342	0.0274	0.0331	0.0381
0.3	0.0327	0.0397	0.0460	0.0282	0.0368	0.0445	0.0391	0.0446	0.0496
0.4	0.0362	0.0412	0.0456	0.0313	0.0382	0.0442	0.0428	0.0461	0.0490
0.5	0.0354	0.0374	0.0391	0.0312	0.0349	0.0381	0.0408	0.0413	0.0417
0.6	0.0313	0.0304	0.0296	0.0284	0.0288	0.0291	0.0342	0.0324	0.0307
0.7	0.0246	0.0217	0.0192	0.0236	0.0213	0.0193	0.0238	0.0209	0.0185
0.8	0.0158	0.0125	0.0096	0.0174	0.0137	0.0103	0.0102	0.0083	0.0066
0.9	0.0054	0.0038	0.0023	0.0103	0.0067	0.0035	-0.0061	-0.0045	-0.0032
h	0.0000	0.0000	0.0000	0.0000	0.0000	0.0000	0.0000	0.0000	0.0000

Table. (3.2): Variations of velocity profile for different values of the nanoparticles volume fraction Φ.

w	Non-tapered artery			Diverging tapering			Converging tapering		
r	H_a=0.3	H_a=0.5	H_a=0.7	H_a=0.3	H_a=0.5	H_a=0.7	H_a=0.3	H_a=0.5	H_a=0.7
ε	0.0000	0.0000	0.0000	0.0000	0.0000	0.0000	0.0000	0.0000	0.0000
0.2	0.0305	0.0294	0.0279	0.0280	0.0269	0.0254	0.0346	0.0335	0.0321
0.3	0.0405	0.0394	0.0380	0.0371	0.0360	0.0345	0.0458	0.0449	0.0436
0.4	0.0413	0.0407	0.0398	0.0379	0.0372	0.0362	0.0464	0.0459	0.0453
0.5	0.0371	0.0369	0.0367	0.0344	0.0341	0.0336	0.0410	0.0410	0.0409
0.6	0.0300	0.0302	0.0305	0.0283	0.0284	0.0285	0.0319	0.0322	0.0327
0.7	0.0215	0.0219	0.0225	0.0211	0.0215	0.0219	0.0205	0.0210	0.0216
0.8	0.0125	0.0129	0.0135	0.0138	0.0142	0.0148	0.0082	0.0084	0.0087
0.9	0.0038	0.0040	0.0043	0.0070	0.0074	0.0079	-0.0045	-0.0047	-0.0049
h	0.0000	0.0000	0.0000	0.0000	0.0000	0.0000	0.0000	0.0000	0.0000

Table. (3.3): Variations of velocity profile for different values of Hartmann number H_a.

Chapter 4

Examination of nanoparticles as a drug carrier on blood flow through catheterized composite stenosed artery with permeable walls

In this chapter, the influence of copper nanoparticles on blood flow through a composite stenosed artery with permeable wall is discussed. The nature of blood is discussed mathematically by considering it as viscous nanofluid. An exact solution of temperature and velocity profile is obtained by solving the governing equations after using non-dimensional parameters. Hemodynamic effects of stenosis are discussed through the graphs of resistance impedance to blood flow and wall shear stress. Results for the effects of permeability on blood flow through composite stenosis have been also discussed graphically. The considered analysis summarizes that with an increase in the permeability of stenosed arteries the resistance impedance to blood flow increases. At the end, it is found from trapping pattern that with an impulsion of nanoparticles in considered base fluid trapped bolus decreases.

4.1 Mathematical formulation

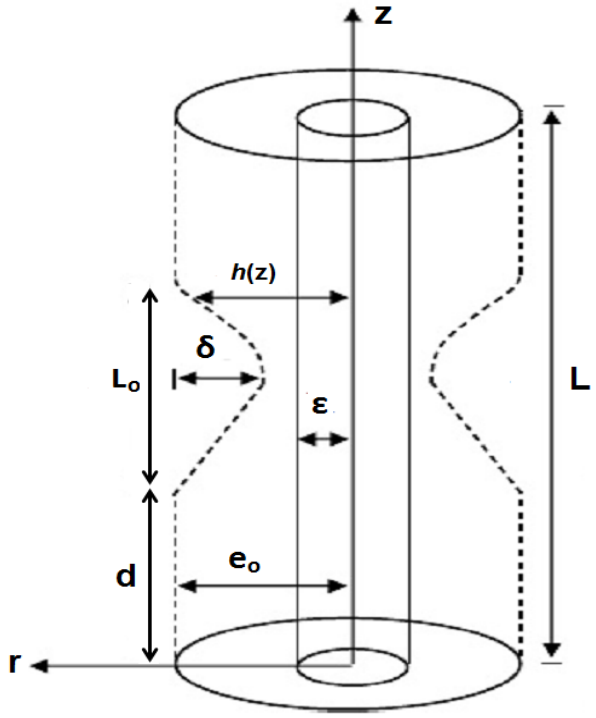

Fig. (4.1): Geometry of composite stenosis.

The heat transfer phenomenon is taken into account by giving temperature T_0 to the wall of the catheter. The geometry of composite stenosis in dimensional form is given as

$$\begin{aligned} \overline{h}(z) &= e_0 - \frac{2\delta}{L_0}(\overline{z} - d), && d \leq \overline{z} \leq d + \frac{L_0}{2}, \\ &= e_0 - \frac{\delta}{2}(1 + \cos\frac{2\pi}{L_0}(\overline{z} - d - \frac{L_0}{2})), && d + \frac{L_0}{2} \leq \overline{z} \leq d + L_0, \\ &= e_0, && \text{otherwise}, \end{aligned} \tag{4.1}$$

where d represents the position of the stenosis, L_0 as the length, while e_0 and $h(z)$ as the radius of the stenosed and normal arteries. The governing equations for conservation of mass, momentum and temperature for viscous nanofluid can be written as

$$\frac{\partial \overline{u}}{\partial \overline{r}} + \frac{\overline{u}}{\overline{r}} + \frac{\partial \overline{w}}{\partial \overline{z}} = 0, \tag{4.2}$$

$$\rho_{nf}\left(\frac{\partial \overline{u}}{\partial \overline{t}} + \overline{u}\frac{\partial \overline{u}}{\partial \overline{r}} + \overline{w}\frac{\partial \overline{u}}{\partial \overline{z}}\right) = -\frac{\partial \overline{p}}{\partial \overline{r}} + \mu_{nf}\left(\frac{\partial^2 \overline{u}}{\partial \overline{r}^2} + \frac{1}{\overline{r}}\frac{\partial \overline{u}}{\partial \overline{r}} + \frac{\partial^2 \overline{u}}{\partial \overline{z}^2} - \frac{\overline{u}}{\overline{r}^2}\right), \tag{4.3}$$

$$\rho_{nf}\left(\frac{\partial \overline{w}}{\partial \overline{t}} + \overline{u}\frac{\partial \overline{w}}{\partial \overline{r}} + \overline{w}\frac{\partial \overline{w}}{\partial \overline{z}}\right) = -\frac{\partial \overline{p}}{\partial \overline{z}} + \mu_{nf}\left(\frac{\partial^2 \overline{w}}{\partial \overline{r}^2} + \frac{1}{\overline{r}}\frac{\partial \overline{w}}{\partial \overline{r}} + \frac{\partial^2 \overline{w}}{\partial \overline{z}^2}\right) + g(\rho\gamma)_{nf}(\overline{T} - T_1), \tag{4.4}$$

$$\left(\frac{\partial \overline{T}}{\partial \overline{t}} + \overline{u}\frac{\partial \overline{T}}{\partial \overline{r}} + \overline{w}\frac{\partial \overline{T}}{\partial \overline{z}}\right) = \frac{K_{nf}}{(\rho c_p)_{nf}}\left(\frac{\partial^2 \overline{T}}{\partial \overline{r}^2} + \frac{1}{\overline{r}}\frac{\partial \overline{T}}{\partial \overline{r}} + \frac{\partial^2 \overline{T}}{\partial \overline{z}^2}\right) + \frac{Q_0}{(\rho c_p)_{nf}}. \tag{4.5}$$

In above equation thermo physical properties are given as

$$\begin{aligned}
&\mu_{nf} = \frac{\mu_f}{(1-\Phi)^{2.5}},\ \alpha_{nf} = \frac{K_{nf}}{(\rho c_p)_{nf}},\ \rho_{nf} = (1-\Phi)\rho_f + \Phi\rho_s,\\
&(\rho c_p)_{nf} = (1-\Phi)(\rho c_p)_f + \Phi(\rho c_p)_s, (\rho\gamma)_{nf} = (1-\Phi)(\rho\gamma)_f + \Phi(\rho\gamma)_s,\\
&\frac{K_{nf}}{K_f} = \frac{(K_s + 2K_f) - 2\Phi(K_f - K_s)}{(K_s + 2K_f) + \Phi(K_f - K_s)}.
\end{aligned} \tag{4.6}$$

Non-dimensional variables are defined as

$$\begin{aligned}
&r = \frac{\overline{r}}{e_0},\ z = \frac{\overline{z}}{L_0},\ w = \frac{\overline{w}}{u_o},\ u = \frac{L_0\overline{u}}{u_o\delta},\ p = \frac{e_0^2\overline{p}}{u_o L_0 \mu_f},\\
&R_{en} = \frac{L_0 u_o \rho_f}{\mu_f},\ G_r = \frac{g\gamma_f\rho_f e_0^2(T_0 - T_1)}{u_0\mu_f},\ \delta^* = \frac{\delta}{e_0},\\
&\beta = \frac{Q_0 e_0^2}{(T_0 - T_1)K_f},\ \theta = \frac{\overline{T} - T_1}{T_0 - T_1},\ d^* = \frac{d}{L_0}.
\end{aligned} \tag{4.7}$$

Using mild stenosis case $\delta^* = \frac{\delta}{e_0} \ll 1$ and taking extra condition $\epsilon = \frac{e_0}{L_0} \approx O(1)$, the constitutive Eqs. (4.3) to (4.5) can be written as

$$\frac{\partial p}{\partial r} = 0, \tag{4.8}$$

$$\frac{\partial p}{\partial z}\frac{\mu_f}{\mu_{nf}} = \frac{\partial^2 w}{\partial r^2} + \frac{1}{r}\frac{\partial w}{\partial r} + \frac{\mu_f}{\mu_{nf}}\frac{(\rho\gamma)_{nf}}{(\rho\gamma)_f}G_r\theta, \tag{4.9}$$

$$\frac{\partial^2 \theta}{\partial r^2} + \frac{1}{r}\frac{\partial \theta}{\partial r} + \left(\frac{K_s(1-\Phi)+K_f(2+\Phi)}{K_s(1+2\Phi)+2K_f(1-\Phi)}\right)\beta = 0, \tag{4.10}$$

The geometry of stenosis in dimensionless form are defined as

$$\begin{aligned} h(z) &= 1 - 2\delta^*(z-d^*), && d^* \le z \le d^* + \frac{1}{2}, \\ &= 1 - \frac{\delta^*}{2}(1+\cos 2\pi(z-d^*-\frac{1}{2})), && d^* + \frac{1}{2} \le z \le d^* + 1, \\ &= 1, && \text{otherwise.} \end{aligned} \tag{4.11}$$

The corresponding boundary conditions are given as [11]

$$w = w_b, \quad \theta = 0, \qquad \text{at} \quad r = h(z), \tag{4.12}$$

$$w = 0, \quad \theta = 1, \qquad \text{at} \quad r = \varepsilon, \tag{4.13}$$

$$\frac{\partial w}{\partial r} = \frac{s}{\sqrt{D_a}}(w_b - w_P), \qquad \text{at} \quad r = h(z). \tag{4.14}$$

where in above equation $D_a(=\frac{R_o}{e_o^2})$ is defined as the Darcy number, R_o as the permeability, s as the dimensionless slip parameter depending on permeable material within the boundary region and w_P as the slip velocity of the permeable boundary that is obtained from Darcy law in the presence of the body forces

$$w_P = \left(-D_a\frac{\mu_f}{\mu_{nf}}\frac{dp}{dz} + g_2\theta\right)\Big|_{r=h}, \tag{4.15}$$

using ($\theta = 0$ at $r = h(z)$), Eq. (4.15) can be written as

$$w_P = -D_a\frac{\mu_f}{\mu_{nf}}\frac{dp}{dz}. \tag{4.16}$$

4.2 Solution of the problem

The exact solutions of Eqs. (4.9) and (4.10) using Eqs. (4.12) and (4.13) are written as

$$\theta = \frac{1}{4(\ln h - \ln \varepsilon)}(4(\ln h - \ln \varepsilon) + \beta g_1(h^2(\ln r - \ln \varepsilon) + r^2(- \ln h + \ln \varepsilon) + (\ln h - \ln r)\varepsilon^2)), \tag{4.17}$$

$$\begin{aligned} w &= \frac{dp}{dz}\frac{(1-\Phi)^{2.5}}{4(\ln h - \ln \varepsilon)}(r^2(\ln h - \ln \varepsilon) + h^2(-\ln r + \ln \varepsilon) + \varepsilon^2 \\ &(-\ln h + \ln r)) + \frac{g_2}{64(\ln h - \ln \varepsilon)^2}(16(h^2(\ln r - \ln \varepsilon) + r^2 \\ &(1 + \ln h - \ln r)(-\ln h + \ln \varepsilon) + (\ln h - \ln r)(1 + \ln h - \\ &\ln \varepsilon)\varepsilon^2) + \beta g_1(r^4(\ln h)^2 + (h^2 - r^2)\ln \varepsilon(4h^2 + (3h^2 - r^2) \\ &\ln \varepsilon) + \ln r(-4h^4 + (-3h^4 + 4h^2r^2)\ln \varepsilon) + \ln h(h^2(4r^2 + \\ &(3h^2 - 4r^2)\ln r) + (-3h^4 + 4h^2r^2 - 2r^4)\ln \varepsilon) - 4(r^2(\ln h)^2 - \\ &2h^2 \ln r + (h^2 - r^2 + r^2 \ln r)\ln \varepsilon + \ln h(h^2 + r^2 - r^2(\ln r + \\ &\ln \varepsilon)))\varepsilon^2 + (\ln h - \ln r)(4 + 3\ln h - 3\ln \varepsilon)\varepsilon^4)) - \\ &\frac{(\ln r - \ln \varepsilon)w_b}{(\ln h - \ln \varepsilon)}, \end{aligned} \tag{4.18}$$

where by using Eq. (4.18) into Eq. (4.14) slip velocity is given as

$$\begin{aligned} w_b &= \frac{1}{4hs(\ln h - \ln \varepsilon) - 4\sqrt{D_a}}(\frac{dp}{dz}\sqrt{D_a}(1-\Phi)^{2.5}(h^2(-1 + 2\ln h - \\ &2\ln \varepsilon) + 4hs(-\ln h + \ln \varepsilon)\sqrt{D_a} + \varepsilon^2) + \frac{1}{64g_3}(\sqrt{D_a}g_2(16h^2(1 \\ &- \ln h + \ln \varepsilon) - (1 + \ln h - \ln \varepsilon)\varepsilon^2) + \beta g_1(-h^4(4 - 7\ln h + \\ &4(\ln h)^2 + (7 - 8\ln h)\ln \varepsilon + 4(\ln \varepsilon)^2) + 4h^2(2 - \ln h + \ln \varepsilon) \\ &\varepsilon^2 + (-4 - 3\ln h + 3\ln \varepsilon)\varepsilon^4))). \end{aligned} \tag{4.19}$$

Flow rate is given as

$$F = \int_{\varepsilon}^{h} rw dr. \tag{4.20}$$

Using Eqs. (4.18) and (4.19) into Eq. (4.20), we get the expression for pressure gradient as follows

$$\frac{dp}{dz} = \frac{F - g_5(z)}{g_4(z)}. \tag{4.21}$$

The pressure drop can be defined as

$$\Delta p = \int_{0}^{L} \left(-\frac{dp}{dz} \right) dz. \tag{4.22}$$

Using Eq. (4.22), the impedance resistance can be evaluated as

$$\lambda = \frac{\Delta p}{F} = \int_{0}^{d^*} \Omega_1(z) \mid_{h=1} dz + \int_{d^*}^{d^*+\frac{1}{2}} \Omega_1(z) dz + \int_{d^*+\frac{1}{2}}^{d^*+1} \Omega_1(z) dz + \int_{d^*+1}^{L} \Omega_1(z) \mid_{h=1} dz, \tag{4.23}$$

where

$$\Omega_1(z) = \frac{1}{F} \left(\frac{-F + g_5(z)}{g_4(z)} \right). \tag{4.24}$$

Using Eq. (4.24) into Eq. (4.23), we get

$$\lambda = (L-1)\Omega_1(z) \mid_{h=1} + \int_{d^*}^{d^*+\frac{1}{2}} \Omega_1(z) dz + \int_{d^*+\frac{1}{2}}^{d^*+1} \Omega_1(z) dz. \tag{4.25}$$

The wall shear stress is evaluated by using Eqs. (4.18) and (4.19), which is given as

$$
\begin{aligned}
S_{rz} &= -\Big(\frac{dp}{dz}\frac{(s(1-\Phi)^{2.5}(-4D_a+h^2(-1+2\ln h-2\ln\varepsilon)+\varepsilon^2))}{(4hs(\ln h-\ln\varepsilon)-4\sqrt{D_a})}+\frac{1}{64g_3}\\
&\quad (sg_2(16(h^2(1-\ln h+\ln\varepsilon)-16(1+\ln h-\ln\varepsilon)\varepsilon^2+\beta g_1(-h^4\\
&\quad (4-7\ln h+4(\ln h)^2+(7-8\ln h)\ln\varepsilon+(4(\ln\varepsilon)^2)+4h^2\\
&\quad (2-\ln h+\ln\varepsilon)\varepsilon^2+(-4-3\ln h+3\ln\varepsilon)\varepsilon^4))))\Big). \qquad (4.26)
\end{aligned}
$$

4.3 Appendix

$$
\begin{aligned}
&g_1=\left(\frac{K_s(1-\Phi)+K_f(2+\Phi)}{K_s(1+2\Phi)+2K_f(1-\Phi)}\right),\ g_2=G_r\left((1-\Phi)+\Phi\frac{\rho_s\gamma_s}{\rho_f\gamma_f}\right)\\
&(1-\Phi)^{2.5},\ g_3=(\ln h-\ln\varepsilon)(hs(\ln h-\ln\varepsilon)-\sqrt{D_a}),\\
&g_4=\frac{-1}{(16(hs(\ln h-\ln\varepsilon)-\sqrt{D_a}))}((1-\Phi)^{2.5}(4hsD_a(h^2(-1+2\ln h\\
&-2\ln\varepsilon)+\varepsilon^2)+\sqrt{D_a}(h^4(3-4\ln h+4\ln\varepsilon)-4h^2\varepsilon^2+\varepsilon^4)+hs(h^4\\
&(-1+\ln h-\ln\varepsilon)+2h^2\varepsilon^2+(-1-\ln h+\ln\varepsilon)\varepsilon^4))),\\
&g_5=\frac{1}{768g_3}(g_2(2hs(6(h^4(-4+3\ln h-3\ln\varepsilon)+4h^2(2+\ln h-\ln\varepsilon)\\
&\varepsilon^2-(4+7\ln h+4(\ln h)^2-(7+8\ln h)\ln\varepsilon+4(\ln\varepsilon)^2)\varepsilon^4)+2\beta g_1\\
&(h^2-\varepsilon^2)(h^4(6-9\ln h+\ 4(\ln h)^2+\ (9-8\ln h)\ln\varepsilon+4(\ln\varepsilon)^2)+\\
&4h^2(-3+(\ln h-\ln\varepsilon)^2)\varepsilon^2+(6+9\ln h+4(\ln h)^2-(9+8\ln h)\\
&\ln\varepsilon+4\ln\varepsilon)^2)\varepsilon^4))+\sqrt{D_a}(12(h^4(9-\ 8\ln h+8(\ln\varepsilon)-4h^2)(3+\\
&2\ln h-2\ln\varepsilon)\varepsilon^2(3+4\ln h-4\ln\varepsilon)\varepsilon^4)+\beta g_1(-h^6(27-46\ln h+\\
&24(\ln h)^2+2(23-24\ln h)\ln\varepsilon+24\ln\varepsilon)^2)+9h^4(7-4\ln h+\\
&4\ln\varepsilon)\varepsilon^2-9h^2(5+2\ln h-2\ln\varepsilon)\varepsilon^4+(9+8\ln h-8\ln\varepsilon)\varepsilon^6)))).
\end{aligned}
$$

4.4 Results and discussion

The momentous influence of different emerging flow parameters on the blood flow with copper nanoparticles is discussed through graphs of wall shear stress, impedance resistance to flow, temperature profile and stream lines. The graphs are plotted by keeping parameters constants

such as $\delta = 0.1 - 0.2$, $d^* = 1.0$, $z = 1.5$, $\varepsilon = 0.1$, $\beta = 2.0$, $F = 0.5$, $G_r = 0.1$, $D_a = 0.01 - 0.9$, $s = 0.1 - 0.9$, $L = 3$. Figs. (4.2) to (4.6) are plotted for wall shear stress versus z in the stenotic region $1.0 \leq z \leq 2.0$. It is observed from these figures that wall shear stress starts increasing from the initial projection of the stenosis (at $z = 1.0$) and then starts decreasing from the upstream of the stenotic throat ($z = 1.5$) to the end of stenotic region (at $z = 2.0$). It is concluded from these figures that stresses on the walls of stenosed artery are maximum at the throat $z = 1.5$. Figs. (4.2) and (4.3) are plotted to analyze the influence of stresses on the stenotic wall for Grashof number G_r and heat source parameter β. The graph of wall shear stress for different values of Grashof number G_r is plotted in Fig. (4.2). It is depicted that the stresses on the wall of arteries decreases with an increase in viscous forces. One can observe from Fig. (4.3), that stresses on the wall of arteries decreases with an increase in the internal heat source parameter. The wall shear stress for different values of Darcy number D_a and slip parameter s is given in Figs. (4.4) and (4.5). It is depicted from Fig. (4.4) that wall shear stress starts increasing with an increase in the values of Darcy number D_a. It is depicted from this figure that the stresses on the wall of arteries increase due to increase in the permeability of the stenosed artery. The variation of wall shear stress for slip parameter s is given in Fig. (4.5). It is observed that wall shear stress increases near the throat of stenosis for Cu blood cases ($1.15 \leq z \leq 1.82$, $1.10 \leq z \leq 1.85$) and for pure blood case ($1.08 \leq z \leq 1.88$), while the opposite trend is observed in the rest of the stenotic segments. The variation of wall shear stress versus z for different values of stenosis height δ is given in Fig. (4.6). It is analyzed from this figure that the wall shear stress increases with an increase in the values of stenosis height δ due to the pressure distribution behavior in the pre and post stenotic regions. Figs. (4.7) to (4.10) are plotted for impedance resistance to flow against stenosis height δ. Figs. (4.7) and (4.8) are plotted for heat source parameter β and Grashof number G_r. It is observed from Fig. (4.7) that viscosity of the fluid decreases with an increase in internal heat source that minimize the effects of resistance impedance to blood flow. The variations of Grashof number G_r from Fig. (4.8) shows that due to decrease in stresses on the wall of stenosed artery resistance to blood flow decreases. The resistance impedance for different values of Darcy number D_a is given in Fig. (4.9). It is analyzed from this figure that with an increase in the D_a resistance to blood flow increases. Such an increase is due to increase in permeability of the artery which result

into damaged, dilated or inflamed arterial wall thickness and tend to increases in resistance. From Figs. (4.10), It is observed that resistance to blood flow decreases with an increase in the values of slip parameter s. It is obtained from this figure that the damage of arteries due to stenosis could be decreased by introducing slip effects and may be exploited for better function of diseased artery. The variations of temperature profile against radial direction r for different values of heat source parameter β and stenosis height δ are plotted through Fig. (4.11) and (4.12). It is observed from these figures that temperature profile increases with an increase in the values of heat source parameter β, while decreases with an increase in the values of the stenosis height δ. These graphs also indicate that temperature is higher for pure blood case ($\Phi = 0.00$) as compared to the Cu blood cases. It is also concluded that the efficiency of heat transfer rate from the flowing blood to the walls increases with increase in thermal conductivity of nanoparticles. Trapping represents an interesting phenomenon and has been plotted here through Figs. (4.13) to (4.17). From Fig. (4.13), it is observed that with an increase in stenosis height number of trapped bolus increases between the catheter and stenotic walls. The trapping for Darcy number D_a and slip parameter s is discussed in Figs. (4.14) and (4.15). It is depicted from this flow pattern that the number of trapping bolus increases with an increase in the permeability of the stenosed artery, while shows random behavior for different values of slip parameter s. Stream lines for different values of the catheter size ε and nanoparticles volume fraction Φ are plotted through Figs. (4.16) and (4.17). It is analyzed from these stream lines behaviors that the number of trapping bolus increases with an increase in the radius of the catheter ε and decreases with an increase in nanoparticles volume fraction Φ. Tables (4.1) and (4.2) are plotted for velocity profile against radial direction r to discuss the different pure and copper blood cases. From tables (4.1) and (4.2), it is observed that the velocity profile for different values of Darcy number D_a and slip parameter s increases near the wall of the catheter between the interval $\varepsilon \leq r \leq 0.7$ and decreases near the wall of the artery between the interval $0.7 < r \leq h$. The tables show that the velocity profile gives higher magnitude for copper blood case near the wall of the catheter, while the opposite trend is observed near the wall of the artery.

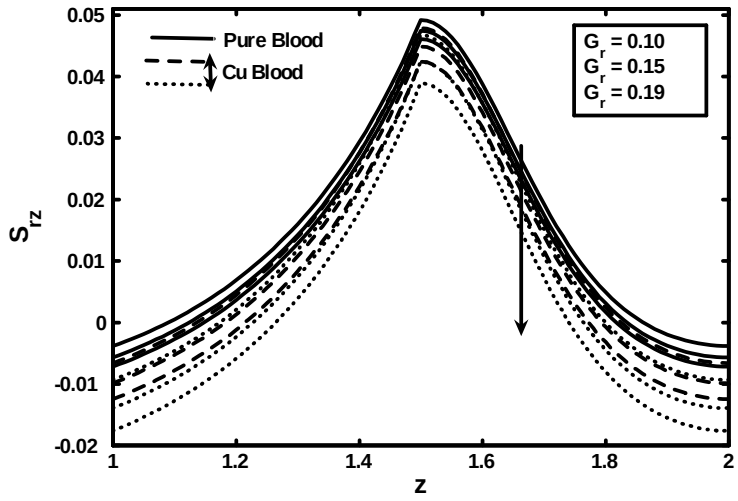

Fig. (4.2): Variation of wall shear stress for different values of Grashof number G_r.

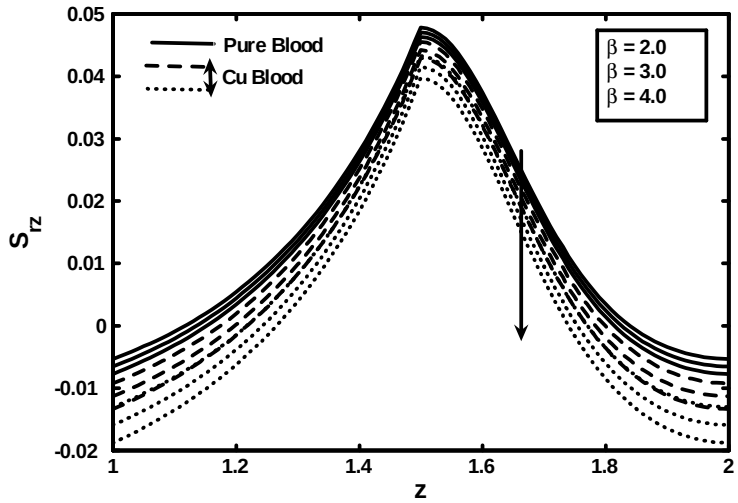

Fig. (4.3): Variation of wall shear stress for different values of heat source parameter β.

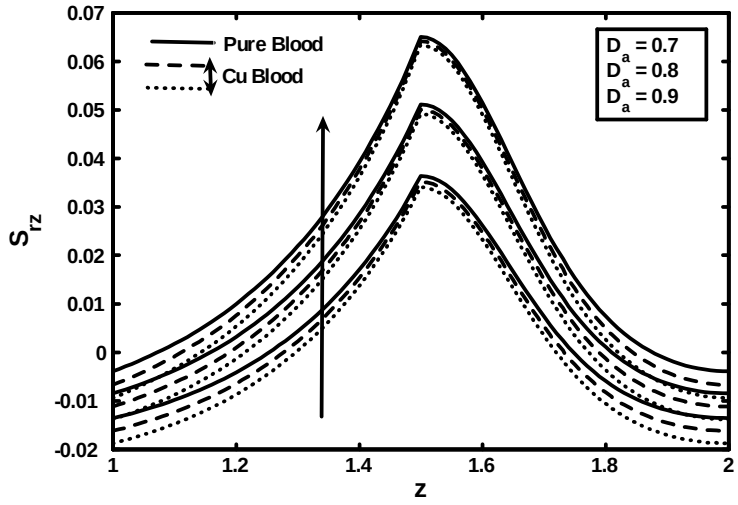

Fig. (4.4): Variation of wall shear stress for different values of Darcy number D_a.

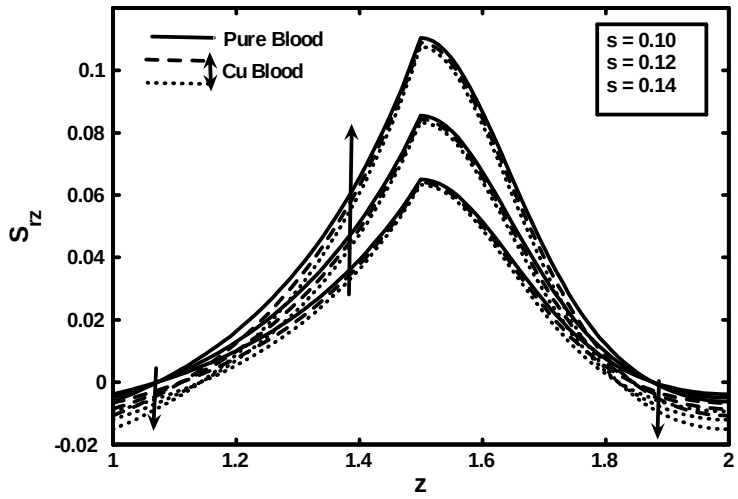

Fig. (4.5): Variation of wall shear stress for different values of for different values of slip parameter s.

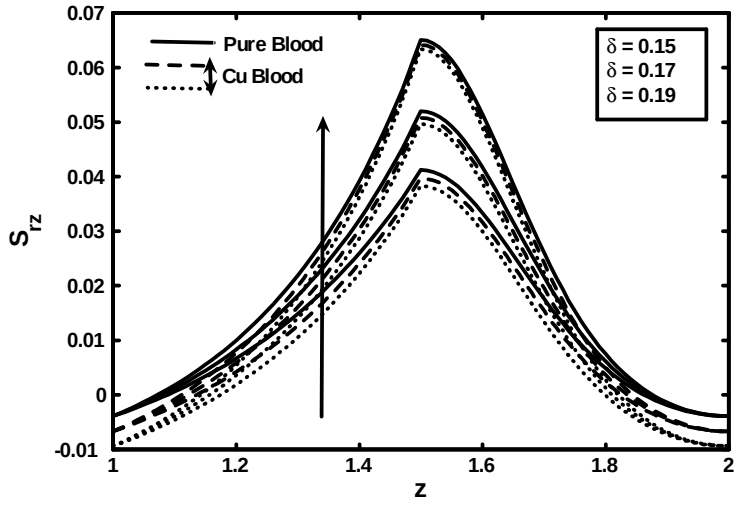

Fig. (4.6): Variation of wall shear stress for different values of stenosis height δ.

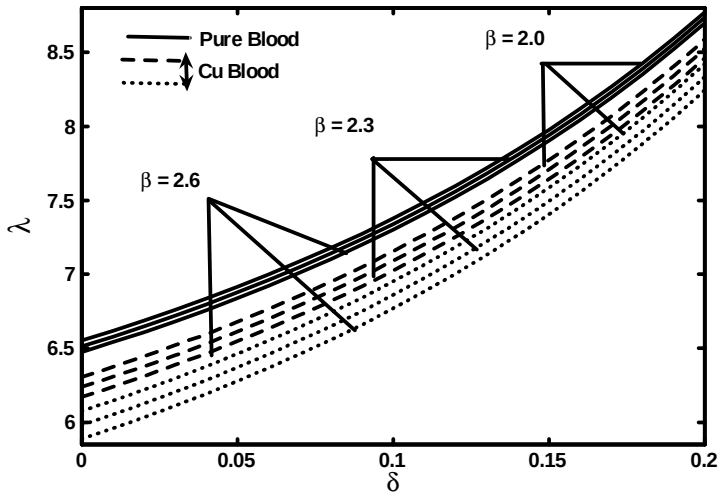

Fig. (4.7): Variation of resistance impedance for different values of heat source parameter β.

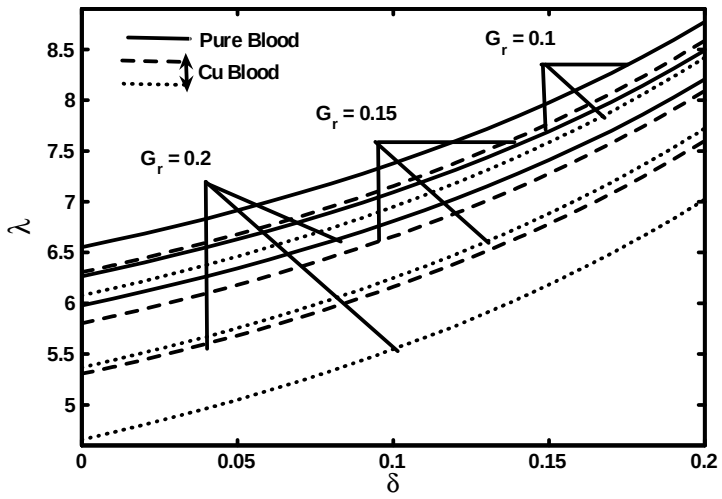

Fig. (4.8): Variation of resistance impedance for different values of Grashof number G_r.

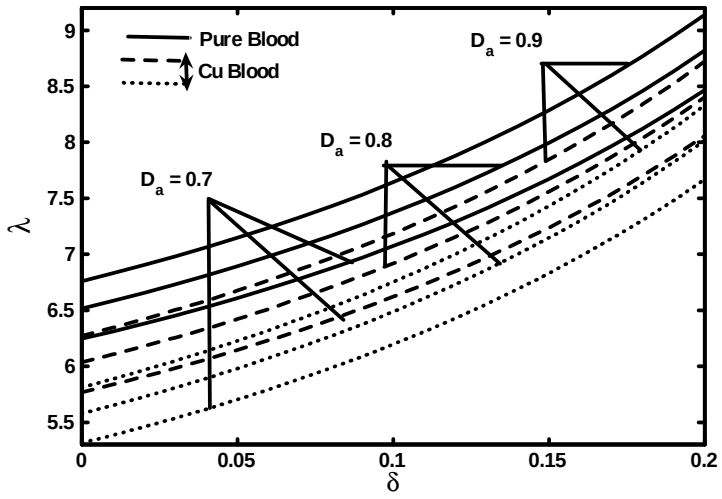

Fig. (4.9): Variation of resistance impedance for different values of Darcy number D_a.

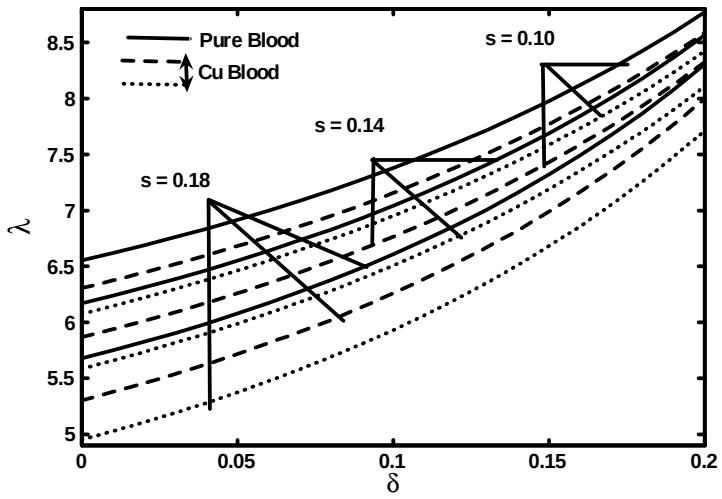

Fig. (4.10): Variation of resistance impedance for different values of slip parameter s.

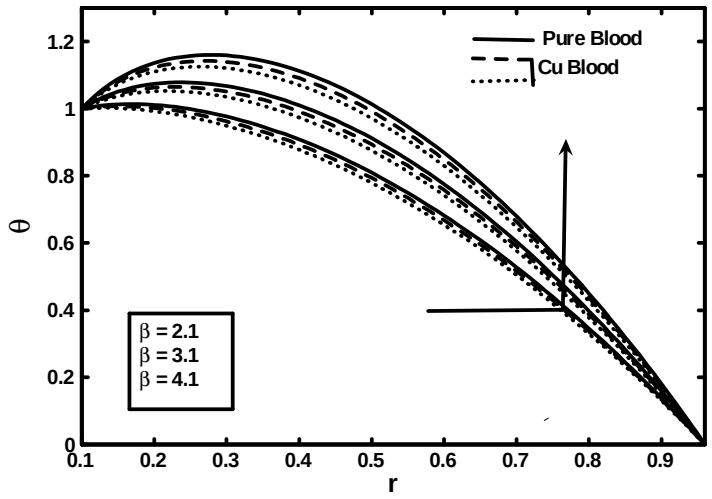

Fig. (4.11): Variation of temperature profile for different values of heat source parameter β.

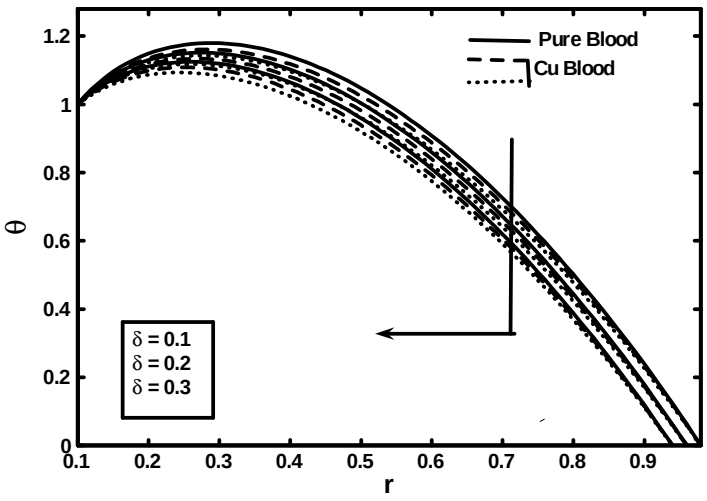

Fig. (4.12): Variation of temperature profile for different values of stenosis height δ.

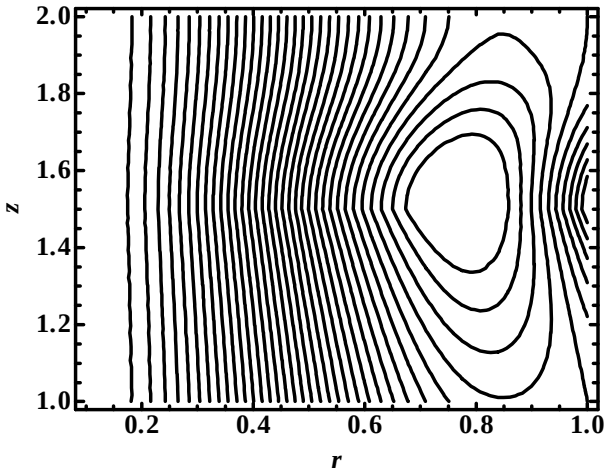

(a)

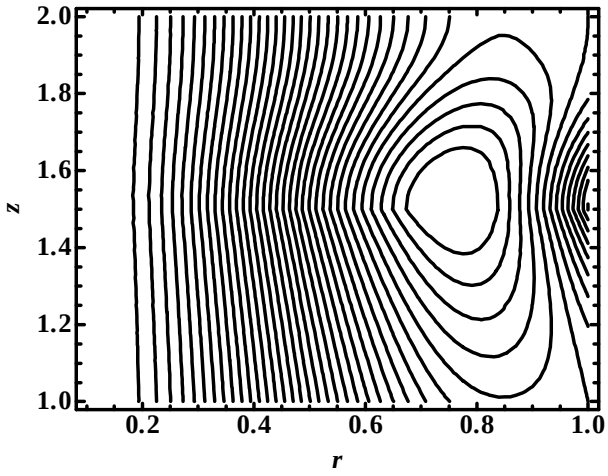

(b)

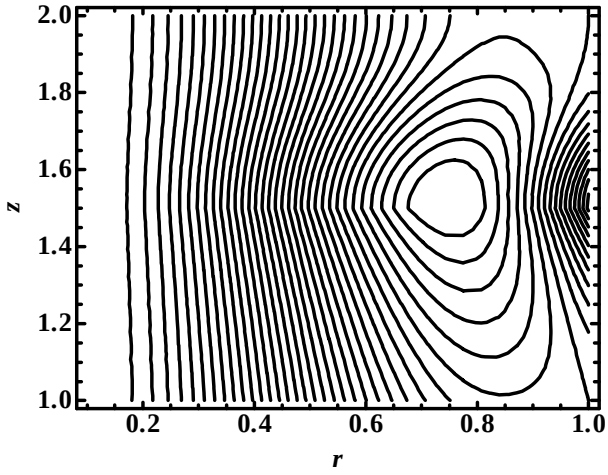

(c)

Figs. (4.13): Blood flow pattern for different values of (a) $\delta = 0.07$, (b) $\delta = 0.08$, (c) $\delta = 0.09$.

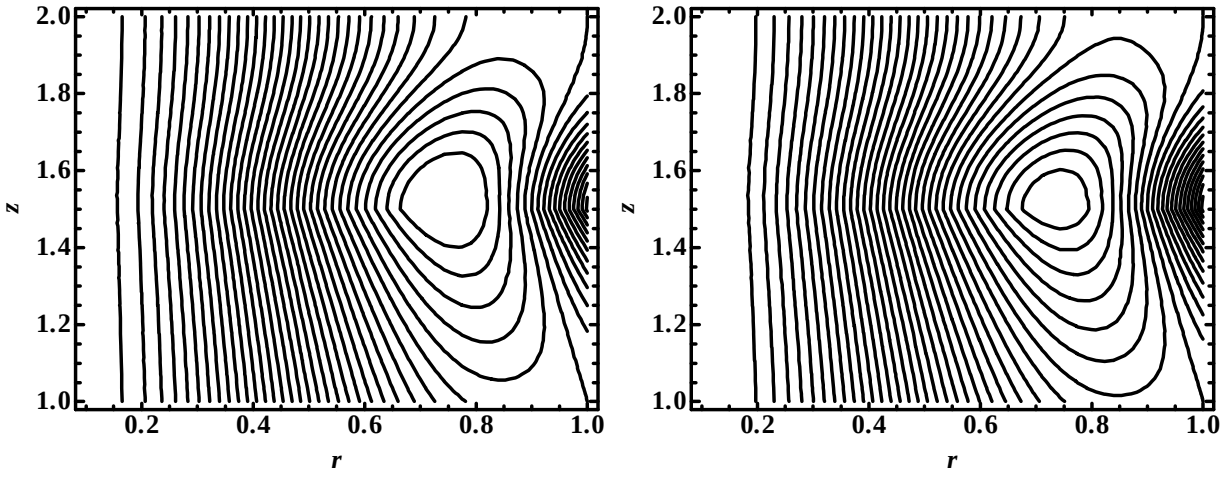

(a) **(b)**

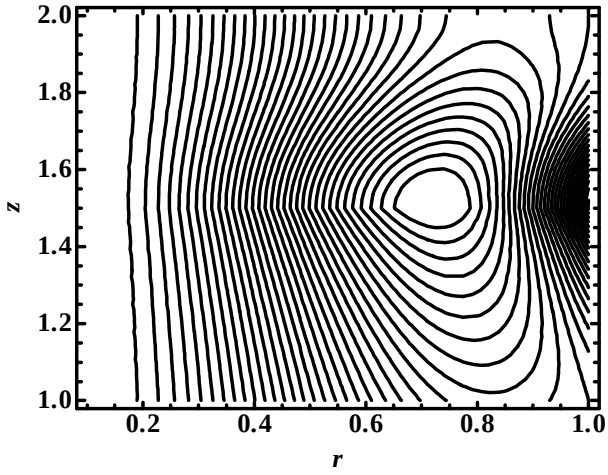

(c)

Figs. (4.14): Blood flow pattern for different values of (a) $D_a = 0.01$, (b) $D_a = 0.02$, (c) $D_a = 0.03$.

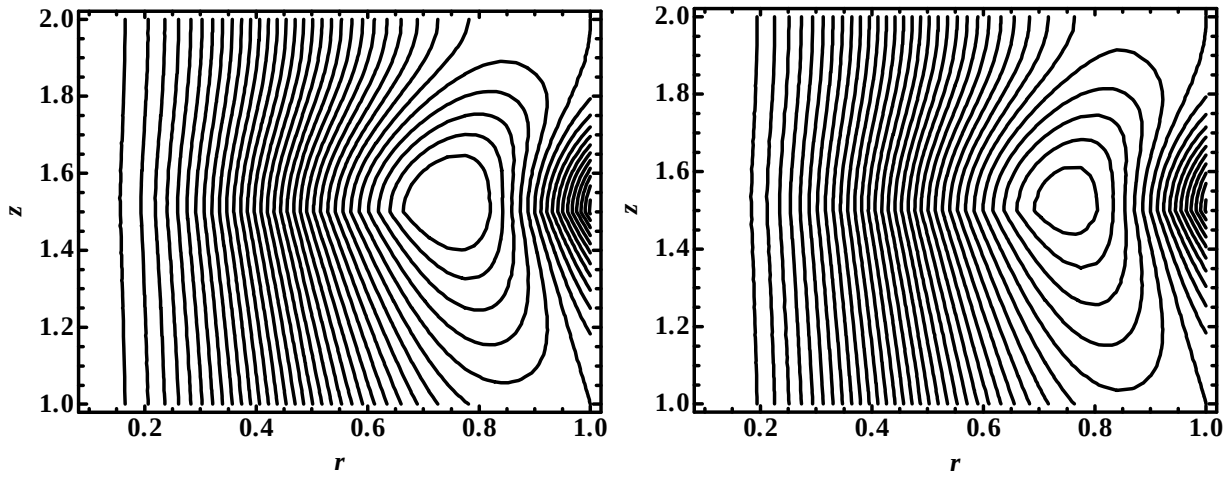

(a) (b)

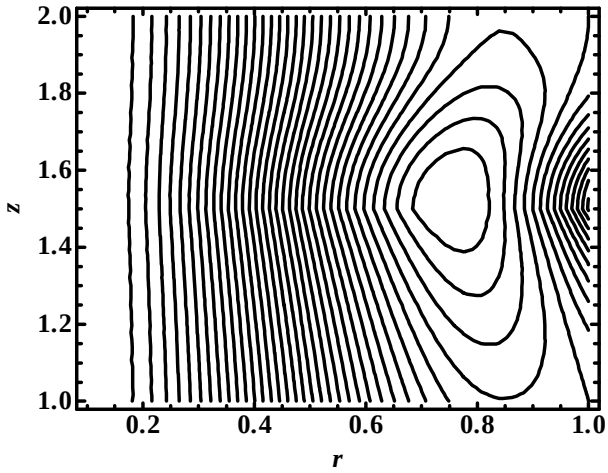

(c)

Figs. (4.15): Blood flow pattern for different values of (a) $s = 0.60$, (b) $s = 0.65$, (c) $s = 0.70$.

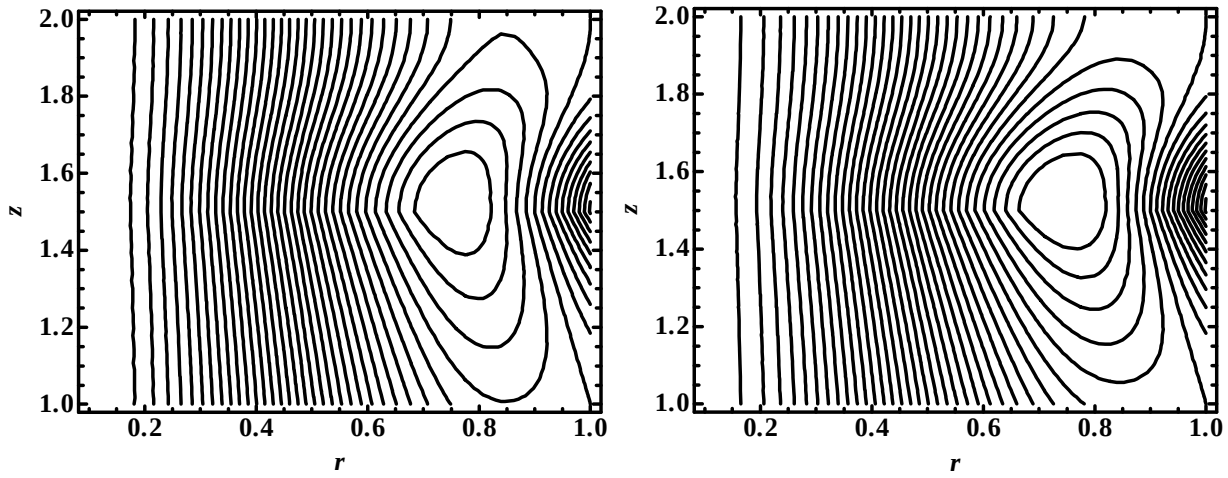

(a) (b)

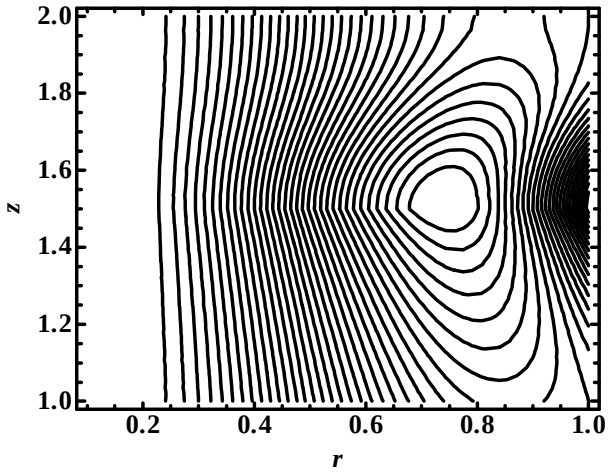

(c)

Figs. (4.16): Blood flow pattern for different values of (a) $\varepsilon = 0.10$, (b) $\varepsilon = 0.13$, (c) $\varepsilon = 0.16$.

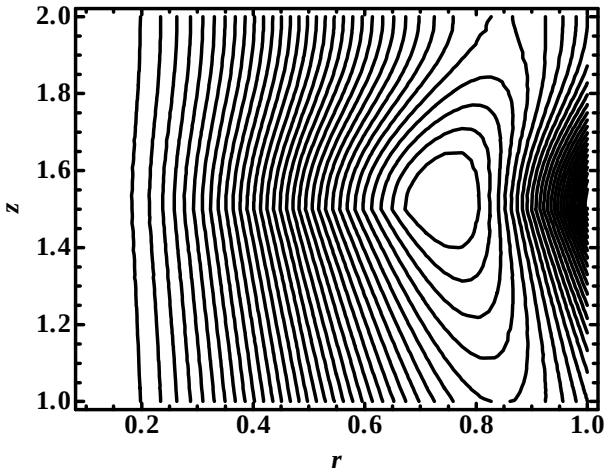

(a)

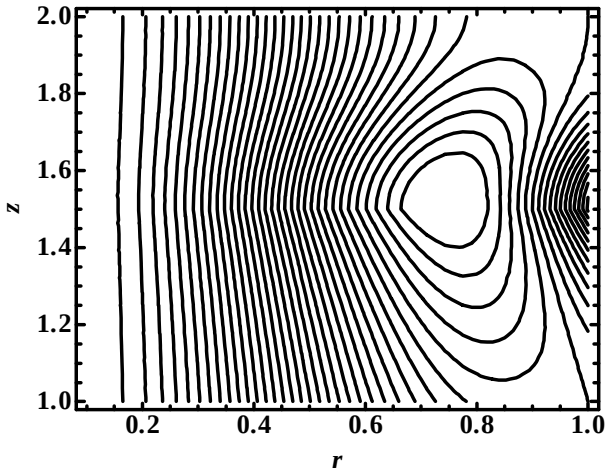

(b)

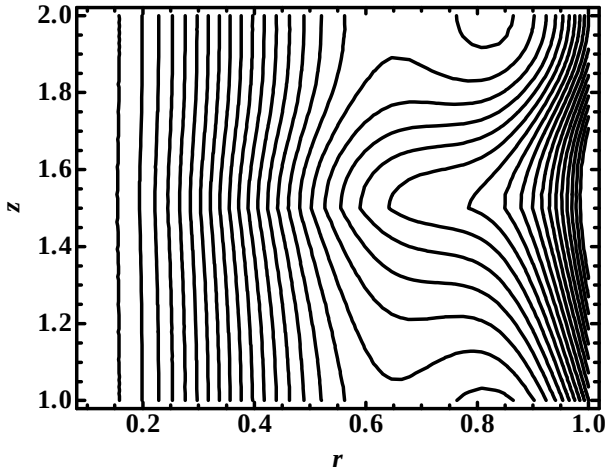

(c)

Figs. (4.17): Blood flow pattern for different values of (a) $\Phi = 0.00$, (b) $\Phi = 0.02$, (c) $\Phi = 0.04$.

w	Pure blood ($\Phi = 0.00$)			Copper Blood($\Phi = 0.01$)			Copper Blood ($\Phi = 0.02$)		
r	D_a=0.6	D_a=0.7	D_a=0.8	D_a=0.6	D_a=0.7	D_a=0.8	D_a=0.6	D_a=0.7	D_a=0.8
ε	0.00000	0.00000	0.00000	0.00000	0.00000	0.00000	0.00000	0.00000	0.00000
0.2	0.49485	0.49672	0.49834	0.50736	0.50885	0.51012	0.51919	0.52033	0.52127
0.3	0.76553	0.76808	0.77030	0.78003	0.78207	0.78379	0.79369	0.79526	0.79653
0.4	0.93971	0.94231	0.94456	0.95153	0.95360	0.95536	0.96264	0.96423	0.96553
0.5	1.05820	1.06037	1.06226	1.06508	1.06682	1.06830	1.07153	1.07287	1.07396
0.6	1.13983	1.14120	1.14238	1.14108	1.14217	1.14310	1.14222	1.14306	1.14375
0.7	1.19529	1.19550	1.19568	1.19144	1.19161	1.19175	1.18782	1.18795	1.18805
0.8	1.23152	1.23025	1.22915	1.22429	1.22327	1.22242	1.21751	1.21672	1.21609
h	1.26176	1.25749	1.25379	1.25554	1.25212	1.24924	1.24967	1.24704	1.24491

Table (4.1): Variations of velocity profile for different values of the Darcy number D_a.

w	Pure blood ($\Phi = 0.00$)			Copper Blood ($\Phi = 0.01$)			Copper Blood ($\Phi = 0.02$)		
r	s =0.10	s =0.15	s =0.2	s =0.10	s =0.15	s =0.20	s =0.10	s =0.15	s =0.20
ε	0.00000	0.00000	0.00000	0.00000	0.00000	0.00000	0.00000	0.00000	0.00000
0.2	0.49979	0.49593	0.49013	0.51122	0.50371	0.49242	0.52205	0.51117	0.49481
0.3	0.77228	0.76701	0.75910	0.78530	0.77505	0.75965	0.79760	0.78275	0.76044
0.4	0.94657	0.94122	0.93317	0.95689	0.94647	0.93081	0.96661	0.95151	0.92882
0.5	1.06395	1.05946	1.05272	1.06958	1.06085	1.04773	1.07486	1.06222	1.04321
0.6	1.14344	1.14063	1.13639	1.14390	1.13842	1.13018	1.14432	1.13638	1.12444
0.7	1.19584	1.19541	1.19476	1.19187	1.19103	1.18977	1.18814	1.18692	1.18509
0.8	1.22817	1.23078	1.23471	1.22167	1.22676	1.23441	1.21556	1.22294	1.23402
h	1.25048	1.25928	1.27250	1.24673	1.26384	1.28957	1.24314	1.26794	1.30521

Table (4.2): Variations of velocity profile for different values of the slip constant s.

Chapter 5

Impulsion of nanoparticles as a drug carrier for the theoretical investigation of stenosed arteries with magnetic effects

In this chapter, hemodynamics of stenosis is discussed to predict effect of atherosclerosis by means of mathematical models in the presence of uniform transverse magnetic field. The analysis is carried out using silver and copper nanoparticles as a drug carrier for the theoretical investigation of blood flow through inclined artery with composite stenosis. Exact solutions for the fluid temperature, velocity and pressure gradient are obtained under mild stenosis approximation. The expressions of current density distribution and axial induced magnetic field are also computed. The results indicate that with an increase in the magnetic Reynolds number and Strommers number resistance impedance to blood flow increases. Moreover, it is concluded from graphical results that hemodynamic effects of stenosed arteries minimize more effectively for Ag case when compared to other cases.

5.1 Fundamental equation of induced magnetic field

The system is stressed by an external magnetic field of strength $\frac{\bar{H}_0\bar{h}}{\bar{r}}$ and the total magnetic field will be $\bar{\mathbf{H}}^{+}(\overline{H}_r(\bar{r},\bar{z})+\frac{\bar{H}_0\bar{h}}{\bar{r}},0,\overline{H}_z(\bar{r},\bar{z}))$, where $\overline{H}_r$ and $\overline{H}_z$ are defined as the radial and axial components of total magnetic field. The steady governing equations are

1. Maxwell equations are

$$\begin{aligned}
\boldsymbol{\nabla}.\bar{\mathbf{H}}^{+} &= 0,\ \boldsymbol{\nabla}.\bar{\mathbf{E}}=0, && (5.1)\\
\boldsymbol{\nabla}\times\bar{\mathbf{H}}^{+} &= \bar{\mathbf{J}},\ \text{where } \bar{\mathbf{J}}=\sigma_{nf}\{\bar{\mathbf{E}}+\mu_{ef}(\bar{\mathbf{V}}\times\bar{\mathbf{H}}^{+})\}, && (5.2)\\
\boldsymbol{\nabla}\times\bar{\mathbf{E}} &= -\mu_{ef}\frac{\partial\bar{\mathbf{H}}^{+}}{\partial\bar{t}}, && (5.3)
\end{aligned}$$

2. Continuity and Navier Stokes equations are

$$\begin{aligned}
\boldsymbol{\nabla}.\bar{\mathbf{V}} &= 0, && (5.4)\\
\rho_{nf}\left(\frac{\partial\bar{\mathbf{V}}}{\partial t}+\bar{\mathbf{V}}.\boldsymbol{\nabla}\bar{\mathbf{V}}\right) &= -\boldsymbol{\nabla}p+\mu_{nf}\boldsymbol{\nabla}^2\bar{\mathbf{V}}+\rho_{nf}\mathbf{f}+\mu_{ef}(\bar{\mathbf{J}}\times\bar{\mathbf{H}}^{+}), && (5.5)
\end{aligned}$$

From Eqs. (5.2) to (5.4), we have

$$\frac{\partial\bar{\mathbf{H}}^{+}}{\partial\bar{t}}=\boldsymbol{\nabla}\times\left\{\bar{\mathbf{V}}\times\bar{\mathbf{H}}^{+}\right\}+\frac{1}{\sigma_{nf}\mu_{ef}}\boldsymbol{\nabla}^2\bar{\mathbf{H}}^{+}. \quad (5.6)$$

in which $\bar{\mathbf{E}}$ is defined as the induced electric field, $\bar{\mathbf{J}}$ as the electric current density, $\bar{\mathbf{V}}$ as the velocity component, $\mathbf{f}$ as the body force and p as the pressure. For the proposed nanofluid model σ_{nf} represents the electrical conductivity, μ_{ef} is the magnetic permeability, ρ_{nf} is the density and μ_{nf} is the nanofluid viscosity.

5.2 Formulation of the problem

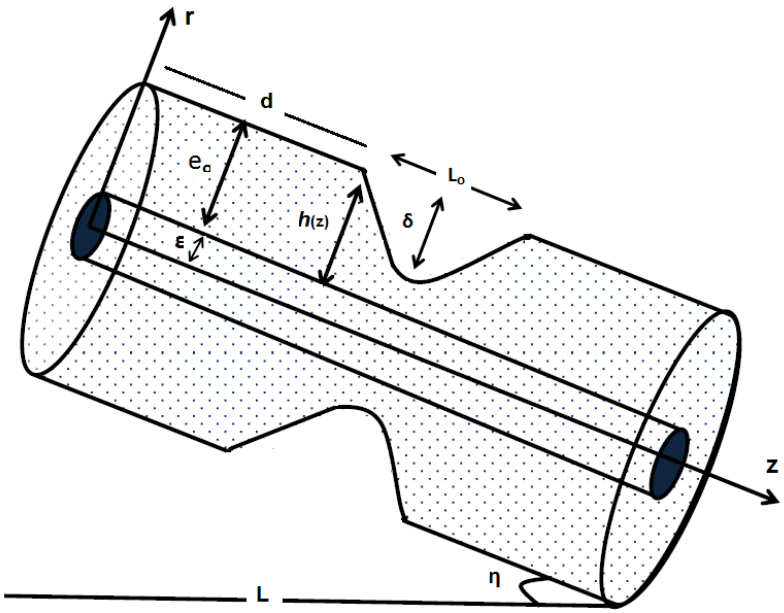

Fig. (5.1): Geometry of composite stenosed artery.

Consider the laminar and the incompressible blood flow in an inclined tube of length L. Let us consider the velocity vector as $\overline{\mathbf{V}} = (\overline{u}, 0, \overline{w})$, where $\overline{u}$ and $\overline{w}$ are defined as the velocity components in the r and z directions respectively. Heat transfer phenomenon is taken into account by giving temperature T_1 to the wall of the catheter and T_0 to the upper wall of the inclined artery. The geometry of composite stenosis in dimensional form is given as

$$\begin{aligned} \overline{h}(z) &= e_0 - \frac{2\delta}{L_0}(\overline{z} - d), && d \leq \overline{z} \leq d + \frac{L_0}{2}, \\ &= e_0 - \frac{\delta}{2}(1 + \cos\frac{2\pi}{L_0}(\overline{z} - d - \frac{L_0}{2})), && d + \frac{L_0}{2} \leq \overline{z} \leq d + L_0, \\ &= e_0, && \text{otherwise}, \end{aligned} \tag{5.7}$$

where d represents the position, L_0 as the length, δ as the height, $h(z)$ as the radius of the stenotic segment, e_0 as the radius of the non-stenotic segment (normal artery), ε as radius of the catheter and η as the inclination angle. The governing flow equations for nanofluid in the

presence of induced magnetic effects can be written as

$$\frac{\partial \overline{u}}{\partial \overline{r}} + \frac{\overline{u}}{\overline{r}} + \frac{\partial \overline{w}}{\partial \overline{z}} = 0, \tag{5.8}$$

$$\frac{\partial \overline{H}_r}{\partial \overline{r}} + \frac{\overline{H}_r}{\overline{r}} + \frac{\partial \overline{H}_z}{\partial \overline{z}} = 0, \tag{5.9}$$

$$\begin{aligned} \rho_{nf}\left(\overline{u}\frac{\partial \overline{u}}{\partial \overline{r}} + \overline{w}\frac{\partial \overline{u}}{\partial \overline{z}}\right) &= -\frac{\partial \overline{p}}{\partial \overline{r}} + \mu_{nf}\left(\frac{\partial^2 \overline{u}}{\partial \overline{r}^2} + \frac{1}{\overline{r}}\frac{\partial \overline{u}}{\partial \overline{r}} + \frac{\partial^2 \overline{u}}{\partial \overline{z}^2} - \frac{\overline{u}}{\overline{r}^2}\right) + \mu_{ef}\left(-\frac{\partial \overline{H}_z}{\partial \overline{r}}\right. \\ &\left. + \frac{\partial}{\partial \overline{z}}\left(\frac{H_o\overline{h}}{\overline{r}} + \overline{H}_r\right)\right)\overline{H}_z - g(\rho\gamma)_{nf}(\overline{T} - T_0)\cos\eta, \end{aligned} \tag{5.10}$$

$$\begin{aligned} \rho_{nf}\left(\overline{u}\frac{\partial \overline{w}}{\partial \overline{r}} + \overline{w}\frac{\partial \overline{w}}{\partial \overline{z}}\right) &= -\frac{\partial \overline{p}}{\partial \overline{z}} + \mu_{nf}\left(\frac{\partial^2 \overline{w}}{\partial \overline{r}^2} + \frac{1}{\overline{r}}\frac{\partial \overline{w}}{\partial \overline{r}} + \frac{\partial^2 \overline{w}}{\partial \overline{z}^2}\right) + \mu_{ef}\left(\frac{H_o\overline{h}}{\overline{r}} + \overline{H}_r\right) \\ &\left(\frac{\partial \overline{H}_z}{\partial \overline{r}} - \frac{\partial}{\partial \overline{z}}\left(\frac{H_o\overline{h}}{\overline{r}} + \overline{H}_r\right)\right) + g(\rho\gamma)_{nf}(\overline{T} - T_0)\sin\eta, \end{aligned} \tag{5.11}$$

$$\begin{aligned} \xi_{nf}\frac{\partial}{\partial \overline{z}}\left(-\frac{\partial \overline{H}_z}{\partial \overline{r}} + \frac{\partial}{\partial \overline{z}}\left(\frac{H_o\overline{h}}{\overline{r}} + \overline{H}_r\right)\right) &= \left(\overline{u}\frac{\partial}{\partial \overline{r}} + \overline{w}\frac{\partial}{\partial \overline{z}}\right)\left(\frac{H_o\overline{h}}{\overline{r}} + \overline{H}_r\right) \\ &- \left(\left(\frac{H_o\overline{h}}{\overline{r}} + \overline{H}_r\right)\frac{\partial \overline{u}}{\partial \overline{r}} + \overline{H}_z\frac{\partial \overline{u}}{\partial \overline{z}}\right), \end{aligned} \tag{5.12}$$

$$\begin{aligned} \xi_{nf}\left(\frac{1}{\overline{r}}\frac{\partial}{\partial \overline{r}}\left(\overline{r}\frac{\partial \overline{H}_z}{\partial \overline{r}}\right) - \frac{\partial}{\partial \overline{z}}\left(\frac{1}{\overline{r}} + \frac{\partial}{\partial \overline{r}}\right)\left(\frac{H_o\overline{h}}{\overline{r}} + \overline{H}_r\right)\right) &= \left(\overline{u}\frac{\partial}{\partial \overline{r}} + \overline{w}\frac{\partial}{\partial \overline{z}}\right)\overline{H}_z - \left(\frac{H_o\overline{h}}{\overline{r}} + \right. \\ &\left. \overline{H}_r\right)\frac{\partial \overline{w}}{\partial \overline{r}} - \overline{H}_z\frac{\partial \overline{w}}{\partial \overline{z}}, \end{aligned} \tag{5.13}$$

$$\left(\frac{\partial \overline{T}}{\partial \overline{t}} + \overline{u}\frac{\partial \overline{T}}{\partial \overline{r}} + \overline{w}\frac{\partial \overline{T}}{\partial \overline{z}}\right) = \frac{K_{nf}}{(\rho c_p)_{nf}}\left(\frac{\partial^2 \overline{T}}{\partial \overline{r}^2} + \frac{1}{\overline{r}}\frac{\partial \overline{T}}{\partial \overline{r}} + \frac{\partial^2 \overline{T}}{\partial \overline{z}^2}\right) + \frac{Q_0}{(\rho c_p)_{nf}}. \tag{5.14}$$

For the proposed nanofluid model thermo physical properties are given as

$$\frac{\mu_{nf}}{\mu_f}=\frac{1}{(1-\Phi)^{2.5}},\ \frac{\mu_{ef}}{\mu_e}=\frac{1}{(1-\Phi)^{2.5}},\ \rho_{nf}=(1-\Phi)\rho_f+\Phi\rho_s,$$
$$(\rho\gamma)_{nf}=(1-\Phi)(\rho\gamma)_f+\Phi(\rho\gamma),\ (\rho c_p)_{nf}=(1-\Phi)(\rho c_p)_f+\Phi(\rho c_p)_s,$$
$$\frac{K_{nf}}{K_f}=\frac{(K_s+2K_f)-2\Phi(K_f-K_s)}{(K_s+2K_f)+\Phi(K_f-K_s)},\ \frac{\sigma_{nf}}{\sigma_f}=1+\frac{3\left(\frac{\sigma_s}{\sigma_f}-1\right)\Phi}{\left(\frac{\sigma_s}{\sigma_f}+2\right)-\left(\frac{\sigma_s}{\sigma_f}-1\right)\Phi},$$
$$\alpha_{nf}=\frac{K_{nf}}{(\rho c_p)_{nf}},\ \xi_{nf}=\frac{1}{\sigma_{nf}\mu_{ef}}. \tag{5.15}$$

The non-dimensional variables are defined as

$$\begin{aligned}
r &= \frac{\overline{r}}{e_0},\ w=\frac{\overline{w}}{u_o},\ u=\frac{L_o\overline{u}}{u_o\delta},\ p=\frac{e_0^2\overline{p}}{u_oL_o\mu_f},\ \beta=\frac{Q_0e_0^2}{(T_1-T_o)K_f},\\
d^* &= \frac{d}{L_o},\ R_{en}=\frac{e_0u_o\rho_f}{\mu_f},\ G_r=\frac{g\gamma_f\rho_fe_0^2(T_1-T_o)}{u_0\mu_f},\ \theta=\frac{\overline{T}-T_o}{T_1-T_o},\\
z &= \frac{\overline{z}}{L_o}, S^2=\frac{H_0^2\mu_e}{\rho u_o^2},\ H_r=\frac{\overline{H}_r}{H_o},\ H_z=\frac{\overline{H}_z}{H_o},\ R_m=e_0\sigma_fu_o\mu_e.
\end{aligned} \tag{5.16}$$

In the above equations S^2 represents the Strommers number and R_m is the magnetic Reynolds number. Using Eq. (5.16), mild stenosis case $\delta^*=\frac{\delta}{e_0}\ll 1$ and taking extra condition $\epsilon=\frac{e_0}{L_0}\approx O(1)$, the constitutive Eqs. (5.9) to (5.14) take the form

$$\frac{\partial H_r}{\partial r}+\frac{H_r}{r}=0, \tag{5.17}$$

$$\frac{\partial p}{\partial r}=0, \tag{5.18}$$

$$\begin{aligned}
\frac{\partial p}{\partial z}\frac{\mu_f}{\mu_{nf}} &= \frac{\partial^2 w}{\partial r^2}+\frac{1}{r}\frac{\partial w}{\partial r}+S^2R_{en}\left(\frac{h}{r}+H_r\right)\left(\frac{\partial H_z}{\partial r}\right)\frac{\mu_f}{\mu_{nf}}\frac{\mu_{ef}}{\mu_e}+\\
&\quad \frac{\mu_f}{\mu_{nf}}\frac{(\rho\gamma)_{nf}}{(\rho\gamma)_f}G_r\theta\sin\eta,
\end{aligned} \tag{5.19}$$

$$\left(\frac{1}{r}\frac{\partial}{\partial r}\left(r\frac{\partial H_z}{\partial r}\right)\right) = -\frac{R_m}{\chi}\left(\frac{h}{r}+H_r\right)\left(\frac{\partial w}{\partial r}\right), \tag{5.20}$$

$$\frac{\partial^2\theta}{\partial r^2}+\frac{1}{r}\frac{\partial\theta}{\partial r}+\frac{K_f}{K_{nf}}\beta = 0, \tag{5.21}$$

where $\chi = \frac{1}{\frac{\sigma_{nf}}{\sigma_f}\frac{\mu_{ef}}{\mu_e}}$. The boundary conditions and geometry of stenosis in dimensionless form are defined as

$$\begin{aligned} h(z) &= 1-2\delta^*(z-d^*), && d^* \le z \le d^*+\frac{1}{2}, \\ &= 1-\frac{\delta^*}{2}(1+\cos 2\pi(z-d^*-\frac{1}{2})), && d^*+\frac{1}{2} \le z \le d^*+1, \\ &= 1, && \text{otherwise.} \end{aligned} \tag{5.22}$$

$$w = 0, \quad \theta = 0, \quad \text{and} \quad H_z = H_r = 0 \qquad \text{at} \quad r = h(z), \tag{5.23}$$

$$w = 0, \quad \theta = 1, \qquad \text{at} \quad r = \varepsilon. \tag{5.24}$$

5.3 Solution of the problem

The solution of Eq. (5.17) shows that $H_r = 0$, substituting into Eq. (5.20) we get

$$J_\theta = \frac{\partial H_z}{\partial r} = -\frac{R_m}{\chi}\frac{hw}{r}+c_1. \tag{5.25}$$

Since $J_\theta = 0$ at $r = h$ from Eq. (5.25), gives $c_1 = 0$, then replace it in Eq. (5.19). The exact solutions of Eqs. (5.19) – (5.21) using Eqs. (5.23) and (5.24) are directly written as

$$\begin{aligned} \theta &= \frac{\ln h-\ln r}{\ln h-\ln\varepsilon}+\left(\frac{K_s(1-\Phi)+K_f(2+\Phi)}{K_s(1+2\Phi)+2K_f(1-\Phi)}\right)\left(\frac{\beta}{4(\ln h-\ln\varepsilon)}\right)((-r^2+\varepsilon^2) \\ &\quad \ln h+(h-\varepsilon)(h+\varepsilon)\ln r+(-h^2+\varepsilon^2)\ln\varepsilon), \end{aligned} \tag{5.26}$$

$$
\begin{aligned}
w &= \frac{dp}{dz}\frac{(1-\Phi)^{2.5}}{(-4+K)(h^{2\sqrt{K}}-\varepsilon^{2\sqrt{K}})} r^{-\sqrt{K}}(h^{2\sqrt{K}}(-r^{-\sqrt{K}}+\varepsilon^{2\sqrt{K}})+r^{\sqrt{K}}\varepsilon^{\sqrt{K}}(-r^{-\sqrt{K}} \\
&\quad \varepsilon^2+r^2\varepsilon^{\sqrt{K}})+h^{2+\sqrt{K}}(r^{2\sqrt{K}}-\varepsilon^{2\sqrt{K}}))+\frac{G_r(1-\Phi)^{2.5}}{2(-4+K)^2}(((1-\Phi)+\Phi\frac{\rho_s\gamma_s}{\rho_f\gamma_f})\sin\eta) \\
&\quad (\frac{8x_2r^2}{(-4+K)^2}+\frac{2x_3r^2}{-4+K}-\frac{2x_1r^4}{-16+K}-2x_5h^{\sqrt{K}}r^{-\sqrt{K}}+\frac{2x_2r^2}{(-4+K)}\ln r)+ \\
&\quad \frac{(x_5-x_6)r^{-\sqrt{K}}(-h^{2\sqrt{K}}+r^{2\sqrt{K}})\varepsilon^{\sqrt{K}}}{-h^{\sqrt{K}}+\varepsilon^{\sqrt{K}}}+\frac{(x_5+x_6)r^{-\sqrt{K}}(h^{2\sqrt{K}}-r^{2\sqrt{K}})\varepsilon^{\sqrt{K}}}{h^{\sqrt{K}}+\varepsilon^{\sqrt{K}}}), \quad (5.27)
\end{aligned}
$$

where $K=\frac{S^2h^2R_mR_{en}}{\chi}$ and flow rate is given as

$$
F=\int_{\varepsilon}^{h} rw dr. \tag{5.28}
$$

Using Eq. (5.27) into Eq. (5.28), we get the expression for pressure gradient as follows

$$
\frac{dp}{dz}=\frac{F-x_8x_7((1-\Phi)+\Phi\frac{\rho_s\gamma_s}{\rho_f\gamma_f})}{(1-\Phi)^{2.5}x_6}. \tag{5.29}
$$

The pressure drop from above Eq. (5.29) can be defined as

$$
\Delta p=\int_0^L\left(-\frac{dp}{dz}\right)dz. \tag{5.30}
$$

Using Eq. (5.30), the impedance resistance can be evaluated as

$$
\begin{aligned}
\lambda=\frac{\Delta p}{F}=\int_0^{d^*}\Omega_2(z)\mid_{h=1}dz+\int_{d^*}^{d^*+\frac{1}{2}}\Omega_2(z)dz+\int_{d^*+\frac{1}{2}}^{d^*+1}\Omega_2(z)dz+ \\
\int_{d^*+1}^{L}\Omega_2(z)\mid_{h=1}dz, \qquad (5.31)
\end{aligned}
$$

where

$$\Omega_2(z) = \frac{1}{F}\left(\frac{-F + x_8 x_7((1-\Phi) + \Phi\frac{\rho_s\gamma_s}{\rho_f\gamma_f})}{(1-\Phi)^{2.5}x_6}\right). \tag{5.32}$$

Using Eq. (5.32) into Eq. (5.31), we get

$$\lambda = \frac{\Delta p}{F} = (L-1)\Omega(z)_2\mid_{h=1} + \int_{d^*}^{d^*+\frac{1}{2}} \Omega(z)_2 dz + \int_{d^*+\frac{1}{2}}^{d^*+1} \Omega(z)_2 dz. \tag{5.33}$$

The expression for axial induced magnetic field H_z and the current density distribution J_θ can be obtained using Eq. (5.27) into Eq. (5.25) and from some straight forward calculation we have

$$\begin{aligned} J_\theta = {} & \frac{1}{(-4+K)(h^{2\sqrt{K}} - \varepsilon^{2\sqrt{K}})\chi}\frac{dp}{dz}((1-\Phi)^{2.5} h r^{-1-\sqrt{K}} R_m (h^{2\sqrt{K}}(r^{2+\sqrt{K}} - \\ & \varepsilon^{2+\sqrt{K}}) + r^{\sqrt{K}}\varepsilon^{\sqrt{K}}(r^{\sqrt{K}}\varepsilon^2 + r^2\varepsilon^{\sqrt{K}}) + h^{2+\sqrt{K}}(-r^{2\sqrt{K}} + \varepsilon^{2\sqrt{K}}))) + \\ & \frac{x_9 h R_m}{2r\chi}(-\frac{8x_2 r^2}{(-4+K)^2} - \frac{2x_3 r^2}{-4+K} + \frac{2x_1 r^4}{-16+K} + 2x_5 h^{\sqrt{K}} r^{-\sqrt{K}} + \\ & \frac{(x_5 - x_6) r^{-\sqrt{K}}(-h^{2\sqrt{K}} + r^{2\sqrt{K}})}{(h^{2\sqrt{K}} - \varepsilon^{2\sqrt{K}})} + \frac{(x_5 + x_6) r^{-\sqrt{K}}(-h^{2\sqrt{K}} + r^{2\sqrt{K}})}{(h^{2\sqrt{K}} - \varepsilon^{2\sqrt{K}})} - \\ & \frac{2x_2 r^2 \ln r}{-4+K}), \end{aligned} \tag{5.34}$$

$$\begin{aligned} H_z = {} & \frac{1}{2(-4+K)\sqrt{K}\chi(h^{2\sqrt{K}} - \varepsilon^{2\sqrt{K}})}\frac{dp}{dz}((1-\Phi)^{2.5}(-4+K) h r^{-\sqrt{K}} R_m (h^{\sqrt{K}} \\ & r^{\sqrt{K}}(-2h^2 r^{\sqrt{K}} + h^{\sqrt{K}}(-h^2(-2+\sqrt{K}) + \sqrt{K} r^2)) + 2(h^{\sqrt{K}} - r^{\sqrt{K}})^2 \\ & \varepsilon^{2+\sqrt{K}} + (-2h^{2+\sqrt{K}} + r^{\sqrt{K}}(h^2(2+\sqrt{K}) - \sqrt{K} r^2))\varepsilon^{2\sqrt{K}})) + \frac{h x_9 R_m}{4\chi}(- \\ & \frac{x_2(-12+K)(h-r)(h+r)}{(-4+K)^2} + \frac{x_1(-h^4 + r^4)}{-16+K} + \frac{4x_5(1 - h^{\sqrt{K}} r^{-\sqrt{K}})}{\sqrt{K}} + \\ & \frac{2(x_5 - x_6) r^{-\sqrt{K}}(h^{\sqrt{K}} - r^{\sqrt{K}})^2}{\sqrt{K}(h^{\sqrt{K}} - \varepsilon^{\sqrt{K}})} + \frac{2(x_5 + x_6) r^{-\sqrt{K}}(h^{\sqrt{K}} - r^{\sqrt{K}})^2}{\sqrt{K}(h^{\sqrt{K}} + \varepsilon^{\sqrt{K}})} + \\ & \frac{2(x_3(h-r)(h+r) + x_2 h^2 \ln h - x_2 r^2 \ln r}{(-4+K)}). \end{aligned} \tag{5.35}$$

The wall shear stress is obtained by using Eq. (5.27) in following expression,

$$S_{rz} = -\frac{\mu_{nf}}{\mu_f}\left(\frac{\partial w}{\partial r}\right)_{r=h}, \tag{5.36}$$

or

$$\begin{aligned} S_{rz} = -\Bigg(&\frac{dp}{dz}\frac{(h^{2+2\sqrt{K}}(-2+\sqrt{K}) - 2h^{\sqrt{K}}\sqrt{K}\varepsilon^{2+\sqrt{K}} + h^2(2+\sqrt{K})\varepsilon^{2\sqrt{K}})}{h(-4+K)(h^{2\sqrt{K}} - \varepsilon^{2\sqrt{K}})} \\ &+ \frac{x_9}{h(1-\Phi)^{2.5}}(-\frac{4x_1h^4}{-16+K} + x_5\sqrt{K} + \frac{h^2(2x_3(-4+K) + x_2(4+K))}{(-4+K)^2} \\ &+\frac{(x_5-x_6)h^{\sqrt{K}}\sqrt{K}}{(-h^{2\sqrt{K}} + \varepsilon^{2\sqrt{K}})} - \frac{(x_5+x_6)h^{\sqrt{K}}\sqrt{K}}{(h^{2\sqrt{K}} + \varepsilon^{2\sqrt{K}})} + \frac{2x_2h^2\ln h}{-4+K}\Bigg)\Bigg). \end{aligned} \tag{5.37}$$

5.4 Appendix

$$x_o = \left(\frac{K_s(1-\Phi) + K_f(2+\Phi)}{K_s(1+2\Phi) + 2K_f(1-\Phi)}\right),\ x_1 = \frac{\beta x_o}{4},\ x_2 = \frac{-4 + \beta x_o(h-\varepsilon)(h+\varepsilon)}{4(\ln h - \ln\varepsilon)},$$
$$x_3 = \frac{1}{4(\ln h - \ln\varepsilon)}(\beta x_o\varepsilon^2 4\ln h\ln h - \beta x_o h^2\ln\varepsilon),\ x_4 = -\frac{x_3h^2}{4-K} + \frac{x_1h^4}{16-K} +$$
$$\frac{x_2h^2(4+(-4+K)\ln h)}{(4-K)^2},\ x_5 = -\frac{x_3\varepsilon^2}{4-K} + \frac{x_1\varepsilon^4}{16-K} + \frac{x_2\varepsilon^2(4+(-4+K)\ln\varepsilon)}{(4-K)^2},$$
$$x_6 = \frac{1}{(4(-4+K)^2(h^{2\sqrt{K}} - \varepsilon^{2\sqrt{K}}))}((1-\Phi)^{2.5}(-16h^{2+\sqrt{K}}\sqrt{K}\varepsilon^{2+\sqrt{K}} + \varepsilon^{2+\sqrt{K}}(h^4$$
$$(2+\sqrt{K})^2 - (-2+\sqrt{K})^2\varepsilon^4) + h^{2\sqrt{K}}(-h^4(-2+\sqrt{K})^2 + (2+\sqrt{K})^2\varepsilon^4))),$$
$$x_7 = \frac{1}{48}(\frac{48h^2x_5}{-2+\sqrt{K}} + \frac{48\varepsilon^2x_6}{2+\sqrt{K}} - \frac{3(-20+K)(h^4-\varepsilon^4)x_2}{2+\sqrt{K}} + \frac{12(h^4-\varepsilon^4)x_3}{-4+K} +$$
$$\frac{8(-h^6+\varepsilon^6)x_1}{-16+K} - \frac{48(h-\varepsilon)(h+\varepsilon)(x_5-x_6)h^{\sqrt{K}}\sqrt{K}}{(-4+K)(h^{\sqrt{K}} - \varepsilon^{\sqrt{K}})} - \frac{48(h^2+\varepsilon^2)(x_5+x_6)h^{\sqrt{K}}\sqrt{K}}{(-4+K)(h^{\sqrt{K}} - \varepsilon^{\sqrt{K}})}$$
$$+\frac{12x_2(h^4\ln h - \varepsilon^4\ln\varepsilon)}{(-4+K)}),\ x_8 = (1-\Phi)^{2.5}G_r\sin\eta,\ x_9 = x_8((1-\Phi) + \Phi\frac{\rho_s\gamma_s}{\rho_f\gamma_f}).$$

5.5 Results and discussion

In order to discuss the implementation of the extended set of Navier-Stokes equations with additional nanoparticle contributions and induced magnetic field we have plotted the graphs of the axial induced magnetic field, current density, wall shear stress, impedance resistance to blood flow, temperature profile and stream lines. The graphs are plotted with the help of different emerging flow parameters by keeping constants such as $\Phi = 0.07$, $R_m = 2$, $S = 0.8$, $\beta = 0.9$, $L = 3$, $z = 1.5$, $\delta = 0.2$, $F = 0.03$, $R_{en} = 1$, $G_r = 2$, $d^* = 1.0$, $\eta = 0$, $\frac{\pi}{4}$, $\frac{\pi}{2}$ (vertical, horizontal, inclined arteries). Figs. (5.2) to (5.7) are plotted for wall shear stress investigation along z in the composite stenotic region. We observed here that for the stenotic curve ($1.0 \leq z \leq 1.5$) wall shear stress starts increasing from the beginning of the stenosis until a maximum constriction (i.e., throat) is obtained then decreases to reach the end of the stenotic segment ($1.5 \leq z \leq 2.0$). Fig. (5.2) is plotted to show the effect of stenosis height δ on the wall of stenosed arteries. It is analyzed from this figure that with an increase in stenosis height δ stresses on the wall of stenosed arteries increases. The wall shear stress for different values of inclination angle η is given in Fig. (5.3). It is found that the stresses on the wall of horizontal composite stenosed arteries are higher when compared to the inclined and vertical composite stenosed arteries. The graph with different variations of Strommers number S and magnetic Reynolds number R_m are discussed through Figs. (5.4) and (5.5). The influence of the Strommers number S and magnetic Reynolds R_m on wall of the inclined stenosed arteries depicts that the magnetic field become stronger with an increase in these parameters. Moreover, these figures also show that the significantly strong magnetic field increases the stresses on the wall of inclined stenosed arteries. Figs. (5.6) and (5.7) are plotted for different values of the heat source parameter β and Grashof number G_r. It is depicted from these figures that the stresses on the wall of inclined stenosed arteries start decreasing with an increase in internal heat source parameter and viscous forces. The resistance impedance to blood flow is important to discuss the disease section properly and plotted here from Fig. (5.8) $-$ (5.12) against the stenosis height δ. The resistance impedance to blood flow for different values of Strommers number S and magnetic Reynolds number R_m is given in Figs. (5.8) and (5.9). It is depicted from these figures that resistance impedance to flow increases because magnetic field becomes more stronger with an in the values of the Strommers number S and magnetic Reynolds number

R_m. This increase in the resistance is due to the fact that when magnetic field is applied to the fluid the Lorentz force will oppose the flow, which tends to retard the flow of blood. The effects of Grashof number G_r and heat source parameter β on the wall of inclined stenosed arteries are discussed in Figs. (5.10) and (5.11). It is observed from these graphs that with an increase in Grashof number G_r and heat source parameter β the resistance impedance to blood flow decreases. In Fig. (5.12), it is observed that resistance to blood flow is little higher for horizontal stenosed arteries as comparing to the vertical and inclined stenosed arteries. The variation of current density distribution J_θ along r (radial direction) is discussed through Figs. (5.13) and (5.14). Fig. (5.13) is plotted to show that the influence of magnetic Reynolds number R_m on current density distribution and concluded that strong magnetic field tend to decrease in current density distribution between the region $\varepsilon \leq r \leq 0.58$, while tend to increase between the region $0.58 < r \leq h$. The effects of Strommers number S on current density distribution are given in Fig. (5.14). It is depicted from this graph that current density distribution increases between the region $\varepsilon \leq r \leq 0.58$, while the opposite trend is observed in the rest of the region $0.58 < r \leq h$. The graphs of axial induced magnetic field are plotted through Figs. (5.15) and (5.16). The variations of magnetic Reynolds number R_m are discussed in Fig. (5.15). It is observed from this figure that the axial induced magnetic field increases between the region $\varepsilon \leq r \leq 0.38$, while decreases between the region $0.38 < r \leq h$. Further, this graph also shows that the axial induced magnetic field increases throughout the inclined stenosed arteries for pure blood case with an increase in the values of the magnetic Reynolds number R_m. Fig. (5.16) is plotted to discuss the effects of Strommers number S and observed that the axial induced magnetic field decreases between the region $\varepsilon \leq r \leq 0.38$, while the opposite trend is observed between the region $0.38 < r \leq h$. The variations of temperature profile against radial direction r are plotted through Figs. $(5.17) - (5.18)$ for different values of interest. The temperature profile is plotted for different values of the heat source parameter β and nanoparticle volume fraction Φ. It is observed that temperature profile increases with an increase in the values of the heat source parameter β and decreases for different values of the nanoparticle volume fraction Φ. Stream lines by trapping represent an interesting phenomenon for blood flow patterns of an internally circulating bolus between the catheter and the artery wall. This flow pattern has been discussed here through Figs. (5.19) to (5.24) for silver and copper nanoparticles. The trapping

phenomenon shows that the size of trapping bolus increases for the copper nanoparticles case. Figs. (5.19) and (5.20) are prepared to discuss the effects of stenosis height δ and it is observed from this blood flow pattern that the number of trapping bolus increases by the closed stream lines. From Figs. (5.21) and (5.22), it is observed that the significantly strong magnetic field tend to increase in the size of trapping bolus with an increases in the values of the magnetic Reynolds number R_m. The effects of Strommers number S are given in Figs. (5.23) and (5.24). It is depicted from these stream lines patterns that with an increase in the values of Strommers number S magnetic effects enhance the trapping phenomenon. The tables (5.1) and (5.2) are illustrated to show the variations of velocity profile for different values of the magnetic Reynolds number R_m and Strommers number S against radial direction r. Tables (5.1) and (5.2), shows that with an increase in the values of the magnetic Reynolds number R_m and Strommers number S velocity profile decreases near the wall of the catheter between the region $\varepsilon \leq r \leq 0.5$, while increases near the wall of the inclined composite stenosed arteries between the region $0.5 < r \leq h$.

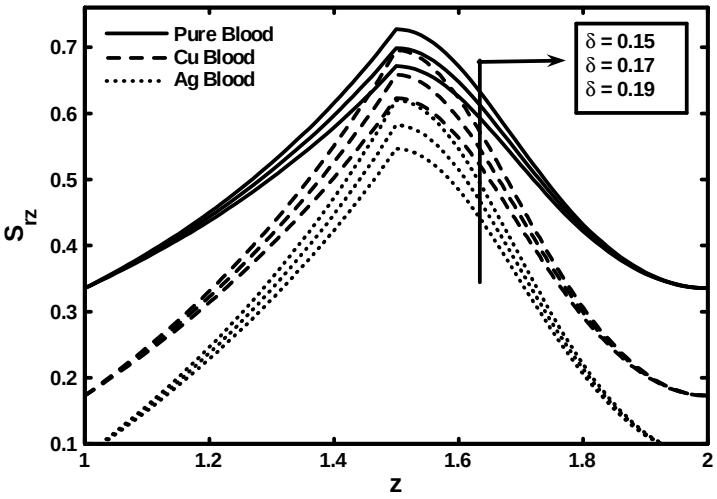

Fig. (5.2): Variation of wall shear stress for different values of the stenosis height δ.

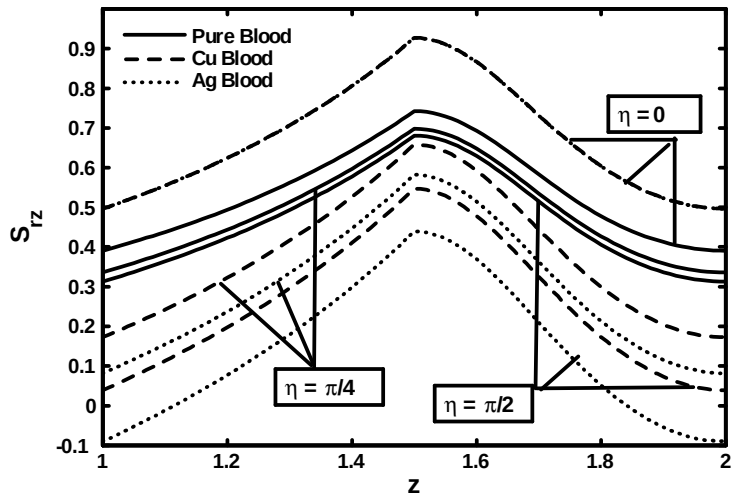

Fig. (5.3): Variation of wall shear stress for different values of the inclination angle η.

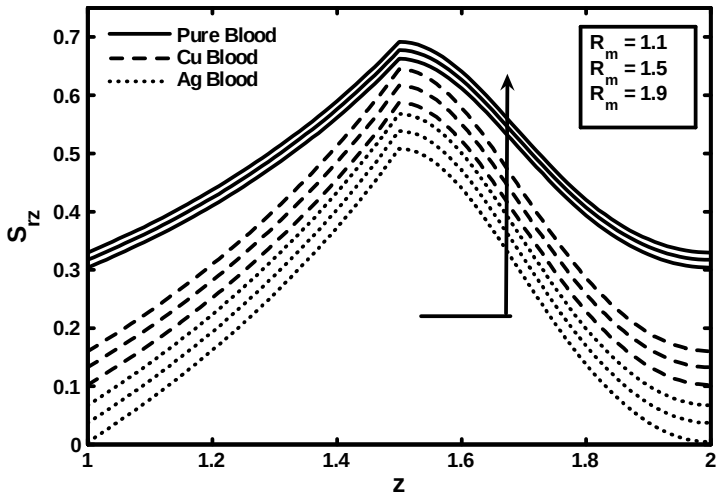

Fig. (5.4): Variation of wall shear stress for different values of magnetic Reynolds R_m.

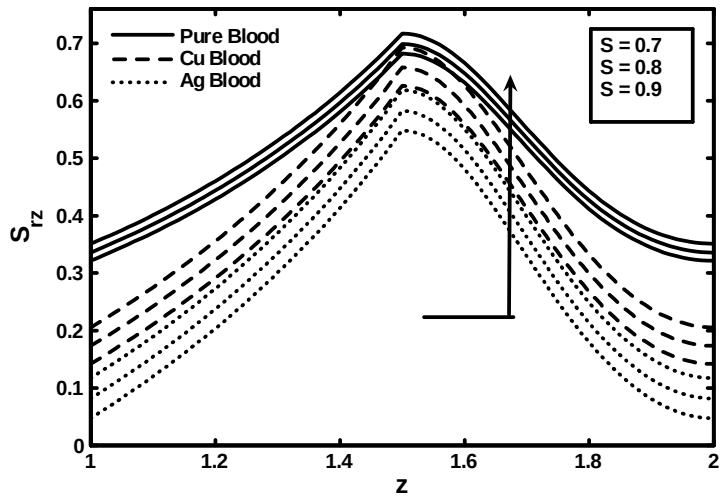

Fig. (5.5): Variation of wall shear stress for different values of values of Strommers number S.

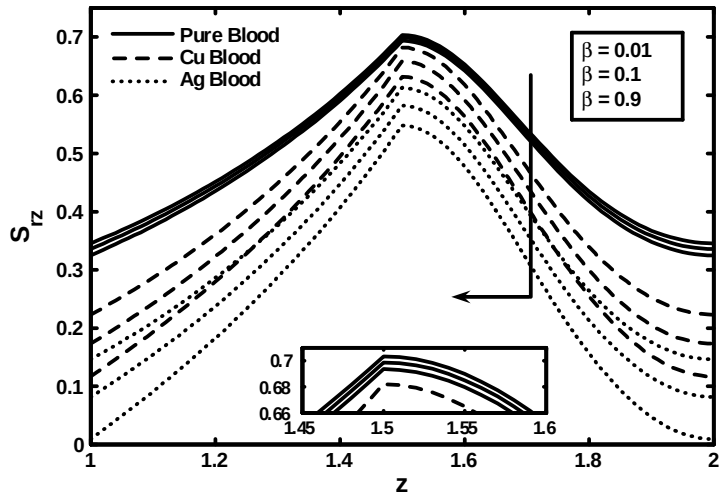

Fig. (5.6): Variation of wall shear stress for different values of the heat source parameter β.

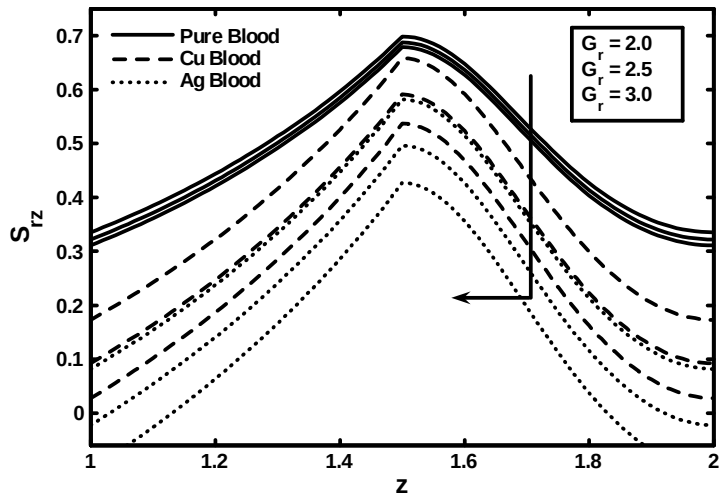

Fig. (5.7): Variation of wall shear stress for different values of the Grashof number G_r.

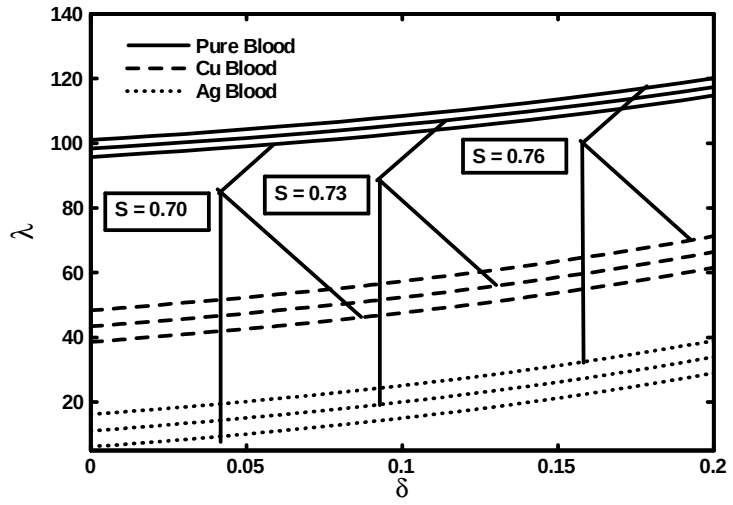

Fig. (5.8): Variation of resistance impedance for different values of Strommers number S.

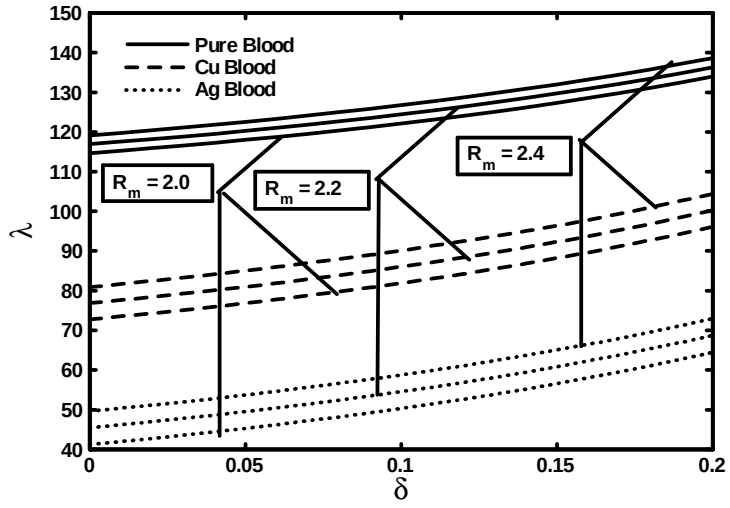

Fig. (5.9): Variation of resistance impedance for different values of magnetic Reynolds R_m.

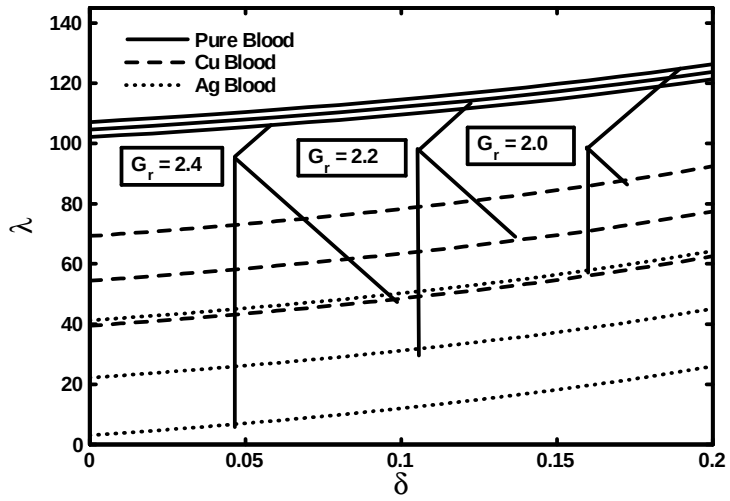

Fig. (5.10): Variation of resistance impedance for different values of Grashof number G_r.

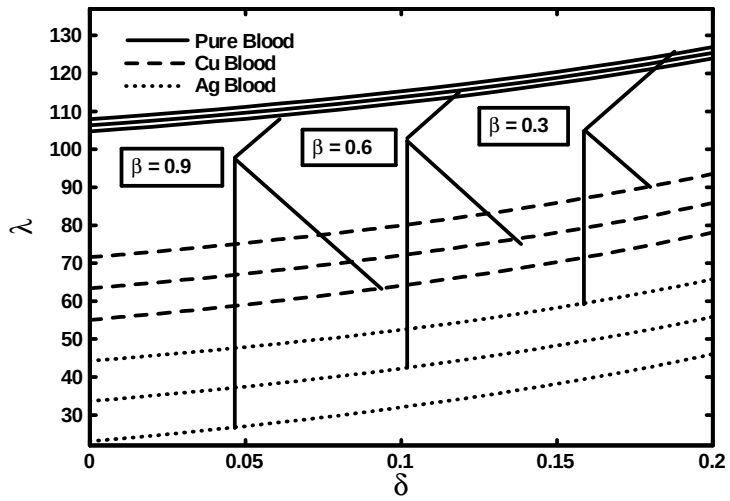

Fig. (5.11): Variation of resistance impedance to blood flow for different values of heat source parameter β.

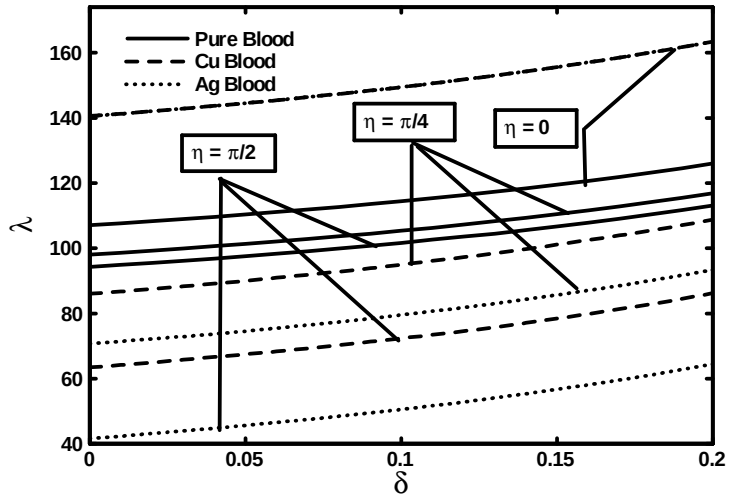

Fig. (5.12): Variation of resistance impedance to blood flow for different values of inclination angle η.

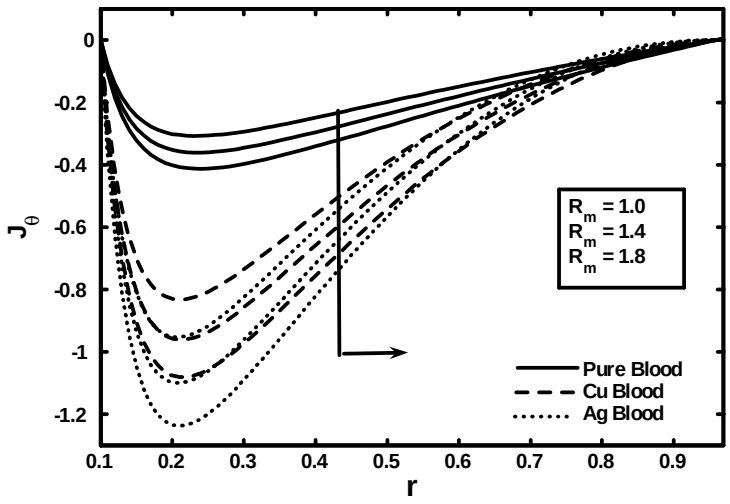

Fig. (5.13): Variation of current density distribution for different values of magnetic Reynolds R_m.

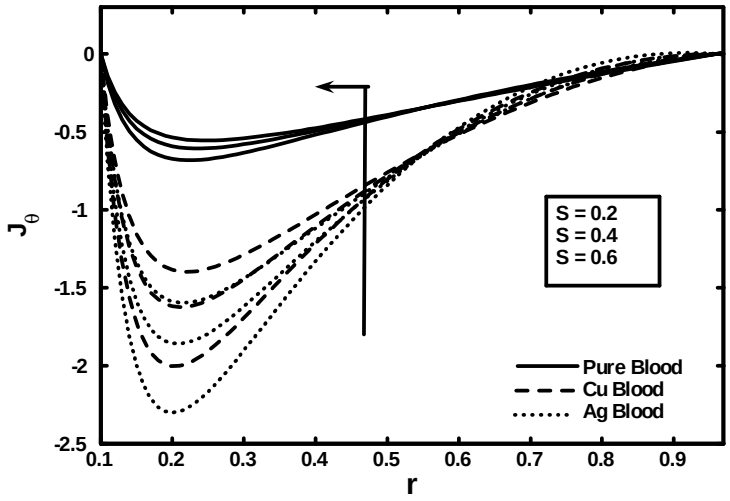

Fig. (5.14): Variation of current density distribution for different values of Strommers number S.

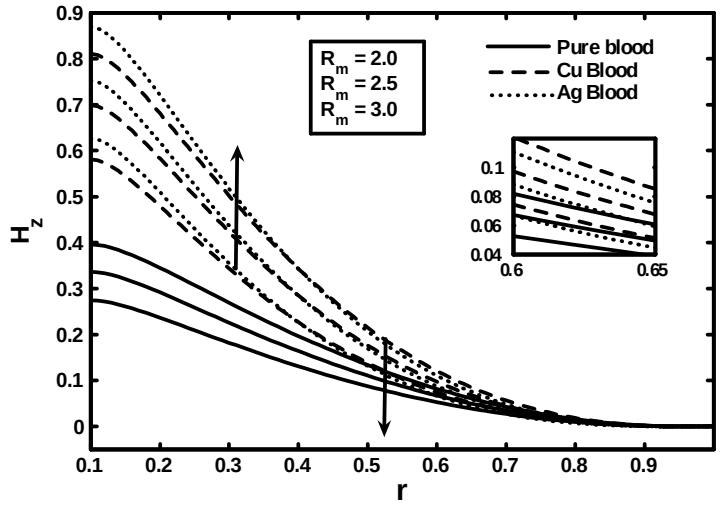

Fig. (5.15): Variation of axial induced magnetic field for different values of magnetic Reynolds R_m.

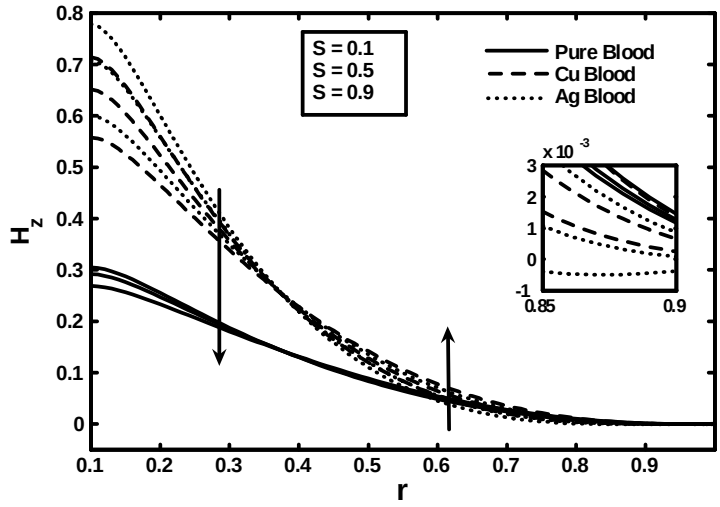

Fig. (5.16): Variation of axial induced magnetic field for different values of Strommers number S.

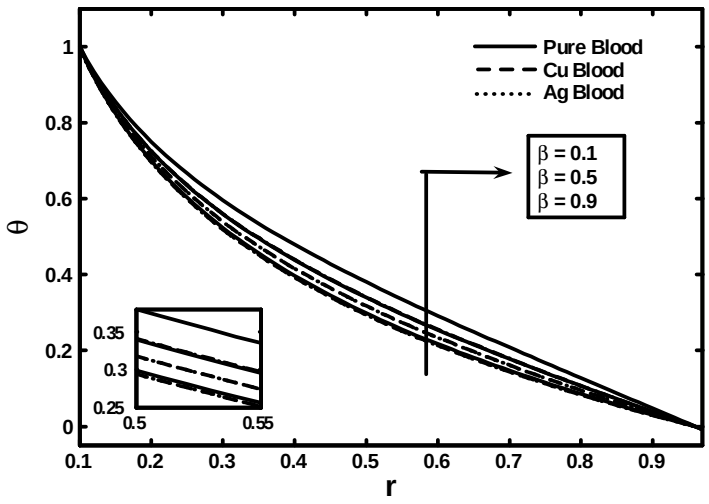

Fig. (5.17): Variation of temperature profile for different values of the heat source parameter β.

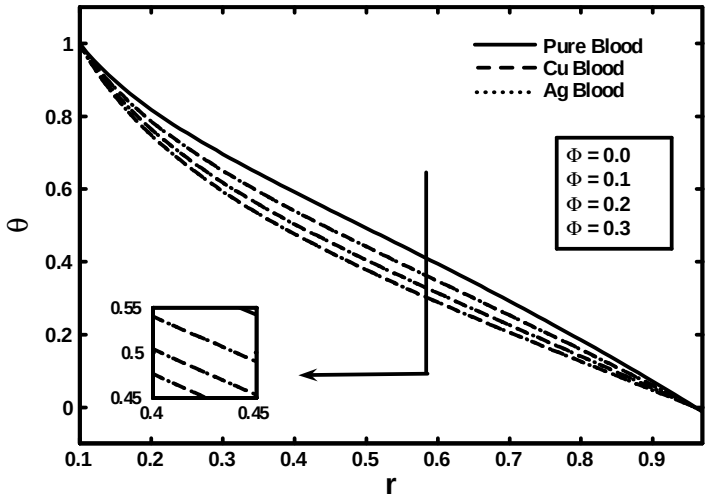

Fig. (5.18): Variation of temperature profile for different values of the nanoparticle volume fraction Φ.

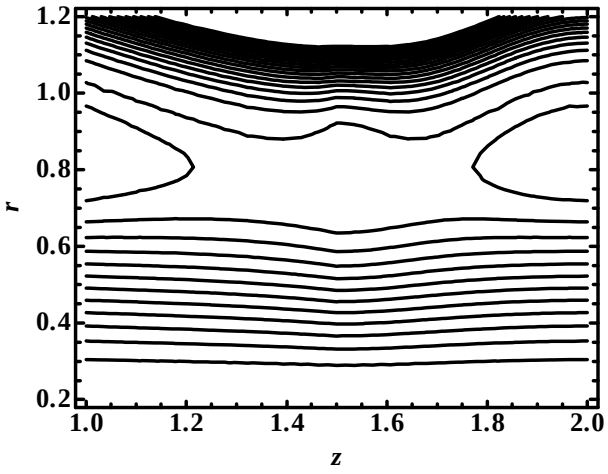

(a)

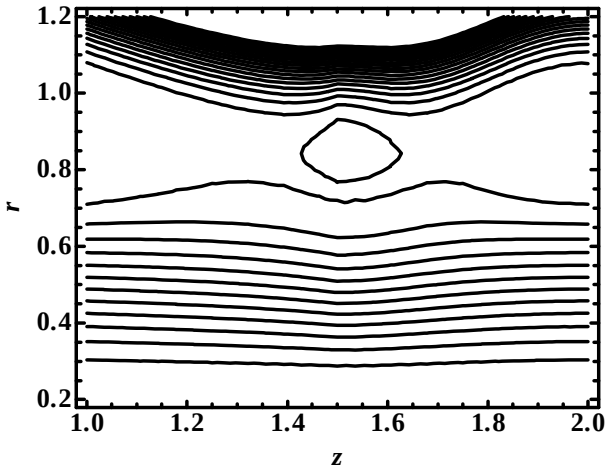

(b)

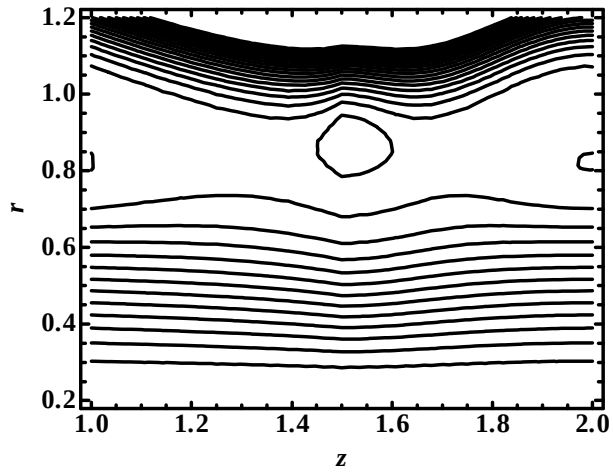

(c)

Figs. (5.19): Blood flow pattern (Cu nanoparticles) for (a) $\delta = 0.25$, (b) $\delta = 0.27$, (c) $\delta = 0.29$.

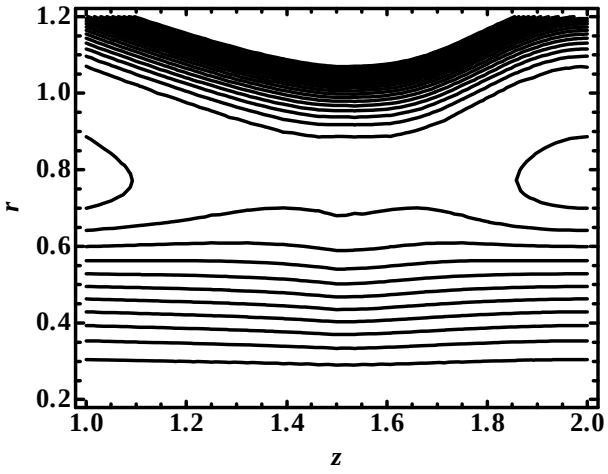

(a)

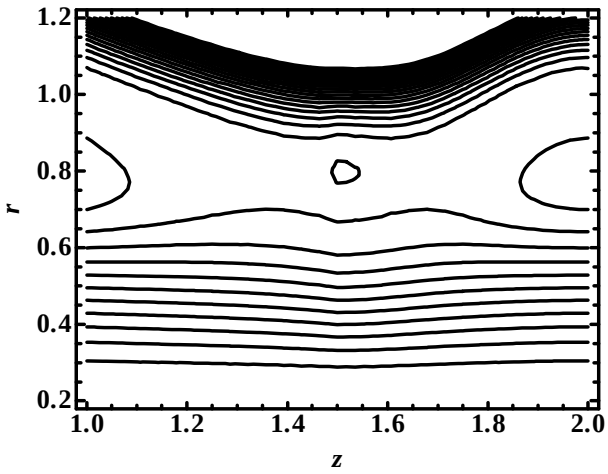

(b)

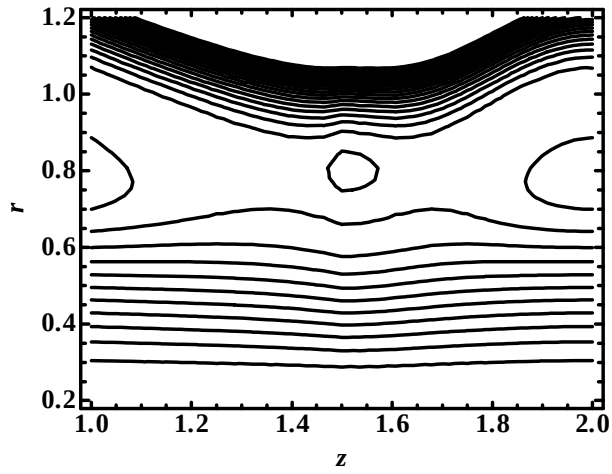

(c)

Figs. (5.20): Blood flow pattern (Ag nanoparticles) for (a) $\delta = 0.25$, (b) $\delta = 0.27$, (c) $\delta = 0.29$.

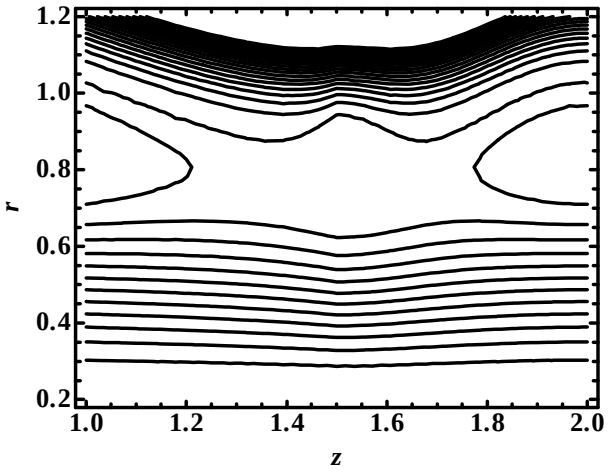

(a)

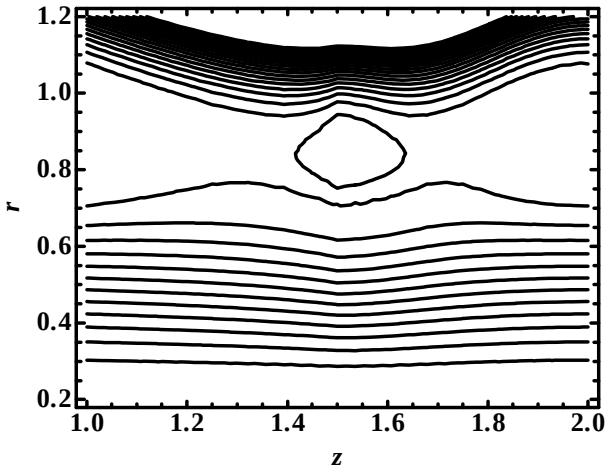

(b)

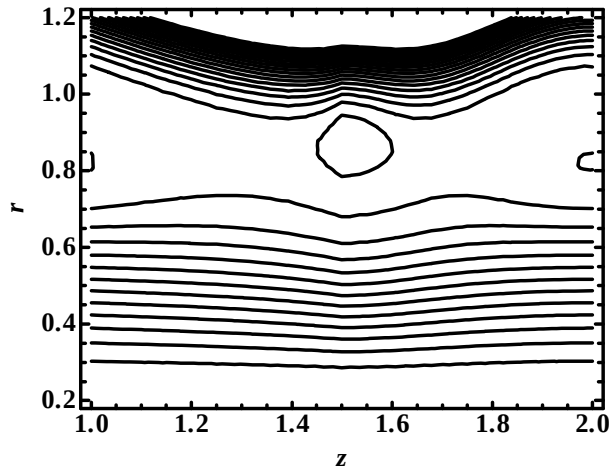

(c)

Figs. (5.21): Blood flow pattern (Cu nanoparticles) for (a) $R_m = 0.36$, (b) $R_m = 0.38$, (c) $R_m = 0.40$.

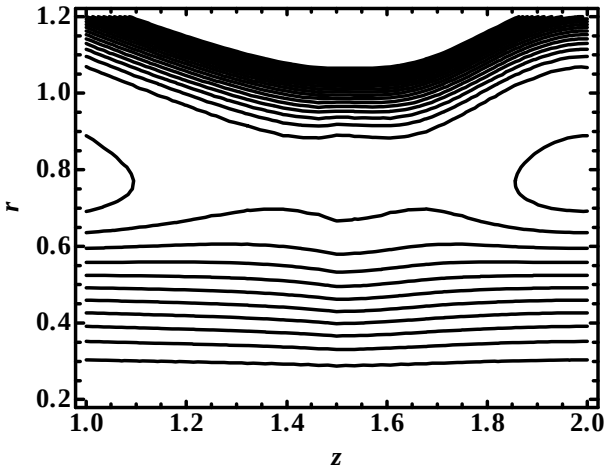

(a)

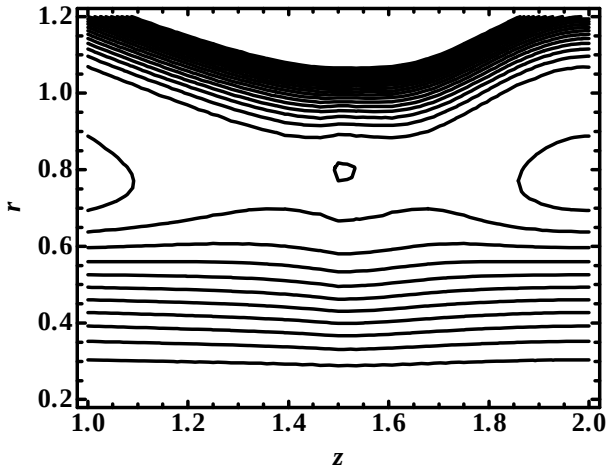

(b)

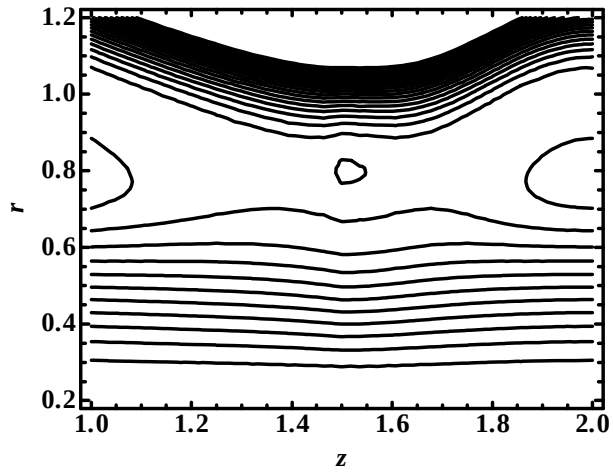

(c)

Figs. (5.22): Blood flow pattern (Ag nanoparticles) for (a) $R_m = 0.36$, (b) $R_m = 0.38$, (c) $R_m = 0.40$.

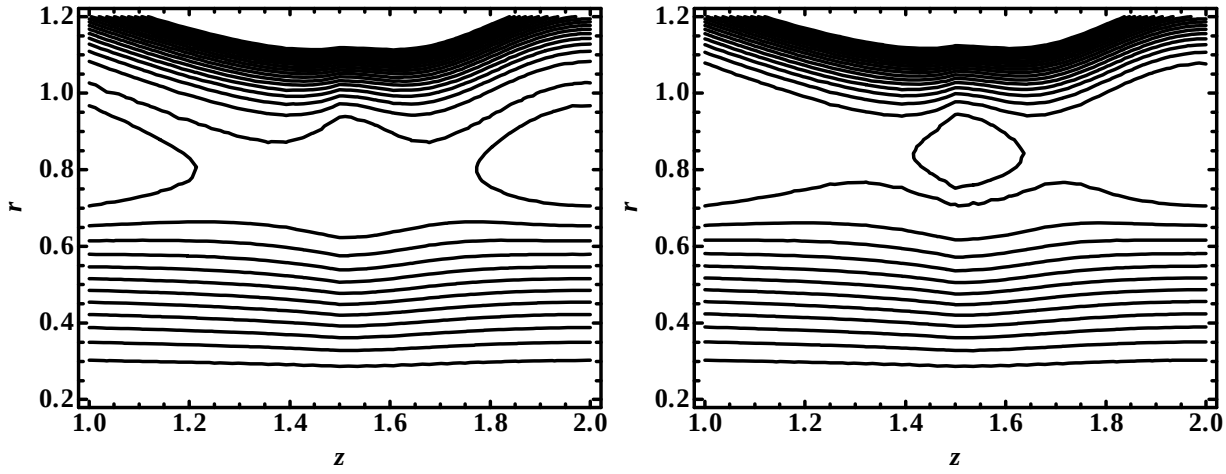

(a) **(b)**

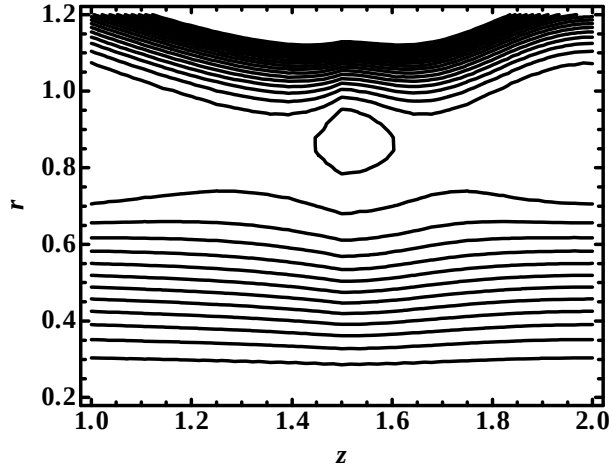

(c)

Figs. (5.23): Blood flow pattern (Cu nanoparticles) for (a) $S = 3.9$, (b) $S = 4.0$, (c) $S = 4.1$.

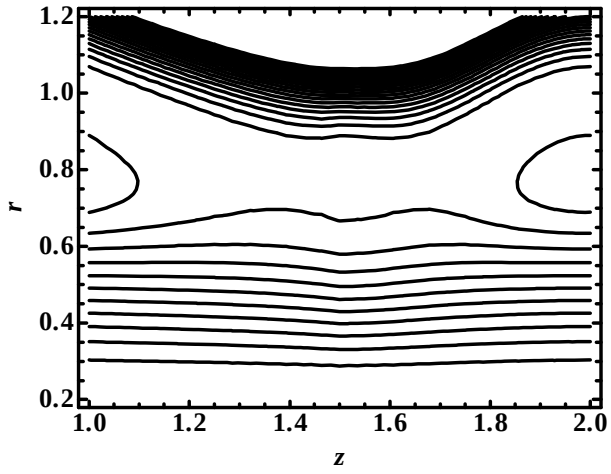

(a)

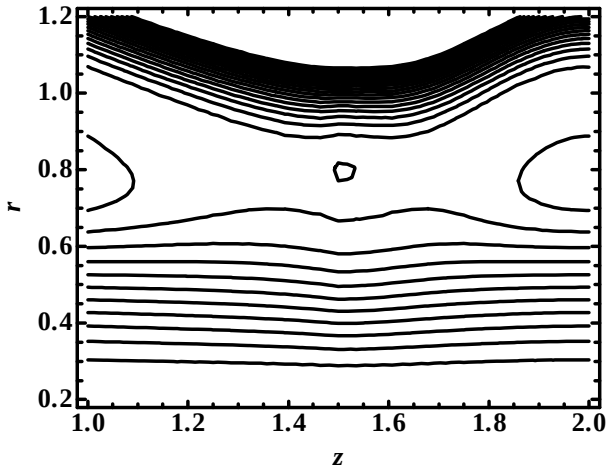

(b)

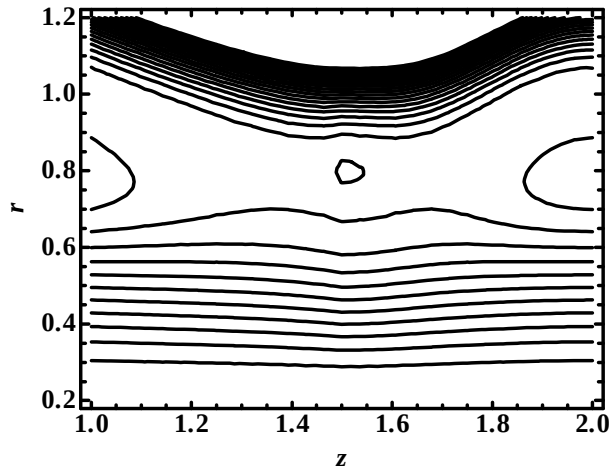

(c)

Figs. (5.24): Blood flow pattern (Ag nanoparticles) for (a) $S = 3.9$, (b) $S = 4.0$, (c) $S = 4.1$.

w	Pure blood ($\Phi = 0.00$)			Copper Blood			Silver Blood		
r	R_m=2.0	R_m=3	R_m=4	R_m=2	R_m=3	R_m=4	R_m=2	R_m=3	R_m=4
ε	0.00000	0.00000	0.00000	0.00000	0.00000	0.00000	0.00000	0.00000	0.00000
0.2	0.05591	0.05048	0.04605	0.07880	0.06873	0.06099	0.08854	0.07717	0.06842
0.3	0.08465	0.07889	0.07405	0.11071	0.10024	0.09190	0.12168	0.10997	0.10065
0.4	0.09883	0.09489	0.09145	0.11919	0.11218	0.10634	0.12759	0.11986	0.11344
0.5	0.10151	0.10001	0.09861	0.11162	0.10912	0.10682	0.11565	0.11299	0.11055
0.6	0.09417	0.09491	0.09545	0.09301	0.09450	0.09552	0.09237	0.09412	0.09534
0.7	0.07789	0.08010	0.08197	0.06770	0.07172	0.07496	0.06343	0.06792	0.07153
0.8	0.05356	0.05609	0.05832	0.03983	0.04430	0.04805	0.03420	0.03912	0.04323
h	0.00000	0.00000	0.00000	0.00000	0.00000	0.00000	0.00000	0.00000	0.00000

Table (5.1): Variations of velocity profile for different values of the magnetic Reynolds R_m.

w	Pure blood ($\Phi = 0.00$)			Copper Blood			Silver Blood		
r	S=0.3	S=0.6	S=0.9	S=0.3	S=0.6	S=0.9	S=0.3	S=0.6	S=0.9
ε	0.00000	0.00000	0.00000	0.00000	0.00000	0.00000	0.00000	0.00000	0.00000
0.2	0.06872	0.06176	0.05288	0.10537	0.09041	0.07310	0.11852	0.10165	0.08211
0.3	0.09764	0.09067	0.08146	0.13690	0.12238	0.10484	0.15099	0.13473	0.11511
0.4	0.10726	0.10281	0.09667	0.13557	0.12667	0.11530	0.14571	0.13585	0.12330
0.5	0.10432	0.10290	0.10070	0.11654	0.11401	0.11026	0.12090	0.11821	0.11421
0.6	0.09218	0.09330	0.09460	0.08853	0.09112	0.09387	0.08721	0.09018	0.09338
0.7	0.07295	0.07559	0.07911	0.05779	0.06326	0.06995	0.05235	0.05847	0.06594
0.8	0.04816	0.05101	0.05495	0.02940	0.03507	0.04231	0.02269	0.02895	0.03693
h	0.00000	0.00000	0.00000	0.00000	0.00000	0.00000	0.00000	0.00000	0.00000

Table. (5.2): Variations of velocity profile for different values of the Strommers number S.

Chapter 6

Nanoparticles analysis on blood flow through tapered catheterized elastic artery with overlapping stenosis

The main purpose of this chapter is to examine the analysis of blood flow between an arterial stenosis and a uniform catheter by using Buongiorno's model. The nature of blood through coaxial tubes is considered as nano viscous fluid. The mild stenosis approximation and corresponding boundary conditions are used to obtain analytic expressions for axial velocity, temperature distribution, nanoparticles concentration, wall shear stress and resistance impedance to flow. The model is also used to study the consequence of thermophoresis parameter and Brownian motion number on the blood flow through stenosed arteries by plotting graphs of wall shear stress and resistance to blood flow. This considered phenomenon presents that the thermal conductivity of the nanofluid enhanced only due to increase in Brownian motion number and hence also useful to minimize the hemodynamic effects of stenosis.

6.1 Fundamental equation of Buongiorno's model

The heat and nanoparticles concentration phenomenon is taken into account by giving temperature T_o and concentration C_o to the wall of the catheter, while temperature T_1 and concentration C_1 to the wall of the artery. Expression of the law of conservation of mass, temperature and

nanoparticles concentration is given as

$$\operatorname{div} \bar{\mathbf{V}} = 0, \tag{6.1}$$

$$\rho_f \frac{d\bar{\mathbf{V}}}{d\bar{t}} = -\boldsymbol{\nabla} p + \mu_f \boldsymbol{\nabla}^2 \bar{\mathbf{V}} \ + \rho_f g \alpha_t (\overline{T} - T_1) + \rho_f g \alpha_c (\overline{\mathbf{C}} - \mathbf{C_1}), \tag{6.2}$$

$$\frac{d\bar{T}}{d\bar{t}} = \frac{k}{(\rho c)_f} \boldsymbol{\nabla}^2 \bar{T} + \frac{(\rho c)_p}{(\rho c)_f} \left[D_{\bar{B}} \boldsymbol{\nabla} \bar{C}.\boldsymbol{\nabla} \bar{T} + \left(\frac{D_{\bar{T}}}{T_1} \right) \boldsymbol{\nabla} \bar{T}.\boldsymbol{\nabla} \bar{T} \right], \tag{6.3}$$

$$\frac{d\bar{C}}{d\bar{t}} = D_{\bar{B}} \boldsymbol{\nabla}^2 \bar{C} + \left(\frac{D_{\bar{T}}}{T_1} \right) \boldsymbol{\nabla}^2 \bar{T}, \tag{6.4}$$

in which $D_{\bar{B}}$ is defined as the Brownian diffusion coefficients and $D_{\bar{T}}$ as the thermophoretic diffusion coefficient respectively. Also, $\tau = \frac{(\rho c)_p}{(\rho c)_f}$ describes the ratio between the effective heat capacity in the case of nanoparticle material and heat capacity of the fluid.

6.2 Mathematical formulation

The governing equations for nano viscous fluid by using Eqs. (6.1) to (6.4), can be written as

$$\frac{\partial \overline{u}}{\partial \overline{r}} + \frac{\overline{u}}{\overline{r}} + \frac{\partial \overline{w}}{\partial \overline{z}} = 0, \tag{6.5}$$

$$\rho_f \left(\frac{\partial \overline{u}}{\partial \overline{t}} + \overline{u} \frac{\partial \overline{u}}{\partial \overline{r}} + \overline{w} \frac{\partial \overline{u}}{\partial \overline{z}} \right) = -\frac{\partial \overline{p}}{\partial \overline{r}} + \left(\frac{\partial^2 \overline{u}}{\partial \overline{r}^2} + \frac{1}{\overline{r}} \frac{\partial \overline{u}}{\partial \overline{r}} + \frac{\partial^2 \overline{u}}{\partial \overline{z}^2} - \frac{\overline{u}}{\overline{r}^2} \right), \tag{6.6}$$

$$\rho_f \left(\frac{\partial \overline{w}}{\partial \overline{t}} + \overline{u} \frac{\partial \overline{w}}{\partial \overline{r}} + \overline{w} \frac{\partial \overline{w}}{\partial \overline{z}} \right) = -\frac{\partial \overline{p}}{\partial \overline{z}} + \left(\frac{\partial^2 \overline{w}}{\partial \overline{r}^2} + \frac{1}{\overline{r}} \frac{\partial \overline{w}}{\partial \overline{r}} + \frac{\partial^2 \overline{w}}{\partial \overline{z}^2} \right) + \rho_f g \alpha_t (\overline{T} - T_1) + \rho_f g \alpha_c (\overline{C} - C_1), \tag{6.7}$$

$$\left(\overline{u}\frac{\partial\overline{T}}{\partial\overline{r}}+\overline{w}\frac{\partial\overline{T}}{\partial\overline{z}}\right) = \alpha\left(\frac{\partial^2\overline{T}}{\partial\overline{r}^2}+\frac{1}{\overline{r}}\frac{\partial\overline{T}}{\partial\overline{r}}+\frac{\partial^2\overline{T}}{\partial\overline{z}^2}\right)+\tau\left[D_{\overline{B}}\left(\frac{\partial\overline{C}}{\partial\overline{r}}\frac{\partial\overline{T}}{\partial\overline{r}}+\frac{\partial\overline{C}}{\partial\overline{z}}\frac{\partial\overline{T}}{\partial\overline{z}}\right)+\frac{D_{\overline{T}}}{T_1}\left\{\left(\frac{\partial\overline{T}}{\partial\overline{r}}\right)^2+\left(\frac{\partial\overline{T}}{\partial\overline{z}}\right)^2\right\}\right], \tag{6.8}$$

$$\left(\overline{u}\frac{\partial\overline{C}}{\partial\overline{r}}+\overline{w}\frac{\partial\overline{C}}{\partial\overline{z}}\right)=D_{\overline{B}}\left(\frac{\partial^2\overline{C}}{\partial\overline{r}^2}+\frac{1}{\overline{r}}\frac{\partial\overline{C}}{\partial\overline{r}}+\frac{\partial^2\overline{C}}{\partial\overline{z}^2}\right)+\frac{D_{\overline{T}}}{T_1}\left(\frac{\partial^2\overline{T}}{\partial\overline{r}^2}+\frac{1}{\overline{r}}\frac{\partial\overline{T}}{\partial\overline{r}}+\frac{\partial^2\overline{T}}{\partial\overline{z}^2}\right). \tag{6.9}$$

For the above equation α_t describes the coefficient of thermal expansion and α_c as the coefficient of thermal expansion with nano concentration. Non-dimensional variables are defined as

$$\begin{aligned}
r &= \frac{\overline{r}}{e_0},\ z=\frac{\overline{z}}{L_0},\ w=\frac{\overline{w}}{u_o},\ u=\frac{L_0\overline{u}}{u_o\delta},\overline{p}=\frac{e_0^2p}{u_oL_0\mu},\ t=\frac{\overline{t}u_o}{L_0},\\
R_{en} &= \frac{L_0u_o\rho}{\mu},\ \theta=\frac{\overline{T}-T_1}{T_0-T_1},\ \sigma=\frac{\overline{C}-C_1}{C_0-C_1},\ N_t=\frac{(\rho c)_pD_{\overline{T}}(T_0-T_1)}{T_1(\rho c)_f\alpha},\\
\alpha &= \frac{k}{(\rho c)_f},\ N_b=\frac{(\rho c)_pD_B(C_0-C_1)}{(\rho c)_f\alpha},\ B_r=\frac{\rho g\alpha_ce_0^2(C_0-C_1)}{\mu u_o},\\
G_r &= \frac{\rho g\alpha_te_0^2(T_0-T_1)}{\mu u_o}.
\end{aligned} \tag{6.10}$$

Here N_b defined as Brownian motion parameter, B_r as the local nanoparticle Grashof number, G_r local temperature Grashof and N_t as the thermophoresis parameter. Using above Eq. (6.10), mild stenosis case $\delta^*=\frac{\delta}{e_0}\ll 1$ and extra condition $\epsilon=\frac{e_0}{b}\approx O(1)$, the constitutive Eqs. (6.6) to (6.9) can be written as

$$\frac{\partial p}{\partial r}=0, \tag{6.11}$$

$$\frac{\partial p}{\partial z}=\frac{1}{r}\left(\frac{\partial}{\partial r}\left(r\frac{\partial w}{\partial r}\right)\right)+G_r\theta+B_r\sigma, \tag{6.12}$$

$$\frac{1}{r}\frac{\partial}{\partial r}\left(r\frac{\partial\theta}{\partial r}\right)+N_b\left(\frac{\partial\sigma}{\partial r}\right)\left(\frac{\partial\theta}{\partial r}\right)+N_t\left(\frac{\partial\theta}{\partial r}\right)^2=0, \tag{6.13}$$

$$\left(\frac{1}{r}\frac{\partial}{\partial r}\left(r\frac{\partial\sigma}{\partial r}\right)\right)+\frac{N_t}{N_b}\left(\frac{1}{r}\frac{\partial}{\partial r}\left(r\frac{\partial\theta}{\partial r}\right)\right)=0. \tag{6.14}$$

The geometry of stenosis in dimensionless form is defined as

$$\begin{aligned} h(z,\ t) &= [(\zeta z+1)-\delta\cos\phi(z-d^*)\{11-\frac{94}{3}(z-d^*)+32(z-d^*)^2-\frac{32}{3} \\ &\quad (z-d^*)^3\}]Q_1(t), \qquad d^*\le z\le d^*+\frac{3}{2}, \\ &= (\zeta z+1)Q_1(t), \qquad \text{otherwise}, \end{aligned} \tag{6.15}$$

where corresponding boundary conditions are defined as

$$w=0 \ \ at \ \ r=h(z), \ \ w=0 \ \ at \ \ r=\varepsilon, \tag{6.16}$$

$$\theta=0 \ \ at \ \ r=h(z), \ \ \theta=1 \ \ at \ \ r=\varepsilon, \tag{6.17}$$

$$\sigma=0 \ \ at \ \ r=h(z), \ \ \sigma=1 \ \ at \ \ r=\varepsilon, \tag{6.18}$$

where in above

$$\delta=\frac{\delta^*}{e_0},\ d^*=\frac{d}{L_0}. \tag{6.19}$$

6.3 Solution of the problem

For the solution of Eqs. (6.13) and (6.14), HPM suggest that we can write these equation as follow

$$H(\Sigma,\theta)=(1-\Sigma)[\Gamma(\theta)-\Gamma(\theta_{10})]+\Sigma\left[\Gamma(\theta)+N_b\left(\frac{\partial\theta}{\partial r}\right)\left(\frac{\partial\sigma}{\partial r}\right)+N_t\left(\frac{\partial\theta}{\partial r}\right)^2\right], \tag{6.20}$$

$$H(\Sigma,\sigma)=(1-\Sigma)\left[\Gamma(\sigma)-\Gamma(\sigma_{10})\right]+\Sigma\left[\Gamma(\sigma)+\frac{N_t}{N_b}\left(\frac{1}{r}\frac{\partial}{\partial r}\left(r\frac{\partial\theta}{\partial r}\right)\right)\right]. \tag{6.21}$$

The linear operator and the initial guesses are chosen and defined as

$$\Gamma_r\theta = \frac{1}{r}\frac{\partial}{\partial r}\left(r\frac{\partial}{\partial r}\right),\ \Gamma_r\sigma = \frac{1}{r}\frac{\partial}{\partial r}\left(r\frac{\partial}{\partial r}\right), \tag{6.22}$$

$$\theta_{10}(r,z) = -\left(\frac{r-h}{h-\varepsilon}\right),\ \sigma_{10}(r,z) = -\left(\frac{r-h}{h-\varepsilon}\right). \tag{6.23}$$

According to HPM, we may define as

$$\begin{aligned} \theta &= \theta_0 + \Sigma\theta_1 + ..., \\ \sigma &= \sigma_0 + \Sigma\sigma_1 + ..., \end{aligned} \tag{6.24}$$

Making use of Eq. (6.24) into Eqs. (6.20) and (6.21) for $\Sigma \to 1$, the expressions of temperature and nanoparticles concentration are written as

$$\begin{aligned} \theta = -\frac{r-h}{h-\varepsilon} + \frac{1}{4(\ln h - \ln\varepsilon)(h-\varepsilon)^2}(4h(r\ln h - h\ln r + (h-r)\ln\varepsilon) - \\ (r^2(\ln h - \ln\varepsilon) + h^2(-\ln r + \ln\varepsilon))(N_b + N_t) - 4((h+r) \\ \ln h - 2h\ln r + (h-r)\ln\varepsilon)\varepsilon + (\ln h - \ln r)(4 + N_b + N_t)\varepsilon^2), \end{aligned} \tag{6.25}$$

$$\sigma = -\frac{r-h}{h-\varepsilon} + \frac{(N_b+N_t)(r\ln h - h\ln r + (h-r)\ln\varepsilon + (-\ln h + \ln r)\varepsilon)}{(\ln h - \ln\varepsilon)N_b(h-\varepsilon)}. \tag{6.26}$$

Using Eqs. (6.25) and (6.26), we can find exact solution for axial velocity of Eq. (6.12)

$$
\begin{aligned}
w &= \frac{dp}{dz}\frac{r^2(\ln h - \ln \varepsilon) + h^2(-\ln r + \ln \varepsilon) + \varepsilon^2(-\ln h + \ln r)}{4(\ln h - \ln \varepsilon)} + \\
&\frac{1}{144(\ln h - \ln \varepsilon)}(h^2(36c_1 - 36c_4 + h(16c_2 + 9c_3 h))\ln r + (-h^2(36c_1 - \\
&36c_4 + 16c_2 h + 9c_3 h^2) + 36(c_1 - c_4)r^2 + 16c_2 r^3 + 9c_3 r^4 + 36c_4 r^2 \ln r) \\
&\ln \varepsilon - \ln h(r^2(36c_1 - 36c_4 + r(16c_2 + 9c_3 r)) + 36c_4((-h^2 + r^2)\ln r + \\
&h^2 \ln \varepsilon)) + (\ln h - \ln r)\varepsilon^2(36(c_1 - c_4 + c_4 \ln \varepsilon) + 16c_2\varepsilon + 9c_3\varepsilon^2)). \qquad (6.27)
\end{aligned}
$$

Flow rate is given as

$$
F = \int_{\varepsilon}^{h} r w dr. \qquad (6.28)
$$

Using Eq. (6.27) into Eq. (6.28), we get the expression for pressure gradient as follows

$$
\frac{dp}{dz} = \frac{F - c_6(z)}{c_5(z)}. \qquad (6.29)
$$

Since F is constant for all sections between the two coaxial tubes, the pressure drop across the length of the overlapping stenosis is given as

$$
\Delta p = \int_{0}^{L} \left(-\frac{dp}{dz}\right) dz. \qquad (6.30)
$$

Using above Eq. (6.30), the impedance resistance can be evaluated as

$$
\lambda = \frac{\Delta p}{F} = \left\{ \int_{0}^{d^*} \Sigma_3(z) \mid_{h=(\zeta z+1)Q_1(t)} dz + \int_{d^*}^{d^*+\frac{3}{2}} \Omega_3(z) dz + \int_{d^*+\frac{3}{2}}^{L} \Sigma(z)_3 \mid_{h=(\zeta z+1)Q_1(t)} dz \right\}, \qquad (6.31)
$$

where

$$\Omega_3(z) = \frac{1}{F}\left(\frac{-F + c_6(z)}{c_5(z)}\right), \tag{6.32}$$

$$\Sigma_3(z) = \Omega_3(z)|_{h=(\zeta z+1)Q_1(t)}. \tag{6.33}$$

Expression for the wall shear stress is given as

$$\begin{aligned} S_{rz} = & -\frac{dp}{dz}\frac{1}{144h(\ln h - \ln \varepsilon)}(36(h^2(-1 + 2\ln h - 2\ln \varepsilon) + \varepsilon^2)) + \\ & \frac{1}{(144h(\ln h - \ln \varepsilon))}(h^2(36c_1 - 36c_4 + h(16c_2 + 9c_3h) - 12\ln h \\ & (6c_1 - 6c_4 + 4c_2h + 3c_3h^2 + 6c_4\ln h) + 12(6c_1 - 3c_4 + 4c_2h + 3c_3 \\ & h^2 + 6c_4\ln h)\ln \varepsilon) - \varepsilon^2(36(c_1 - c_4 + c_4\ln \varepsilon) + 16c_2\varepsilon^3 + 9c_3\varepsilon^2)). \end{aligned} \tag{6.34}$$

6.4 Appendix

$c_1 = \frac{1}{(4(\ln h - \ln \varepsilon)N_b}(4B_rN_t(h-\varepsilon)(h\ln \varepsilon - \varepsilon \ln h) + G_rN_b^2(-h^2$
$\ln \varepsilon + \varepsilon^2 \ln h) + N_b(4(B_r + G_r)(h-\varepsilon)^2 \ln h + G_rN_t(-h^2 \ln \varepsilon + \varepsilon^2 \ln h))),$
$c_2 = \frac{B_rN_t}{N_b}(h-\varepsilon)^2,\ c_3 = \frac{-G_r(N_t+N_b)}{4(h-\varepsilon)^2},\ c_4 = \frac{1}{4(\ln h - \ln \varepsilon)N_b(h-\varepsilon)}$
$(4B_rN_t(-h+\varepsilon) + G_rN_b^2(h+\varepsilon) + N_b(-4(B_r+G_r)(h-\varepsilon) + G_rN_t(h+\varepsilon))),$
$c_5 = \frac{1}{16(\ln h - \ln \varepsilon)}(h^4(1 - \ln h + \ln \varepsilon) - 2h^2\varepsilon^2 + (1 + \ln h - \ln \varepsilon)\varepsilon^4),$
$c_6 = \frac{1}{2880(\ln h - \ln \varepsilon)}(h^4(-5(36c_1 - 36c_4 + h(16c_2 + 9c_3h)) + 3(\ln h)(60$
$c_1 - 105c_4 + 4h(8c_2 + 5c_3h) + 60c_4\ln h) - 3(60c_1 - 45c_4 + 4h(8c_2 + 5c_3h) +$
$60c_4\ln h)\ln \varepsilon) + \varepsilon^2(5h^2(72c_1 - 72c_4 + h(16c_2 + 9c_3h) + 36c_4(\ln h +$
$\ln \varepsilon)) + \varepsilon(80c_2h^2 + \varepsilon(45(-4c_1 + 4c_4 + c_3h^2 + (\ln h)(-4c_1 + 3c_4 - 4c_4\ln \varepsilon) +$
$(\ln \varepsilon)(4c_1 - 7c_4 + 4c_4\ln \varepsilon)) - 16c_2(5 + 6\ln h - 6\ln \varepsilon)\varepsilon - 15c_3(3 + 4\ln h -$
$4\ln \varepsilon)\varepsilon^2)))).$

6.5 Results and discussion

In order to understand the quantitative effects of thermophoresis parameter N_t and Brownian motion number N_b, we have plot the graphs of wall shear stress, impedance resistance to flow, nanoparticles concentration, temperature distribution and axial velocity by considering three distinct arteries. The graphs are plotted by keeping the parameter constant such as $B_r = 2$, $L = 3$, $\delta = 0.2$, $F = 0.01$, $d^* = 0.75$, $G_r = 2$, $\alpha_o = 0.1$, $\omega = 7.854$, $z = 1.5$, $t = 0.5$, $N_t = 2.0$, $N_b = 2.0$, $\varepsilon = 0.1$. Figs. (6.1) and (6.2) are plotted to observe the influence of axial velocity w on blood flow through overlapping stenosis. From these figures, it is observed that velocity profile increases near the wall of the catheter ($0.1 \leq r \leq 0.65$ ($\phi < 0$), $0.1 \leq r \leq 0.70$ ($\phi > 0$), $0.1 \leq r \leq 0.67$ ($\phi = 0$)) with an increase in the values of Brownian motion number N_b and decreases with an increase in the values of thermophoresis parameter N_t, while the opposite trend is observed near the wall of arteries in the segments between ($0.65 < r \leq h$ ($\phi < 0$), $0.70 < r \leq h$ ($\phi > 0$), $0.67 < r \leq h$ ($\phi = 0$)). The variations of temperature distribution θ for different values of thermophoresis parameter N_t and Brownian motion number N_b are given in Figs. (6.3) and (6.4). It is analyzed that temperature profile increases with an increase in the values of thermophoresis parameter N_t and Brownian motion number N_b near the wall of arteries between the interval $0.35 < r \leq h$, while the opposite trend is observed between the interval $\varepsilon \leq r \leq 0.35$. This temperature profile pattern shows that the random motion of the nanoparticles is dominating near the wall of the arteries then near the wall of the catheter. The variations of nanoparticles concentration profile σ for different values of thermophoresis parameter N_t and Brownian motion number N_b are presented in Figs. (6.5) and (6.6). It is observed from Fig. (6.5), that nanoparticles concentration profile σ increases with an increase in Brownian motion number N_b. This result justifies that with an increase in random motion of particles the density of fluid increases which also enhance the mass flux and hence nanoparticles concentration profile increases. From Fig. (6.6), it is depicted that nanoparticles concentration profile decreases with an increase in thermophoresis parameter N_t. At the end, it is concluded from these results that for thermophoresis parameter and Brownian motion number temperature profile possess same behavior, while opposite trend is observed for nanoparticles concentration profile. In Figs. (6.7) and (6.8) the variations of wall shear stress versus z is plotted between the stenotic segment $0.75 \leq z \leq 2.25$ to understand the development of arterial disease with

different flow parameters. We can see that wall shear stress gives higher results for convergent tapering as associated with other tapering arteries. The variation of wall shear stress for different values of Brownian motion number N_b and thermophoresis parameter N_t versus axial distance z is given in Figs. (6.7) and (6.8). It is illustrated from these graphs that stresses on the wall of arteries decreases with an increase in N_b and this increase in random motion of nanoparticles accelerates the flow of blood to minimize stresses, while opposite behavior is taken into account for thermophoresis parameter N_t. Figs. (6.9) and (6.10) presented to observe the variation of the resistance impedance to flow along the maximum height of stenosis δ for different values of tapering angle φ. It is analyzed that resistance impedance to flow gives higher results for converging tapering as comparing to other tapering arteries. Fig. (6.9) is plotted for different values of thermophoresis parameter N_t. It is observed from this graph that resistance impedance to flow increases with an increase in N_t. The resistance impedance to flow for Brownian motion number N_b is plotted in Fig.(6.10). This figures depicts that the random motion of particles enhanced the thermal conductivity of the nanofluid due to which resistance to blood flow decreases. Figs. (6.11) and (6.12) are plotted versus time t for almost four and three cardiac phases. In these graphs we can see that the magnitude of first cycle starts decreasing to obtain its minimum then starts increasing to obtain its maximum then replicate its form again to obtain the starting point of the second cycle and so on. It is also observed that these graphs decay as the time t increases. The trapping phenomenon for the blood flow in an overlapping stenosed artery is discussed through Figs. (6.13) to (6.15). The stream line phenomena for tapering effects are plotted in Fig. (6.13). It is observed from this flow pattern that trapping bolus shift towards lower side for divergent tapering, while shift towards upper side for convergent tapering. The trapping for thermophoresis parameter N_t and Brownian motion number N_b is discussed through figs. (6.14) and (6.15) and it is observed that trapping increases with an increase in the values of Brownian motion number N_b and thermophoresis parameter N_t.

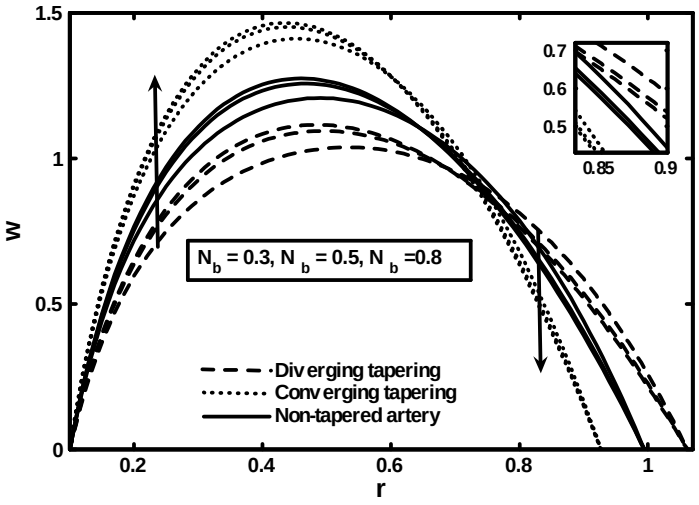

Fig. (6.1): Variation of axial velocity for different values of Brownian motion number N_b.

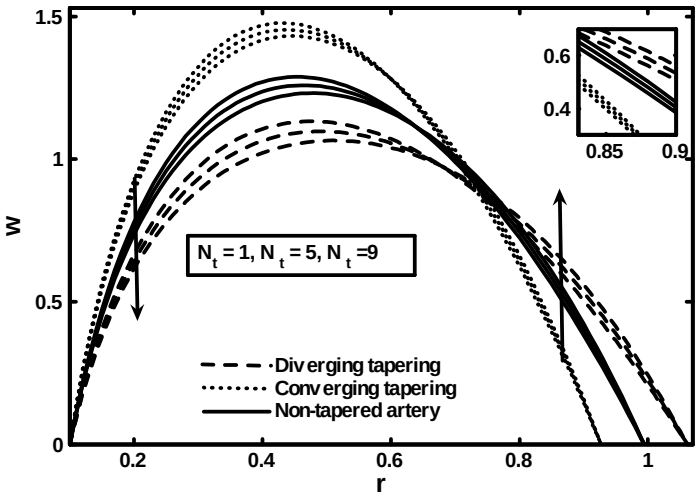

Fig. (6.2): Variation of axial velocity for different values of thermophoresis parameter N_t.

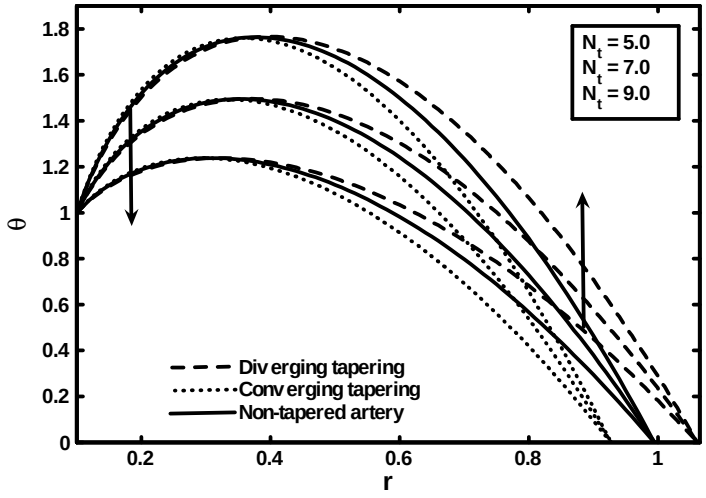

Fig. (6.3): Variation of temperature distribution for different values of thermophoresis parameter N_t.

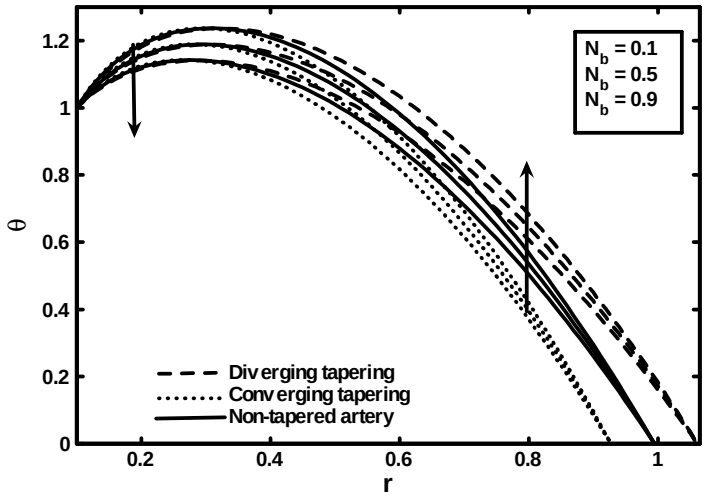

Fig. (6.4): Variation of temperature distribution for different values of Brownian motion number N_b.

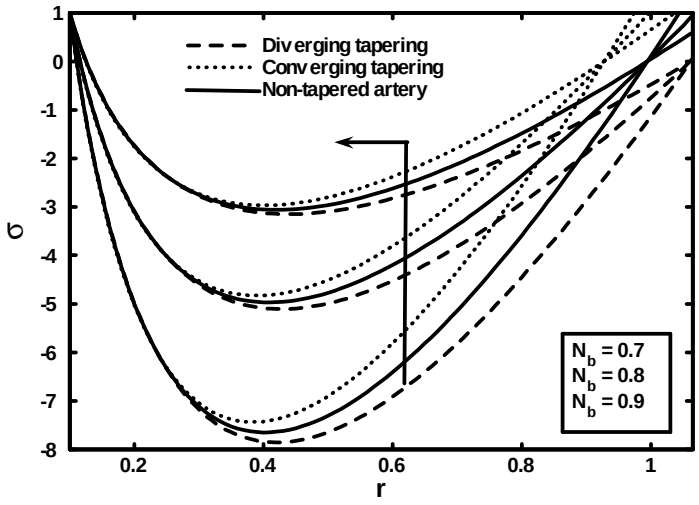

Fig. (6.5): Variation of nanoparticles concentration for different values of Brownian motion number N_b.

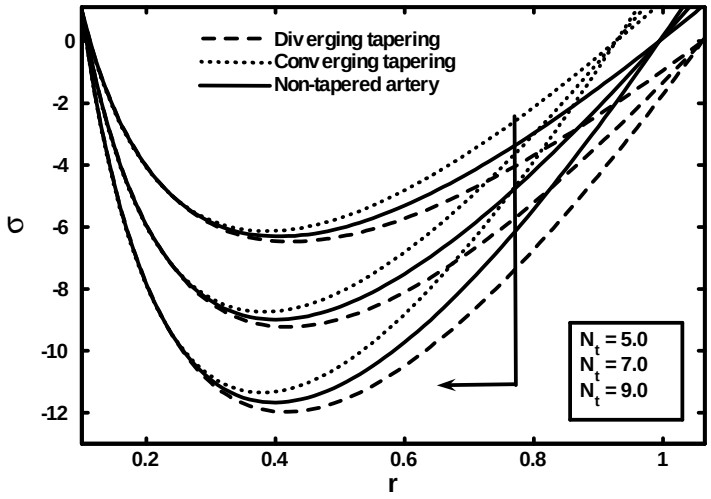

Fig. (6.6): Variation of nanoparticles concentration for different values of thermophoresis parameter N_t.

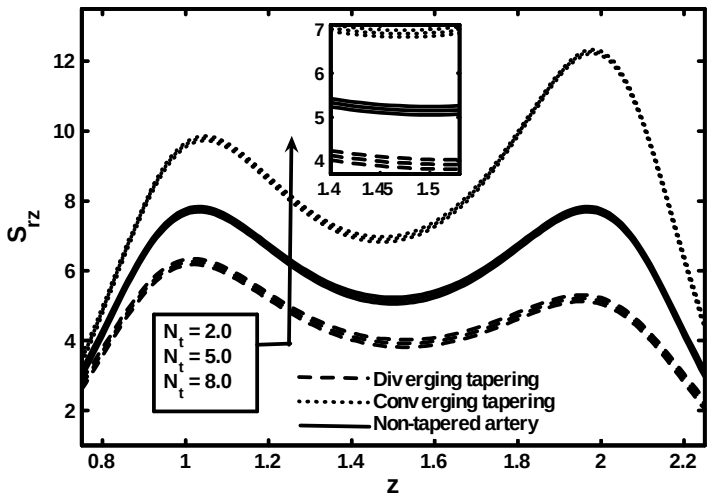

Fig. (6.7): Variation of wall shear stress for different values of thermophoresis parameter N_t.

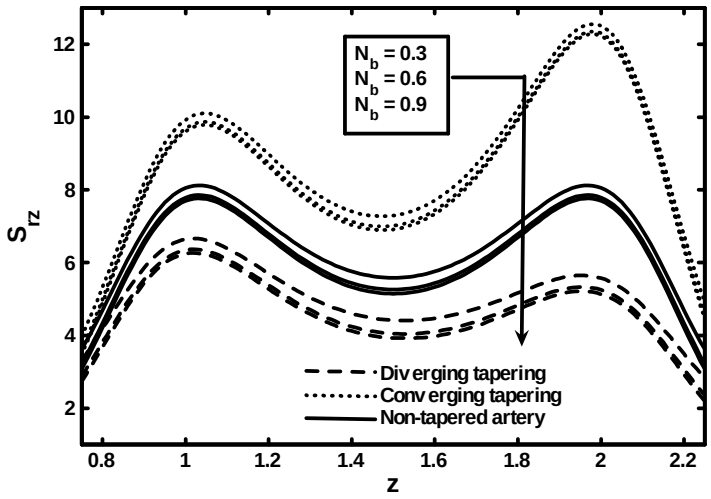

Fig. (6.8): Variation of wall shear stress for different values of Brownian motion number N_b.

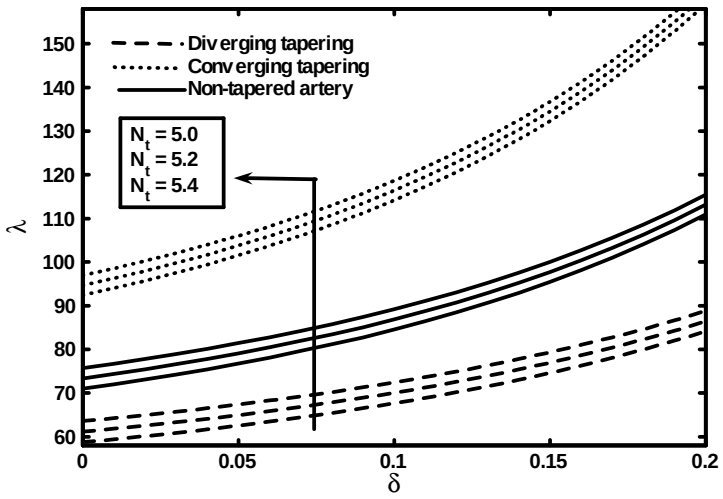

Fig. (6.9): Variation of resistance impedance for different values of thermophoresis parameter N_t.

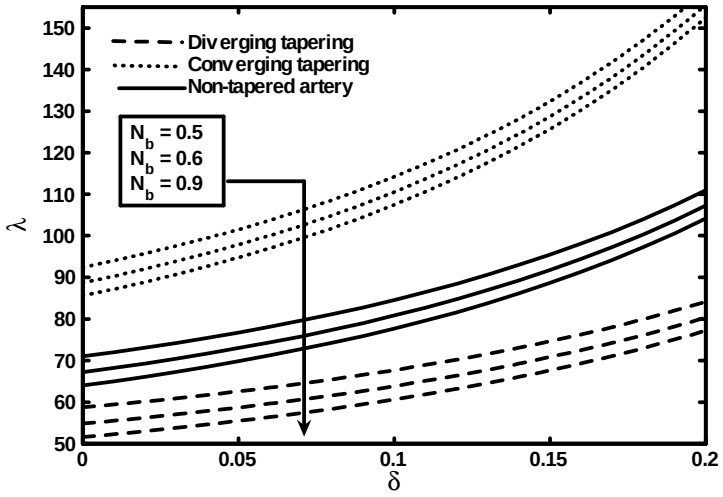

Fig. (6.10): Variation of resistance impedance for different values of Brownian motion number N_b.

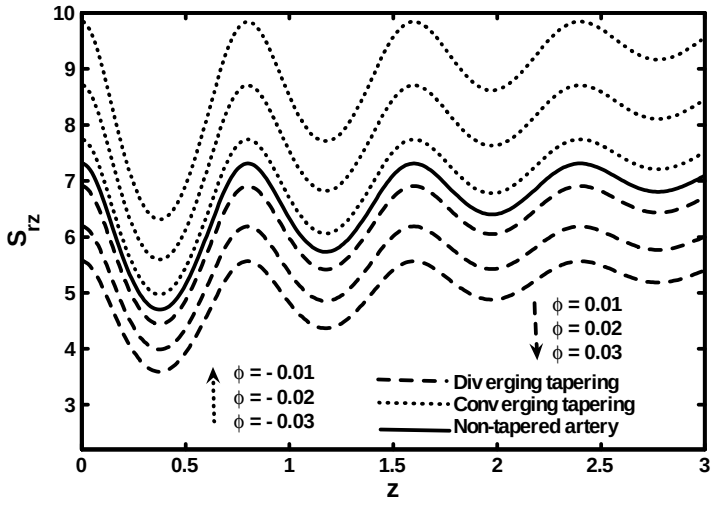

Fig. (6.11): Variation of wall shear stress for different values tapering angles against t.

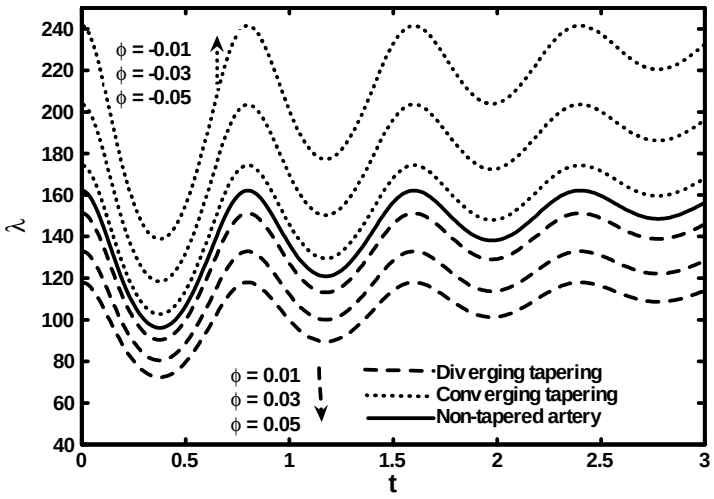

Fig. (6.12): Variation of resistance impedance for different values tapering angles against t.

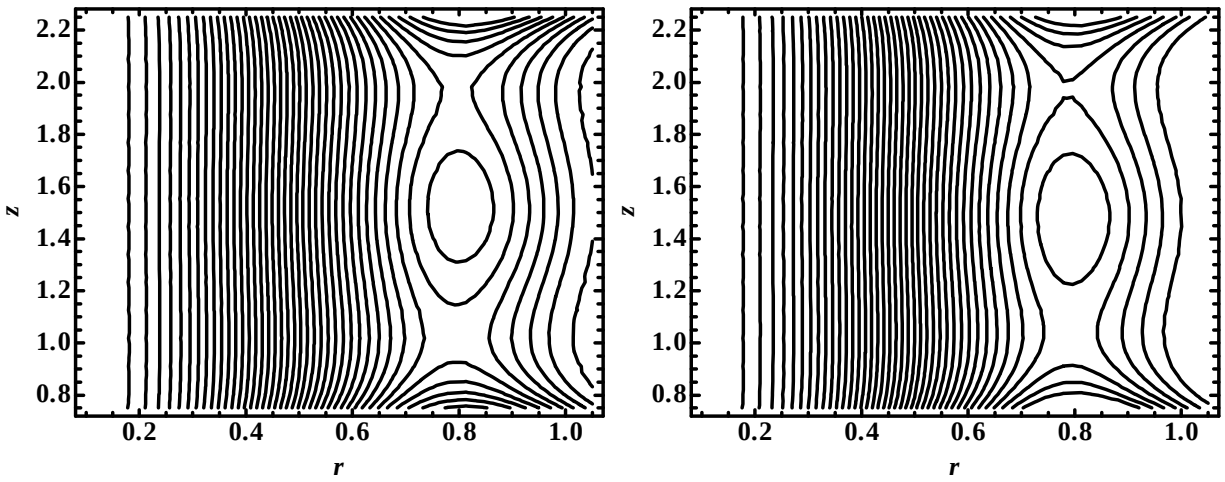

(a) (b)

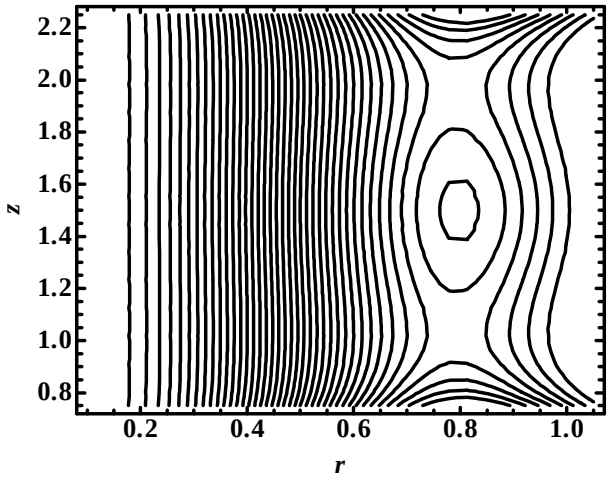

(c)

Fig. (6.13): Blood flow pattern for different values of (a) $\varphi > 0$, (b) $\varphi < 0$, (c) $\varphi = 0$.

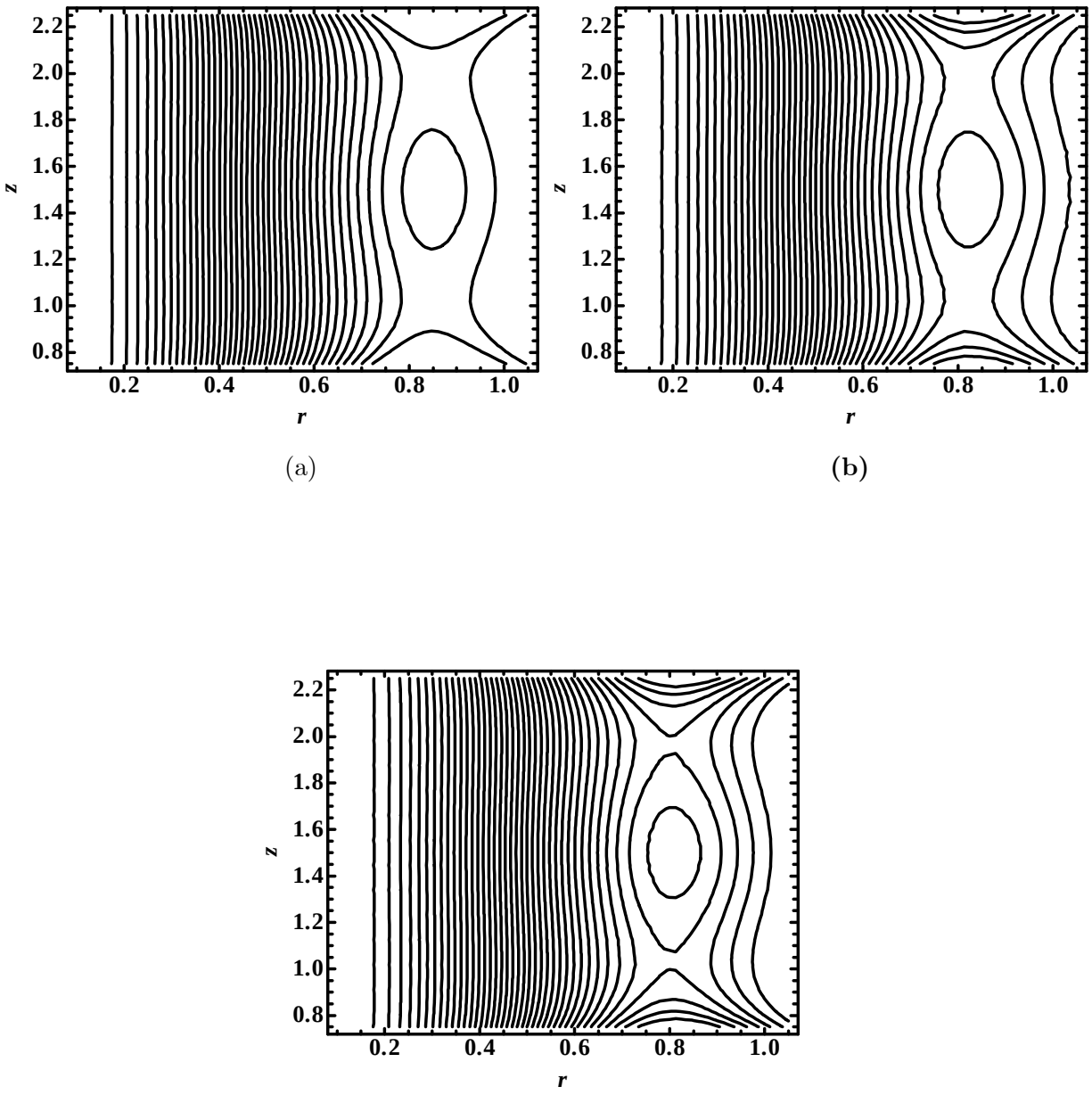

Fig. (6.14): Blood flow pattern for different values of (a) $N_b = 0.9$, (b) $N_b = 1.9$, (c) $N_b = 2.9$.

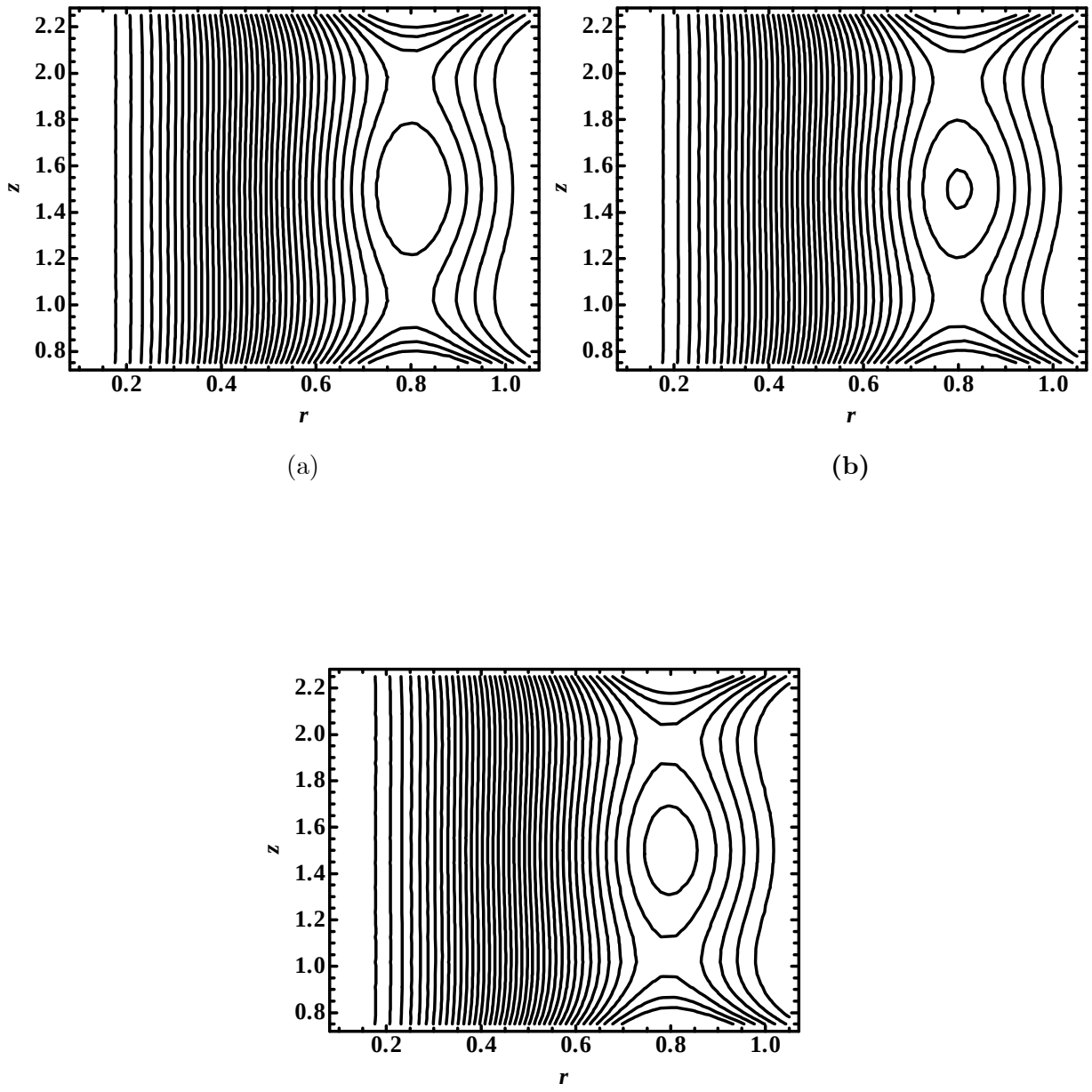

Fig. (6.15): Blood flow pattern for different values of (a) $N_t = 0.1$, (b) $N_t = 0.2$, (c) $N_t = 0.9$.

Chapter 7

Single wall carbon nanotube (SWCNT) examination on blood flow through a multiple stenosed artery with variable nanofluid viscosity

In this chapter, the theoretical model which deals with the analysis of variable viscosity and thermal conductivity of a single wall carbon nanotube within the considered base fluid flowing through multiple stenosed arteries is presented. A mathematical model is presented for the mild stenosis case and then solved by using symmetry boundary conditions to determine the exact solution of temperature, axial velocity and pressure gradient. The main hemodynamics due to multiple stenosis are also computed under the influence of an SWCNT. Numerical simulations are presented for the SWCNT with different values of nanoparticles volume fraction. The behavior of fluid flow for blood based SWCNT is discussed through graphs and streamlines. It is found that the resistance to blood flow increases for SWCNT case as compared to the pure blood case.

7.1 Mathematical formulation

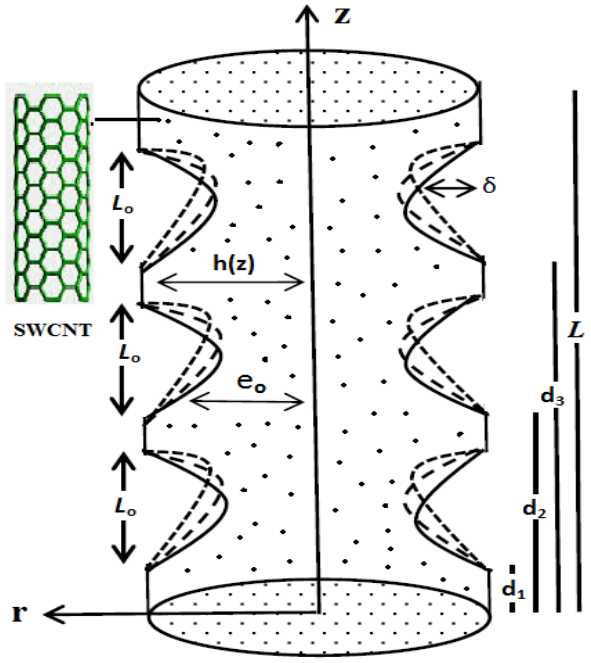

Fig. (7.1): Geometry of multiple stenosed artery.

The axis-symmetric geometry of stenosis in dimensional form is given as

$$\begin{aligned} \overline{h}(z) &= e_0[1-\eta^*(L_o^{n-1}(\overline{z}-d_i)-(\overline{z}-d_i)^n)] \quad d_i \leq \overline{z} \leq d_i + L_o, \\ &= e_0, \qquad\qquad\qquad\qquad\qquad\qquad \text{otherwise}, \end{aligned} \tag{7.1}$$

where $(i = 1, 2, 3)$ the radius of the non-stenotic arterial segment is e_0, length of stenosis is L_o, d_i measures the location of the stenosis and $n \geq 2$ determines the shape of stenosis. The parameter η^* is defined as

$$\eta^* = \frac{\delta n^{\frac{n}{n-1}}}{e_0 L_o^n (n-1)}. \tag{7.2}$$

The governing equations for conservation of mass, momentum and temperature for variable viscous nanofluid for a vertical stenosed artery can be written as,

$$\frac{\partial \overline{u}}{\partial \overline{r}} + \frac{\overline{u}}{\overline{r}} + \frac{\partial \overline{w}}{\partial \overline{z}} = 0, \tag{7.3}$$

$$\begin{aligned} \rho_{nf}\left(\overline{u}\frac{\partial \overline{u}}{\partial \overline{r}} + \overline{w}\frac{\partial \overline{u}}{\partial \overline{z}}\right) &= -\frac{\partial \overline{p}}{\partial \overline{r}} + \frac{1}{\overline{r}}\frac{\partial}{\partial \overline{r}}\left(2\overline{r}\mu_{nf}\frac{\partial \overline{u}}{\partial \overline{r}}\right) + \frac{\partial}{\partial \overline{z}}\left(\mu_{nf}\left(\frac{\partial \overline{u}}{\partial \overline{z}} + \frac{\partial \overline{w}}{\partial \overline{r}}\right)\right) \\ &\quad -2\mu_{nf}\frac{\overline{u}}{\overline{r}^2}, \end{aligned} \tag{7.4}$$

$$\begin{aligned} \rho_{nf}\left(\overline{u}\frac{\partial \overline{w}}{\partial \overline{r}} + \overline{w}\frac{\partial \overline{w}}{\partial \overline{z}}\right) &= -\frac{\partial \overline{p}}{\partial \overline{z}} + \frac{1}{\overline{r}}\frac{\partial}{\partial \overline{r}}\left(\overline{r}\mu_{nf}\left(\frac{\partial \overline{u}}{\partial \overline{z}} + \frac{\partial \overline{w}}{\partial \overline{r}}\right)\right) + \frac{\partial}{\partial \overline{z}}\left(2\mu_{nf}\left(\frac{\partial \overline{w}}{\partial \overline{z}}\right)\right) \\ &\quad +g(\rho\gamma)_{nf}(\overline{T} - T_o), \end{aligned} \tag{7.5}$$

$$\left(\frac{\partial \overline{T}}{\partial \overline{t}} + \overline{u}\frac{\partial \overline{T}}{\partial \overline{r}} + \overline{w}\frac{\partial \overline{T}}{\partial \overline{z}}\right) = \frac{K_{nf}}{(\rho c_p)_{nf}}\left(\frac{\partial^2 \overline{T}}{\partial \overline{r}^2} + \frac{1}{\overline{r}}\frac{\partial \overline{T}}{\partial \overline{r}} + \frac{\partial^2 \overline{T}}{\partial \overline{z}^2}\right) + \frac{Q_0}{(\rho c_p)_{nf}}. \tag{7.6}$$

In the above equations for the proposed nanofluid model μ_{nf} is the variable nanofluid viscosity, K_{nf} is the thermal conductivity, ρ_{nf} is the density, γ_{nf} is the thermal expansion coefficient and $(\rho c_p)_{nf}$ is the heat capacitance. The thermo physical properties with variable nanofluid viscosity is given as,

$$\begin{aligned} &\mu_{nf} = \frac{\mu_f(\theta)}{(1-\Phi)^{2.5}},\ \alpha_{nf} = \frac{K_{nf}}{(\rho c_p)_{nf}},\quad \rho_{nf} = (1-\Phi)\rho_f + \Phi\rho_{_{SWCNT}}, \\ &(\rho c_p)_{nf} = (1-\Phi)(\rho c_p)_f + \Phi(\rho c_p)_{_{SWCNT}},\quad (\rho\gamma)_{nf} = (1-\Phi)(\rho\gamma)_f + \Phi(\rho\gamma)_{_{SWCNT}}, \\ &\frac{K_{nf}}{K_f} = \frac{(1-\Phi) + 2\Phi\frac{k_{SWCNT}}{k_{SWCNT}-k_f}\ln\frac{k_{SWCNT}+k_f}{2k_f}}{(1-\Phi) + 2\Phi\frac{k_f}{k_{SWCNT}-k_f}\ln\frac{k_{SWCNT}+k_f}{2k_f}}. \end{aligned} \tag{7.7}$$

For the base fluid ρ_f is the density, μ_f is the viscosity, γ_f is the thermal expansion coefficient, $(\rho c_p)_f$ is the heat capacitance and k_f is the thermal conductivity, while for single carbon nanotubes $\rho_{_{SWCNT}}$ is the density, $\gamma_{_{SWCNT}}$ is the thermal expansion coefficient, $(\rho c_p)_{_{SWCNT}}$ is the heat capacitance, k_{SWCNT} is the thermal conductivity and Φ is the volume fraction. Reynolds model's of viscosity is defined as

$$\mu_f(\theta) = \mu_o e^{-\alpha\theta}, \tag{7.8}$$

where α is defined as coefficient of Reynolds model's of viscosity. Non-dimensional variables are defined as

$$r = \frac{\overline{r}}{e_0},\ w = \frac{\overline{w}}{u_o},\ u = \frac{L\overline{u}}{u_o\delta},\ p = \frac{e_0^2\overline{p}}{u_o L_o \mu_o},\ \beta = \frac{Q_0 e_0^2}{T_0 k_f},\ L = \frac{\overline{L}}{L_0},$$
$$R_{en} = \frac{e_0 u_o \rho_f}{\mu_o}, G_r = \frac{g\gamma_f \rho_f e_0^2 T_0}{u_0 \mu_o},\ \theta = \frac{\overline{T} - T_o}{T_o},\ z = \frac{\overline{z}}{L_o}. \tag{7.9}$$

Using the mild stenosis case $\delta^* = \frac{\delta}{e_0} \ll 1$ and taking the extra condition $\epsilon = \frac{e_0}{L_o} \approx O(1)$, the constitutive Eqs. (7.4) to (7.6) can be written as

$$\frac{\partial p}{\partial r} = 0, \tag{7.10}$$

$$\frac{\partial p}{\partial z} = \frac{1}{r}\frac{\partial}{\partial r}\left(\frac{\mu_{nf}(\theta)}{\mu_o}\left(r\frac{\partial w}{\partial r}\right)\right) + \frac{(\rho\gamma)_{nf}}{(\rho\gamma)_f} G_r \theta, \tag{7.11}$$

$$\frac{\partial^2 \theta}{\partial r^2} + \frac{1}{r}\frac{\partial \theta}{\partial r} + \beta\frac{K_f}{K_{nf}} = 0. \tag{7.12}$$

Boundary conditions and geometry of stenosis in dimensionless form are defined as

$$h(z) = 1 - \eta((z - \sigma_i) - (z - \sigma_i)^n)] \quad \sigma_i \le z \le \sigma_i + 1,$$
$$= 1 \qquad \text{otherwise.} \tag{7.13}$$
$$w = 0, \quad \theta = 0, \qquad \text{at} \quad r = h(z), \tag{7.14}$$
$$\frac{\partial w}{\partial r} = 0, \frac{\partial \theta}{\partial r} = 0 \qquad \text{at} \quad r = 0, \tag{7.15}$$

where

$$\eta = \frac{\delta^* n^{\frac{n}{n-1}}}{(n-1)},\ \delta^* = \frac{\delta}{e_0},\ d_i^* = \frac{d_i}{L_o}. \tag{7.16}$$

7.2 Solution of the problem

The exact solutions of Eqs. (7.11) and (7.12) using Eqs. (7.14) and (7.15) are written as

$$\theta = -\beta\left(\frac{r^2-h^2}{4}\right)\left[\frac{(1-\Phi)+2\Phi\frac{k_f}{k_{SWCNT}-k_f}\ln\frac{k_{SWCNT}+k_f}{2k_f}}{(1-\Phi)+2\Phi\frac{k_{SWCNT}}{k_{SWCNT}-k_f}\ln\frac{k_{SWCNT}+k_f}{2k_f}}\right], \tag{7.17}$$

$$\begin{aligned} w &= \frac{dp}{dz}(1-\Phi)^{2.5}\left(\frac{m_3(r^2-h^2)}{4}-\frac{m_4(r^4-h^4)}{8}\right)+\left((1-\Phi)+\Phi\frac{(\rho\gamma)_{SWCNT}}{(\rho\gamma)_f}\right) \\ &\quad G_r(1-\Phi)^{2.5}\left(\frac{m_5(h^2-r^2)}{2}+\frac{m_6(h^4-r^4)}{4}+\frac{m_7(h^6-r^6)}{6}\right). \end{aligned} \tag{7.18}$$

Flow rate is given as

$$F = \int_0^h rw dr. \tag{7.19}$$

Substituting Eq. (7.18) into Eq. (7.19), we obtain an expression for the pressure gradient as follows

$$\frac{dp}{dz} = \frac{F - m_9(z)(1-\Phi)^{2.5}\left((1-\Phi)+\Phi\frac{(\rho\gamma)_{SWCNT}}{(\rho\gamma)_f}\right)h^4}{m_8(z)(1-\Phi)^{2.5}h^4}. \tag{7.20}$$

The pressure drop between the segment $z = 0$ to $z = L$ through the stenosis that is calculated from above Eq. (7.20) can be defined as

$$\Delta p = \int_0^L \left(-\frac{dp}{dz}\right)dz. \tag{7.21}$$

Using Eq. (7.21), the impedance resistance can be given after simplifying all the stenotic and non-stenotic segments as

$$\lambda = \frac{\Delta p}{F} = \int_{0}^{\sigma_1} \Omega_4(z)|_{h=1} dz + \int_{\sigma_1}^{\sigma_1+1} \Omega_4(z) dz + \int_{\sigma_1+1}^{\sigma_2} \Omega_4(z)|_{h=1} dz + \int_{\sigma_2}^{\sigma_2+1} \Omega_4(z) dz + \int_{\sigma_2+1}^{\sigma_3} \Omega_4(z)|_{h=1} dz + \int_{\sigma_3}^{\sigma_3+1} \Omega_4(z) dz + \int_{\sigma_3+1}^{L} \Omega_4(z)|_{h=1} dz, \tag{7.22}$$

where

$$\Omega_4(z) = \frac{1}{F}\left(\frac{m_9(z)(1-\Phi)^{2.5}\left((1-\Phi)+\Phi\frac{(\rho\gamma)_{SWCNT}}{(\rho\gamma)_f}\right)h^4 - F}{m_8(z)(1-\Phi)^{2.5}h^4}\right). \tag{7.23}$$

Substituting Eq. (7.23) into Eq. (7.22), we have

$$\lambda = \frac{\Delta p}{F} = (L-3)m_{10} + \int_{\sigma_1}^{\sigma_1+1} \Omega_4(z) dz + \int_{\sigma_2}^{\sigma_2+1} \Omega_4(z) dz + \int_{\sigma_3}^{\sigma_3+1} \Omega_4(z) dz. \tag{7.24}$$

Expression for the wall shear stress is given as

$$S_{rz} = -\frac{\mu_{nf}}{\mu_o}\left(\frac{\partial w}{\partial r}\right)_{r=h}. \tag{7.25}$$

Substituting Eq. (7.18) into Eq. (7.25), we have

$$S_{rz} = -\frac{1}{(1-\Phi)^{2.5}(m_3 - m_4h^2)}\left((1-\Phi)^{2.5}\left((1-\Phi)+\Phi\frac{(\rho\gamma)_{SWCNT}}{(\rho\gamma)_f}\right)G_r (-m_5h - m_6h^3 - m_7h^5) + \frac{dp}{dz}\frac{(1-\Phi)^{2.5}}{2}(m_3h - m_4h^3)\right). \tag{7.26}$$

7.3 Appendix

$$m_o = \left[\frac{(1-\Phi)+2\Phi\frac{k_f}{k_{SWCNT}-k_f}\ln\frac{k_{SWCNT}+k_f}{2k_f}}{(1-\Phi)+2\Phi\frac{k_{SWCNT}}{k_{SWCNT}-k_f}\ln\frac{k_{SWCNT}+k_f}{2k_f}}\right],\ m_1(z)=\frac{\beta m_o}{4},\ m_2(z)=\frac{\beta h^2 m_o}{4},$$
$$m_3(z)=1+\alpha m_2(z),\ m_4(z)=\alpha m_1(z),\ m_5(z)=\frac{m_2(z)m_3(z)}{2},\ m_7(z)=\frac{m_1(z)m_4(z)}{4},$$
$$m_6(z)=-\frac{m_1(z)m_3(z)}{4}-\frac{m_2(z)m_4(z)}{2},\ m_8(z)=-\frac{m_3}{16}+\frac{m_4h^2}{24},\ m_9(z)=G_r\left(\frac{m_5}{8}+\right.$$
$$\left.\frac{m_6h^2}{12}+\frac{m_7h^4}{16}\right),\ m_{10}=\Omega_4(z)|_{h=1},\sigma_1=d_1^*,\ \sigma_2=d_1^*+d_2^*+1,\ \sigma_3=d_1^*+d_2^*+d_3^*+2.$$

7.4 Thermophysical properties of blood and SWCNT

Some experimental values of parameters useful for next section are given as

Physical properties	blood	SWCNT
$c_p(J/kgK)$	3594	425
$\rho(kg/m^3)$	1063	2600
$K(W/mK)$	0.492	6600
$\gamma\times10^{-5}(1/K)$	0.18	1.5

Table (7.1): Thermo physical properties.

7.5 Results and discussion

For evaluating reliability and accuracy of our exact solutions numerical measures of the pertinent parameters are lighted through graphs in this section of chapter 7. The graphs of temperature, wall shear stress and resistance impedance to flow are plotted for the heat source parameter β, Grashof number G_r, viscosity parameter α, stenosis shape n and height of the stenosis δ respectively. These graphs are considered for pure blood and SWCNT ($\Phi=0.04$, $\Phi=0.07$) cases by keeping parameters constant such as $\beta=2.0$, $G_r=2.0$, $\delta=0.1$, $F=0.06$, $n=2$, $d_1^*=d_2^*=d_3^*=0.5$, $\alpha=0.01$, $z=2.5$, $L=5$. The magnitude of wall shear stress is very essential to understand arterial disease because of its strong correlation with constriction of the arteries. The graphs of wall shear stress along axial displacement are plotted in Figs. (7.2)−(7.6)

for different cases. It is observed from these figures that wall shear stress having stenosis gives higher results for SWCNT case when compared to the pure blood case. From these figures it is concluded that for the first stenotic region the wall shear stress starts increasing from the beginning of the stenosis until a maximum constriction (i.e., throat) is attained, then start decreasing to reach the end of the stenotic section ($0.5 \leq z \leq 1.5$). This statement is also true for other stenotic segments of multiple stenosis ($2.0 \leq z \leq 3.0$) and ($3.5 \leq z \leq 4.5$). Fig. (7.2), It is interesting to note that symmetry of considered stenosis is destroyed with an increase in stenosis shapes. The wall shear stress for different values of the stenosis height δ is plotted in Fig. (7.3). It is observed that the significance of wall shear stress is directly proportional to the maximum height of stenosis. Figs. $(7.4) - (7.5)$ are plotted for different values of the heat source parameter β and the Grashof number G_r. The stress on the wall of the arteries for the different cases decreases with an increase in the values of the heat source parameter β and the Grashof number G_r. The wall shear stress for different values of the viscosity parameter α is plotted in Fig. (7.6). It is important to note here that the significance of wall shear stress decreases with an increase in the values of the viscosity parameter α. Stresses on the wall of the arteries are higher for constant nanofluid when compared to the variable nanofluid viscosity. The resistance impedance to flow is plotted against the maximum height of stenosis in Figs. $(7.7) - (7.10)$. These graphs depict that resistance impedance to flow increases with an increase in the maximum height of stenosis and gives higher results for the SWCNT case as compared to the pure blood case. The resistance impedance to flow for different values of Grashof number G_r and heat source parameter β is given through Figs. $(7.7) - (7.8)$. Resistance impedance to blood flow decreases with an increase in the values of Grashof number G_r and heat source parameter β. In Fig. (7.9) we observe that resistance in blood flow through diseased arteries decreases with an increase in the values of the stenosis shape n. The variations for different values of viscosity parameter α for pure blood and SWCNT are depicted in Fig. (7.10). it is analyzed that resistance to blood flow decreases with an increase in the viscosity parameter α and resistance to flow is higher for constant nanofluid viscosity then for variable nanofluid viscosity. It is concluded from this result that viscosity of the fluid plays significant roll to circulate the flow properly during diseased state of the artery. The temperature profile for different values of the stenosis height δ and the heat source parameter β are given in Figs.

(7.11) and (7.12). Temperature profile decreases with an increase in the values of stenosis height δ, while increases with an increase in the values of heat source parameter β. Trapping, describing an interesting phenomenon for the blood flow pattern in an artery having stenosis is discussed in Figs. $(7.13) - (7.16)$. In Fig. (7.13), we observe that the symmetry of trapped bolus destroyed with an increase in the values of stenosis shape n. The trapping phenomenon for stenosis height δ is given in Fig. (7.14). The number of trapping bolus increases with the closed stream lines. The important significance of nanoparticles volume fraction Φ is discussed in Fig. (7.15). The trapping bolus decreases with an increase in the nanoparticle volume fraction as compared to the pure blood case $\Phi = 0.00$. Fig. (7.16) shows the effects of viscosity parameter α and observed that the trapping bolus increases for variable nanofluid viscosity as compared to constant nanofluid viscosity. Tables (7.2) and (7.3) illustrate for different values of stenosis shape n, velocity profile and temperature profile give maximum results at $r = 0$ that is the axis of symmetry. From table (7.2), it is observed that the temperature profiles increases throughout the stenosed artery between $-h \leq r \leq h$. The table (7.3) shows that the velocity decreases at the center of the arteries with an increase in values of the stenosis shape n between the region $-0.6 \leq r \leq 0.6$, while the opposite trend is observed near the wall of the arteries.

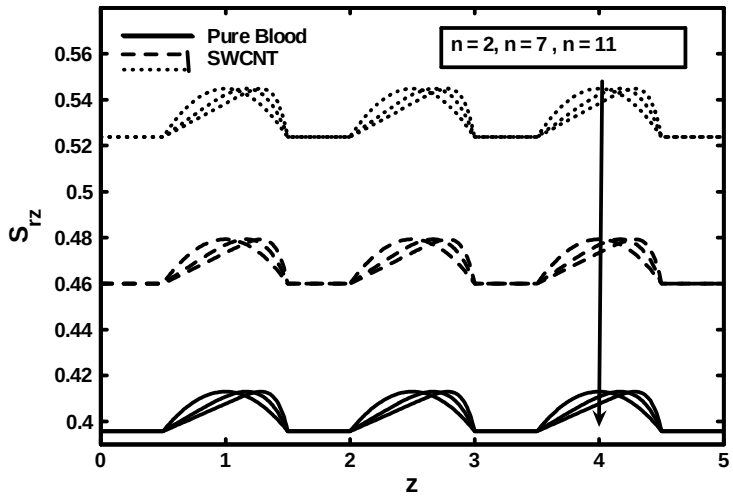

Fig. (7.2): Variation of wall shear stress for different values of stenosis shape n.

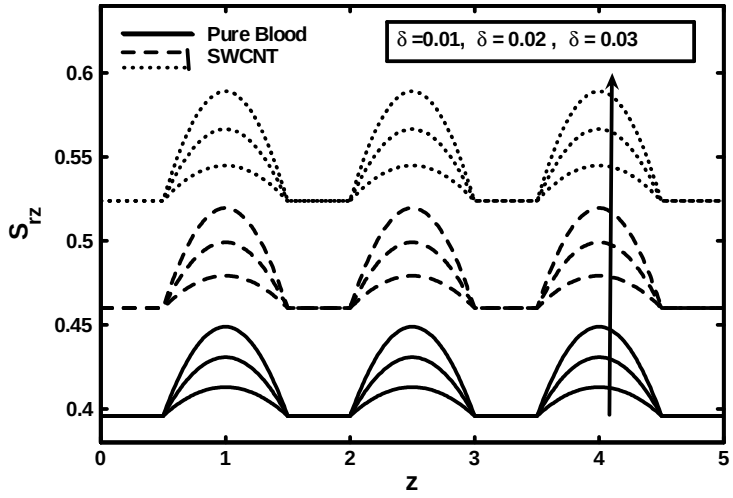

Fig. (7.3): Variation of wall shear stress for different values of stenosis height δ.

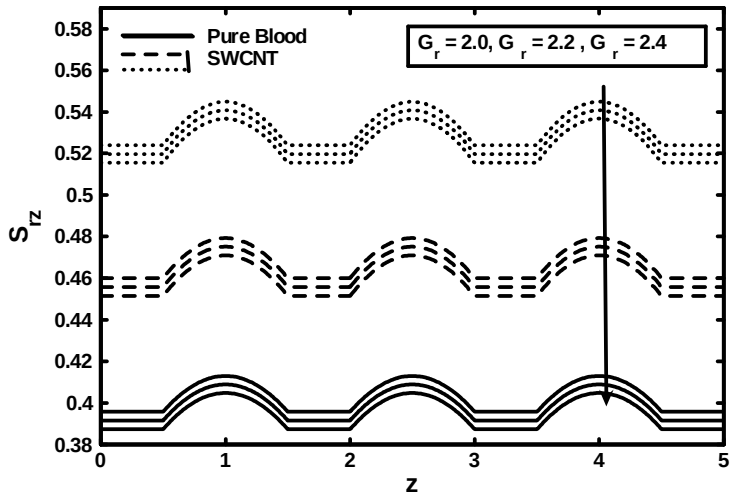

Fig. (7.4): Variation of wall shear stress for different values of Grashof number G_r.

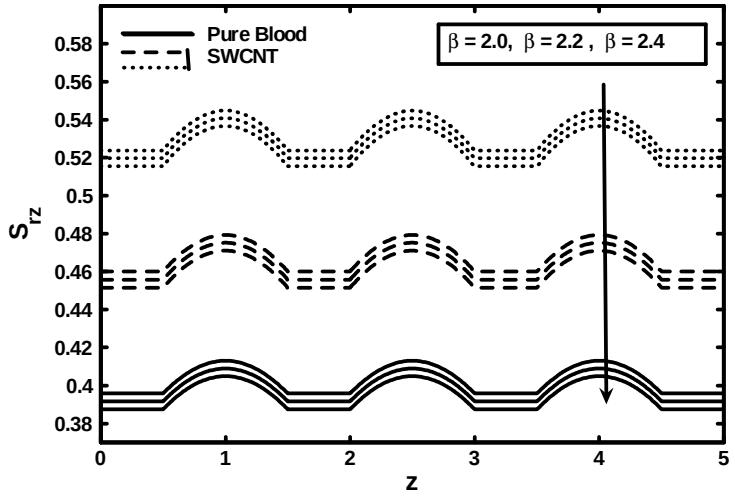

Fig. (7.5): Variation of wall shear stress for different values of the heat source parameter β.

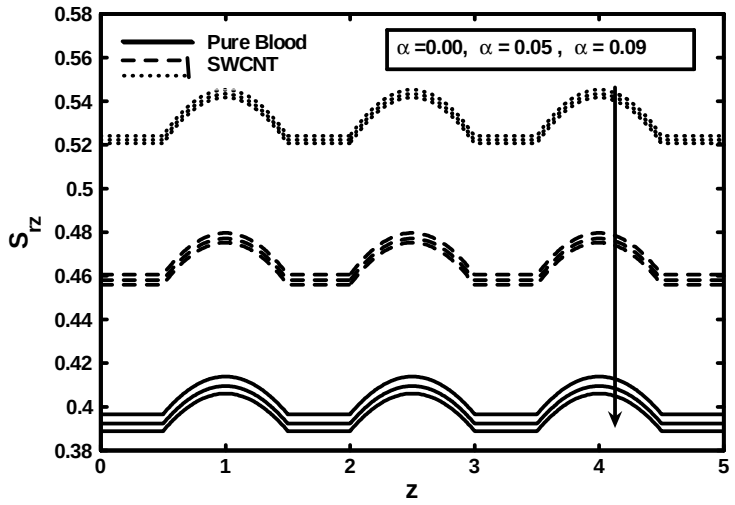

Fig. (7.6): Variation of wall shear stress for different values of the viscosity parameter α.

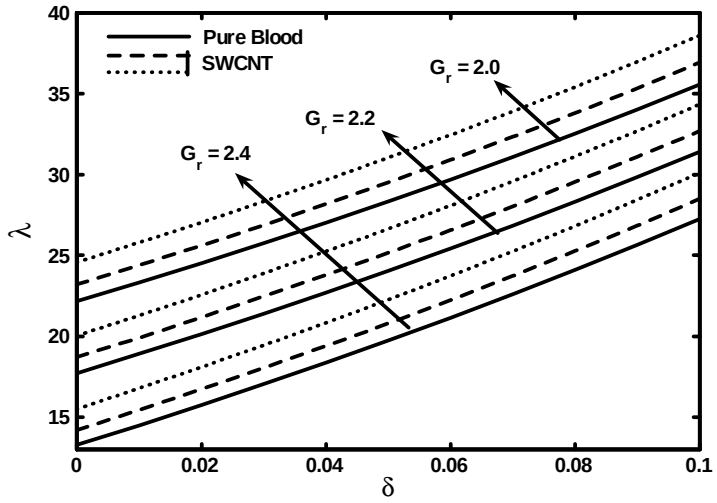

Fig. (7.7): Variation of resistance impedance for different values of the Grashof number G_r.

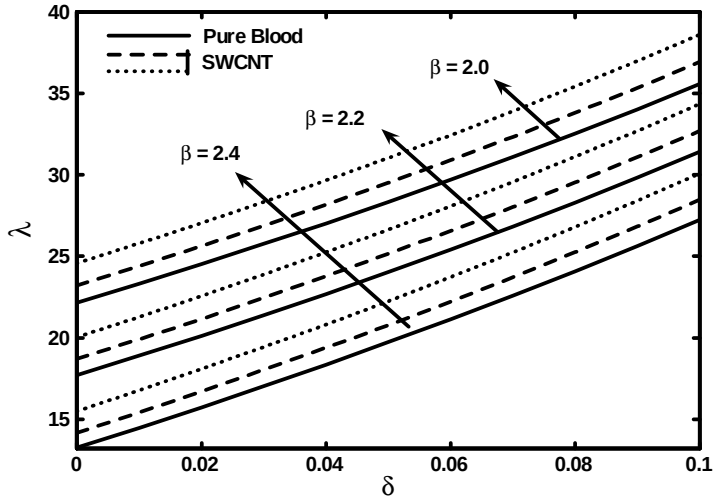

Fig. (7.8): Variation of resistance impedance for different values of the heat source parameter β.

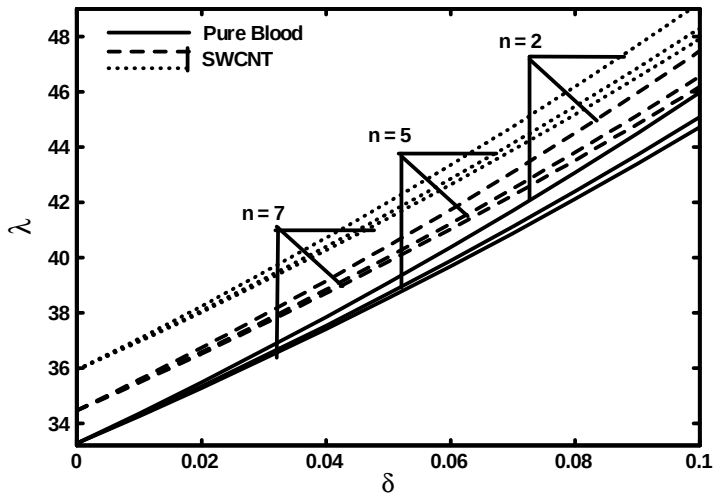

Fig. (7.9): Variation of resistance impedance for different values of the stenosis shape n.

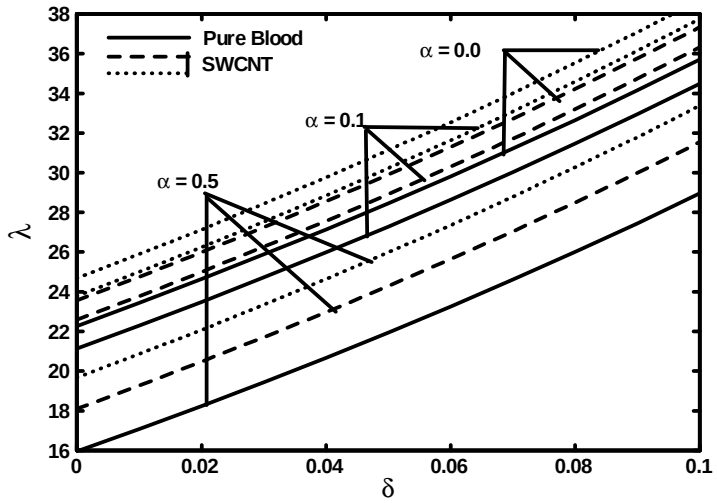

Fig. (7.10): Variation of resistance impedance for different values of the viscosity parameter α.

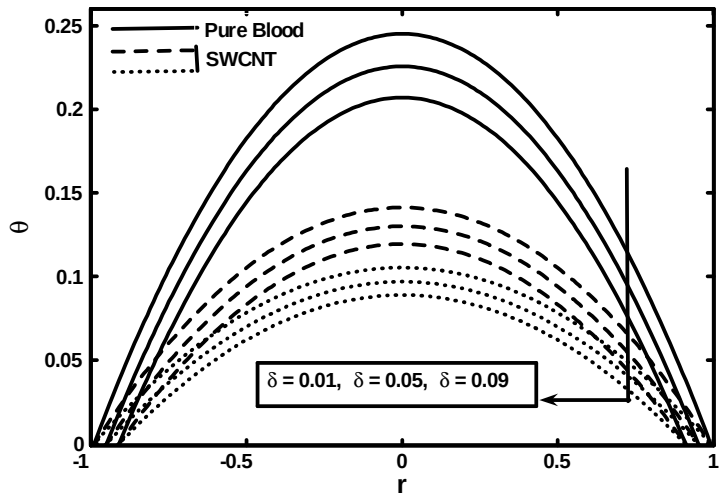

Fig. (7.11): Variation of temperature profile different values of stenosis height δ.

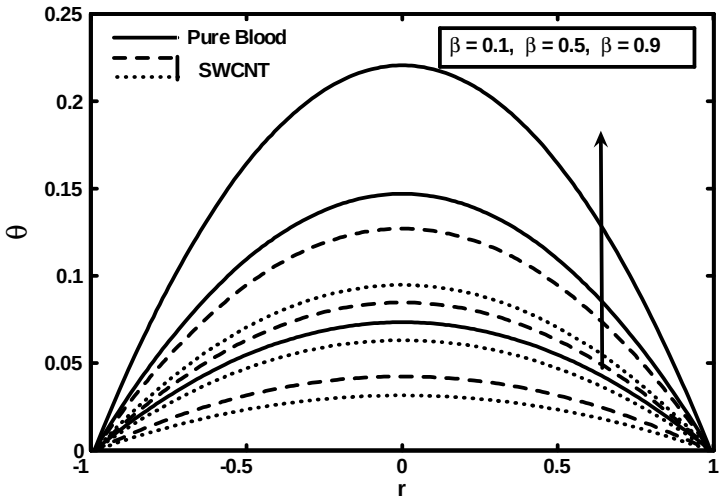

Fig. (7.12): Variation of temperature profile different values of the heat source parameter β.

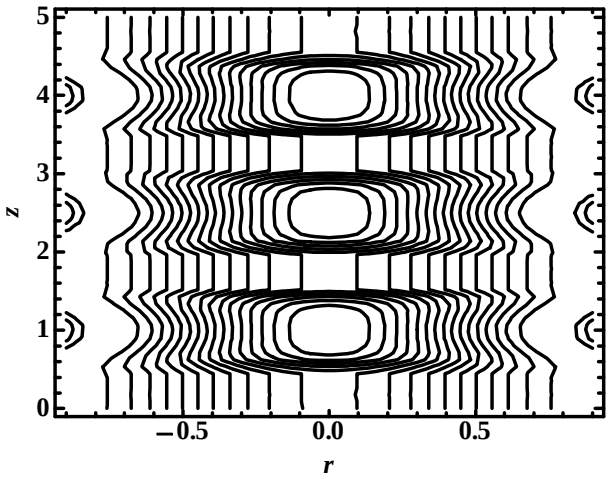

(a)

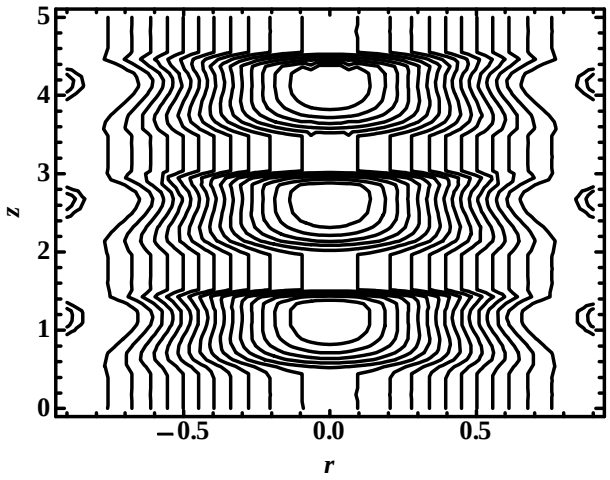

(b)

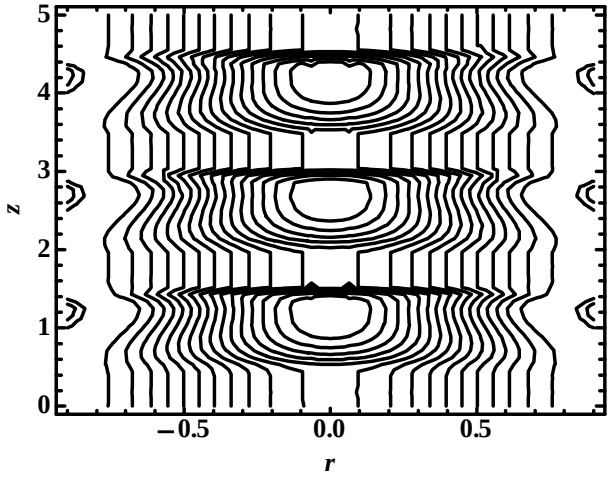

(c)

Figs. (7.13): Blood flow pattern for different values of stenosis shape (a) $n = 2$, (b) $n = 5$, (c) $n = 7$.

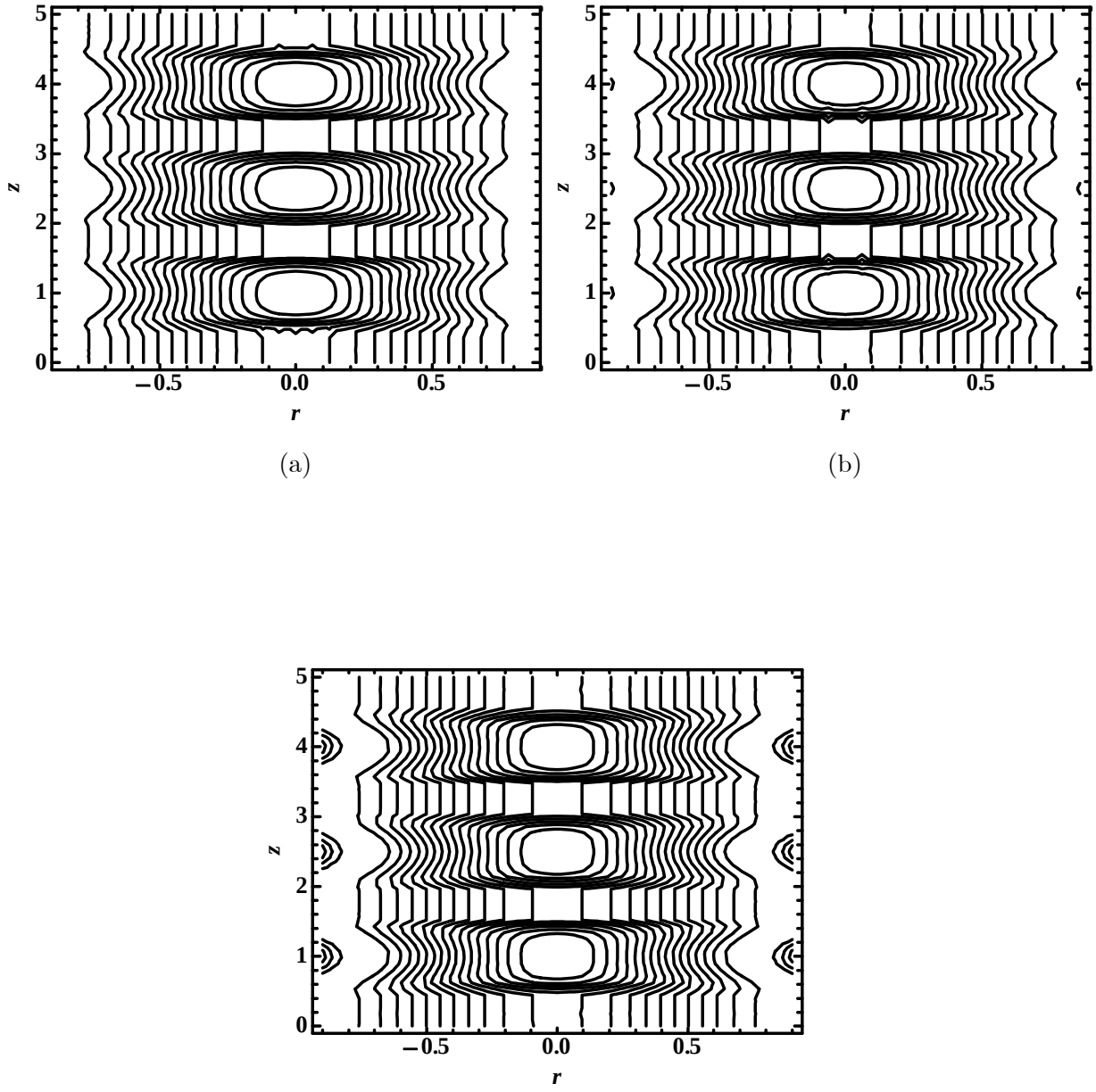

Fig. (7.14): Blood flow pattern for different values of stenosis height (a) $\delta = 0.22$, (b) $\delta = 0.24$, (c) $\delta = 0.26$.

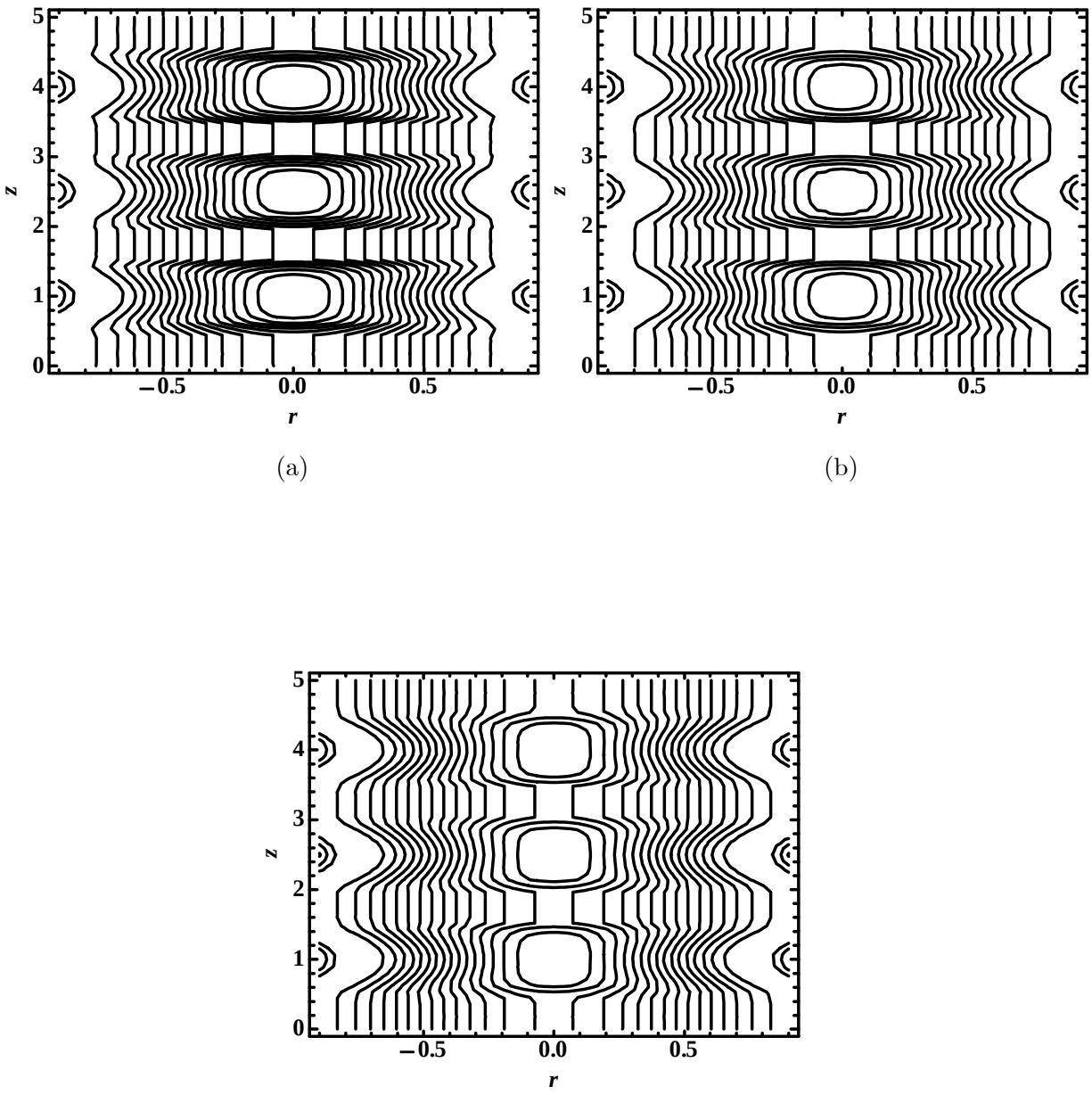

Fig. (7.15): Blood flow pattern for different values of the nanoparticle volume fraction (a), $\Phi = 0.00$ (pure blood), (b) $\Phi = 0.1$, (c) $\Phi = 0.2$.

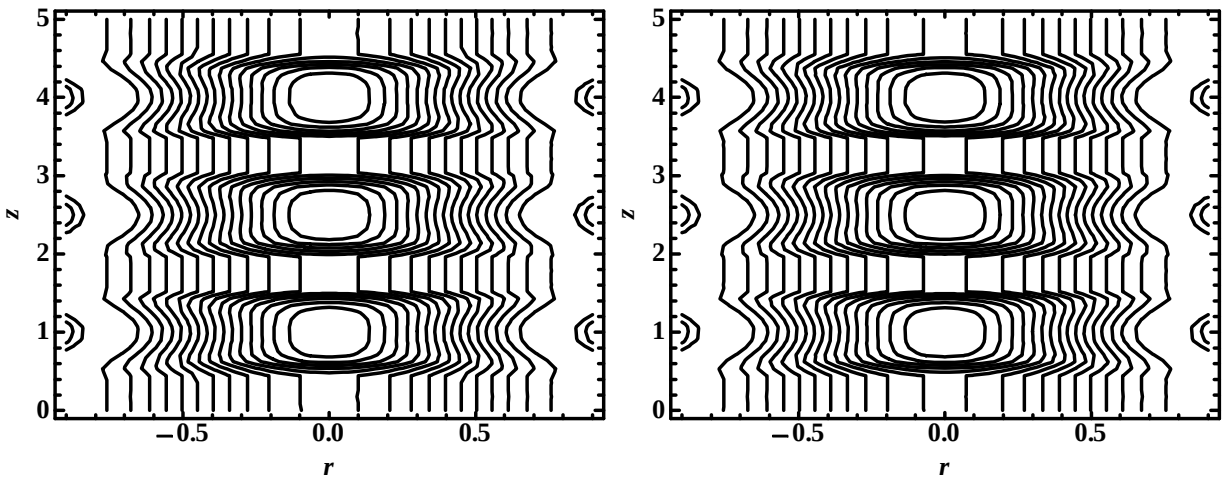

(a) (b)

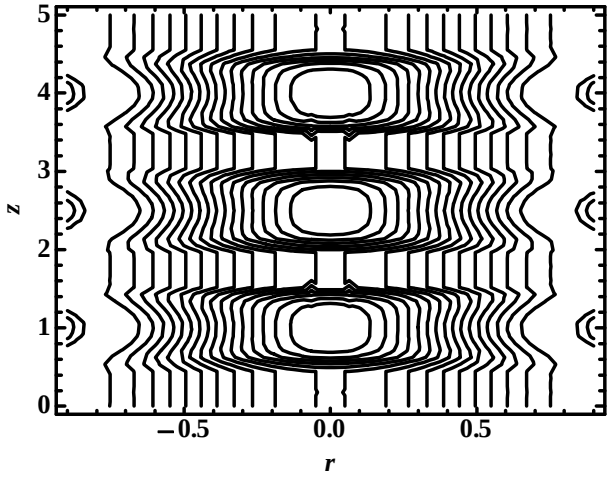

(c)

Fig. (7.16): Blood flow pattern for different values of the for different values of the viscosity parameter (a) $\alpha = 0.0$, (b) $\alpha = 0.05$, (c) $\alpha = 0.09$.

θ	Pure blood ($\Phi = 0.00$)			SWCNT ($\Phi = 0.04$)			SWCNT ($\Phi = 0.07$)		
r	$n = 2$	$n = 7$	$n = 11$	$n = 2$	$n = 7$	$n = 11$	$n = 2$	$n = 7$	$n = 11$
h	0.00000	0.00000	0.00000	0.00000	0.00000	0.00000	0.00000	0.00000	0.00000
0.8	0.09405	0.11108	0.11912	0.05423	0.06405	0.06869	0.04043	0.04775	0.05121
0.6	0.23405	0.25108	0.25912	0.13496	0.14478	0.14942	0.10061	0.10793	0.11139
0.4	0.33405	0.35108	0.35912	0.19262	0.20244	0.20708	0.14360	0.15092	0.15438
0.2	0.39405	0.41108	0.41912	0.22722	0.23704	0.24168	0.16939	0.17671	0.18017
0.0	0.41405	0.43108	0.43912	0.23875	0.24857	0.25321	0.17799	0.18531	0.18877
-0.2	0.39405	0.41108	0.41912	0.22722	0.23704	0.24168	0.16939	0.17671	0.18017
-0.4	0.33405	0.35108	0.35912	0.19262	0.20244	0.20708	0.17799	0.15092	0.15438
-0.6	0.23405	0.25108	0.25912	0.13496	0.14478	0.14942	0.10061	0.10793	0.11139
-0.8	0.09405	0.11108	0.11912	0.05423	0.06405	0.06869	0.04043	0.04775	0.05121
$-h$	0.00000	0.00000	0.00000	0.00000	0.00000	0.00000	0.00000	0.00000	0.00000

Table (7.2): Variations of temperature profile for different values of the stenosis shape n.

w	Pure blood ($\Phi = 0.00$)			SWCNT ($\Phi = 0.04$)			SWCNT ($\Phi = 0.07$)		
r	$n = 2$	$n = 7$	$n = 11$	$n = 2$	$n = 7$	$n = 11$	$n = 2$	$n = 7$	$n = 11$
h	0.00000	0.00000	0.00000	0.00000	0.00000	0.00000	0.00000	0.00000	0.00000
0.8	0.00668	0.00704	0.00716	0.00701	0.00742	0.00756	0.00735	0.00781	0.00799
0.6	0.02483	0.02473	0.02468	0.02503	0.02491	0.02485	0.02522	0.02509	0.02503
0.4	0.04383	0.04339	0.04323	0.04346	0.04296	0.04277	0.04307	0.04252	0.04229
0.2	0.05765	0.05702	0.05677	0.05675	0.05603	0.05575	0.05582	0.05501	0.05468
0.0	0.06266	0.06196	0.06161	0.06155	0.06075	0.06044	0.06040	0.05951	0.05915
-0.2	0.05765	0.05702	0.05677	0.05675	0.05603	0.05575	0.05582	0.05501	0.05468
-0.4	0.04383	0.04339	0.04323	0.04346	0.04296	0.04277	0.04307	0.04252	0.04229
-0.6	0.02483	0.02473	0.02468	0.02503	0.02491	0.02485	0.02522	0.02509	0.02503
-0.8	0.00668	0.00704	0.00716	0.00701	0.00742	0.00756	0.00735	0.00781	0.00799
$-h$	0.00000	0.00000	0.00000	0.00000	0.00000	0.00000	0.00000	0.00000	0.00000

Table (7.3): Variations of velocity profile for different values of the stenosis shape n.

Chapter 8

Influence of metallic nanoparticles on blood flow through arteries having both stenosis and aneurysm

In this chapter, the main objective is to discuss the blood flow analysis through inclined arteries by treating its nature as viscous fluid. The effects of both dilatation and constriction are considered to investigate the behavior of the both abnormal wall segments with variable nanofluid viscosity. The nonlinear momentum equation for proposed model is simplified by considering the non-dimensionless parameters to find the exact solutions of the formulated problem. The main hemodynamic effects of stenosis and aneurysm are discussed for different values of the interest by plotting the graphs of wall shear stress and resistance impedance to flow and opposite behavior is observed for both cases. The results also reveal that the nanoparticles with high concentration are important to reduce the resistance impedance to blood flow. The graphs of stream lines show the formation of bolus appears in the aneurysm segment but no formation is observed or seen in the stenotic segment.

8.1 Mathematical formulation

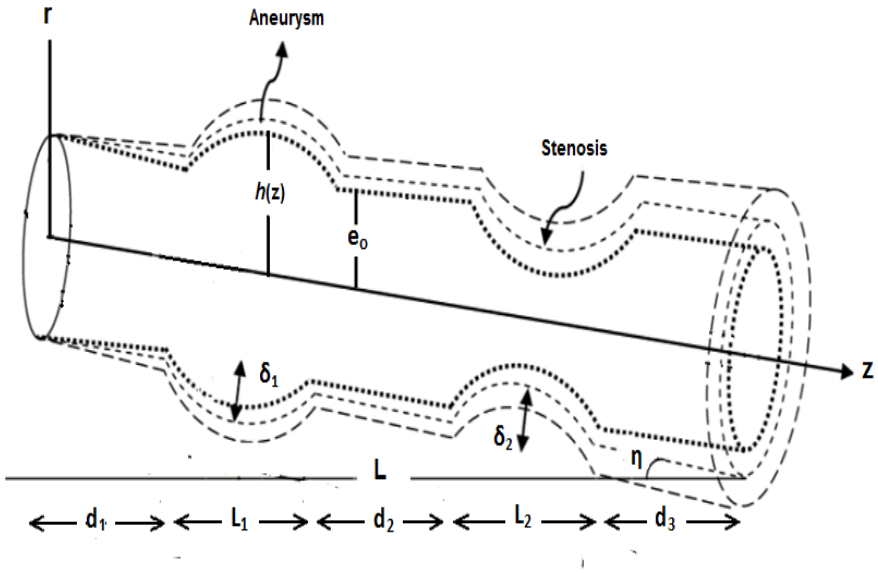

Fig. (8.1): Geometry of the problem.

Consider an incompressible and laminar nanofluid flowing through a vessel of finite length L and inclined at an angle η to the axis. Also heat transfer phenomenon is taken into account by giving temperature T_0 to the wall of the artery. The geometry of the arterial wall is defined as

$$\begin{aligned} \overline{h}(z) &= (\zeta\overline{z}+e_0)\left[e_0-\frac{\delta_i}{2}\left(1+\cos\frac{2\pi}{L_i}\left(\overline{z}-\alpha_i-\frac{L_i}{2}\right)\right)\right], \quad \alpha_i \le \overline{z} \le \beta_i, \\ &= (\zeta\overline{z}+e_0), \qquad\qquad \text{otherwise}, \end{aligned} \tag{8.1}$$

where in above equation $\overline{h}(z)$ is define as the radius of the abnormal arteries, δ_i as the maximum distance of the i^{th} abnormal segment projects into the lumen and is negative for aneurysms and positive for stenosis, L_i as the length of the i^{th} abnormal segment, α_i as the distance from the origin to the start of the i^{th} abnormal segment and is given by

$$\alpha_i = \sum_{j=1}^{i}(d_j+L_j)-L_i, \tag{8.2}$$

and β_i as the distance from the origin to the end of the i^{th} abnormal segment is given as

$$\beta_i = \sum_{j=1}^{i} (d_j + L_j), \tag{8.3}$$

in which d_i is the distance separating the start of the i^{th} abnormal segment from the start of the segment if $i = 1$. In above geometry e_0 is defined as constant radius of the normal artery in the non-stenotic region, ϕ as the tapering angle, L_1 and L_2 as the lengths of aneurysm and stenosis, δ_1 and δ_2 as the critical heights of the aneurysm and stenosis, ζ =tanϕ as the slope of the tapered artery. The possibility of different shapes of the arteries are defined as the converging tapering ($\phi < 0$), as the non-tapered artery ($\phi = 0$) and as the diverging tapering ($\phi > 0$). The governing equations for conservation of mass, momentum and temperature for viscous fluid for an inclined artery can be written as

$$\frac{\partial \overline{u}}{\partial \overline{r}} + \frac{\overline{u}}{\overline{r}} + \frac{\partial \overline{w}}{\partial \overline{z}} = 0, \tag{8.4}$$

$$\begin{aligned} \rho_{nf}\left(\overline{u}\frac{\partial \overline{u}}{\partial \overline{r}} + \overline{w}\frac{\partial \overline{u}}{\partial \overline{z}}\right) &= -\frac{\partial \overline{p}}{\partial \overline{r}} + \frac{1}{\overline{r}}\frac{\partial}{\partial \overline{r}}\left(2\overline{r}\mu_{nf}\frac{\partial \overline{u}}{\partial \overline{r}}\right) + \frac{\partial}{\partial \overline{z}}\left(\mu_{nf}\left(\frac{\partial \overline{u}}{\partial \overline{z}} + \frac{\partial \overline{w}}{\partial \overline{r}}\right)\right) \\ &\quad -2\mu_{nf}\frac{\overline{u}}{\overline{r}^2} - g(\rho\gamma)_{nf}(\overline{T} - T_o)\cos\eta - g\rho_{nf}\cos\eta, \end{aligned} \tag{8.5}$$

$$\begin{aligned} \rho_{nf}\left(\overline{u}\frac{\partial \overline{w}}{\partial \overline{r}} + \overline{w}\frac{\partial \overline{w}}{\partial \overline{z}}\right) &= -\frac{\partial \overline{p}}{\partial \overline{z}} + \frac{1}{\overline{r}}\frac{\partial}{\partial \overline{r}}\left(\overline{r}\mu_{nf}\left(\frac{\partial \overline{u}}{\partial \overline{z}} + \frac{\partial \overline{w}}{\partial \overline{r}}\right)\right) + \frac{\partial}{\partial \overline{z}}\left(2\mu_{nf}\left(\frac{\partial \overline{w}}{\partial \overline{z}}\right)\right) \\ &\quad +g(\rho\gamma)_{nf}(\overline{T} - T_o)\sin\eta + g\rho_{nf}\sin\eta, \end{aligned} \tag{8.6}$$

$$\left(\frac{\partial \overline{T}}{\partial \overline{t}} + \overline{u}\frac{\partial \overline{T}}{\partial \overline{r}} + \overline{w}\frac{\partial \overline{T}}{\partial \overline{z}}\right) = \frac{K_{nf}}{(\rho c_p)_{nf}}\left(\frac{\partial^2 \overline{T}}{\partial \overline{r}^2} + \frac{1}{\overline{r}}\frac{\partial \overline{T}}{\partial \overline{r}} + \frac{\partial^2 \overline{T}}{\partial \overline{z}^2}\right) + \frac{Q_0}{(\rho c_p)_{nf}}. \tag{8.7}$$

In above equations the thermo physical properties with respect to blood and copper nanoparticles are given as

$$\mu_{nf} = \frac{\mu_f(\theta)}{(1-\Phi)^{2.5}}, \quad \alpha_{nf} = \frac{K_{nf}}{(\rho c_p)_{nf}}, \quad \rho_{nf} = (1-\Phi)\rho_f + \Phi\rho_s,$$
$$(\rho c_p)_{nf} = (1-\Phi)(\rho c_p)_f + \Phi(\rho c_p)_s, \quad (\rho\gamma)_{nf} = (1-\Phi)(\rho\gamma)_f + \Phi(\rho\gamma)_s,$$
$$\frac{K_{nf}}{K_f} = \frac{(K_s+2K_f) - 2\Phi(K_f - K_s)}{(K_s+2K_f) + \Phi(K_f - K_s)}, \ \mu_f(\theta) = \mu_o e^{-\alpha\theta}. \tag{8.8}$$

Non-dimensional variables are defined as

$$\begin{aligned} r &= \frac{\overline{r}}{e_0}, \ w = \frac{\overline{w}}{u_o}, \ u = \frac{\widetilde{L}\overline{u}}{u_o\widetilde{\delta}}, \ p = \frac{e_0^2\overline{p}}{u_o\widetilde{L}\mu_o}, \ t = \frac{\overline{t}u_o}{\widetilde{L}}, \\ \beta &= \frac{Q_0 e_0^2}{T_0 K_f}, \ H = \frac{F_r}{R_{en}}, \ R_{en} = \frac{e_0 u_o \rho_f}{\mu_o}, \ G_r = \frac{g\gamma_f\rho_f e_0^2 T_0}{u_0\mu_o}, \\ \theta &= \frac{\overline{T} - T_o}{T_o}, \ z = \frac{\overline{z}}{\widetilde{L}}, \ F_r = \frac{u_o^2}{g e_0}, \ L = \frac{\overline{L}}{\widetilde{L}}. \end{aligned} \tag{8.9}$$

Here $\widetilde{\delta}$ represents as $\widetilde{\delta} = \max(\delta_1,\ \delta_2)$, $\widetilde{L}$ as $\widetilde{L} = \min(L_1,\ L_2)$ and F_r as the Froud number. Utilizing above Eq. (8.9), by assuming $\epsilon = \frac{e_0}{\widetilde{L}} \approx O(1)$ and taking mild stenosis and aneurysm condition the governing Eqs. (8.5) to (8.7) can be written as

$$\frac{\partial p}{\partial r} = 0, \tag{8.10}$$

$$\frac{\partial p}{\partial z} = \frac{1}{r}\frac{\partial}{\partial r}\left(\frac{\mu_{nf}(\theta)}{\mu_o}\left(r\frac{\partial w}{\partial r}\right)\right) + \frac{(\rho\gamma)_{nf}}{(\rho\gamma)_f}G_r\theta\sin\eta + \frac{\rho_{nf}}{\rho_f}\frac{R_{en}\sin\eta}{F_r}, \tag{8.11}$$

$$\frac{\partial^2\theta}{\partial r^2} + \frac{1}{r}\frac{\partial\theta}{\partial r} + \beta\frac{K_f}{K_{nf}} = 0. \tag{8.12}$$

The geometry of the arterial wall in dimensionless form is defined as

$$\begin{aligned} h(z) &= (\zeta^* z + 1)\left[1 - \frac{\delta_i^*}{2}\left(1 + \cos\frac{2\pi}{\nu_i}\left(z - \alpha_i^* - \frac{\nu_i}{2}\right)\right)\right] \ \text{for } \alpha_i^* \le z \le \beta_i^*, \\ &= (\zeta^* z + 1), \qquad \text{otherwise.} \end{aligned} \tag{8.13}$$

where

$$\delta_i^* = \frac{\delta_i}{e_0},\ d_i^* = \frac{d_i}{\widetilde{L}},\ \nu_i = \frac{L_i}{\widetilde{L}}. \tag{8.14}$$

Corresponding boundary conditions are defined as

$$w = 0 \ \ at \ \ r = h(z), \ \ \frac{\partial w}{\partial r} = 0 \ \ at \ \ r = 0, \tag{8.15}$$

$$\theta = 0 \ \ at \ \ r = h(z), \ \ \frac{\partial \theta}{\partial r} = 0 \ \ \ at \ \ r = 0. \tag{8.16}$$

8.2 Solution of the problem

The exact solutions of temperature distribution and velocity profile using Eqs. (8.15) and (8.16) are written as

$$\theta = -\frac{1}{4}\beta(r^2 - h^2)\left(\frac{K_s(1-\Phi) + K_f(2+\Phi)}{K_s(1+2\Phi) + 2K_f(1-\Phi)}\right), \tag{8.17}$$

$$\begin{aligned} w \ = \ & \frac{dp}{dz}\frac{(h-r)(h+r)(1-\Phi)^{2.5}(-6Hk_3(z) - 3H(h^2+r^2)k_4(z))}{24H} + \\ & \frac{1}{24H}(h-r)(h+r)(2H\sin\eta\ (6k_5(z) + 3(h^2+r^2)k_6(z) + 2(h^4 + \\ & h^2r^2 + r^4)k_7(z))A_2 + 6(1-\Phi)^{2.5}\sin\eta\ k_3(z)A_3 + 3(1-\Phi)^{2.5} \\ & (h^2+r^2)\sin\eta\ k_4(z)A_3). \end{aligned} \tag{8.18}$$

Flow rate is given as

$$F = \int_0^h rw dr. \tag{8.19}$$

Using Eq. (8.18) into Eq. (8.19), we get the expression for pressure gradient as follows

$$\frac{dp}{dz} = -\frac{(F - h^4\sin\eta\ k_9(z))}{h^4(1-\Phi)^{2.5}k_8(z)}. \tag{8.20}$$

Since F is constant for all sections, the pressure drop across the length of the abnormal artery is given as

$$\Delta p = \int_0^{L^*} \left(-\frac{dp}{dz}\right) dz. \tag{8.21}$$

Using above Eq. (8.21), the impedance resistance can be given after simplifying the i^{th} abnormal segment from $i = 1$ as

$$\lambda = \frac{\Delta p}{F} = \left\{ \int_0^{\alpha_1^*} \Sigma_5(z)dz + \int_{\alpha_1^*}^{\beta_1^*} \Omega_5(z)dz + \int_{\beta_1^*}^{\alpha_2^*} \Sigma_5(z)dz + \int_{\alpha_2^*}^{\beta_2^*} \Omega_5(z)dz + \int_{\beta_2^*}^{L} \Sigma_5(z)dz \right\}, \tag{8.22}$$

where

$$\Omega_5(z) = \frac{(F - h^4 \sin\eta \; k_9(z))}{h^4 F(1-\Phi)^{2.5} k_8(z)}, \tag{8.23}$$

$$\Sigma_5(z) = \Omega_5(z) \mid_{h=(\zeta^* z+1)} . \tag{8.24}$$

Using Eq. (8.18) expression for the wall shear stress is given as

$$\begin{aligned} S_{rz} = & -\frac{1}{(1-\Phi)^{2.5}(k_3(z) + h^2 k_4(z))}\Big(\frac{dp}{dz}\frac{-h(1-\Phi)^{2.5}(-6Hk_3(z) - 6h^2 H k_4(z))}{12H} - \\ & \frac{1}{12H}(h(2H\sin\eta(6k_5(z) + 6h^2 k_6(z) + 6h^4 k_7(z))A_2 + 6(1-\Phi)^{2.5}\sin\eta \\ & k_3(z)A_3 + 6(1-\Phi)^{2.5} h^2 \sin\eta k_4(z)A_3)). \end{aligned} \tag{8.25}$$

8.3 Appendix

$$A_1 = \left(\frac{K_s(1-\Phi)+K_f(2+\Phi)}{K_s(1+2\Phi)+2K_f(1-\Phi)}\right),\ A_2 = G_r\left((1-\Phi)+\Phi\frac{\rho_s\gamma_s}{\rho_f\gamma_f}\right)(1-\Phi)^{2.5}$$

$$A_3 = \left((1-\Phi)+\Phi\frac{\rho_s}{\rho_f}\right),\ k_1(z) = \frac{\beta A_1}{4},\ k_2(z) = \frac{\beta h^2 A_1}{4},\ k_3(z) = 1+\alpha\ k_2(z),$$

$$k_4(z) = -\alpha\ k_1(z),\ k_5(z) = \frac{k_2(z)k_3(z)}{2},\ k_6(z) = -\frac{k_1(z)k_3(z)}{4}+\frac{k_2(z)k_4(z)}{2},$$

$$k_7(z) = -\frac{k_1(z)k_4(z)}{4},\ k_8(z) = -\frac{(3k_3(z)+2h^2k_4(z))}{48},$$

$$k_9(z) = \frac{(H(6k_5(z)+4h^2k_6(z)+3h^4k_7(z))A_2+(1-\Phi)^{2.5}(3k_3(z)+2h^2k_4(z))A_3)}{48H}.$$

$$\alpha_1^* = d_1^*,\ \beta_1^* = d_1^*+\upsilon_1,\ \alpha_2^* = d_1^*+d_2^*+\upsilon_1,\ \beta_2^* = d_1^*+d_2^*+\upsilon_1+\upsilon_2.$$

8.4 Results and discussion

In this present model computer codes are used to calculate the results obtained for the resistance impedance to flow and the wall shear stress distribution in order to perceive the quantitative effects of the heat source parameter β, the Grashof number G_r, the nanoparticles volume fraction Φ, the viscosity parameter α, the critical height of the aneurysm δ_1 and the critical height of the stenosis δ_2 respectively. The graphs are plotted by considering three different types of tapering effects for mild stenosis and aneurysm cases by keeping the parameters constants such as $\Phi = 0.01$, $F_r = 0.9$, $\beta = 2.0$, $\alpha = 0.1$, $\beta = 0.9$, $\delta_1 = 0.15$, $\delta_2 = 0.15$, $F = 0.7$, $G_r = 2.0$, $d_1^* = d_2^* = 0.5$, $\nu_1 = \nu_2 = 1.0$, $\eta = \frac{\pi}{4}$ (inclined arteries), $R_{en} = 1$. Since the aneurysm and stenosis are the contraction and expansion of the lumen respectively, so the projection of aneurysm into the lumen is considered as negative and considered as positive projection for stenosis to plot the graphs of the obtained expressions. The magnitude of wall shear stress is very essential to understand the arterial disease because of its strong correlation with the constriction or expansion of the arteries. The graphs of wall shear stress along axial displacement are plotted in Figs. (8.2) − (8.7) with different tapering effects. For the case of aneurysm segment between $0.5 \leq z \leq 1.5$, it is important to note that wall shear stress starts decreasing towards the downstream of the aneurysm segment (0.5 to 1.0) to approach its minimum value (at $z = 1.0$) and then starts steeply increasing from its minimum value towards

the end of the aneurysm segment (1.0 to 1.5). Now, for the case of stenosis wall shear stress between the stenotic segment $2.0 \leq z \leq 3.0$ starts steeply increasing towards the upstream of the stenotic segment (2.0 to 2.5) to approach its maximum value (at $z = 2.5$) and then starts rapidly decreasing from its maximum value towards the end of the stenotic segment (2.5 to 3.0). Figs. (8.2) and (8.3) are plotted for different values of the heat source parameter β and the Grashof number G_r. These figures show that the stress on the wall of arteries under the different tapering effects start decreasing with an increase in the values of the heat source parameter β and the Grashof number G_r. In Fig. (8.4), it is observed that the stresses on the wall of arteries start decreasing with an increase in the values of the inclination angle η. The wall shear stress for different values for the viscosity parameter α is plotted in Figs. (8.5). In this graph of wall shear stress along axial displacement depicts that the stress on the wall of arteries decreases for the viscosity parameter α. The wall shear stress for different values of the nanoparticles volume fraction Φ is plotted in Fig. (8.6) and observed that the significance of wall shear stress increases with an increase in nanoparticles volume fraction. The graphs of the wall shear stress along axial displacement for different values of the critical height of the aneurysm δ_1 and the critical height of the stenosis δ_2 is plotted in Fig. (8.7). It is analyzed in the Fig. (8.7) that the stresses on the wall of arteries decreases with an increase in the values of the critical height of aneurysm δ_1 between the interval 0.5 to 1.5, while the stresses on the wall of arteries increases with an increase in the values of the critical height of stenosis δ_2 in the stenotic section between the interval 2.0 to 3.0. To investigate the resistance impedance to flow containing two diseased portion of wall in proximity three dimensional surfaces is utilized to characterize that how the resistance impedance to flow varies with different combination of disease section. The resistance impedance to flow is plotted for non-tapered arteries from Figs. $(8.8) - (8.13)$, while Fig. (8.14) is plotted for diverging and converging tapering effects. These graphs depict that resistance impedance to flow decreases with an increase in the critical height of aneurysm δ_1, while increases with an increase in the values of critical height of stenosis δ_2. The resistance impedance to flow for different values of Grashof number G_r and heat source parameter β is given through Figs. $(8.8) - (8.9)$. It is observed from these figures that resistance impedance to flow decreases with an in the values of Grashof number G_r and heat source parameter β. In Fig. (8.10), it is observed that resistance in blood flow through diseased inclined arteries

decreases with an increase in the values of the viscosity parameter α. Fig. (8.11), shows that the resistance impedance to blood flow increases with an increase in the Froud number. The variations for different values of nanoparticles volume fraction Φ and inclination angle η are depicted in Figs. (8.12) and (8.13). It is observed that the resistance to blood flow decreases with an increase in the nanoparticles volume fraction and also decreases with an increase in the values of inclination angle η. The tapering is a substantial aspect in the mammalian system and is discussed in Fig. (8.14). It is depicted in this graph the resistance impedance to flow gives higher results for converging tapering when compare to other tapering arteries for both the aneurysm and stenosis segments. Trapping described an interesting phenomenon for the blood flow pattern in an inclined artery having aneurysm and stenosis that is discussed through Figs. (8.16) − (8.19) for non-tapered arteries, while other associated arteries are discussed in Fig. (8.15). Fig. (8.15) is strategized to show converging and diverging tapering effects on the arteries. It is depicted that trapping bolus moves toward right side of the inclined arteries for converging case by the closed stream lines, while for diverging case trapping bolus moves towards left side of the inclined arteries when compared to the non-tapered arteries panel. In Figs (8.16), it is observed that with an increase in the critical height δ_1 the trapped bolus increases in the aneurysm segment ($0.5 \leq z \leq 1.5$), while stream lines become wider with an increase in the critical height δ_2 in the stenotic segment ($2.0 \leq z \leq 3.0$). From Fig. (8.17), it is observed that no bolus is seen for horizontal stenosed arteries when compared to the panel of vertical and inclined stenosed arteries. The possessions of nanoparticles volume fraction Φ is discussed in Fig. (8.18) and observed that the trapping bolus decreases with an in increase in metallic nanoparticles when compare to the panel of pure blood case $\Phi = 0.00$. The trapping phenomenon for the viscosity parameter α is discussed in Figs. (8.19) and it is depicted from these figures that the trapping bolus shows random behavior for different values of viscosity parameter α.

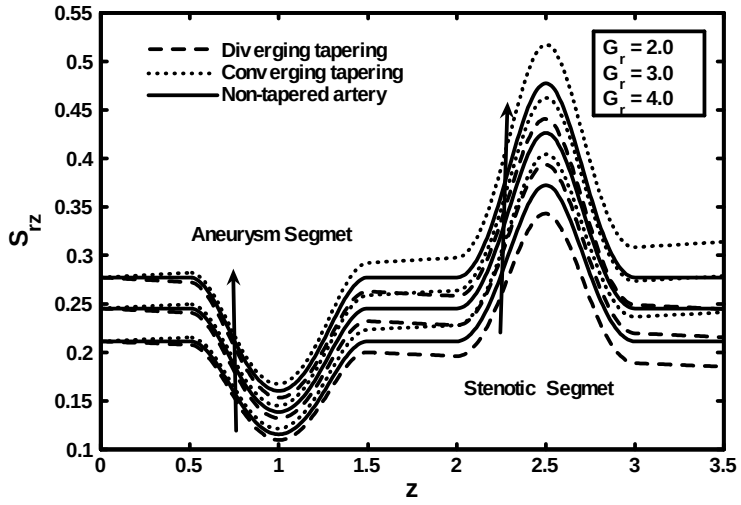

Fig. (8.2): Variation of wall shear stress for different values of Grashof number G_r.

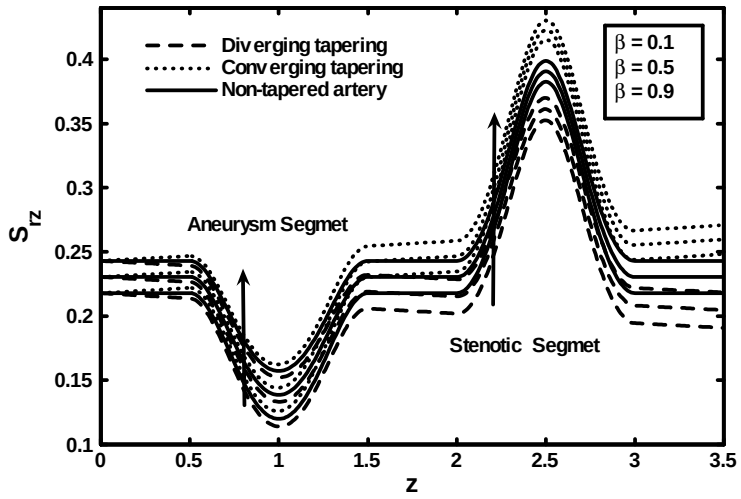

Fig. (8.3): Variation of wall shear stress for different values the heat source parameter β.

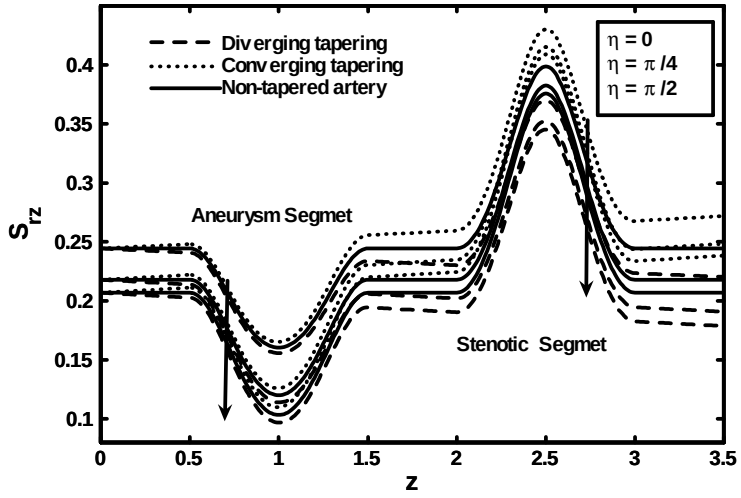

Fig. (8.4): Variation of wall shear stress for different values inclination angle η.

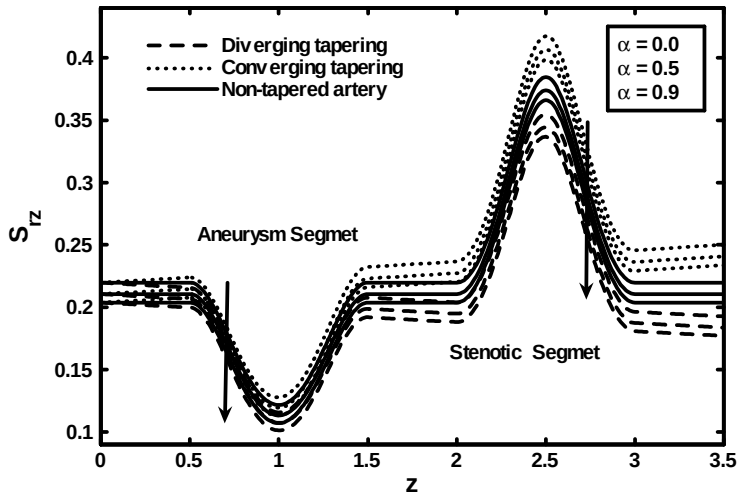

Fig. (8.5): Variation of wall shear stress for different values the viscosity parameter α.

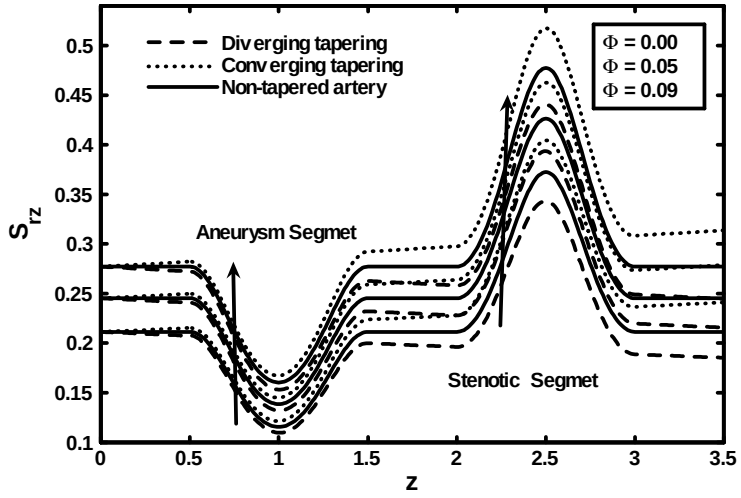

Fig. (8.6): Variation of wall shear stress for different values the nanoparticle volume fraction Φ.

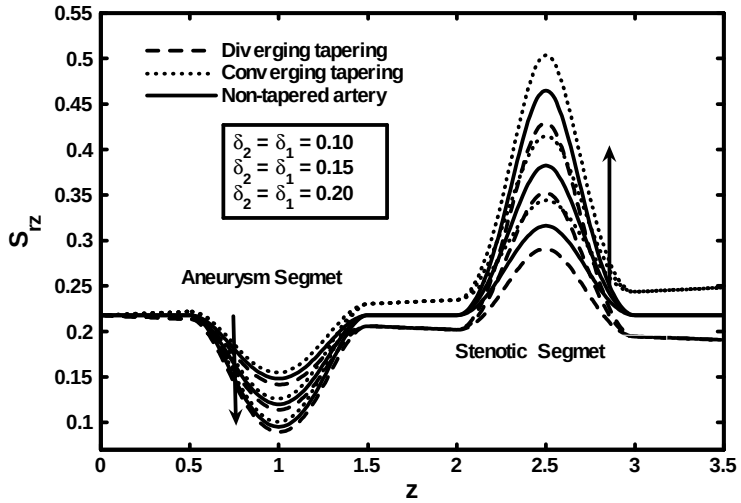

Fig. (8.7): Variation of wall shear stress for different values the critical height of the aneurysm δ_1 and stenosis δ_2.

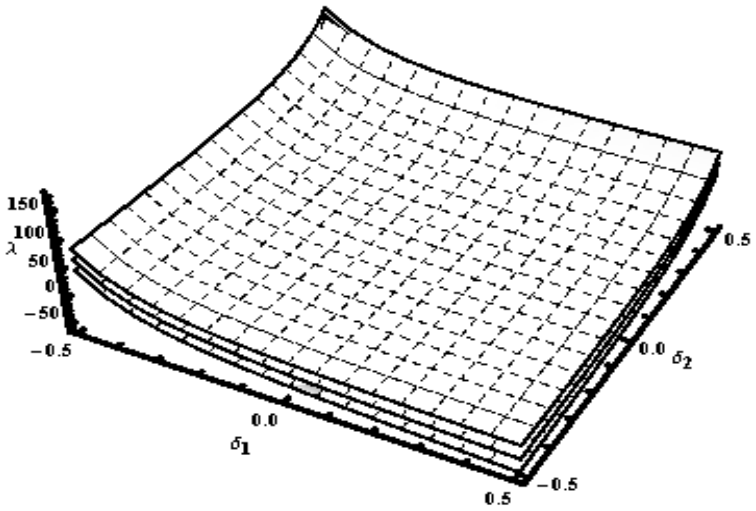

Fig. (8.8): Variation of resistance impedance for different values of the Grashof number $G_r = 2.0$, $G_r = 5.0$, $G_r = 9.0$.

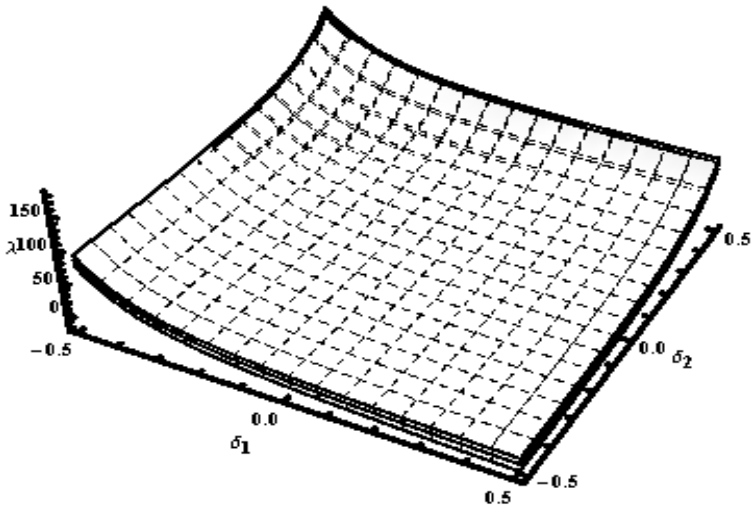

Fig. (8.9): Variation of resistance impedance for different values of the heat source parameter $\beta = 2.0$, $\beta = 5.0$, $\beta = 9.0$.

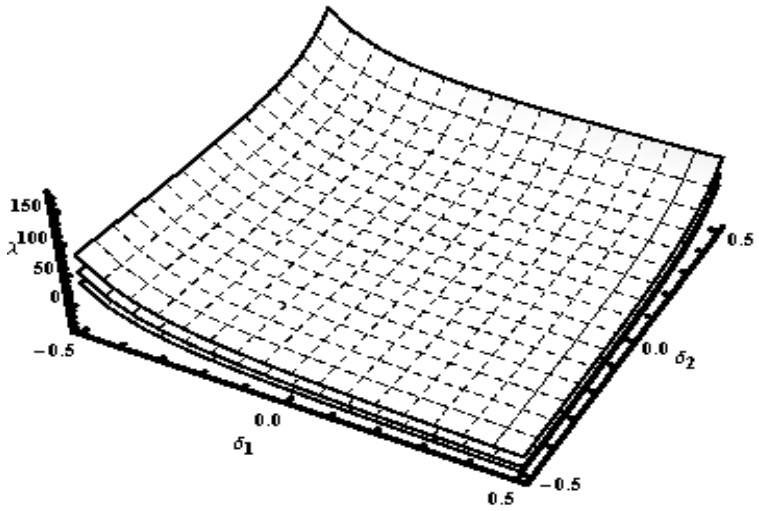

Fig. (8.10): Variation of resistance impedance for different values of the viscosity parameter $\alpha = 0.0$, $\alpha = 0.5$, $\alpha = 0.9$.

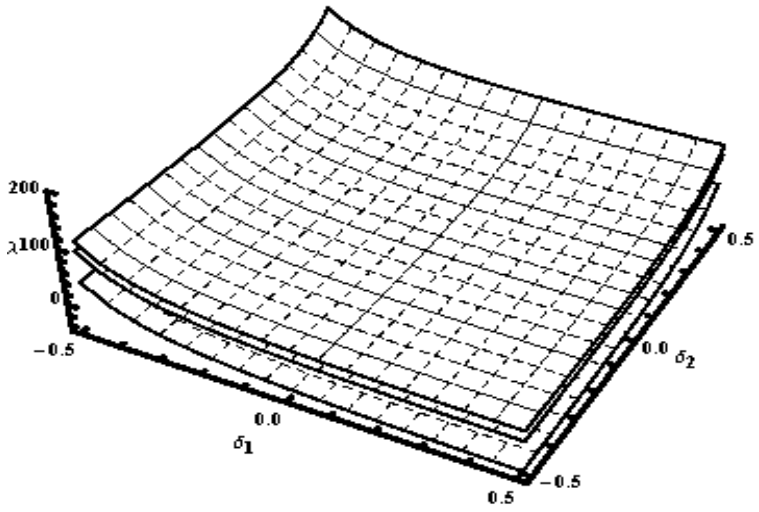

Fig. (8.11): Variation of resistance impedance for different values of the Froud number $F_r = 0.1$, $F_r = 0.3$, $F_r = 0.9$.

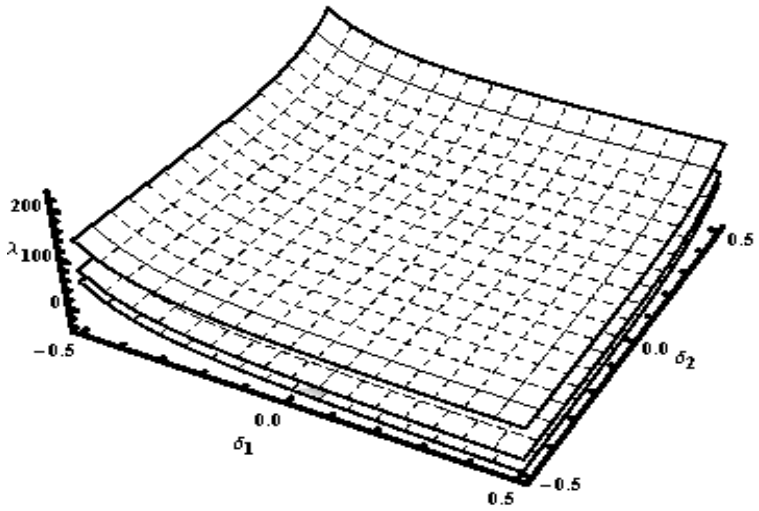

Fig. (8.12): Variation of resistance impedance for different values of the inclination angle $\eta = 0$ (horizontal arteries), $\eta = \frac{\pi}{4}$ (inclined arteries), $\eta = \frac{\pi}{2}$ (vertical arteries).

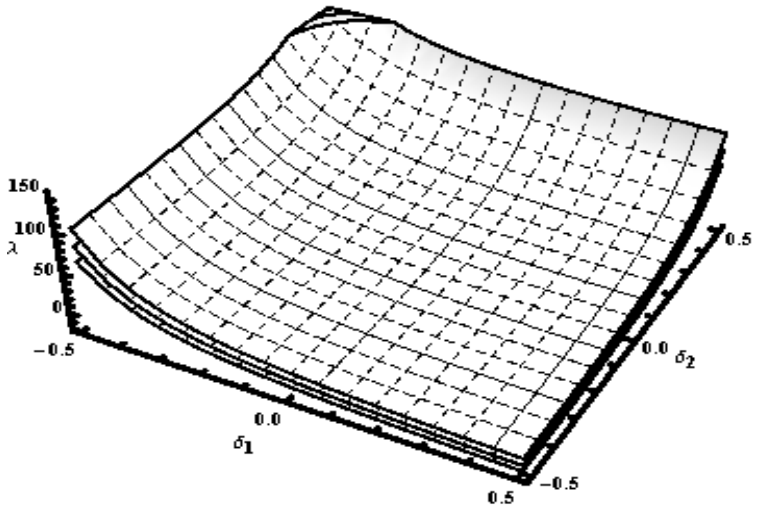

Fig. (8.13): Variation of resistance impedance for different values of the nanoparticle volume fraction $\Phi = 0.00$ (pure blood), $\Phi = 0.05$, $\Phi = 0.09$.

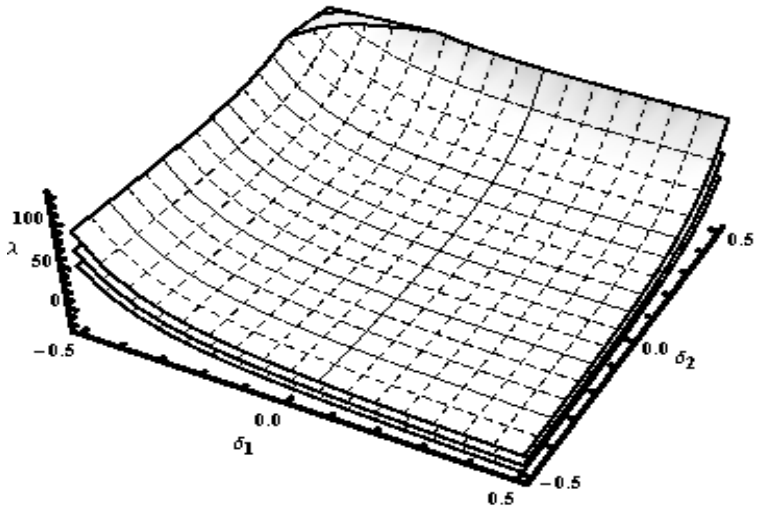

Fig. (8.14): Variation of resistance impedance for the different tapering effects $\phi = 0.00$, $\phi = 0.01$, $\phi = -0.01$.

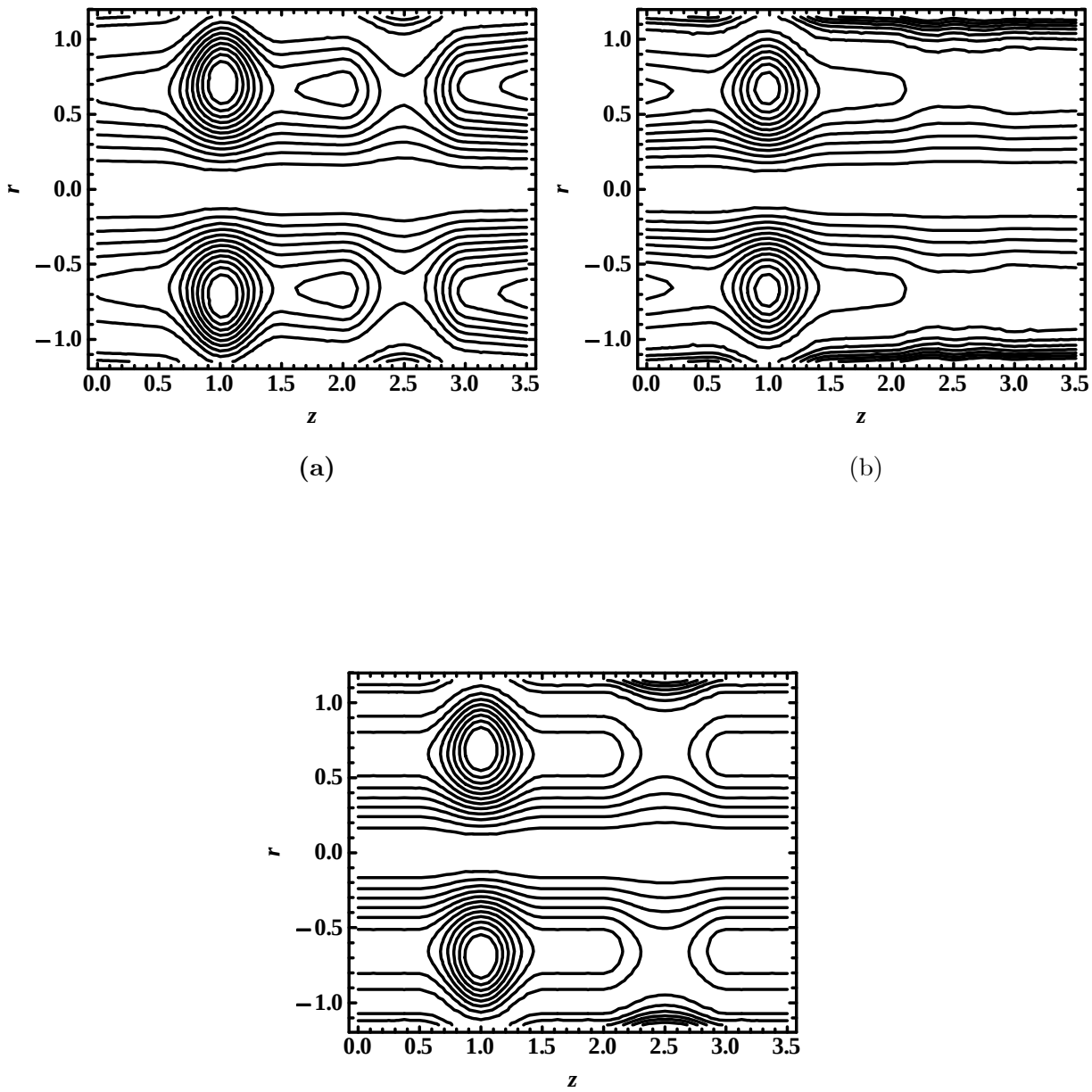

Fig. (8.15): Blood flow pattern for different values of the tapering angle, (a) diverging tapering $\phi \succ 0$, (b) converging tapering $\phi \prec 0$, (c) non-tapered artery $\phi = 0.00$.

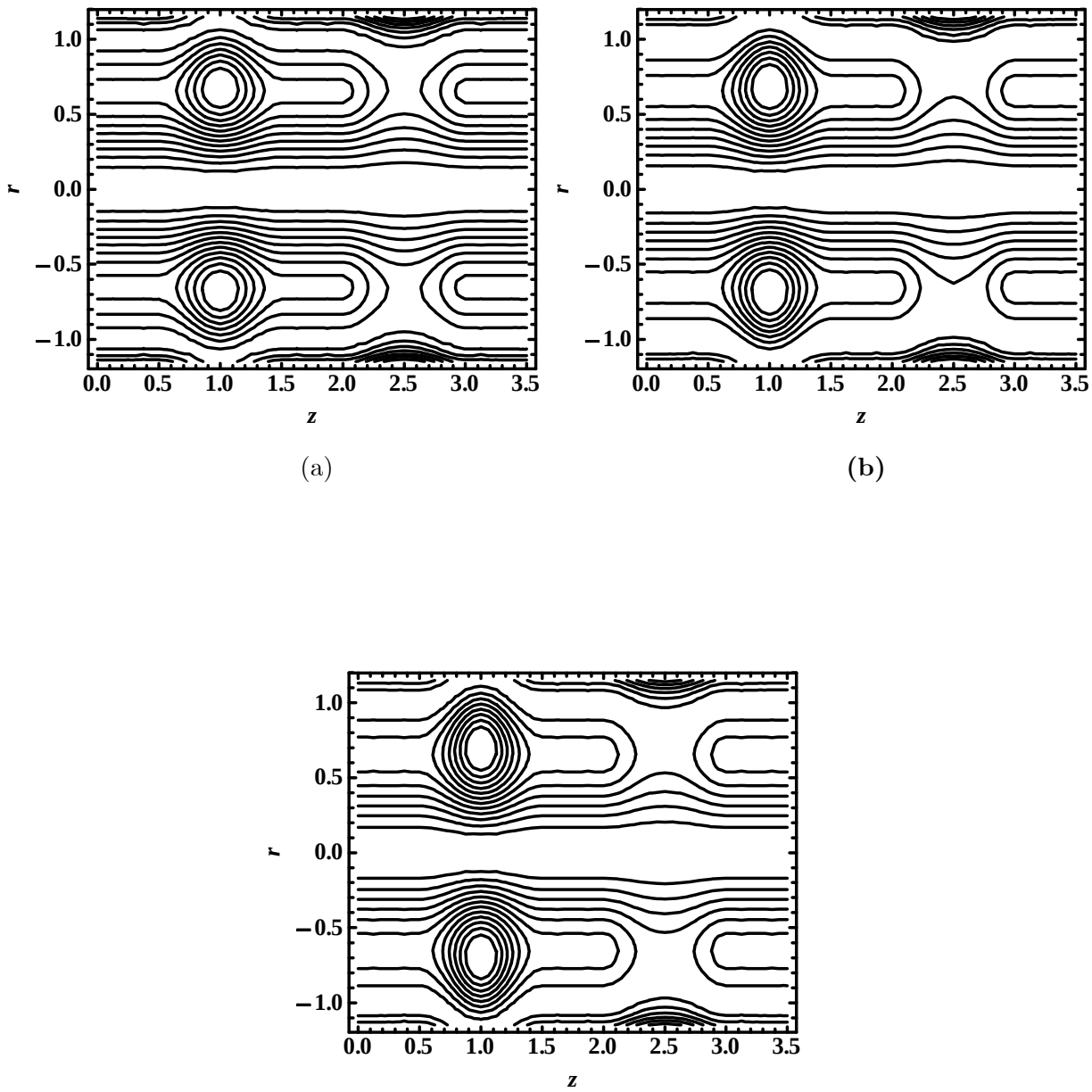

Fig. (8.16): Blood flow pattern for different values of the critical height of the aneurysm and stenosis (a) $\delta_2 = \delta_1 = 0.10$, (b) $\delta_1 = \delta_2 = 0.13$, (c) $\delta_1 = \delta_2 = 0.16$.

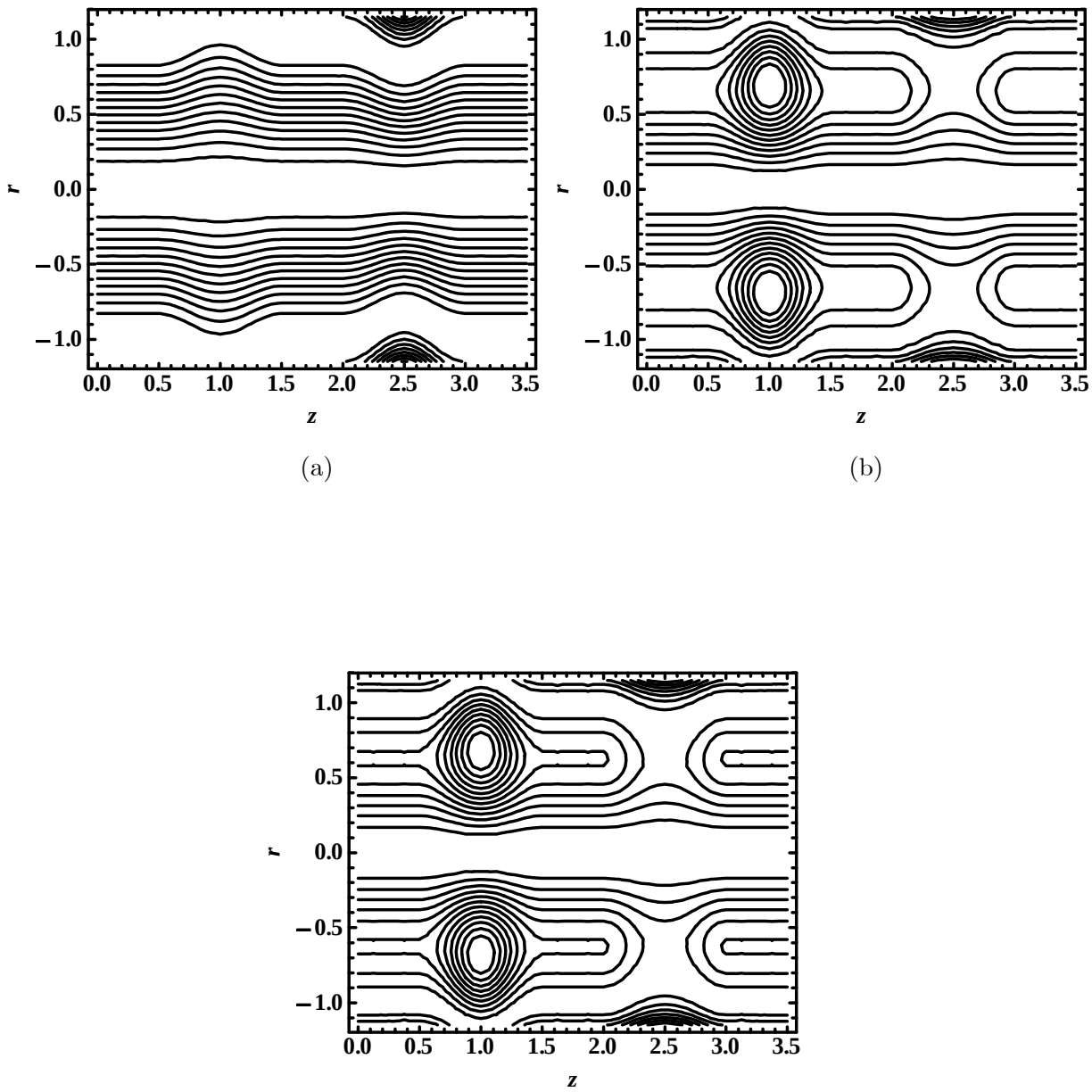

Fig. (8.17): Blood flow pattern for different values of the inclination angle (a) $\eta = 0$, (b) $\eta = \frac{\pi}{4}$, (c) $\eta = \frac{\pi}{2}$.

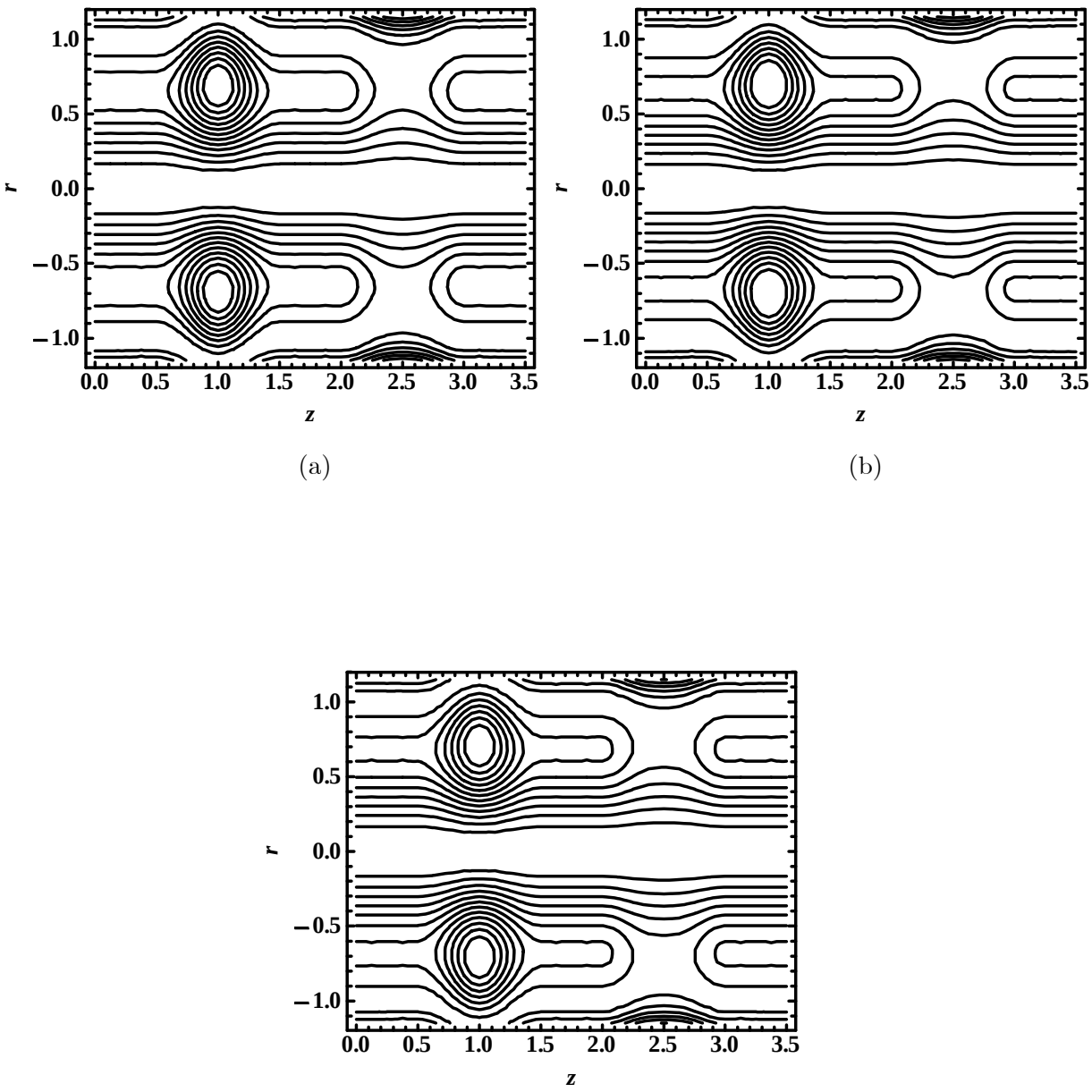

Fig. (8.18): Blood flow pattern for different values of the nanoparticle volume fraction (a) $\Phi = 0.00$, (b) $\Phi = 0.01$, (c) $\Phi = 0.02$.

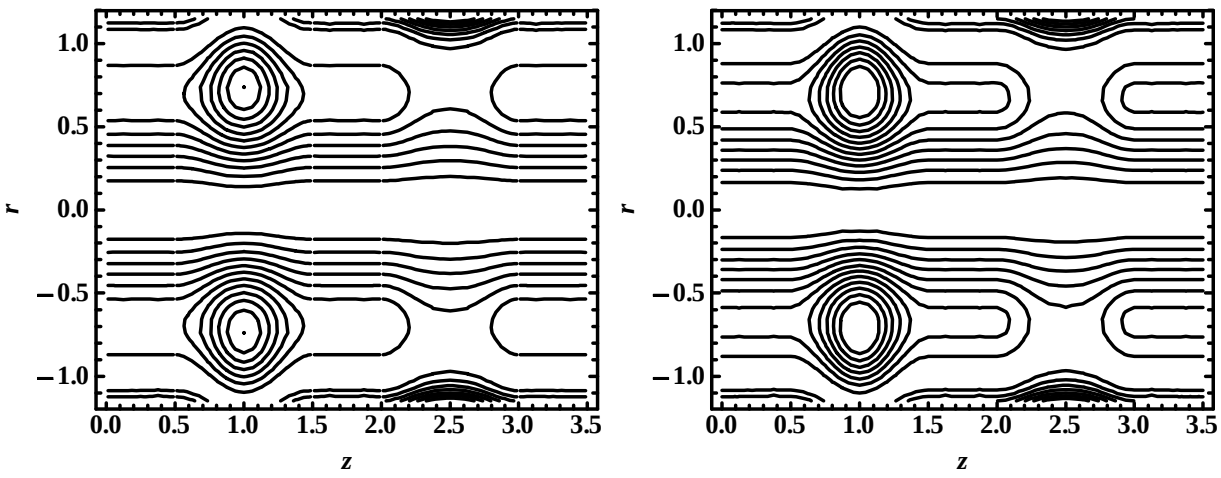

(a) (b)

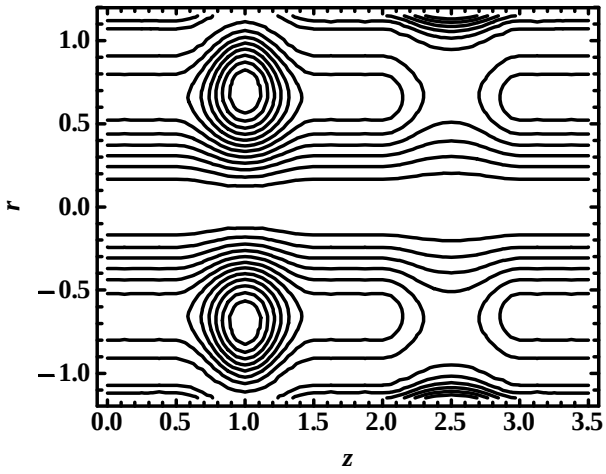

(c)

Fig. (8.19): Blood flow pattern for different values of the viscosity parameter (a) $\alpha = 0.0$, (b) $\alpha = 0.5$, (c) $\alpha = 0.9$.

Chapter 9

Theoretical examination of nanoparticles as a drug carrier with slip effects on the wall of stenosed arteries

The main purpose of this chapter is to deal with the effects of nanoparticles on the characteristics of the blood flow through the bell shaped stenosed arteries by using a suitable mathematical model. Investigation is carried out using copper and silver nanoparticles as a drug carrier. The velocity and thermal slip effects are incorporated on the wall of stenosed artery. The governing equations are considered for viscous nature of blood model and then solved by using mild stenosis approximations to calculate the hemodynamic effect of stenosis. It is observed that the impedance resistance to blood flow decreases with an increase in the values of thermal and velocity slip parameters. Therefore, the present analysis is able to conclude some important features of interest in some biomedical applications.

9.1 Mathematical formulation

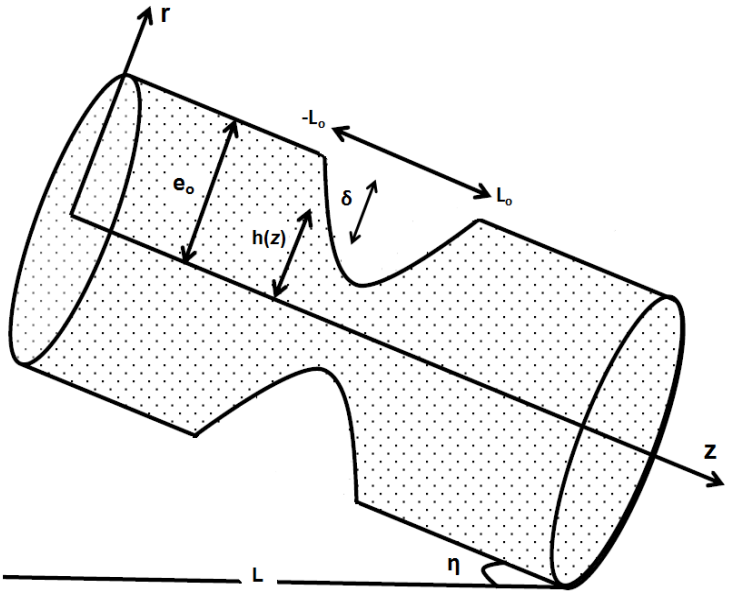

Fig. (9.1): Geometry of bell stenosed artery.

Consider an incompressible flow of viscous nanofluid inside an inclined bell shaped artery having angle of inclination is η. The heat transfer phenomenon is taken into account by giving temperature T_0 to the upper wall of the artery. The geometry of bell shape stenosis in dimensional form is given as

$$\begin{aligned} \frac{\overline{h}(z)}{e_0} &= 1-\frac{\delta}{e_0}exp[\frac{-m^2\epsilon^2\overline{z}^2}{e_0^2}], \qquad |\overline{z}| \leq L_0, \\ &= 1, \qquad\qquad\qquad\qquad \text{otherwise}, \end{aligned} \tag{9.1}$$

here L_0 represents the length of the stenosis, δ is the height of stenosis, ϵ is the relative length of the stenosis that is defined as the ratio of the radius to half length of the stenosis i.e., $\epsilon = e_0/L_0$, m is the parametric constant or bell shape stenosis parameter, while e_0 and $h(z)$ as the radius of the stenosed and normal arteries. The governing equations for conservation of mass, momentum and temperature for viscous nano fluid can be written as

$$\frac{\partial \overline{u}}{\partial \overline{r}} + \frac{\overline{u}}{\overline{r}} + \frac{\partial \overline{w}}{\partial \overline{z}} = 0, \tag{9.2}$$

$$\begin{aligned} \rho_{nf}\left(\overline{u}\frac{\partial \overline{u}}{\partial \overline{r}} + \overline{w}\frac{\partial \overline{u}}{\partial \overline{z}}\right) &= -\frac{\partial \overline{p}}{\partial \overline{r}} + \frac{1}{\overline{r}}\frac{\partial}{\partial \overline{r}}\left(2\overline{r}\mu_{nf}\frac{\partial \overline{u}}{\partial \overline{r}}\right) + \frac{\partial}{\partial \overline{z}}\left(\mu_{nf}\left(\frac{\partial \overline{u}}{\partial \overline{z}} + \frac{\partial \overline{w}}{\partial \overline{r}}\right)\right) - \\ & 2\mu_{nf}\frac{\overline{u}}{\overline{r}^2} - g(\rho\gamma)_{nf}(\overline{T} - T_o)\cos\eta, \end{aligned} \tag{9.3}$$

$$\begin{aligned} \rho_{nf}\left(\overline{u}\frac{\partial \overline{w}}{\partial \overline{r}} + \overline{w}\frac{\partial \overline{w}}{\partial \overline{z}}\right) &= -\frac{\partial \overline{p}}{\partial \overline{z}} + \frac{1}{\overline{r}}\frac{\partial}{\partial \overline{r}}\left(\overline{r}\mu_{nf}\left(\frac{\partial \overline{u}}{\partial \overline{z}} + \frac{\partial \overline{w}}{\partial \overline{r}}\right)\right) + \frac{\partial}{\partial \overline{z}}\left(2\mu_{nf}\left(\frac{\partial \overline{w}}{\partial \overline{z}}\right)\right) \\ & + g(\rho\gamma)_{nf}(\overline{T} - T_o)\sin\eta, \end{aligned} \tag{9.4}$$

$$\left(\overline{u}\frac{\partial \overline{T}}{\partial \overline{r}} + \overline{w}\frac{\partial \overline{T}}{\partial \overline{z}}\right) = \frac{K_{nf}}{(\rho c_p)_{nf}}\left(\frac{\partial^2 \overline{T}}{\partial \overline{r}^2} + \frac{1}{\overline{r}}\frac{\partial \overline{T}}{\partial \overline{r}} + \frac{\partial^2 \overline{T}}{\partial \overline{z}^2}\right) + \frac{Q_0}{(\rho c_p)_{nf}}. \tag{9.5}$$

Thermo physical properties are given as

$$\begin{aligned} &\mu_{nf} = \frac{\mu_f}{(1-\Phi)^{2.5}},\ \alpha_{nf} = \frac{K_{nf}}{(\rho c_p)_{nf}},\ \rho_{nf} = (1-\Phi)\rho_f + \Phi\rho_s, \\ &(\rho\gamma)_{nf} = (1-\Phi)(\rho\gamma)_f + \Phi(\rho\gamma)_s,\ (\rho c_p)_{nf} = (1-\Phi)(\rho c_p)_f + \Phi(\rho c_p)_s, \\ &\frac{K_{nf}}{K_f} = \frac{(K_s + 2K_f) - 2\Phi(K_f - K_s)}{(K_s + 2K_f) + \Phi(K_f - K_s)},\ \mu_f = \mu_o e^{-\alpha\theta}. \end{aligned} \tag{9.6}$$

Non-dimensional variables are defined as

$$\begin{aligned} r &= \frac{\overline{r}}{e_0},\ w = \frac{\overline{w}}{u_o},\ u = \frac{\overline{L}\overline{u}}{u_o\delta},\ p = \frac{e_0^2\overline{p}}{u_o\overline{L}\mu_o},\ \beta = \frac{Q_0 e_0^2}{T_0 K_f}, \\ R_{en} &= \frac{e_0 u_o \rho_f}{\mu_o},\ G_r = \frac{g\gamma_f\rho_f e_0^2 T_0}{u_0\mu_o},\ \theta = \frac{\overline{T} - T_o}{T_o},\ z = \frac{\overline{z}}{\overline{L}}. \end{aligned} \tag{9.7}$$

Using mild stenosis case $\delta^* = \frac{\delta}{e_0} \ll 1$ and taking extra condition $\epsilon = \frac{e_0}{L_0} \approx O(1)$, the constitutive Eqs. (9.3) to (9.5) can be written as

$$\frac{\partial p}{\partial r} = 0, \tag{9.8}$$

$$\frac{\partial p}{\partial z} = \frac{1}{r}\frac{\partial}{\partial r}\left(\frac{\mu_{nf}(\theta)}{\mu_o}\left(r\frac{\partial w}{\partial r}\right)\right) + \frac{(\rho\gamma)_{nf}}{(\rho\gamma)_f}G_r\theta\sin\eta, \tag{9.9}$$

$$\frac{\partial^2\theta}{\partial r^2} + \frac{1}{r}\frac{\partial\theta}{\partial r} + \beta\frac{K_f}{K_{nf}} = 0. \tag{9.10}$$

Boundary conditions and geometry of stenosis in dimensionless form are defined as

$$\begin{aligned} h(z) &= 1 - \delta^* \exp[-m^2 z^2], \qquad |z| \ \leq L_0, \\ &= 1, \qquad\qquad\qquad\qquad \text{otherwise.} \end{aligned} \tag{9.11}$$

$$w + \kappa\frac{\mu_{nf}}{\mu_o}\frac{\partial w}{\partial r} = 0 \quad \text{and} \quad \theta + \gamma\frac{\partial\theta}{\partial r} = 0, \quad \text{at} \quad r = h(z), \tag{9.12}$$

$$\frac{\partial w}{\partial r} = 0 \quad \text{and} \quad \frac{\partial\theta}{\partial r} = 0, \quad \text{at} \quad r = 0, \tag{9.13}$$

where κ $(= \frac{\mu_o\kappa^*}{e_o})$ and γ $(= \frac{\gamma^*}{e_o})$ are defined as the velocity and thermal slip parameters respectively.

9.2 Solution of the problem

The exact solutions of Eqs. (9.9) and (9.10) using boundary conditions Eqs. (9.12) and (9.13) are directly written as

$$\theta = \beta\left(\frac{h^2 - r^2 + 2h\gamma}{4}\right)\left(\frac{K_s(1-\Phi) + K_f(2+\Phi)}{K_s(1+2\Phi) + 2K_f(1-\Phi)}\right), \tag{9.14}$$

$$\begin{aligned} w \ = \ & \frac{1}{8}\frac{dp}{dz}((1-\Phi)^{2.5}(2a_3(-h^2+r^2) + a_4(h^4 - r^4)) - 4h\kappa) + \frac{1}{48}(G_r \\ & \left((1-\Phi) + \Phi\frac{\rho_s\alpha_s}{\rho_f\alpha_f}\right)\sin\eta)((1-\Phi)^{2.5}(6a_1(2a_3(h-r)(h+r) + a_4(-h^4 + \\ & r^4)) + a_2(3a_3(-h^4+r^4) + 2a_4(h^6 - r^6))) - 12h(-2a_1 + a_2h^2)\kappa). \end{aligned} \tag{9.15}$$

Flow rate is given as

$$F = \int_0^h rw dr. \tag{9.16}$$

Using Eq. (9.15) into Eq. (9.16), we get the expression for pressure gradient as follows

$$\frac{dp}{dz} = \frac{F - a_6(z)h^3\left(G_r\left((1-\Phi) + \Phi\frac{\rho_s\gamma_s}{\rho_f\gamma_f}\right)\sin\eta\right)}{a_5(z)h^3}. \tag{9.17}$$

The pressure drop through the stenosis that is calculated from above Eq. (9.17) can be defined as

$$\Delta p = \int_{-L}^{L}\left(-\frac{dp}{dz}\right)dz. \tag{9.18}$$

Using Eq. (9.18), the impedance resistance can be evaluated as

$$\lambda = \frac{\Delta p}{F} = \int_{-L}^{-L_o}\Omega_6(z)\mid_{h=1} dz + \int_{-L_o}^{L_o}\Omega_6(z)dz + \int_{L_o}^{L}\Omega_6(z)\mid_{h=1} dz, \tag{9.19}$$

where

$$\Omega_6(z) = \frac{1}{F}\left(\frac{-F + a_6(z)h^3\left(G_r\left((1-\Phi) + \Phi\frac{\rho_s\gamma_s}{\rho_f\gamma_f}\right)\sin\eta\right)}{a_5(z)h^3}\right). \tag{9.20}$$

Using Eq. (9.20) into Eq. (9.19), we get

$$\lambda = \frac{\Delta p}{F} = a_7(L - L_o) + \int_{-L_o}^{L_o}\Omega_6(z)dz. \tag{9.21}$$

Using Eq. (9.15) expression for the wall shear stress is given as,

$$S_{rz} = -\left(\frac{(-2a_1h + a_2h^3)}{4}\left(G_r\left((1-\Phi) + \Phi\frac{\rho_s\gamma_s}{\rho_f\gamma_f}\right)\sin\eta\right) + \frac{h}{2}\frac{dp}{dz}\right). \tag{9.22}$$

9.3 Appendix

$$a_o = \left(\frac{K_s(1-\Phi)+K_f(2+\Phi)}{K_s(1+2\Phi)+2K_f(1-\Phi)}\right),\ a_1 = \frac{\beta a_o}{4}\left(h^2+2\gamma h\right),\ a_2 = \frac{\beta a_o}{4},$$
$$a_3 = 1+\alpha a_1,\ a_4 = \alpha a_2,\ a_5 = \frac{1}{48}(-3(1-\Phi)^{2.5}a_3 h + 2(1-\Phi)^{2.5}a_4 h^3 -$$
$$12\kappa a_3 + 12h^2\kappa a_4),\ a_6 = \frac{1}{192}((1-\Phi)^{2.5}h(12a_1a_3 - 4(a_2a_3+2a_1a_4)h^2 +$$
$$3a_2a_4h^4) + 24(2a_1 - a_2h^2)(a_3 - a_4h^2)\kappa),\ a_7 = 2\Omega_6(z)|_{h=1}.$$

9.4 Results and discussion

This section is devoted for the study of copper and silver nanoparticles with the help of some different emerging flow parameters on the characteristics of blood flow through the graphs of wall shear stress, impedance resistance to blood flow, temperature profile and stream lines. The graphs are plotted by keeping the parameters constants such as $\Phi = 0.00 - 0.2$, $\kappa = 0.0 - 0.9$, $\gamma = 0.0 - 0.9$, $\alpha = 0.0 - 0.9$, $L_o = 1.5$, $L = 3.0$, $\delta = 0.2$, $z = 1.5$, $F = 0.3$, $\beta = 2.0$, $G_r = 2.0$, $m = 2$, $\eta = 0$, $\frac{\pi}{4}$, $\frac{\pi}{2}$ (vertical, horizontal, inclined arteries). Figs. (9.2) to (9.8) are prepared for wall shear stress analysis versus z in the bell shape stenotic region. All of these figures show that stresses on the wall of inclined arteries start steeply increasing towards the upstream of the stenotic segment and then start rapidly decreasing towards the end of the bell shape stenotic segment $-1.5 \leq z \leq 1.5$. Moreover, it is analyzed that the altitude of stresses on the wall of stenosed arteries for pure blood case is little higher when compared with the nanoparticles cases. The wall shear stress for different values of the Grashof number G_r is given in Figs. (9.2) and observed that the stresses on the wall of inclined stenosed arteries start decreasing with an increase in the viscous forces. From Fig. (9.3), it is noted that stresses on the wall of arteries decreases with an increase in internal heat source parameter ($\beta > 0$). Figs. (9.4) and (9.5) describes the effect of stenosis shape m and stenosis height δ on the wall of inclined arteries. It is obtained from these figures that stresses on the wall of inclined arteries are directly related with the stenosis height δ and inversely related for the stenosis shape m. Figs. (9.6) and (9.7) are prepared for different values of the thermal slip γ and velocity slip parameters κ. It is observed form these figures that the stresses on the wall of inclined arteries give the higher altitude for

pure blood case when compared to the other cases and decreases with an increase in thermal and velocity slip parameters. It is found that the stresses on the walls are high for no slip condition when compared to slip condition. The graph with different variations of inclination angle η is given in Fig. (9.8) and show that the stresses on the wall of stenosed arteries are higher for horizontal stenosed arteries when compare to the vertical and inclined arteries. The variation of wall shear stress versus z for different values viscosity parameter α is given in Fig. (9.9) and observed that the stresses on the wall of inclined arteries decreases for variable temperature dependent viscosity α. It is also analyzed that the stresses on the wall of inclined arteries are lesser for variable nanofluid viscosity then for the case of constant nanofluid viscosity. The influence of nanoparticles volume fraction Φ on wall shear stress is given in the Fig. (9.10). It is observed that the stresses on the wall of inclined arteries decrease with an increase in the nanoparticles volume fraction. To discuss the disease section resistance impedance to blood flow is important and plotted from Figs. $(9.11)-(9.18)$ against the stenosis height δ. It is important to note here that the addition of silver nanoparticles reduces the resistance impedance to blood flow slightly more when compare to the copper nanoparticles. The resistance impedance for different values of Grashof number G_r and heat source parameter β is given in Figs. (9.11) and (9.12). It is observed from these graphs that resistance impedance to flow decreases with an increase in the values of Grashof number G_r and heat source parameter β. Figs. (9.13) and (9.14) are prepared for different values of the thermal γ and velocity κ slip parameters. It is analyzed from these figures that the impedance resistance to blood flow decreases with an increase in the values of the slip parameters. So, taking slip condition at the wall of stenotic artery is important and justify that resistance to blood flow decreases more effectively for slip case when compare to the no slip case ($\gamma = \kappa = 0$). The resistance impedance to blood flow for inclination angle η is given in Fig. (9.15). It is observed that the resistance is higher for horizontal stenosed arteries when compare to the vertical and inclined stenosed arteries. From Fig. (9.16), it is depicted that the resistance to blood flow decreases with an increase in the values of viscosity parameter α. The variation of stenosis shape m is given in Fig. (9.17) and observed that with an increase in the values of the stenosis shape m the resistance impedance to blood flow decreases. Fig. (9.18) is prepared to show that the influence of nanoparticle volume fraction Φ on resistance impedance to blood flow and concluded that the nanoparticles helps to

reduce the resistance impedance to the blood flow. The variations of temperature profile against radial direction r are plotted from Figs. (9.19) and (9.20). The temperature profile for different values of the heat source parameter β is given in Fig. (9.19). It is observed that the temperature profile increases throughout the inclined stenosed arteries with an increase in the values of the heat source parameter β. Fig. (9.20) is plotted for different values of the nanoparticle volume fraction Φ. It is analyzed that the heat transfers rate throughout the inclined arteries decreases with an increase in the nanoparticle volume fraction. A stream line represents an interesting phenomenon for fluid flow of an internally circulating bolus and has been discussed here for silver and copper nanoparticles through Figs. (9.21) to (9.28). The trapping phenomena show that more bolus appears for the silver nanoparticles case when compare to other cases. The blood flow pattern for stenosis shape m is given in Figs. (9.21) and (9.22). It is observed from these stream lines that with an increase in the values of stenosis shapes the size of trapped bolus reduces and then enhance the trapping. Figs. (9.23) and (9.24) are plotted for different values of viscosity parameter α. It is observed from these blood flow patterns that no bolus appear for constant nanofluid viscosity, while number of trapping bolus decreases for variable nanofluid viscosity with an increase in the values of parameter α. The trapping phenomena for the thermal γ and velocity κ slip parameters are discussed through Figs. (9.25) – (9.28). These graphs depict that the number of trapping bolus increases for thermal slip parameter, while decreases for velocity slip parameter. The tables (9.1) and (9.2) are plotted to show the variations of temperature profile and velocity profile for different values of the thermal γ and velocity κ slip parameters against radial direction r. Table (9.1) illustrates that the variations of temperature profile increases throughout the stenosed inclined arteries between the region $-h \leq r \leq h$, which shows that temperature of the considered fluid increases with increase in the thermal slip parameter. Table (9.2) is prepared for velocity profile and observed that velocity decreases between the region $-0.8 < r < 0.8$, while the opposite trend is observed between the regions $-h \leq r \leq -0.8$ and $0.8 \leq r \leq h$.

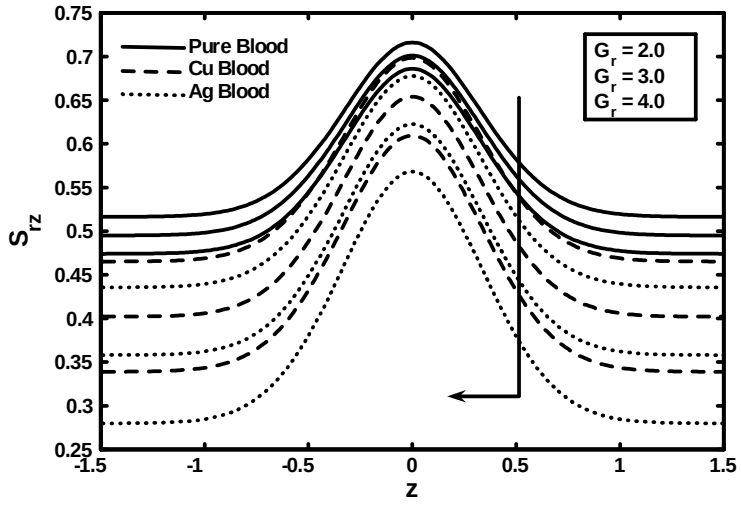

Fig. (9.2): Variation of wall shear stress for different values of Grashof number G_r.

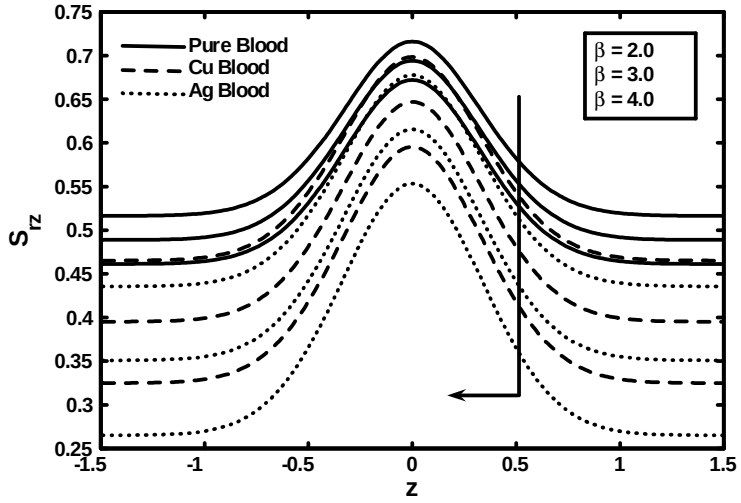

Fig. (9.3): Variation of wall shear stress for different values of heat source parameter β.

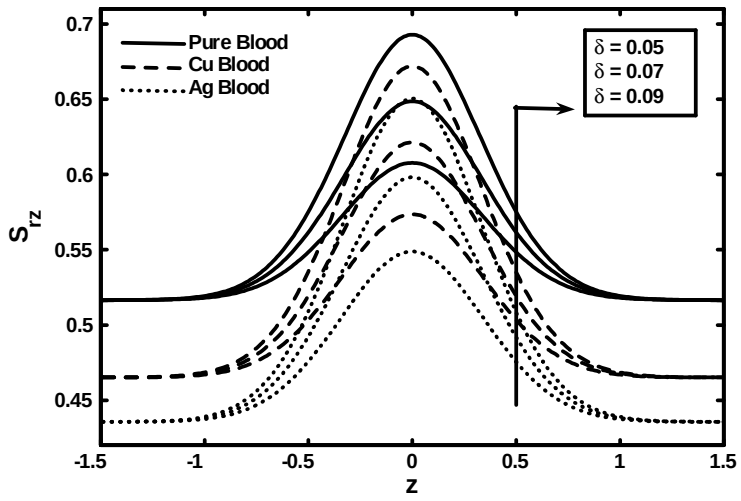

Fig. (9.4): Variation of wall shear stress for different values of stenosis height δ.

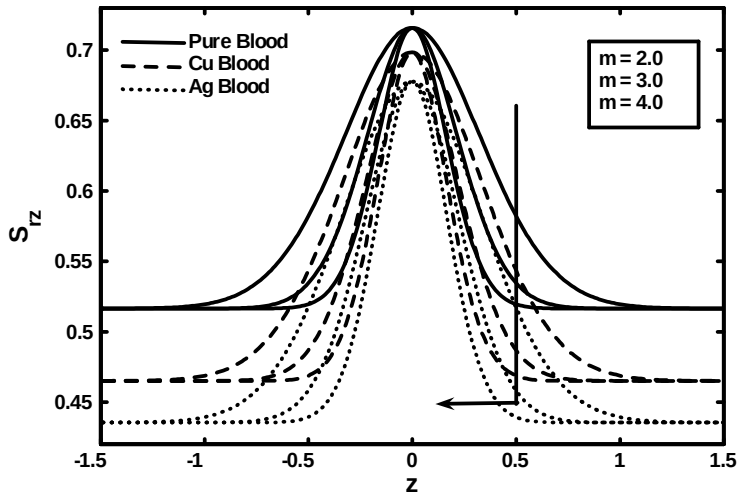

Fig. (9.5): Variation of wall shear stress for different values of stenosis shape m.

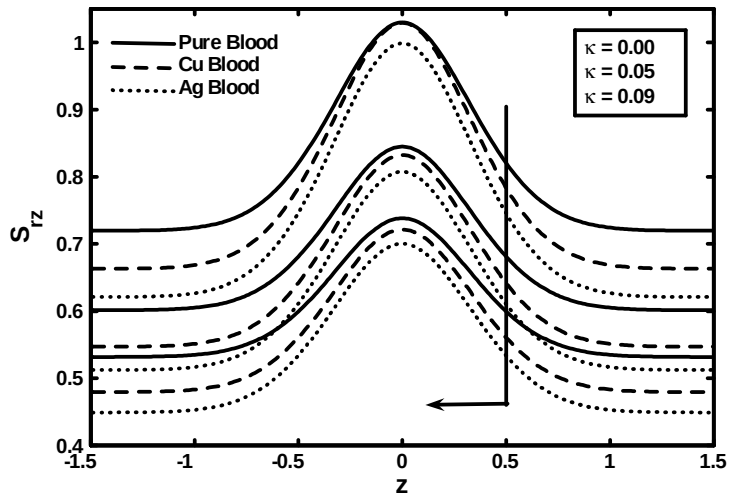

Fig. (9.6): Variation of wall shear stress for different values of velocity slip parameter κ.

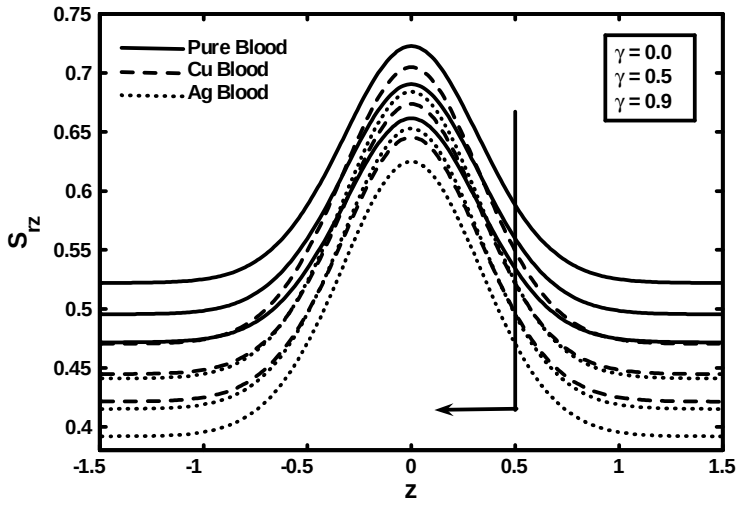

Fig. (9.7): Variation of wall shear stress for different values of thermal slip parameter γ.

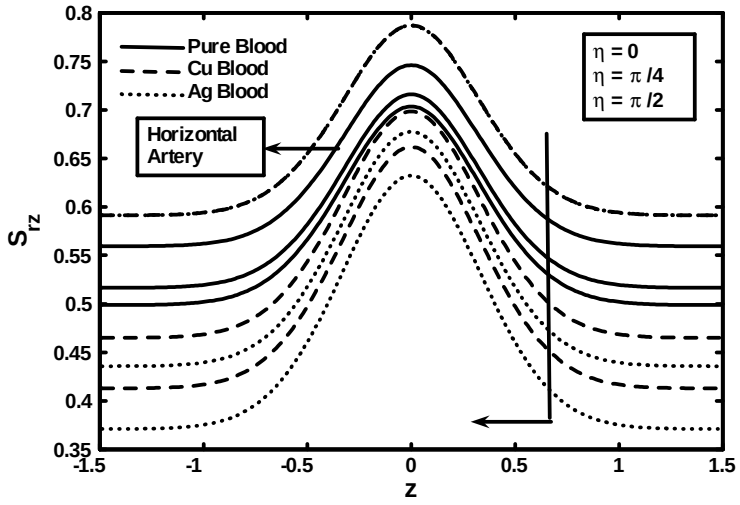

Fig. (9.8): Variation of wall shear stress for different values of inclination angle η.

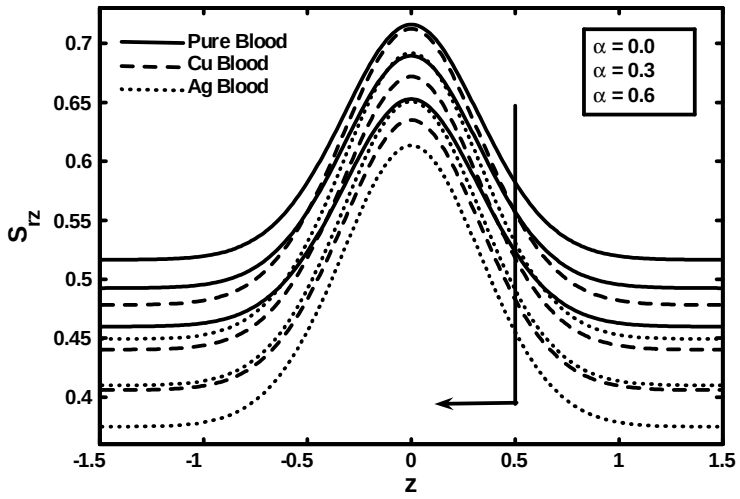

Fig. (9.9): Variation of wall shear stress for different values of viscosity parameter α.

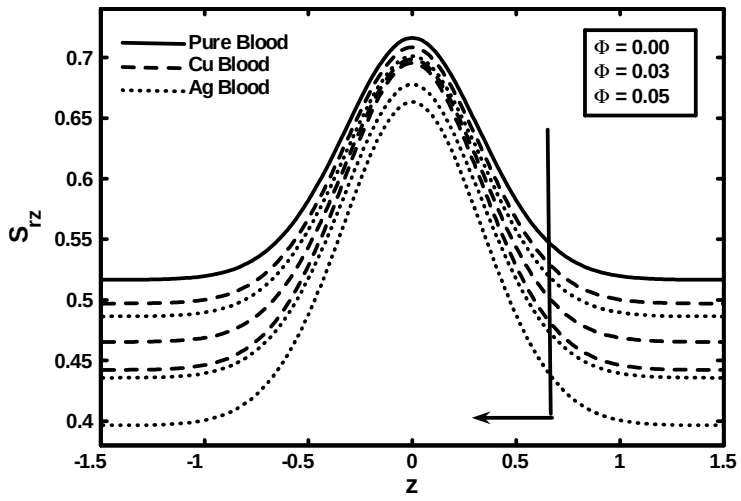

Fig. (9.10): Variation of wall shear stress for different values of nanoparticles volume fraction Φ.

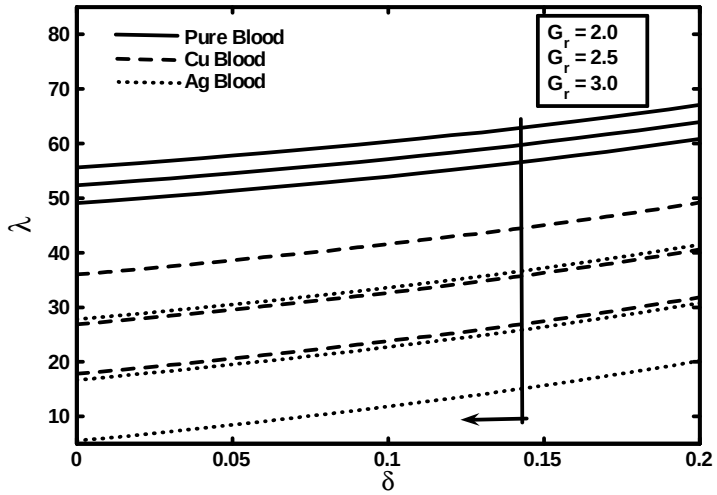

Fig. (9.11): Variation of resistance impedance to blood flow for different values of Grashof number G_r.

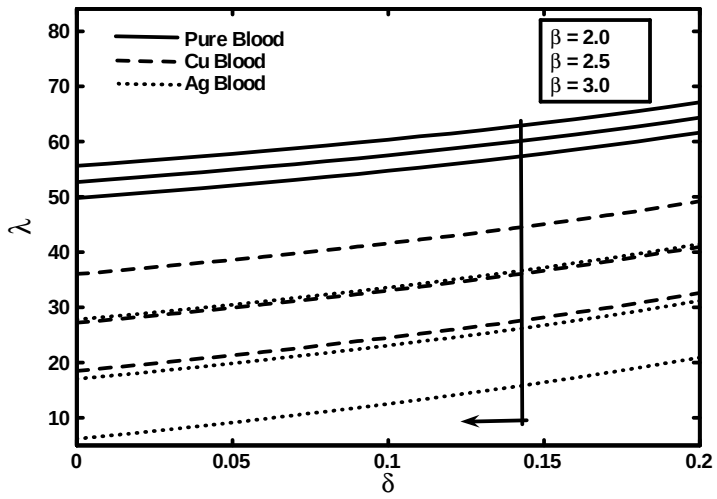

Fig. (9.12): Variation of resistance impedance to blood flow for different values of heat source parameter β.

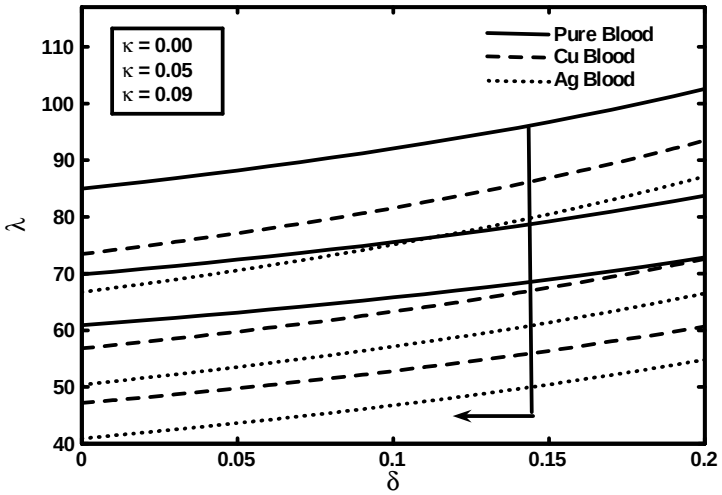

Fig. (9.13): Variation of resistance impedance to blood flow for different values of velocity slip parameter κ.

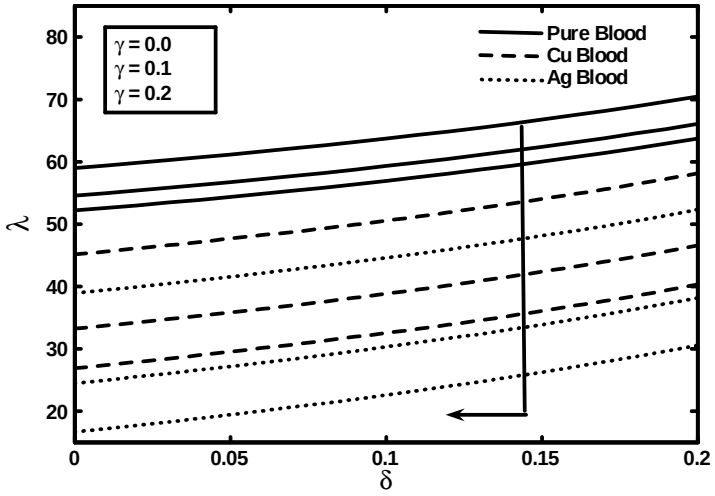

Fig. (9.14): Variation of resistance impedance to blood flow for different values of thermal slip parameter γ.

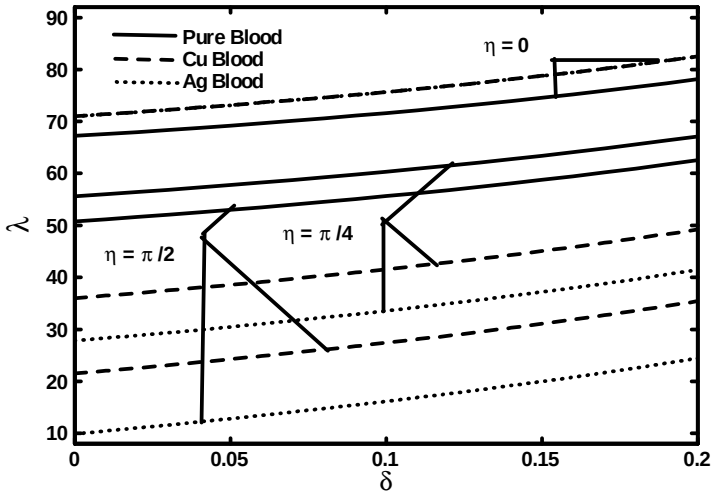

Fig. (9.15): Variation of resistance impedance to blood flow for different values of inclination angle η.

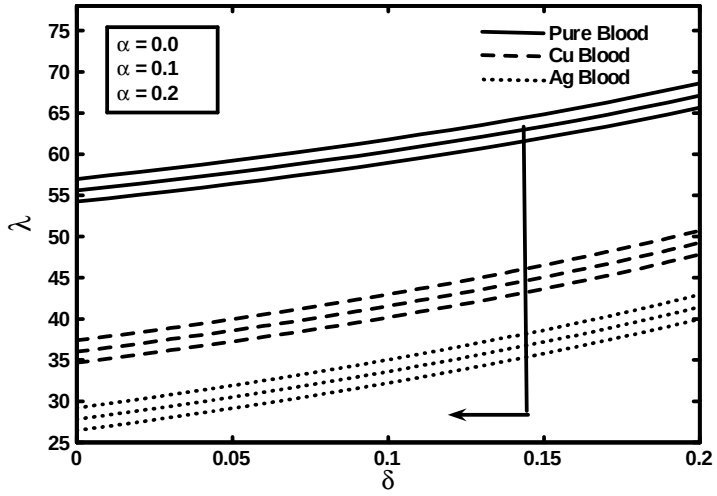

Fig. (9.16): Variation of resistance impedance for different values of viscosity parameter α.

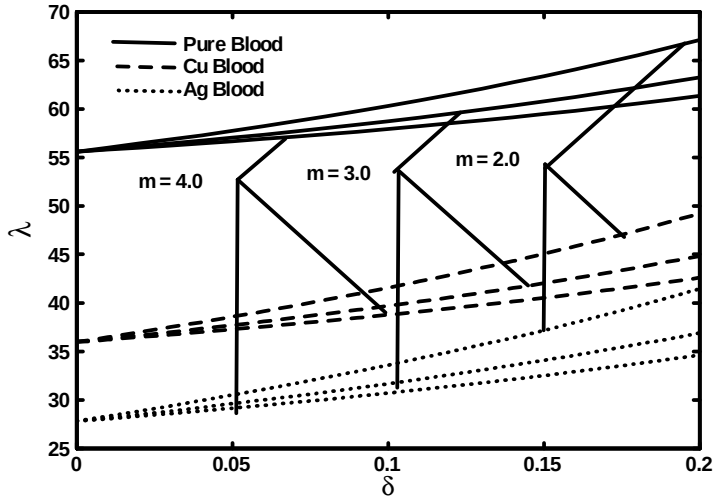

Fig. (9.17): Variation of resistance impedance for different values of stenosis shape m..

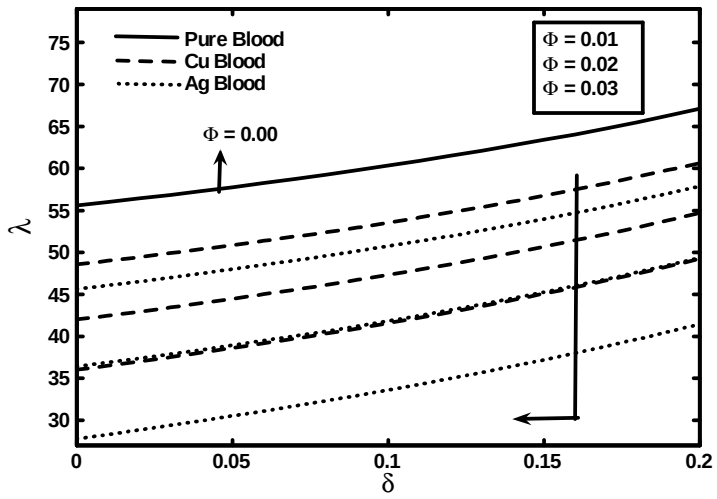

Fig. (9.18): Variation of resistance impedance for different values of nanoparticles volume fraction Φ.

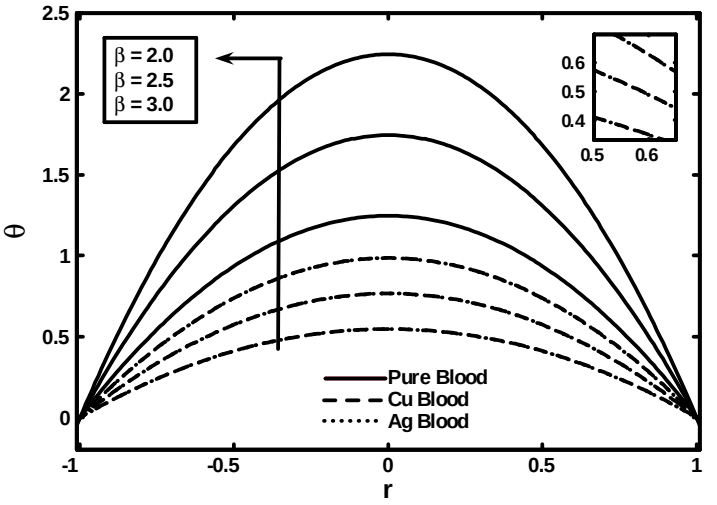

Fig. (9.19): Variation of temperature profile for heat source parameter β.

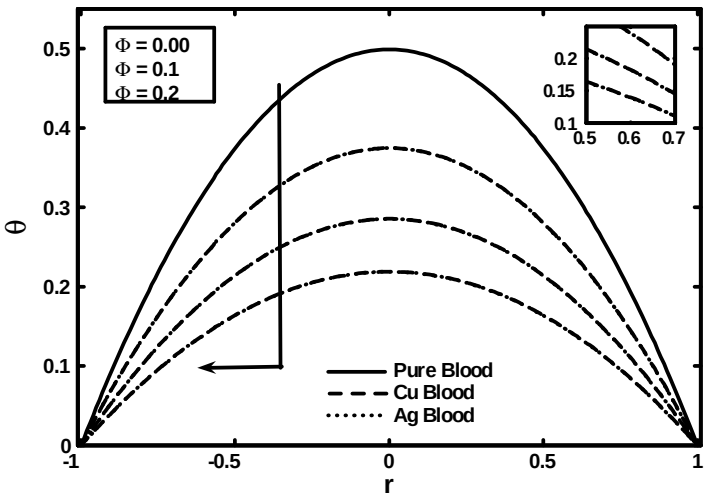

Figs. (9.20): Variation of temperature profile for different values of nanoparticles volume fraction Φ.

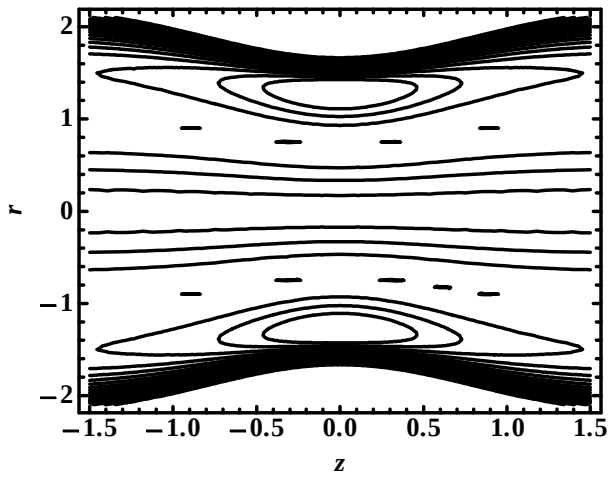

(a)

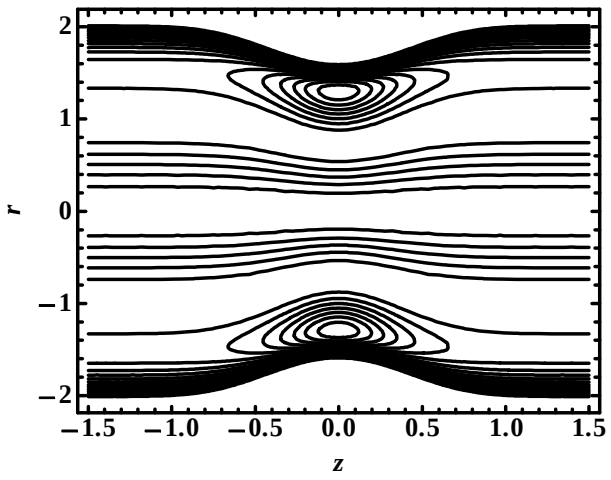

(b)

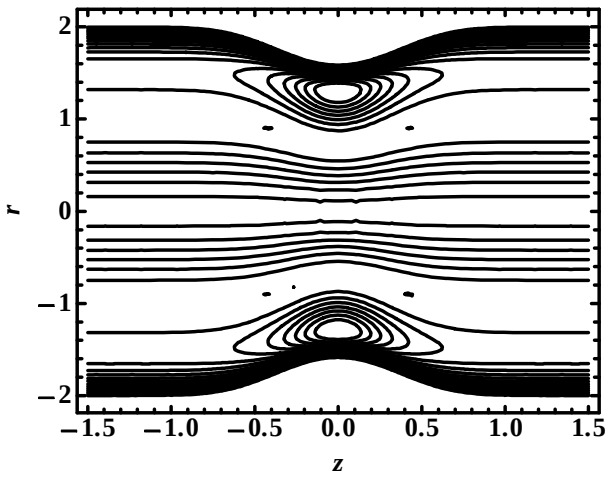

(c)

Figs. (9.21): Blood flow pattern (Cu nanoparticles) for different values of (a) $m = 1.0$, (b) $m = 2.0$, (c) $m = 3.0$.

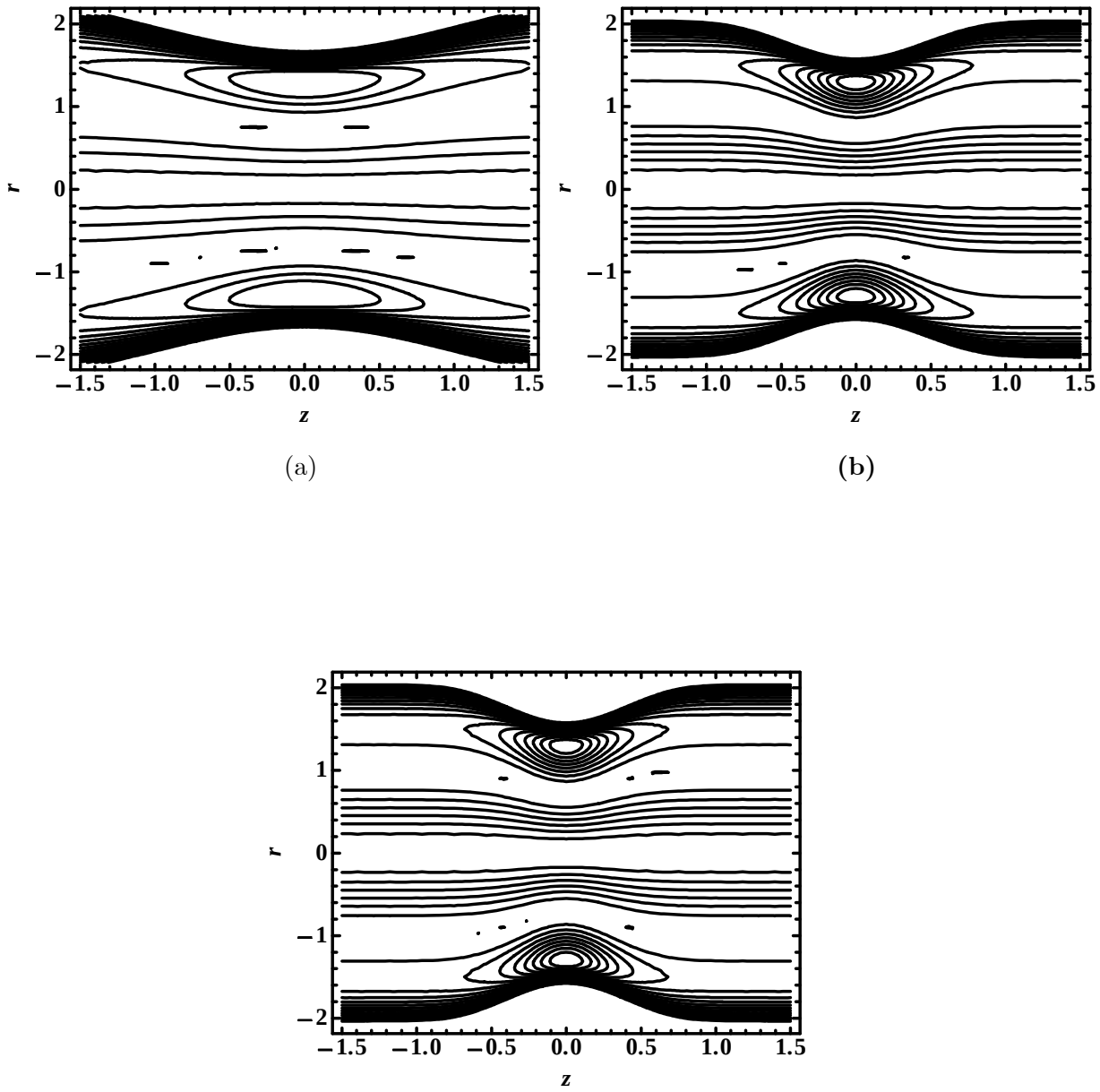

Figs. (9.22): Blood flow pattern (Ag nanoparticles) for different values of (a) $m = 1.0$, (b) $m = 2.0$, (c) $m = 3.0$.

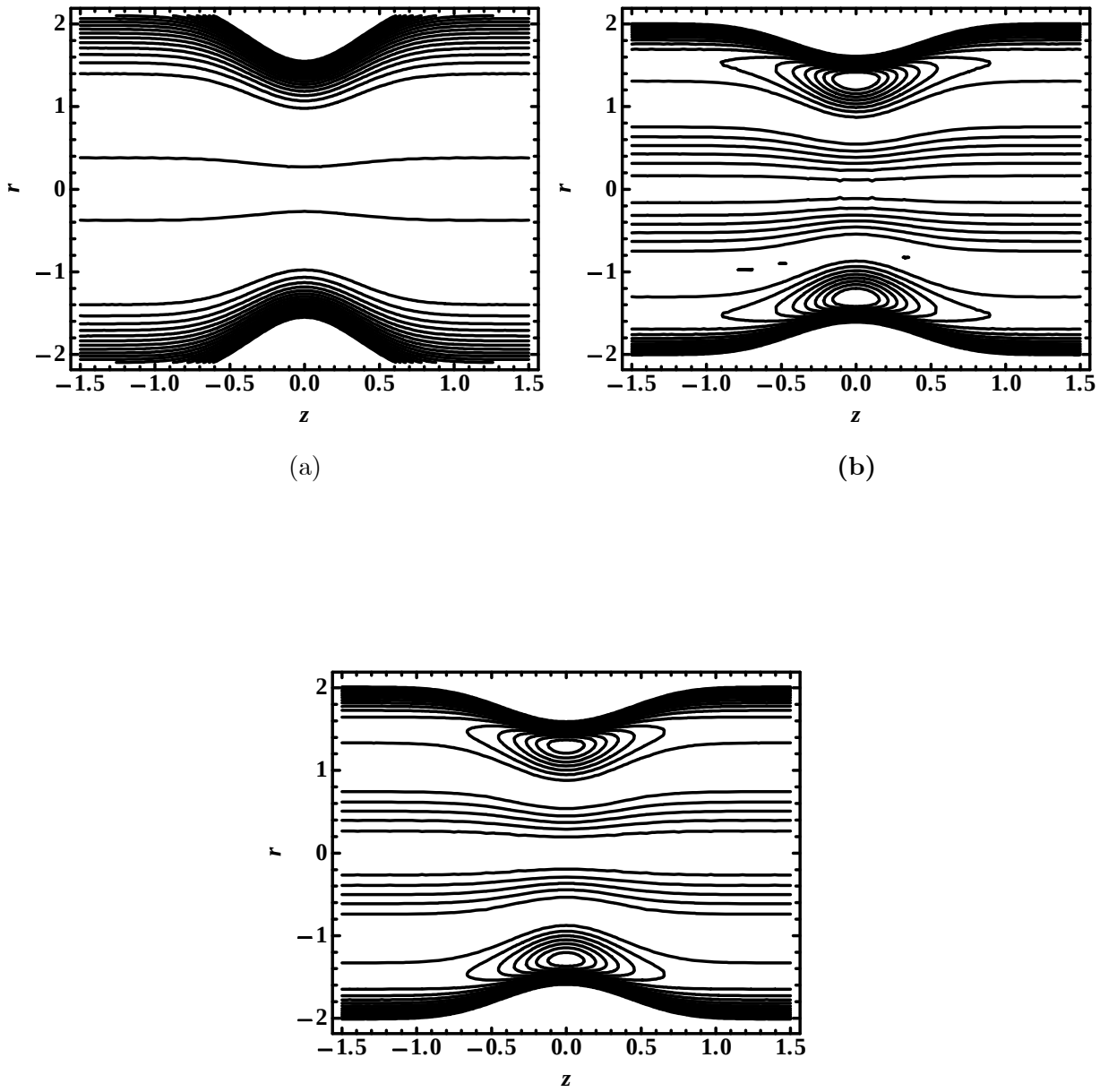

Figs. (9.23): Blood flow pattern (Cu nanoparticles) for different values of (a) $\alpha = 0.0$, (b) $\alpha = 1.5$, (c) $\alpha = 1.7$.

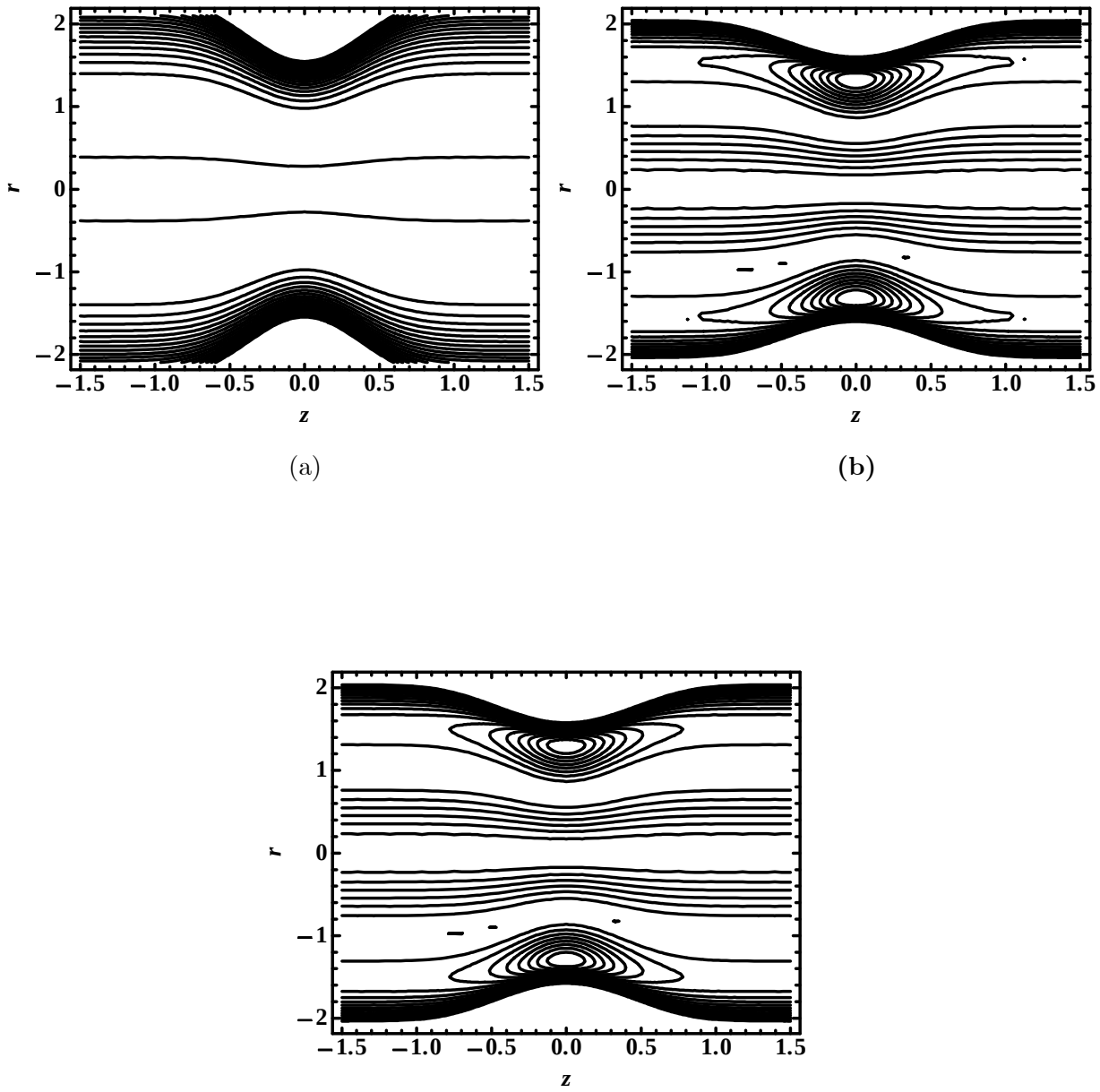

Figs. (9.24): Blood flow pattern (Ag nanoparticles) for different values of (a) $\alpha = 0.0$, (b) $\alpha = 1.5$, (c) $\alpha = 1.7$.

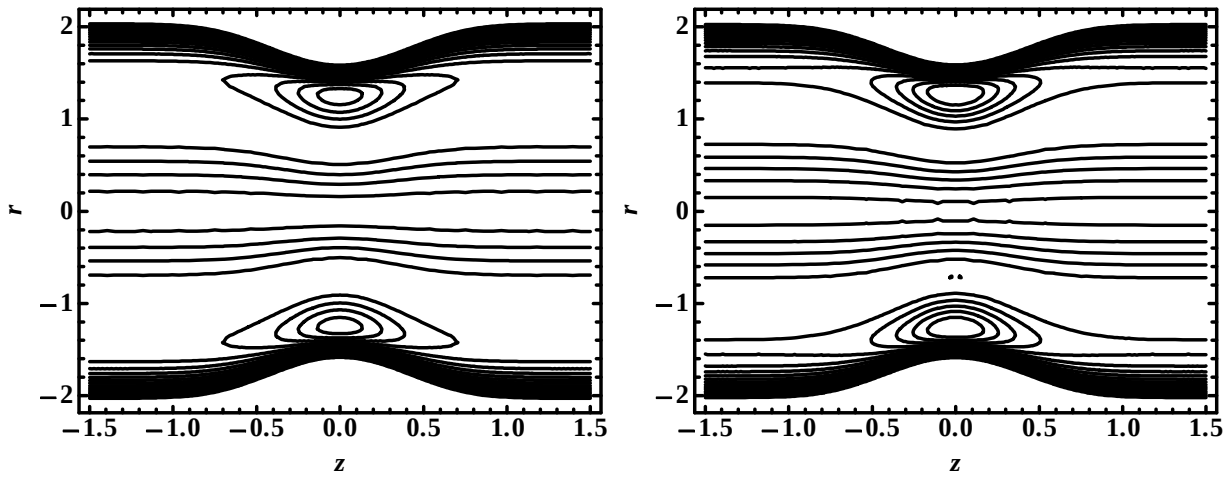

(a) **(b)**

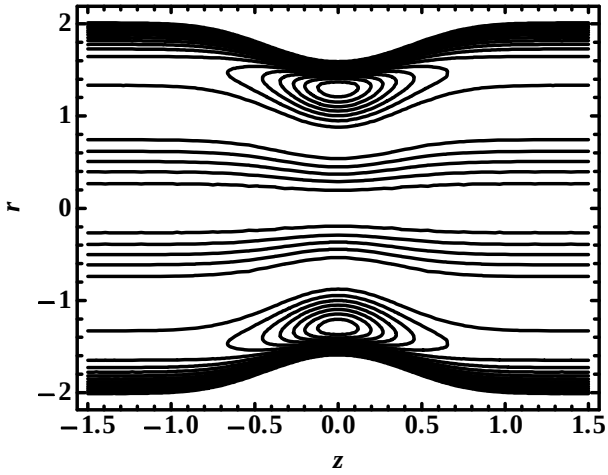

(c)

Figs. (9.25): Blood flow pattern (Cu nanoparticles) for different values of (a) $\gamma = 0.0$, (b) $\gamma = 0.02$, (c) $\gamma = 0.04$.

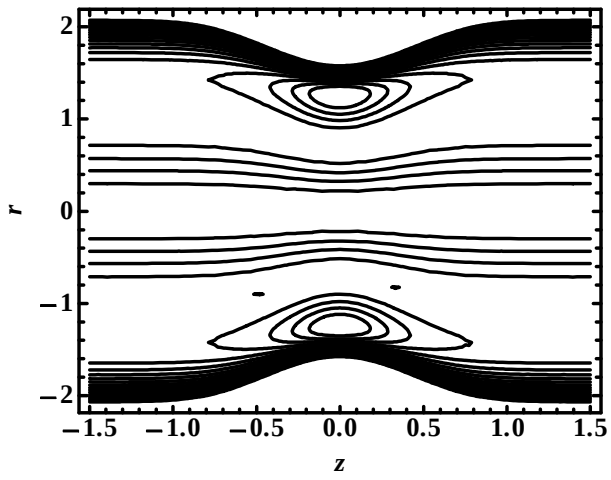

(a)

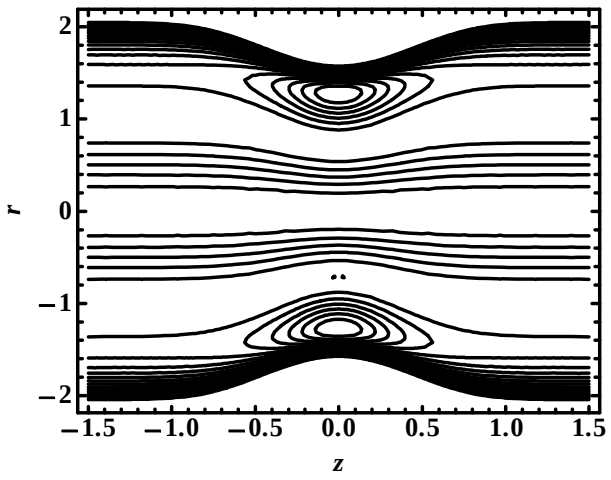

(b)

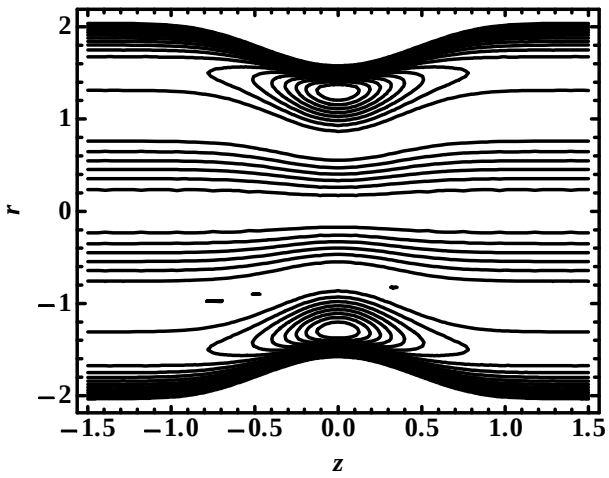

(c)

Figs. (9.26): Blood flow pattern (Ag nanoparticles) for different values of (a) $\gamma = 0.0$, (b) $\gamma = 0.05$, (c) $\gamma = 0.09$.

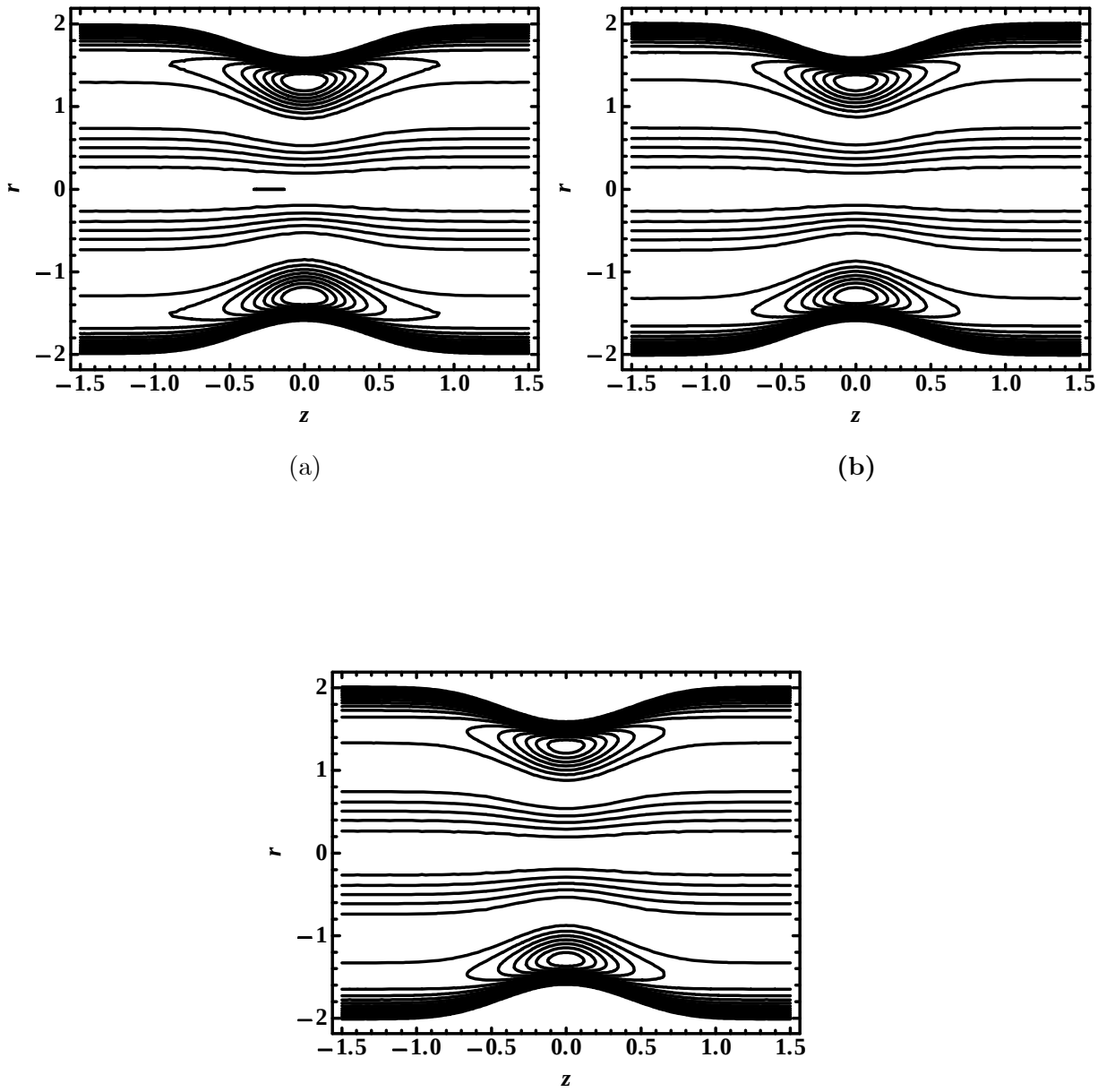

Figs. (9.27): Blood flow pattern (copper nanoparticles) for different values of (a) $\kappa = 0.0$, (b) $\kappa = 0.01$, (c) $\kappa = 0.015$.

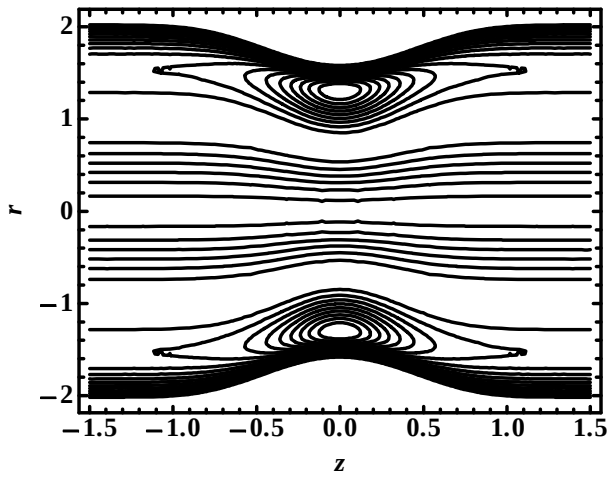

(a)

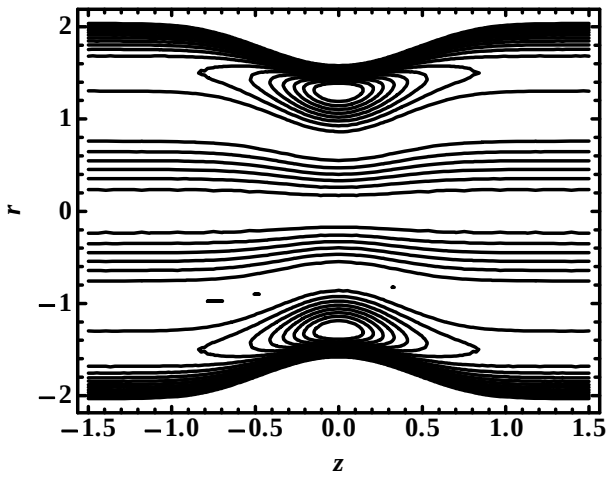

(b)

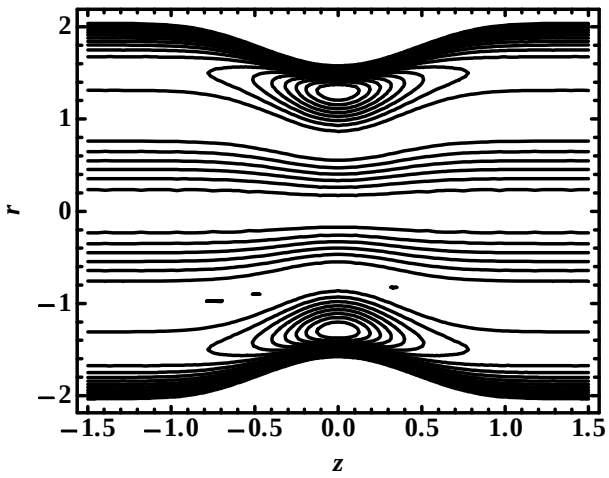

(c)

Figs. (9.28): Blood flow pattern (silver nanoparticles) for different values of (a) $\kappa = 0.0$, (b) $\kappa = 0.01$, (c) $\kappa = 0.015$.

θ	Pure blood ($\Phi = 0.00$)			Copper Blood ($\Phi = 0.09$)			Silver Blood ($\Phi = 0.09$)		
r	γ=0.00	γ=0.05	γ=0.09	γ=0.00	γ=0.05	γ=0.09	γ=0.00	γ=0.05	γ=0.09
$-h$	0.00000	0.04519	0.08135	0.00000	0.03488	0.06279	0.00000	0.03488	0.06279
-0.8	0.08853	0.13373	0.16989	0.06834	0.10322	0.13113	0.06833	0.10322	0.13113
-0.6	0.22853	0.27373	0.30989	0.17640	0.21129	0.23920	0.17639	0.21128	0.23918
-0.4	0.32853	0.37373	0.40989	0.25359	0.28848	0.31639	0.25358	0.28846	0.31637
-0.2	0.38853	0.43373	0.46989	0.29991	0.33479	0.36270	0.29989	0.33477	0.36268
0.0	0.40853	0.45373	0.48989	0.31534	0.35023	0.37814	0.31533	0.35021	0.37812
0.2	0.38853	0.43373	0.46989	0.29991	0.33479	0.36270	0.29989	0.33477	0.36268
0.4	0.32853	0.37373	0.40989	0.25359	0.28848	0.31639	0.25358	0.28846	0.31637
0.6	0.22853	0.27373	0.30989	0.17640	0.21129	0.23920	0.17639	0.21128	0.23918
0.8	0.08853	0.13373	0.16989	0.06834	0.10322	0.13113	0.06833	0.10322	0.13113
h	0.00000	0.04519	0.08135	0.00000	0.03488	0.06279	0.00000	0.03488	0.06279

Table (9.1): Variations of temperature profile for thermal slip parameter γ.

w	Pure blood ($\Phi = 0.00$)			Copper Blood ($\Phi = 0.01$)			Silver Blood ($\Phi = 0.01$)		
r	κ=0.00	κ=0.01	κ=0.02	κ=0.00	κ=0.01	κ=0.02	κ=0.00	κ=0.01	κ=0.02
$-h$	0.00000	0.00059	0.00114	0.00000	0.00032	0.00061	0.00000	0.00021	0.00041
-0.8	0.00757	0.00790	0.00821	0.00559	0.00577	0.00593	0.00487	0.00499	0.00510
-0.6	0.02548	0.02540	0.02533	0.02423	0.02419	0.02416	0.02379	0.02376	0.02373
-0.4	0.04281	0.04244	0.04210	0.04506	0.04486	0.04468	0.04588	0.04574	0.04562
-0.2	0.05507	0.05452	0.05401	0.06062	0.06032	0.06005	0.06263	0.06243	0.06225
0.0	0.05947	0.05885	0.05829	0.06630	0.06599	0.06569	0.06880	0.06858	0.06838
0.2	0.05507	0.05452	0.05401	0.06062	0.06032	0.06005	0.06263	0.06243	0.06225
0.4	0.04281	0.04244	0.04210	0.04506	0.04486	0.04468	0.04588	0.04574	0.04562
0.6	0.02548	0.02540	0.02533	0.02423	0.02419	0.02416	0.02379	0.02376	0.02373
0.8	0.00757	0.00790	0.00821	0.00559	0.00577	0.00593	0.00487	0.00499	0.00510
h	0.00000	0.00059	0.00114	0.00000	0.00032	0.00061	0.00000	0.00021	0.00041

Table. (9.2): Variations of velocity profile for velocity slip parameter κ.

Chapter 10

Conclusions

In this chapter we have summarized the main findings about the theoretical analysis of a blood flow through arteries. The parametric studies and key findings of the entire thesis are stated as:

10.1 Heat and mass transfer results

- The temperature profile decreases with an increase in the nanoparticle volume fraction, which means high thermal conductivity of nanoparticles plays a key role in quick dissipation of the temperature.
- It is noted that the temperature inside the stenotic artery increases for heat source parameter ($\beta > 0$). This result is obtained due to increase in internal heat source of the fluid i.e. through metabolic process.
- Temperature profile gives higher results for diverging tapering ($\phi > 0$) as comparing to other tapering.
- The temperature distribution shows random behavior for Brownian motion number N_b and thermophoresis parameter N_t.
- The nanoparticle concentration increases with an increase in Brownian motion number N_b and decreases with an increases in thermophoresis parameter N_t.

10.2 Hemodynamic theoretical results

10.2.1 Nanoparticles effects

- It is concluded that copper and silver nanoparticles with their high thermal conductivity characteristics are useful as drug carriers to minimize the wall shear stress and resistance impedance that is experienced by blood flowing through stenosed arteries.
- The Ag nanoparticles are more helpful as drug carriers to minimize resistance as comparing to the Cu blood case.
- The wall shear stress phenomenon gives higher altitude for the pure blood case then compare to the Cu blood case.
- Increase in Brownian motion number reveals that the thermal conductivity of the base fluid enhances and reduces resistance to blood flow.
- It is observed that the hemodynamic effects possesses same behavior for thermophoresis parameter N_t and Brownian motion number N_b parameters.
- The magnitude of stresses on the wall of arteries and resistance impedance to flow shows higher results for the SWCNT case than for the pure blood case.

10.2.2 Permeable wall and slip effects

- Increase in permeability of the artery through Darcy number results in damaged, dilated or inflamed arterial wall thickness and tend to increase resistance.
- It is also noted that resistance to flow decreases with an increase in the values of the permeable slip parameter s and hence accelerate the blood flow.

10.2.3 Magnetic effects

- It is observed with an increase in the intensity of magnetic field resistance impedance to flow and wall shear stress increases. This result is concluded from the fact that the external magnetic field slows down the random motion of nanoparticles and hence also tends down the blood movement.

- Hemodynamic of stenosis increases with an increase in the magnetic Reynolds number R_m and Strommers number S. This increase is due to increase in Lorentz force which tends to retard the flow of blood. It is concluded from this result that magnetic effects can be used to regulate or controlled the blood flow.

10.2.4 Thermal and velocity slip effects

- The amplitude of resistance to blood flow is higher for no slip case ($\gamma = \kappa = 0$) and amplitude is smaller for slip case ($\gamma = \kappa \neq 0$).
- The hemodynamic effects of the stenosed arteries decreases with an increase in the thermal and velocity slip parameters. Therefore, slip effects are important to heal up the consequences of diseased artery.

10.2.5 Variable nanofluid viscosity effects

- For variable nanofluid viscosity resistance to blood flow decrease as compared to constant nanofluid viscosity ($\alpha = 0$). So, considering variable nanofluid viscosity is useful for the blood to flow through diseased artery to minimize the coagulation factors.
- It is obtained from graphical illustration that stress on the wall of diseased arteries are also decreases for variable nanofluid viscosity case when compare to the constant nanofluid viscosity case.

10.2.6 Combination of aneurysm and stenosis effects

- The resistance impedance to blood flow decreases with an increase in the critical height of aneurysm δ_1 and increases with an increase in critical height of stenosis δ_2, which means that resistance impedance to flow has an opposite behavior for the aneurysm and stenosis cases.
- The wall shear stress in the aneurysm segment is observed to decrease rapidly towards its minimum value and then starts steeply increase to the end of aneurysm segment, while the opposite trend of wall shear stress is observed in the stenotic segment as compared with the aneurysm segment.

10.2.7 Other important findings

- The increase in resistance to flow creates more stresses on the wall of stenosed arteries and vice versa. From graphical illustration it is noted that the stresses and resistance impedance to blood flow possess same behavior for tapering and other fluid flow parameters.
- Amplitude of resistance decreases for vertical stenosed arteries as compared to the horizontal and inclined arteries.
- The wall shear stress and resistance impedance to flow possess same variation against t and this oscillation is decaying as the time t increases.

10.3 Axial velocity results

- The velocity profile increases near the wall of the artery and decreases near the wall of the catheter with an increase in the Hartmann number H_a.
- The axial velocity possesses opposite results for Brownian motion number N_b and thermophoresis parameter N_t.

10.4 Trapping results

- The number of trapping bolus increases with an increases in the values of N_b, N_t, δ, ε, H_a, R_m, S, γ, α and η, while decreases with an increases in the values of Φ and κ.
- The blood flow pattern shows that the trapping bolus appears in the aneurysm segment, while no formation is observed or seen in the stenotic segment.
- The variable nanofluid viscosity phenomena shows that more bolus appears for the Ag nanoparticles case, while constant nanofluid viscosity phenomena shows trapped bolus increases for the copper nanoparticles case when compare to other cases.

References

[1] F. C. Mann, J. F. Herrick, H. E. Essex, E. J. Blades, Effects on blood flow of decreasing the lumen of blood vessels, Surgery, (1938), 4:249-252.

[2] D. F. Young, Effect of a time dependent stenosis on flow through a tube, Journal of Engineering for Industry, (1968), 90:248-254.

[3] K. M. Channon, The endothelium and pathogenesis of atherosclerosis, Medicine, (2006), 4:173-177.

[4] R. Johnston, D. Kilpatrick, Mathematical modelling of flow through an irregular arterial stenosis, Journal of Biomechanics, (1991), 24:1069-1077.

[5] P. R. F. D. Young, F. Y. Tsai, Flow characteristics in model of arterial stenosis steady flow, Journal of Biomechanics, (1973), 6:395-410.

[6] H. V. Anderson, G. S. Roubin, P. P. Leimgruber, W. R. Cox, J. S. Douglas Jr., S. B. King, A. R. Gruentzig, Measurement of trans-stenotic pressure gradient during percutaneous transluminal coronary angioplasty, Circulation, (1986), 73:1223-1230.

[7] R. Ponalagusamy, The blood flow through an artery with mild stenosis: A two-layered Model, Different shapes of stenosis and slip velocity at the wall, Journal of Applied Sciences, (2007), 7:1071-1077.

[8] G. T. Liu, X. J. Wang, B. Q. Ai, L. G. Liu, Numerical study of pulsatile flow through a tapered artery with stenosis, Chinese Journal of Physics, (2004), 42:401-409.

[9] J. M. Siegel, C. P. Markou, S. R. Hanson, A scaling law for wall shear rate through an arterial stenosis, Journal of Biomechanical Engineering Transactions, ASME, (1994), 116:446-451.

[10] B. E. Morgan, D. F. Young, An integral method for the analysis of flow in arterial stenoses, Bulletin of Mathematical Biology, (1974), 36:39-53.

[11] G. S. Beavers, D. D. Joseph, Boundary conditions at a naturally permeable walls, Journal of Fluid Mechanics, (1967), 30:197-207.

[12] V. P. Srivastava, M. Tandon and R. K. Srivastav, A macroscopic two-phase blood flow through a bell shaped stenosis in an artery with permeable wall, Applications and Applied Mathematics, (2012), 7:37-51.

[13] S. Chakravarty, P. K. Mandal, A nonlinear two-dimensional model of blood flow in an overlapping arterial stenosis subjected to body acceleration, Mathematical and Computer Modelling, (1996), 24:43-58.

[14] R. Ellahi, S. U. Rahman, M. Gulzar, S. Nadeem, K. Vafai, A mathematical study of non-Newtonian micropolar fluid in arterial blood flow through composite stenosis, Applied Mathematics and Information Sciences, (2014), 4:1567-1573.

[15] Kh. S. Mekheimer, M. H. Haroun, M. A. El Kot, Effects of magnetic field, porosity and wall properties for anisotropically elastic multi-stenosis arteries on blood flow characteristics, Applied Mathematics and Mechanics, (2011), 32:1047-1064.

[16] A. Medhavi, Suspension two-layered blood flow through a bell shaped stenosis in arteries, Applied Bionics and Biomechanics, (2013), 10:11-18.

[17] A. K. Singh, Effects of shape parameter and length of stenosis on blood flow through improved generalized artery with multiple stenosis, Advances in Applied Mathematical Biosciences, (2012), 3:41-48.

[18] J. C. Misra, G. C. Shit, Blood flow through arteries in a pathological state: A theoretical study, International Journal of Engineering Science, (2006), 44:662-671.

[19] J. Bernsdorf, D. Wang, Non-Newtonian blood flow simulation in cerebral aneurysms, Computers and Mathematics with Applications, (2009), 58:1024-1029.

[20] A. R. Mantha, G. Benndorf, A. Hernandez, R. W. Metcalfe, Stability of pulsatile blood flow at the ostium of cerebral aneurysms, Journal of Biomechanics, (2009), 42:1081-1087.

[21] S. Mukhopadhyay, G. C. Layek, Analysis of blood flow through a modelled artery with an aneurysm, Applied Mathematics and Computation, (2011), 217:6792-6801.

[22] B. V. R. Kumar, K. B. Naidu, Finite element analysis of nonlinear pulsatile suspension flow dynamics in blood vessels with aneurysm, Computers in Biology and Medicine, (1995), 25:1-20.

[23] B. Pincombe, J. mazumdar, The effects of Post-stenotic dilatations on the flow of a blood analogue through stenosed coronary arteries, Mathematical and Computer Modelling, (1997), 25:57-70.

[24] K. M. Prasad, R. B. Vijaya, C. Umadevi, Effects of stenosis and post stenotic dilatation on Jeffrey fluid flow in arteries, International Journal of Research in Engineering and Technology, (2014), 4:195-201.

[25] A. K. Singh, D. P. Singh, A computational study of Bingham plastic flow of blood through an artery by multiple stenosis and post dilatation, Advances in Applied Science Research, (2012), 3:3285-3290.

[26] S. Priyadharshini, R. Ponalagusamy, Biorheological model on flow of Herschel-Bulkley fluid through a tapered arterial stenosis and dilatation, Applied Bionics and Biomechanics, (2015), 2015: 406195.

[27] D. Biswas, U. S. Chakraborty, Steady flow of blood through a catheterized tapered artery with stenosis: A theoretical model, Assam University Journal of Science & Technology: Physical Sciences and Technology, (2009), 4:7-16.

[28] A. Zaman, N. Ali, M. Sajid, T. Hayat, Effects of unsteadiness and non-Newtonian rheology on blood flow through tapered time-variant stenotic artery, AIP Advances, (2015), 5:037129.

[29] D. S. Sankar, J. Goh, A. I. M. Ismail, FDM analysis for blood flow through stenosed tapered arteries, Boundary Value Problems, (2010), 2010: 917067.

[30] Kh. S. Mekheimer, M.A. El. Kot, Mathematical modelling of unsteady flow of a Sisko fluid through an anisotropically tapered elastic arteries with time-variant overlapping stenosis, Applied Mathematical Modelling, (2012), 36:5393-5407.

[31] Kh. S. Mekheimer, M. A. El Kot, Suspension model for blood flow through arterial catheterization, Chemical Engineering Communications, (2010), 197:1195-1214.

[32] V. P. Srivastava, R. Rastogi, Blood flow through stenosed catheterized artery: effects of hematocrit and stenosis shape, Computers & Mathematics with Applications, (2010), 59:1377-1785.

[33] Kh. S. Mekheimer, M. A. El Kot, Mathematical modeling of axial flow between two eccentric cylinders: Application on the injection of eccentric catheter through stenotic arteries, International Journal of Non-Linear Mechanics, (2012), 47:927-937.

[34] R. K. Srivastav, Mathematical model of blood flow through a composite stenosis in catheterized artery with permeable wall, Application and Applied Mathematics, (2014), 99:58-74.

[35] N. K. Verma, S. Mishrab, S. U. Siddiqui, R. S. Gupta, Study of blood flow through a catheterized artery, Advances in Applied Science Research, (2011), 2:114-122.

[36] M. F. Barnothy (Ed.), Biological Effects of Magnetic Fields, Plenum Press, New York, (1964).

[37] A. Kolin, An electromagnetic flow meter: Principle of method and its application to blood flow acceleration, Experimental Biology and Medicine, (1936), 35:53-56.

[38] V. K. Stud, G. S. Sephon, R. K. Mishra, Pumping action on blood flow by a magnetic field, Bulletin of Mathematical Biology, (1977), 39:385-390.

[39] E. M. Korchevskii, L. S. Marochnik, Magneto hydrodynamic version of movement of blood, Biophysics, (1965), 10:411-413.

[40] Y. Abd. elmaboud, Influence of induced magnetic field on peristaltic flow in an annulus, Communications in Nonlinear Science and Numerical Simulation, (2012), 17:685-698.

[41] R. Ellahi, A. Riaz, S. Nadeem, M. Mushtaq, Series solutions of magnetohydrodynamic peristaltic flow of a Jeffrey fluid in eccentric cylinders, Applied Mathematics & Information Sciences, (2013), 7:1441-1449.

[42] P. K. Mandal, An unsteady analysis of non-Newtonian blood flow through tapered arteries with a stenosis, International Journal of Non-Linear Mechanics, (2005), 40:151-164.

[43] G. C. Shit, M. Roy, Pulsatile flow and heat transfer of a magneto-micropolar fluid through a stenosed artery under the influence of body acceleration, Journal of Mechanics in Medicine and Biology, (2011), 11:643-661.

[44] J. C. Misra, M. K. Patra, S. C. Misra, A non-Newtonian fluid model for blood flow through arteries under stenotic conditions, Journal of Biomechanics, (1993), 26:1129-1141.

[45] A. Sinha, G. C. Shit, P. K. Kundu, Slip effects on pulsatile flow of blood through a stenosed arterial segment under periodic body acceleration, ISRN Biomedical Engineering, (2013), 2013:925876.

[46] R. Ponalagusamy, Blood flow through an artery with mild stenosis: a two-layered model, different shapes of stenoses and slip velocity at the wall, Journal of Applied Sciences, (2007), 7:1071-1077.

[47] U. S. Chakraborty, D. Biswas, M. Paul, Suspension model blood flow through an inclined tube with an axially non-symmetrical stenosis, Korea Australia Rheology Journal, (2011), 23:25-32.

[48] Kh. S. Mekheimer, F. Salama, M. A. El. Kot, The unsteady flow of a Carreau fluid through inclined catheterized arteries having a balloon with time-variant overlapping stenosis, Walailak Journal of Science and Technology, (2015), 12:863-883.

[49] D. Biswas, M. Paul, Suspension model for blood flow through a tapering catheterized inclined artery with asymmetric stenosis, Applications and Applied Mathematics, (2015), 10:474-495.

[50] A. Zaman, N. Ali, M. Sajid, Slip effects on unsteady non-Newtonian blood flow through an inclined catheterized overlapping stenotic artery, AIP Advances, (2016), 6:015118.

[51] N. Srivastava, Analysis of flow characteristics of the blood flowing through an inclined tapered porous artery with mild stenosis under the influence of an inclined magnetic field, Journal of Biophysics, (2014), (2014):797142.

[52] L. Obdulia, K. Taehong, Calculation of arterial wall temperature in atherosclerotic arteries: effect of pulsatile flow, arterial flow, arterial geometry and plaque structure, Journal BioMedical Engineering, (2007), 6:1-18.

[53] Kh. S. Mekheimer, M. H. Haroun, M. A. El Kot, Influence of heat and chemical reactions on blood flow through an anisotropically tapered elastic arteries with overlapping stenosis, Applied Mathematics & Information Sciences, (2012), 2:281-292.

[54] A. Ogulu, T.M. Abbey, Simulation of heat transfer on an oscillatory blood flow in an indented porous artery, International Communications in Heat and Mass Transfer, (2005), 32:983-989.

[55] S. Chakravarty, S. Sen, Dynamic response of heat and mass transfer in blood flow through stenosed bifurcated arteries, Korea-Australia Rheol, (2005),17:47-62.

[56] B. Tashtoush, A. Magableh, Magnetic field effect on heat transfer and fluid flow characteristics of blood flow in multi-stenosis arteries, Heat Mass Transfer, (2008), 44:297-304.

[57] Y. Cinar, N. Kosku, Hypothesis: temperature stress and blood viscosity affects the leukocyte flexibility, coagulation, intracranial hypertension, and hemodynamics, International Conference on Life Science and Technology, IACSIT Press, (2011), 3:120-126.

[58] G. C. Shit, M. Roy, A. Sinha, Mathematical modelling of blood flow through a tapered overlapping stenosed artery with variable viscosity, Applied Bionics and Biomechanics, (2014), 11:185-195.

[59] N. S. Akbar, S. Nadeem, Simulation of variable viscosity and Jeffrey fluid model for blood flow through a tapered artery with a stenosis, (2012), Communications in Theoretical Physics, 57:133-140.

[60] J. C. Misra, A. Sinha, G. C. Shit, Mathematical modeling of blood flow in a porous vessel having double stenosis in the presence of an external magnetic field, International Journal of Biomathematics, (2011), 4:207-225.

[61] P. Singh, A. Singh, S. P. Singh, Effect of radial viscosity variation on non-Newtonian flow

of blood in a stenosed artery, International Journal of Current Engineering and Scientific Research, (2012), 8:51-61.

[62] K. Aslan, T. A. J. Grell, Rapid and sensitive detection of troponin I in human whole blood samples by using silver nanoparticle films and microwave heating, Clinical Chemistry, (2011), 57:5746-752.

[63] S. Shaw, P. V. S. N. Murthy, P. Sibanda, Magnetic drug targeting in a permeable microvessel, Microvascular Research, (2013), 85:77-85.

[64] B. Godin, J. H. Sakamoto, R. E. Serda, A. Grattoni, A. Bouamrani, M. Ferrari, Emerging applications of nanomedicine for the diagnosis and treatment of cardiovascular diseases, Trends in Pharmacological Sciences, (2010), 31:199-205.

[65] Y. Jiang, C. Reynolds, C. Xiao, W. Feng, Z. Zhou, W. Rodriguez, S. C. Tyagi, J. W. Eaton, J. T. Saari, Y. J. Kang, Dietary copper supplementation reverses hypertrophic cardiomyopathy induced by chronic pressure overload in mice, The Journal of Experimental Medicine, (2007), 204:657-666.

[66] F. Gentile, M. Ferrari, P. Decuzzi, The transport of nanoparticles in blood vessels, The effect of vessel permeability and blood rheology, Annals of Biomedical Engineering, (2007), 36:254-261.

[67] S. U. S. Choi, Enhancing thermal conductivity of fluids with nanoparticles, In: Siginer DA, Wang HP (eds), Developments and applications of non-Newtonian flows, ASME, (1995), 36:99-105.

[68] F. M. Abbasi, T. Hayat, F. Alsaadi, Hydromagnetic peristaltic transport of water-based nanofluids with slip effects through an asymmetric channel, International Journal of Modern Physics B, (2015), 29:1550151.

[69] R. Ellahi, S. U. Rahman, S. Nadeem, N. S. Akbar, Blood flow of nanofluid through an artery with composite stenosis and permeable walls, Applied Nanoscience, (2014), 4:919-926.

[70] F. M. Abbasi, T. Hayat, B. Ahmad, G. Q. Chen, Slip effects on mixed convective peristaltic transport of copper-water nanofluid in an inclined channel, Plos One, (2014), 9(8): e105440.

[71] N. S Akbar, S. U Rahman, R. Ellahi, S. Nadeem, Nano fluid flow in tapering stenosed arteries with permeable walls, International Journal of Thermal Sciences, (2014), 85:54-61.

[72] J. c. Maxwell, Electricity and magnetism, 3rd edn., Clarendon, Oxford, (1904).

[73] R. L. Hamilton, O. K. Crosser, Thermal conductivity of heterogeneous two component systems, Industrial & Engineering Chemistry Fundamentals, (1962), 1:187-191.

[74] J. Buongiorono, Convective transport in nanofluids, ASME, Journal of Heat Transfer, (2006), 128:240-250.

[75] S. C. McBain, H. H. Yiu, J. Dobson, Magnetic nanoparticles for gene and drug delivery, International Journal of. Nanomedicine, (2008), 3:169-180.

[76] V. V. Mody, A. Cox, S. Shah, A. Singh, W. Bevins, H. Parihar, Magnetic nanoparticle drug delivery systems for targeting tumor, Applied Nanoscience, (2004), 4:385-394.

[77] S. M. S. Murshed, C. A. N. Castro, M. J. V. Lourenco, M. L. M. Lopes, F. J. V. Santos, A review of boiling and convective heat transfer with nanofluids, Renewable and Sustainable Energy Reviews, (2011), 15:2342-2354.

[78] S. Iijima, T. Ichihashi, Single-shell carbon nanotubes of 1-nm diameter, Nature, (1993), 363:603-605.

[79] N. S. Akbar, A. W. Butt, Carbon nanotubes analysis for the peristaltic flow in curved channel with heat transfer, Applied Mathematics and Computataion, (2015), 259:231-241.

[80] N. S. Akbar, Entropy generation analysis for a CNT suspension nanofluid in plumb ducts with peristalsis, Entropy, (2015), 17:1411-1424.

[81] J. H. He, Homotopy Perturbation technique, Computer Methods in Applied Mechanics and Engineering, (1999), 178:257-262.